Inhibition of Cell Migration using PARG Inhibitors

Daniel John Harrison

A thesis submitted in partial fulfilment of the requirements for the degree of Doctor of Philosophy

The University of Sheffield
Faculty of Medicine, Dentistry and Health
Department of Oncology and Metabolism

May 2023

Acknowledgements

First and foremost, I would like to thank Dr Helen Bryant for her patience and passion for science. It has been a privilege to have been mentored by you and to have worked with you. I cannot thank you enough for taking a chance on me and despite the difficulties, I hope you have enjoyed it as much as I have.

Secondly, I would like to thank the University of Sheffield for funding this project which made it possible for me to undertake this work. A big thank you to Dr Paul Heath for his contributions with the microarray during the hights of the pandemic. I would also like to thank Dr Barbara Ciani and Dr Chris Toseland for their insights and expertise. Also, a big thank you to Dr David King. You had left by the time I started the PhD but my first major lab experience was in large part influenced by you and I'll never forget it. Thank you Dr Polly Gravells as well for teaching me westerns, even if I do say that through slightly gritted teeth.

I would like to give thanks to everyone past and present in the Bryant, Collis, and Thompson labs. There are too many to name and I couldn't be concise in what I wanted to say to each of you, but you know who you are and I wish you all the best in the future. I have no doubt each one of you will go far. Stay in touch. Thank you to Dr Spencer Collis for his contributions in lab meetings and privately. The same can be said for Dr Ola Rominiyi.

An extra special thank you to Connor, Kathryn and Tobi. I hope we continue to remain friends and thank you for being there to share in the good days and the bad days. Tim, never change, I hope you continue to have that positive aura and thank you as well.

Thank you to all my friends outside the lab for tolerating me particularly when I was grumpy. Honourable mentions include Callum, Sam, Lewis H, Brandon, Martin, Lewis B and Charlie.

I would also like to thank all my family for their belief and encouragement over the years and during my life. Honourable mentions include Deb and Mark, Charlotte and Dave, Lynn and

Colin, Jill and Brian, and Aimie and Shaun. Thank you to Jill for all your help at the very beginning.

Regarding family, an extra special thank you is owed to my parents who without, I would not be the person that I am today, and I owe more to you than I even probably realise. Thank you. I hope you would be proud Dave; I would have loved to have sat down with you in the garden and discussed all of this with you before I got a real job. You've got red on you.

Abstract

The ability of a cancer cells to migrate, contributes to their metastatic potency and effective therapies are urgently needed. Five of the seventeen Poly(ADP-Ribose) polymerase (PARP) family members are capable of catalysing polymers of ADP-Ribose, a post translational modification implicated in many biological processes. It's the activity of these PARP members that Poly(ADP-Ribose) Glycohydrolase (PARG) reverses by degrading ADP-Ribose chains. Depletion of PARG has been reported to reduce cellular migration *in vitro* in a range of cancer types and reduce metastasis *in vivo* in breast cancer. We wanted to investigate if PARG inhibitors (PARGi) reduced cellular migration of the aggressive and highly migratory breast cancer cell line MDA-MB-231.

In this thesis, we provide evidence that molecular inhibition of PARG's catalytic activity with effective non-cytotoxic doses of PARGi reduces MDA-MB-231 cell migration. Cellular supplementation with the NAD+ precursor β-NMN, restored the migration of PARGi treated cells. Furthermore, inhibitors selective against different PARylating PARP's also reduced migration. Intriguingly, combined PARP and PARG inhibition restored cell migration, suggesting that the ratio of PARP and PARG's catalytic activity is important for maintaining favourable migration conditions. PARGi treated cells had elevated cytoskeletal components and the dynamics of actin associated sub-structures (stress fibres, filipodia and podosomes) were affected. PARGi treated cells also had an increase in nuclear envelope ruptures, invaginations, and blebs. PARGi also reduced the total protein levels of mesenchymal markers YAP1, β-catenin, C-MYC and vimentin. Finally, we explored the effects of PARGi on global transcription and identified 139 differentially expressed genes (DEG) that when interrogated using bioinformatics, providing insight into a wide range of biological processes that PAR biology may be involved in. E2F1 was a DEG, confirmed to be downregulated at the protein level and is involved in breast cancer migration. PARGi's have a potential future as anti-migratory agents.

Table of Contents

List of Figures

List of Tables

Abbreviations

A	Alpha Helical Domain
ABC	ATP-binding cassette
ABRO1	BRCA1-interacting protein, Abraxas
ADP	Adenosine Dipohosphate
AIF	Apopotosis Inducing Factor
ALC1	Amplified in Liver Cancer Protein 1
AMOT	Angiomotins
A-NHEJ	Alternative Non-Homologus End Joining
ANOVA	Analysis of Variance
AP	Apurinic/apyrimidinic
APC2	Adenomatous polyposis coli protein 2
APLF	Aprataxin And PNKP Like Factor
ACL1	Ankyrin Repeat Cluster
ARID1A	AT-Rich Interactive Domain-Containing Protein 1A
ART	ADP-Ribosyltransferase
ARTD	ADP-Ribosyltransferase Domain
ATG9A	Autophagy Related 9A
ATM	Ataxia-telangiectasia mutated
ATMIN	ATM Interactor
ATP	Adenosine Triphosphate
ATR	Ataxia telangiectasia and Rad3 related
Axin	Axis Inhibition Protein 1
BARD1	BRCA1 associated RING domain 1
Bcl-2	B-cell lymphoma 2
BCR	BCR Activator Of RhoGEF And GTPase
BER	Break Excision Repair
BLZF1	Basic Leucine Zipper Nuclear Factor 1
BP	Branched Polymer
BRCA1	Breast cancer type 1 susceptibility protein
BRCA2	Breast cancer type 2 susceptibility protein

BRCT	BRCA1 C Terminus Domain
Bub3	BUB3 Mitotic Checkpoint Protein
BubR1	BUB1 mitotic checkpoint serine/threonine kinase B
CASC3	Cancer Susceptibility Candidate Gene 3 Protein
CCND1	Cyclin D1
CD2AP	CD2-Associated Protein
Cenpa	Centromere Protein A
Cenpb	Centromere Protein B
CHFR	Checkpoint With Forkhead And Ring Finger Domains
C-NHEJ	Classical Non-Homology End Joining
CPAP	Centrosomal P4.1-Associated Protein
CSB	Cockayne Syndrome group B
CTC	CST Telomere Replication Complex Component 1
CTCF	CCCTC-binding factor
DBM	DNA Binding Motif
DDR	DNA Damage Response
DEG	Differentially Expressed Genes
DNA	Deoxyribonucleic Acid
DSB	Double Strand Break
DUSP22	Dual Specificity Phosphatase 22
EMT	Epithelial to Mesenchymal Transition
FOV	Field of Vision
GAPDH	Glyceraldehyde 3-phosphate dehydrogenase
GG-NER	Global Genome-NER
GLUT4	Glucose Transporter 4
GO	Gene Ontology
GOE	Gene Ontology Enrichment
GSE	Gene Set Enrichment
HCC	Hepatocellular Carcinoma
HR	Homologous Recombination
HRR	Homologous Recombination Repair
HU	Hydroxy Urea

HuR	Human antigen R
KDM5B	Lysine Demethylase 5B
KEGG	Kyoto Encyclopedia of Genes and Genomes
KM/plot	Kaplain Meier/Plot
MAR	Mono-ADP-Ribose
MD	Macro Domain
MEF	Mouse Embryonic Fibroblast
MF	Molecular Functions
MIF	Macrophage Inhibitory Factor
Miki	Mitotic Kinetics Regulator
MMP2	Matrix Metalloprotease 2
MMP9	Matrix Metalloprotease 9
MMS	Methyl methanesulfonate
MNNG	Methylnitronitrosoguanidine
MNU	Methylnitrosourea
MVPI	MVP Interacting Domain
NAD+	Nicotinamide adenine dinucleotide
NADH	Nicotinamide adenine dinucleotide
NELF-E	Negative Elongation Factor Complex Member E
NER	Nucleotide Excision Repair
NHEJ	Non-Homology End Joining
NMD	Nonsense Mediated Decay
NuMa	Nuclear Mitotic Apparatus
PAP	Poly(A) Polymerase
PAR	Poly(ADP-Ribose)
PARG	Poly(ADP-Ribose) Glycohydrolase
PARGi	Poly(ADP-Ribose) Glycohydrolase Inhibition/Inhibitor
PARP	Poly(ADP-Ribose) Polymerase
PARPi	Poly(ADP-Ribose) Polymerase Inhibition/Inhibitor
PCNA	Proliferating Cell Nuclear Antigen
PCR	Polymerase Chain Reaction
PDX	Patient Derived Xenograft

PNKP	Polynucleotide Kinase-Phosphatase
PTEN	Phosphatase and tensin homolog
PUMA	p53 Upregulated Modulator of Apoptosis
RB	Retionblastoma Protein
RBMX	RNA Binding Motif Protein X-Linked
RECQ1	RecQ Like Helicase
RNA	Ribonucleic Acid
RNABP	RNA Binding Protein
RNF146	Ring Finger Protein 146
RPA	Replication Protein A
RRM	RNA Recongnition Motif
SAM	Sterile Alpha Motif
SAP	SAF-A/B, Acinus & PIAS Motif
SCE	Sister Chromatid Exchange
SD	Standard Deviation
SEM	Standard Error of the Mean
SSB	Single Strand Break
SSBR	Single Strand Break Repair
TCA	Tricarboxylic Acid
TC-NER	Transcription Coupled NER
TDP-43	TAR DNA-binding protein 43
TFPI2	Tissue factor pathway inhibitor 2
TNBC	Triple Negative Breast Cancer
TNKS	Tankyrase
TNKSi	Tankyrase Inhibitor/Inhibition
TRF1	Telomeric Repeat Factor 1
U	Ubiquitin Interacting Motif
UPS25	Ubiquitin Specific Peptidase 25
VIT	Vault Protein Inter Alpha Trypsin Domain
vWA	Von Willebrand Factor Type A Domain
WGR	WGR Domain
XPC	Xeroderma pigmentosum complementation group C

XPE	Xeroderma pigmentosum complementation group E
XRCC1	X-ray repair cross-complementing protein 1
YAP1	yes-associated protein 1
Z/Znf	Zing Finger Motif

1.0 Introduction

1.1 Overview of the Poly(ADP-Ribose) Cycle

Poly(ADP-ribose) polymerases (PARPs) are a superfamily of 17 multi-domain proteins each possessing a highly conserved (ADP-ribosyl)transferase (ART) domain that catalyses the cleavage of nicotinamide adenine dinucleotide (NAD+) into nicotinamide and ADP-ribose (Amé et al., 2004). The ADP-ribose is then transferred to an acceptor protein or itself (figure 1.1). This transfer can occur in a monomeric or polymeric (linear or branched chain) manner depending on the PARP enzyme (figure 1.1). The ADP-ribose moieties are normally considered to be added to the most distal ADP-ribose terminus (Alvarez-Gonzalez, 1988; Taniguchi, 1987), however other models exist (Ikejima et al., 1987). Poly (ADP-ribose) glycohydrolase (PARG) and PAR erasers are responsible for the removal of the polymer of ADP-ribose (PAR) (figure 1.1).

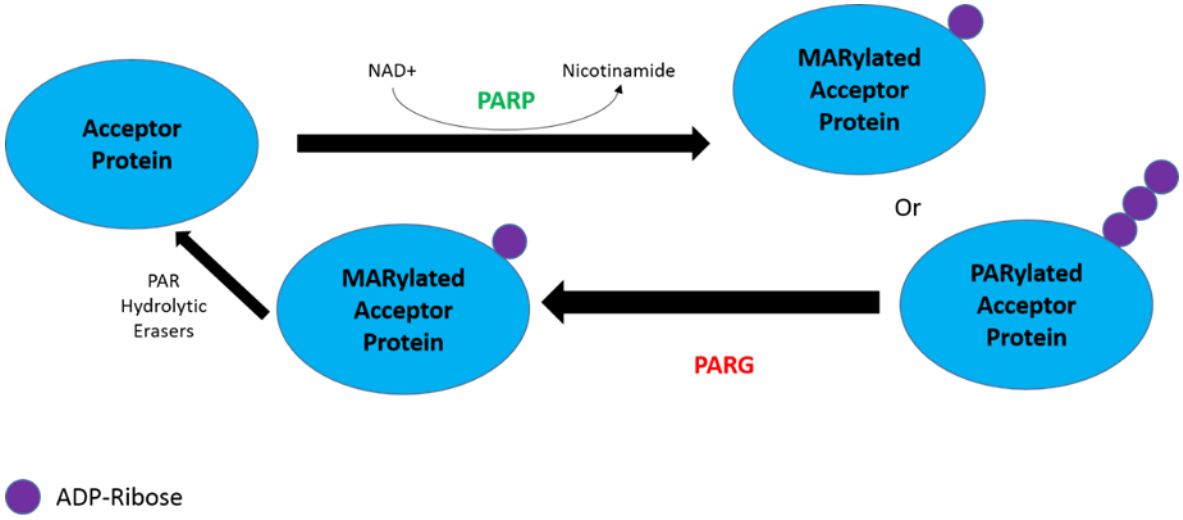

Figure 1.1. **Overview of the PAR Cycle.** PARP enzyme uses NAD+ as a substrate to catalyse the transfer of the ADP-ribose moiety of NAD+ to a target acceptor protein. Nicotinamide is cleaved off in the reaction. The mono-ADP-ribosylated protein is referred to as being MARylated. Some PARP enzymes are also capable of catalysing the addition of ADP-ribose to distal ADP-ribose residues forming a polymer of ADP-ribose – PAR. PARG and additional PAR Hydrolytic erasers are responsible for PAR removal returning the acceptor protein back into its native state.

To facilitate understanding and gain insight into the potential effects of PARG inhibitors, it is important to provide an overview of PARP structure and function.

1.2 Overview of PARP Protein Structure, Activity and Function

1.2.1 PARP Family Structure and Activity

The PARP family consists of 17 family members. These PARP's have different names within the literature and can be sub-classified by domain structure or activity. The subcellular location of each PARP, along with a summary of the functions of each PARP is shown in table 1.1. PARPs1-5b share a conserved His-Tyr-Glu (H-Y-E triad – table 1.1) within the NAD+ binding pocket of the ART domain (Otto et al., 2005). This triad is predicative of PARylation capabilities. PARP1 was the first PARP enzyme to be discovered and is the most intensely researched (Chambon et al., 1963, 1966). PARP1 is classified as a nuclear DNA activated PARylator, capable of adding multiple ADP-ribose residues to a single acceptor (figure 1.2). These PAR units have been reported to get up to hundreds of residues in size (Alvarez-gonzalez & Jacobson, 1987; Murcial et al., 1983). Furthermore, it can promote branching within a growing PAR chain (Miwa et al., 1979; Rolli et al., 1997; Ruf et al., 1998). PARP2 is similar to PARP1 (Amé et al., 1999), and their structure can be seen in figure 1.3, along with the rest of the PARP family. PARP1 and 2 therefore display multiple catalytic capabilities emerging from within the same domain. They can catalyse the following: initiating the initial transferal of ADP-ribose to an acceptor protein, elongating this chain further by catalysing a 2'-1'' ribose-ribose glycosidic bond and additionally, instigating branching by catalysing a 2'' – 1''' ribose-ribose bond (figure 1.2). Both PARP1 and PARP2 are activated by DNA damage, with different lesions reported induce activity to varying degrees (Amé et al., 1999; Benjamin & Gill, 1980; Eustermann et al., 2015).

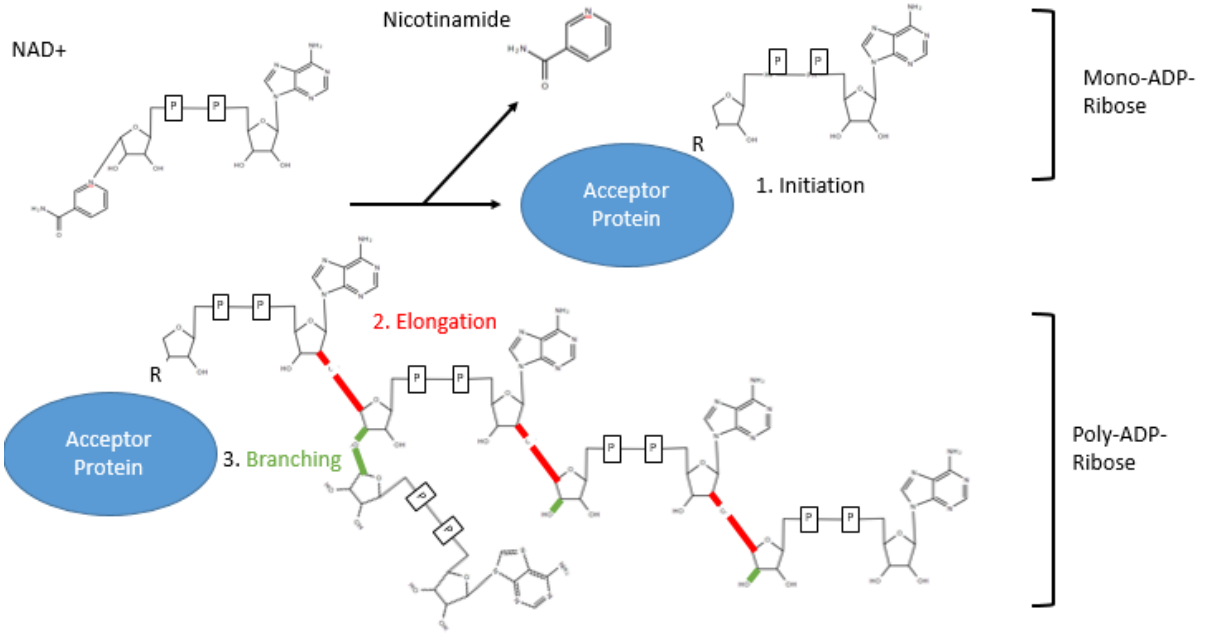

Figure 1.2. **The catalytic reaction of PARylators.** 1. PARP initiates the PAR reaction by transfer of ADP-ribose to a receptive amino acid residue on an acceptor protein. 2. Elongation is performed by the addition of ADP-ribose to form a polymer, catalysing the formation of a 2'-1'' ribose-ribose glycosidic bond, highlighted in red. 3. Branching can be performed by catalysing a 2'' – 1''' ribose-ribose glycosidic bond.

PARP3 is also activated by DNA damage and is shorter in length that PARP1 and 2 (figure 1.3). Despite containing the H-Y-E triad (table 1.1), there is conflicting evidence regarding PARP3's MARylation and PARylation activity. Initially, PARP3 was considered only capable of MARylation, however, PARP3 is now known to MARylate PARP1 (Loseva et al., 2010) and PARylate the nuclear mitotic apparatus (NuMa) (Boehler et al., 2011) and KU80 (Beck et al., 2014a) in addition to MARylating and PARylating free double strand break (DSB) ends (Zarkovic et al., 2018). This is possibly due to experimental context but may be reflective of a more complex and nuanced role of PARP3 in different cellular processes. PARP4 is associated with the vault complex (table 1.1), a massive ribonucleoprotein complex and has MARylation activity (Van Zon et al., 2003).

PARP Family Name	Transferase Name	Alternative Names	Sub-Class	Triad Motif	Enzymatic Activity	Motifs and Domains	Subcellular Localisation	Functions	Reference
PARP1	ARTD1		DNA-Dependant	H-Y-E	BP	ZnF, BRCT, WGR	N	Aging, Antiviral, Cell Cycle regulation, differentiation, Chromosome structure and DNA repair, inflammation, Metabolic regulation, RNA processing, Transcription, migration	(J.-R. Choi et al., 2016; Ji & Tulin, 2010; Ke, Wang, et al., 2019; Ke, Zhang, et al., 2019; Ko & Ren, 2012; Ray Chaudhuri & Nussenzweig, 2017; Westera et al., 2019; Liu Yang et al., 2013; Zha et al., 2018)
PARP2	ARTD2		DNA-Dependant	H-Y-E	BP	DBD, WGR	N	Chromosome Structure and DNA repair, Cell cycle regulation, inflammation, metabolic regulation, transcription	(P. Bai & Cantó, 2012; Dantzer & Santoro, 2013; Fouqin et al., 2017; Szántó et al., 2012)
PARP3	ARTD3		DNA-Dependant	H-Y-E	M/P	WGR	N, C	Cell cycle regulation, DNA repair	(Beck et al., 2014b; Christian Boehler et al., 2011)
PARP4	ARTD4	vPARP		H-Y-E	M	BRCT	CP, N, Ex, CM, S	Cancer Biology, vault biology	(Raval-Fernandes, 2005; Van Zon et al., 2003)

PARP5A	ARTD5	Tankyrase 1, TNKS1	Tankyrase	H-Y-E	OP	ARC, SAM	N, CP, T, G	Antiviral, cell cycle regulation, cytosolic RNA processing, inflammation, metabolic regulation, mitotic spindle formation, telomere maintenance	(Haikarainen et al., 2014; M. Kim, 2018; Smith, 2015)
PARP5B	ARTD6	Tankyrase 2, TNKS2	Tankyrase	H-Y-E	OP	ARC, SAM	N, CP, T, G	Inflammation, metabolic regulation, telomere maintenance	(Haikarainen et al., 2014; M. Kim, 2018; Smith, 2015)
PARP6	ARTD17			H-Y-Y	M		N, CP	Cell proliferation, Cell Cycle, Tumorigenesis	(J. Y. Huang et al., 2016; Tatsuka, 2012)
PARP7	ARTD14	TiPARP	CCCH PARP	H-Y-I	M	ZnF, WWE	N, CP	Antiviral effects, Chromosome structure? cytosolic RNA processing, protein degradation, transcription	(Ahmed et al., 2015; Bindesbøll et al., 2016; Bock et al., 2015; Macpherson et al., 2013)
PARP8	ARTD16			H-Y-I	M		N, CP		
PARP9	ARTD9	BAL1	macroPARP	Q-Y-T	-	Macro	N, CP	Antiviral response, Cell migration, inflammation?, tumour formation	(Iwata et al., 2016; Kamata & Paschal, 2019; Tang et al., 2018)
PARP10	ARTD10			H-Y-I	M			Antiviral, Cell Proliferation, Cell cycle, cytosolic RNA processing, DNA replication, metabolism, migration, transcription	(Chou et al., 2006; Márton, Fodor, et al., 2018; Munnur et al., 2019; Schleicher et al., 2018; Mengbin Yu et al., 2011; Y. Zhao et al., 2018)

PARP11	ARTD11			H-Y-I	M	WWE	NE	Antiviral	(T. Guo et al., 2019; Kirby et al., 2018)
PARP12	ARTD12	ZC3HDC1	CCCH PARP	H-Y-I	M	ZnF, WWE	G, CP	Antiviral effects, cytosolic RNA processing, Golgi Trafficking, Inflammation	(Catara et al., 2017; L. Li et al., 2018; Welsby et al., 2014)
PARP13	ARTD13	ZC3HAV1, ZAP	CCCH PARP	H-Y-V	-	ZnF, WWE	N, CP	Apoptosis, Cytosolic RNA processing, DNA repair, Tumorigenesis	(Bock et al., 2015; Fujimoto et al., 2017; Todorova et al., 2014, 2015)
PARP14	ARTD8	BAL2, COAST6	macroPARP	H-Y-L	M	Macro, WWE	N, CP	Apoptotic, DNA repair, Inflammation, metabolic regulation, nuclear RNA processing, transcription, tumour formation	(Bock et al., 2015; Caprara et al., 2018; Schweiker et al., 2018)
PARP15	ARTD7	BAL3	macroPARP	H-Y-L	M	Macro	N	Cytosolic RNA processing	(Anthony et al., 2011; Bock et al., 2015)
PARP16	ARTD15			H-Y-I	M		N, RER	Unfolded protein response	(Di Paola et al., 2012; Jwa & Chang, 2012)

Table 1.1 **The PARP Family.** PARP names, transferase name (Hottiger, Hassa, Lüscher, Schüler, & Koch-Nolte, 2010) and alternative names are included. Each PARP's respective sub group is included. The catalytic triad of each PARP is included. The enzymatic activity of each PARP is included. BP, OP, M and '–' donate branched polymer, oligo-polymer, mono ADP-ribose activity and '-' indicates no catalytic activity respectively. Notable motifs and domains are included: Zinc Finger Domain (Znf), BRCA C-terminal domain (BRCT), WGR domain, Akyrin Repeat Cluster (ARC), Sterile Alpha Motif (SAM), WWE domain, and Macro domain (MD). Subcellular localisations included: Nucleus (N), Centrosomes (C), Cytoplasm (CP), Exosomes (Ex), Cell Membrane (CM), Telomeres (T), Spindle (S), Golgi Apparatus (G) Nuclear Envelope (NE) and Rough Endoplasmic Reticulum (RER). PARP functions and associated references are included.

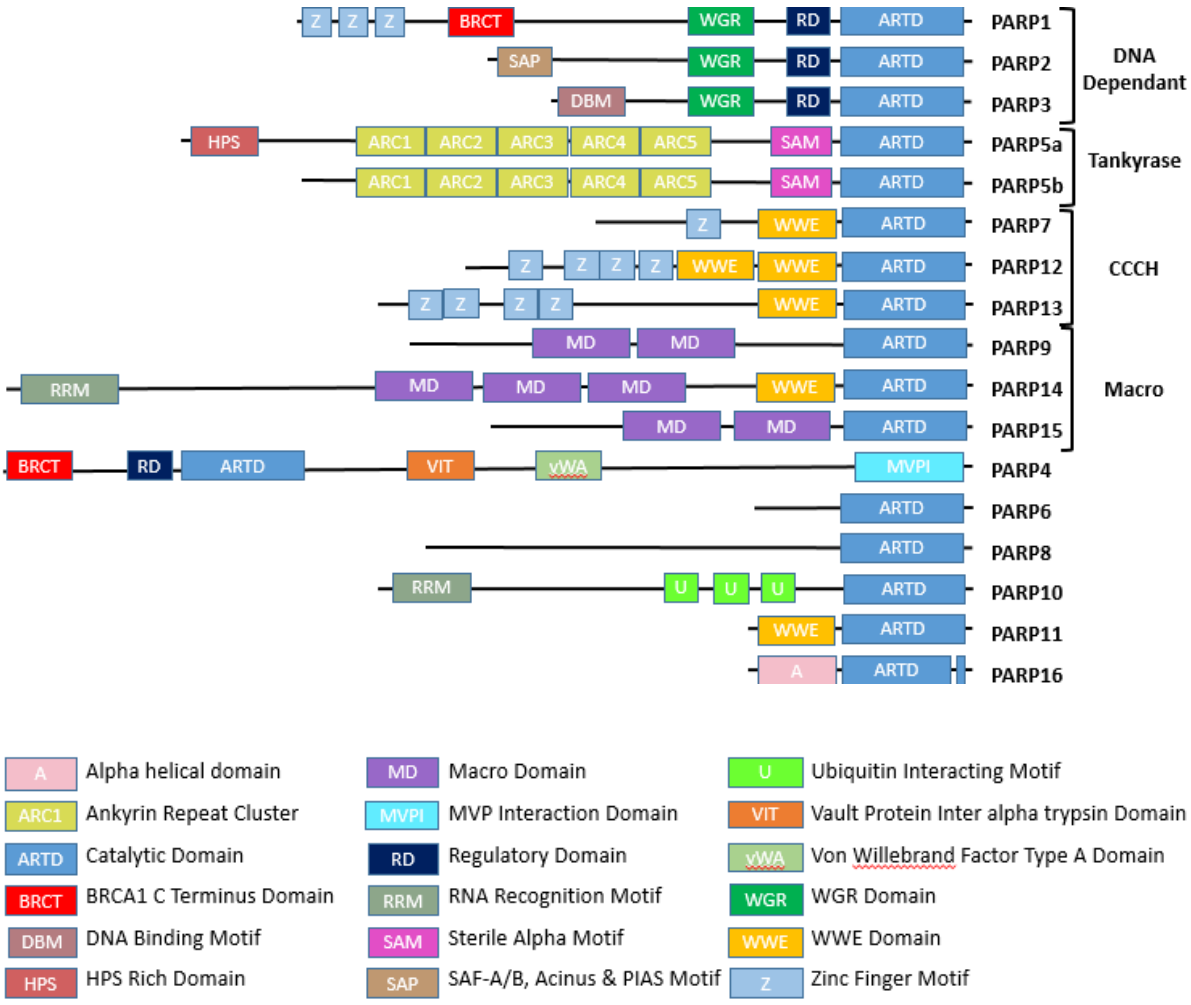

Figure 1.3. **Schematic Diagram of PARP Family Domains.** PARPs group based on subclass. See the figure key for full domain names.

PARP 5a and 5b (commonly referred to as Tankyrase 1/2, TNKS1/2), do not need DNA damage to be activated and are located more widely throughout the cell. They are capable of PARylation activity however typically produce oligomers up to around 20 ADP-ribose residues in length. The significance of PAR length and size is not fully understood. The rest of the family (PARP6-17) are MARylaters. However, it has not been demonstrated that PARP13 exhibits catalytic activity (Vyas et al., 2014), due to a closed cleft preventing NAD+ binding (Karlberg et al., 2015). The PARP name is therefore a misnomer. The family's expansion and previous nomenclatures inaccuracies/inconsistencies has resulted in a new

nomenclature proposal (Hottiger et al., 2010). This nomenclature revolves around the enzymatic reaction (ART) and enzymatic structural markers (diphtheria-like, in reference to the presence of the H-Y-E triad motif in secreted ADP-ribosylating pathogenic diphtheria toxins by *Corynecbacterium diphtheria)*, hence the name ARTD. However, for clarity and consistency with the literature, the PARP nomenclature will be used. As the focus of this review is PARG, which reverses PAR and not MAR, the known functions of the PARylators will be discussed.

1.2.2 PARP 1, 2 and 3 Functions

PARP1, 2 and 3 contain DNA binding domains that facilitate their interaction with DNA and enable them to ADP-ribosylate target proteins, perform auto modification and even ADP-ribosylate free DNA ends (Vyas et al., 2014). ADP-ribosylation has been observed to have different consequences. One consequence is that it operates as a recruitment platform. For example, efficient resolution of single strand breaks (SSB) by SSB repair and recruitment of the scaffold protein X-ray repair cross complementing 1 (XRCC1) is facilitated by PARP1 and 2 auto modification (Hanzlikova et al., 2017). XRCC1 is then more efficiently recruited to SSB due to its BRCT domain which has an affinity for PAR (Masson et al., 1998). Additional consequences of ADP-ribosylation of an acceptor protein include DNA/RNA dissociation due to the strong negative charge of PAR (Satoh & Lindahl, 1992), acceptor protein topography changes influencing protein-protein interactions and modulating acceptor protein catalytic activity (Fischbach et al., 2018; Muthurajan et al., 2014; G. Yang et al., 2020; Zhen & Yu, 2018). This enables PARPs to be involved in a wide array of biological processes. PARP1 is thought to account for approximately 90% of the cells PAR activity. PARylation still occurs in mice deficient of PARP1 suggesting PARP1 and 2 have overlapping roles and PARP2 may be able partially compensate for PARP1 loss (Beneke et al., 2000; Dantzer et al., 2000; Masutani et al., 2000; Shieh et al., 1998). For example, both are capable of recruiting

XRCC1 to chromatin (Fisher et al., 2007; Hanzlikova et al., 2017). Indeed, deletion of PARP1 and PARP2 results in embryonic lethality (Menissier De Murcia, 2003), however, PARP1 -/- mice exhibit higher mutation frequencies (Shibata et al., 2009) and while spontaneous tumour formation rates in PARP1 -/- and PARP1 +/+ mice are similar, they appear earlier in PARP1 -/- mice and have a greater chance of harbouring a malignant tumour across a range of cancer types (Piskunova et al., 2008; Shibata et al., 2009). This suggests PARP2 cannot fully compensate for the loss of PARP1. Homozygous deletion of PARP3 is non-lethal but does increase sensitivity to DNA damaging agents (Boehler et al., 2011). PARP3 -/- mice cells have been reported to display reduced association of Ku80 with DSB ends, reducing the levels of classical non-homologous end joining (C-NHEJ) and increasing DNA end resection (Beck et al., 2014a), DNA end resection at a double strand break being prerequisite for homologous recombination (HR) and alternative non-homologous end joining (A-NJEH). PARP3 depletion results in a suppression of HR despite an increase in DNA end resection and an increase in mutagenic deletions that is thought to be due to PARP3 increasing the levels of the error prone A-NHEJ that occur (Beck et al., 2014a). This suggests PARP3 is involved in modulating which repair pathway is deployed at a DSB which may explain the sensitivity to DNA damage agents. PARP1-3 are localized to the nucleus and have been implicated in many cellular processes to varying degrees. These processes will now be discussed.

In this thesis, where a clear role for a particular PARP protein has been indicated, it will be stated. In other places where the particular PARP(1-3) is not known – for example when the result has been shown with a PARP inhibitor, the term PARP will be used.

1.2.2.1 The Role of PARP1, 2 and 3 in DNA Repair, Chromosome Structure and Cell Cycle Regulation

The most heavily studied function of PARPs1-3 is their role in DNA repair. A depletion in NAD+ and increase in PARP activity in response to DNA damaging agents was noted early

in the field of PARP research. The first paper to demonstrate PARP inhibition and NAD+ depletion enhanced DNA damage was published by Dukacz et al., (1980), demonstrating PARP involvement in DNA repair and increasing the prospect of it being targeted for its potential as an anti-cancer drug target. In the interim, the roles of PARP1-3 in DNA repair have been elucidated extensively and will now be summarised.

1.2.2.1.1 Single Strand break repair

PARP1, 2 and 3 have multifaceted roles in different aspects of single strand break repair (SSBR). PARP1, 2 and 3 contain DNA binding motifs that facilitate binding at single strand break sites and enables PARP dimerization. Homo and heterodimerization is possible between the PARPs (Ali et al., 2012; Jean-christophe Ame et al., 2002; Menissier De Murcia, 2003), however the context and precise functional consequences are still being elucidated. PARP can also bind monomerically at DNA damage sites (Eustermann et al., 2011). PARP1 accounts for 80-90% of detectable PAR following DNA damage and has been demonstrated to be responsible for the majority of repair. PARP1 hyperactivation in response to DNA damage depletes cellular NAD+ to critical levels (Murata et al., 2019). Perhaps PARP2 and 3 compete with PARP1 at DNA damage sites to help mitigate NAD+ consumption. Binding to DNA stimulates polymerase activity and production of the PARylation chain via auto modification or on one of the dimerised partners (Ali et al., 2012; G. de Murcia & de Murcia, 1994; Langelier & Pascal, 2013). PARylation in this context functions to recruit repair factors and eventually disassociate PARP from the break stie to facilitate efficient repair due to repulsion between the negatively charged DNA and PAR chain (Ferro & Olivera, 1982; Zahradka & Ebisuzaki, 1982). PARP1 and 2 PARylation have been demonstrated to recruit XRCC1, which is key scaffold protein for the recruitment of the rest of the cohort of repair factors and is integral for driving efficient repair (Breslin et al., 2015; El-Khamisy et al., 2003; Hanzlikova et al., 2017; Okano et al., 2003; Polo et al., 2019; Taylor et al., 2002). However, some of these downstream repair factors, such as Aprataxin and PNK-like factor (APLF) and polynucleotide kinase 3'-phosphatase (PNKP), the latter of

which is stimulated by XRCC1 (Mani et al., 2007; Whitehouse et al., 2001), have also been shown to have an affinity for PAR suggesting they may also be directly recruited by PARP (Eustermann et al., 2010; M. Li et al., 2013; Rulten et al., 2008). Interestingly, recent work shows the binding of PARP and XRCC1 is dependent on each other during genotoxic stress, suggesting a reciprocal regulation of each other (Reber et al., 2022). The role of PARP3 in single strand break repair is less well understood. PARP3 has been shown to sense SSBs and accelerate SSBR, however with differential affinities compared to PARP1 depending on the type of single strand damage (Grundy et al., 2016).

1.2.2.1.2 Base excision repair

Indirect SSBs form because of the activation of base excision repair (BER) related apurinic/apyrimidinic (AP) endonucleases. BER is required for the resolution of nucleotides with lost bases (abasic sites) or damaged bases via oxidation or alkylation. PARP1 and 2 are likely required for downstream processing of the indirect SSBs formed during BER however there is conflicting evidence. Differential sensitivity to base damaging lesions have been reported when PARP1 is deficient or inhibited (Dantzer et al., 1999; Ménissier De Murcia et al., 1997; Pachkowski et al., 2009; Vodenicharov et al., 2000). PARP1 has also been reported to reduce the repair kinetics of BER (Allinson et al., 2003). PARP inhibitors do trap PARP on the SSB that's formed downstream (Ström et al., 2011). Excess PARP1 activity can also impede BER and is tamed by XRCC1 (Adamowicz et al., 2021; Demin et al., 2021). A possible explanation to account for all these reports is that PARP is redundant and possibly interferes with BER in some contexts, yet is indispensable for a sub-set of lesions which BER resolves (Reynolds et al., 2015).

1.2.2.1.3 Nucleotide excision repair

Nucleotide excision repair (NER) is responsible for the resolution of bulky/helix distorting DNA lesions. There are two subtypes of NER which consist of different proteins; transcription coupled NER (TC-NER) and global-genome NER (GG-NER), which get activated in their named contexts and downstream overlap to form the NER pre-incision complex. PARP1 associates with Cockayne syndrome group B (CSB) (Flohr et al., 2003) in TC-NER and recruits xeroderma pigmentosum complementation group C (XPC), xeroderma pigmentosum complementation group E (XPE) (Luijsterburg et al., 2012; Robu et al., 2013) and Amplified in liver cancer protein 1 (ALC1) (Pines et al., 2012) in GG-NER and xeroderma pigmentosum complementation group A (XPA) (Fahrer et al., 2007; King et al., 2012) in the pre-incision complex. PARP1 enables efficient NER.

1.2.2.1.4 Double strand break repair

Double stranded breaks are the most cytotoxic DNA lesion. They can be resolved via multiple pathways and repair is essential to maintain genome stability. PARP1-3 have been implicated in each of these different pathways.

1.2.2.1.4.1 Homologous Recombination Repair (HRR)

Changes in the levels of PARP1 activity impact sister chromatid exchange (SCE), implicating it in homologous recombination repair (HRR). Loss of PARP1 or inhibition of PARP increases HRR as indicated by increased spontaneous SCE (Ménissier De Murcia et al., 1997; G. D. E. Murcia & Murcia, 1995; Oikawa et al., 1980), RAD51 foci formation (Schultz et al., 2003) and direct assays of HRR (Saleh-gohari et al., 2005). Consistent with this, overexpression of PARP1 reduces the levels of DNA damage-induced SCE's (R. Meyer et al., 2000). PARP accelerates HRR by recruiting and stabilising the breast cancer type 1 susceptibility protein (BRCA1) and BRCA1 associated ring domain 1 (BARD1) heterodimer

at double strand breaks (M. Li & Yu, 2013). Additionally, RNA binding motif protein X-linked (RBMX) is recruited in a PARP1 dependant manner, which recruits and stabilises the breast cancer type 2 susceptibility protein BRCA2 (Adamson et al., 2012). The recruitment of these proteins is integral for efficient HRR.

1.2.2.1.4.2 Non-Homologous End Joining (NHEJ)

Non homologous end joining (NHEJ) is an alternative DSBR pathway that can repair DSBs without the need for a homologous DNA template. Classical-NHEJ (C-NHEJ) is the pathway most people regard as NHEJ and is contingent on DNA-PKcs activity. PARP1 has been shown to PARylate DNA-PKcs, inhibiting its activity (Yang Han et al., 2019). PARP1 has been shown to PARylate KU70/80, reducing its affinity for DSBs, and suppressing C-NHEJ (B. Li et al., 2004). PARP3 recruits KU80 at DSB sites (Beck et al., 2014b) and interacts with a number of NHEJ associated proteins – Lig3, KU70, KU80 and DNA-PKcs (Rouleau et al., 2007). NHEJ is mediated by a PARP3 and APLF axis, the latter of which functions as a major recruitment platform for efficient NHEJ mediated repair (Grundy et al., 2012; Rulten et al., 2011). Alternative-NHEJ (A-NHEJ) gets activated predominantly during G2 phase of the cell cycle and is only detectable when there is reduced C-NHEJ activity (W. Wu et al., 2008). A-NHEJ is also required for class switch recombination and telomeric fusions, and is dependent on PARP1 function (Robert et al., 2009; Sfeir, Agnel J, de Lange, 2012).

1.2.2.1.5 The Cell Cycle

Due to PARPs involvement in DNA repair, its function is integrally entwined with the progression of the cell cycle. However, PARPs have been shown to exert cell cycle effects independently of their direct DNA-repair roles and the resulting signalling cascades that occur in response to damage. In some cases, this is a direct transcriptional effect and in others, it is due to functions of PARP during replication or mitosis.

For example, PARP2 has been shown to reduce the expression of various cell cycle coupled genes for example, p21, RB, E2F1 and C-MYC (Liang et al., 2013). This transcriptional repression was independent of PARylation and the overexpression of PARP2 was shown to delay/block G1 exit (Liang et al., 2013). In addition, loss of PARP2 has been reported to produce a G2/M transition arrest in mouse erythroid progenitor cells, but likely through a loss of replication stress protection rather than a direct transcriptional effect (Farrés et al., 2015). Like PARP2, the overexpression of PARP3 also interfered with G1/S progression in the absence of exogenous DNA damage, although the mechanism was not elucidated (Augustin et al., 2003). Like PARP2, PARP1 has also been shown to have function at replication forks and promotes progression of S-phase as it is required for primase activity and replication-coupled repair (Bryant et al., 2009; Petermann et al., 2010; Sugimura et al., 2008; Vaitsiankova et al., 2022; Yamashita et al., 2022).

PARylation is highly prevalent during mitosis (Y. Kanai et al., 1981; Kidwell & Mage, 1976). During mitotic stress, PARP1 autoribosylates and interacts with the mitotic checkpoint and E3 ligase checkpoint with forehead and ring finger domains (CHFR), which degrades PARP1, halting the cells in prophase (Kashima et al., 2012), which suggests in the absence of stress, PARP1 permits mitotic progression. PARP is catalytically active and present within metaphase chromosomes (Holtlund et al., 1980). In addition, PARP1 is located at centrosomes (Kanai et al., 2003). When PARP1 is deletion or PARP1-3 inhibited, centrosomes are hyper-amplified in mouse embryonic fibroblasts (MEFs) due to PARP being unable to PARylate P53 localised at the centrosomes (M. Kanai et al., 2003). Consistent with this, centrosome amplification was also observed in PARP1 deficient mice (Tong et al., 2007). PARP1 has been shown to interact with and Poly(ADP-Riboslyate) the centrosomal proteins Cenpa and Cenpb, implicating PARP1 in kinetochora attatchment. (Alka Saxena et al., 2002). PARP1 deficient fibroblasts treated with a spindle disrupting agent (colcemid) had an accelerated mitotic progression and became polyploidy, suggesting PARP1 is involved in the mitotic spindle checkpoint. Indeed, PARP1 has also been reported to interact with the

spindle assembly checkpoint proteins BubR1 and Poly(ADP-Riboslyate) Bub3 (Fang et al., 2006; Alka Saxena et al., 2002).

PARP3 is also present at centrosomes, where it colocalises with PARP1 and overexpression of PARP3 does not alter centrosome amplification. The study did not look at the effect of deleting PARP3 (Augustin et al., 2003), thus the function of PARP3 at centrosomes is not clear. PARP3 has been reported to be involved in mitotic spindle assembly via an interaction with NuMa (C Boehler et al., 2011).

1.2.2.1.6 Chromatin Remodelling

PARPs have been shown to regulate chromatin remodelling, and many PARP functions are mediated though this role. PARP1 has been shown to PARylate histones directly (Otake et al., 1969) (with linker histone H1 being most studied), resulting in nucleosome disassembly and chromatin relaxation (Martinez-Zamudio & Ha, 2012; Poirier et al., 1982). This is likely due the negative charge of PAR leading to dissociation of histone H1. Interestingly, PARP1 can bind to linker DNA of nucleosomes and this causes PARylation independent reorganization of the nucleosome via direct displacement of H1 (Maluchenko et al., 2021). Other histones reported to be PARylated include all 4 core histones (Huletskyl et al., 1989; Karch et al., 2017). Histone variants H2A.Z and macroH2A have also both been shown to have functional relationships with PARP1 (H. Chen et al., 2014; Donnell et al., 2013).

In addition, PARP1's ability to modulate the local chromatin environment extends to regulating other histone post-translational modifications. For example, lysine demethylase 5B (KDM5B) when in a PARylated state, cannot demethylate H3K4me3. Thus PARP promotes persistence of H3K4me3 and localised opening of chromatin (Krishnakumar & Kraus, 2010). Further PARP can promote recruitment of chromatin remodellers. For example, ALC1 is a SNF2-like ATPase recruited by PARP1 mediated PARylation of UV-

damaged DNA. Once recruited, ALC1 modulates chromatin structure via nucleosome sliding which in turn promotes XPC recruitment and efficient GG-NER (Pines et al., 2012).

1.2.2.2 The Role of PARP1 and 2 in Transcription and RNA processing

PARP1 and to a lesser extent PARP2, have extensive roles in transcription, ribosomal biogenesis, and the processing of RNA ranging from alternative splicing, export and subcellular condensates. The roles of PARP1 and 2 in these processes will be discussed as the events proceed during the life cycle of mRNA.

PARP mediated chromatin remodelling contributes to the ability of PARP to alter cellular transcription (see below). For example in order to drive gene expression, PARP1 binds near the promoter of actively transcribed genes, which impedes the transcriptional repressive function of histone H1 (Krishnakumar et al., 2008). In line with this, PARP1 has also been shown to modulate large scale 3D organization of chromatin via the CCCTC-binding factor (CTCF), co-localizing at specific DNA sites (Nalabothula et al., 2015), also impacting transcription (H. Zhao et al., 2015). CTCF is the master regulator of 3D chromatin structure and shares a complex co-regulatory function with PARP1 (Guastafierro et al., 2008; Lupey-Green et al., 2018). Indeed, histone H1 and PARP1 are thought to compete for binding of promoters of target genes to have reciprocal roles in transcription (M. Y. Kim et al., 2004; Krishnakumar et al., 2008). For example, in collaboration with GATA3, PARP1 competes with H1 to maintain euchromatin and allow cyclin D1 (CCND1) transcription (Shan et al., 2014). In addition, PARP1 can function as a transcription factor directly (Akiyama et al., 2001; K. Huang et al., 2004) and has been seen to interact with numerous other transcription factors to exert binding partner dependant co-activation (Simbulan-Rosenthal et al., 2003) or co-repression (Lin et al., 2011). Another way PARP is suggested to regulate transcription is via direct or indirect interactions with the basal transcription machinery (Hassa & Hottiger,

2008; Meisterernst et al., 1997; Slatterys et al., 1983). In these ways, PARP has been seen to regulate many different cellular processes via changes in transcription initiation.

Following initiation, efficient transcription relies on a process known as proximal pausing, which allows for recruitment of splicing factors; RNA Polymerase II is paused in early elongation, and then released in a regulated way that promotes productive RNA synthesis. One of the proteins involved in establishing proximal pausing is negative elongation factor complex member E (NELF-E). PARP1 PARylates NELF-E, causing it to disassociate and allowing RNA elongation to proceed to productive elongation (Gibson et al., 2016; E. A. Matveeva et al., 2019).

Another way PARP can alter gene expression is via regulation of alternative splicing. PARP has been seen to bind nucleosomes and pre-mRNA at exon/intron boundaries (E. Matveeva et al., 2016). Further, inhibition of PARP or depletion of PARP1 altered the pattern of alternative splicing. Interestingly different patterns were seen with depletion compared to inhibition suggesting catalytic and non-catalytic dependent functions (E. Matveeva et al., 2016). It is postulated that both PARP-dependent changes to chromatin structure and PARP-dependent recruitment of splicing factors are responsible for this (E. Matveeva et al., 2016; E. A. Matveeva et al., 2019). In addition, RNA binding proteins (RNABP) also impact the splicing fate of pre-processed mRNA. PARP1 has been shown to interact with multiple RNABP via protein-protein interactions (Isabelle et al., 2010), to PARylate RNABP directly (Jungmichel et al., 2013) plus many RNABP have affinity for PAR (Teloni & Altmeyer, 2016), these findings suggest that PARP may also alter splicing via recruitment of RNABP.

The final steps to produce a mature mRNA is the synthesis of a Poly (A) tail and mature mRNA export. Polyadenylation is performed by Poly(A)polymerases (PAP), which prior to Poly(A) synthesis endonucleolytically cleave the mRNA. PARP1 under thermal stress PARylates PAP, resulting in PAP's disassociation from the immature mRNA, preventing polyadenylation of non-heat shock proteins (Di Giammartino et al., 2013). This reduces the half-life of the mRNA, impedes export and ultimately, effects protein translation. It is not

known how PARP recognises specific transcripts. Following Polyadenylation, a variety of receptors and complexes facilitate mRNA export. PARP1 has been shown to interact with some of these proteins, exerting a role on mRNA export that is still yet to be fully elucidated (Isabelle et al., 2010). PARP1 has been implicated in impacting mRNA stability that extends beyond the suppression of poly(A) tail synthesis. Depletion of PARP1 has been shown to increase the transcription of non-sense mediated decay (NMD) genes, a cellular program directly involved in modulating mRNA turnover (Melikishvili et al., 2017). Additionally, PARP1 has been shown to PARylate the RNA-binding protein Hu antigen R (HuR) impacting gene mRNA stability (Ke et al., 2017). How selectivity of stabilisation is induced is unknown.

Once mRNA is exported, it is translated into protein by ribosomes. PARP1 exerts a role in ribosomal biogenesis in the nucleolus. In Drosophila, PARP1 was seen in the nucleolus, and its activity was required for correct nucleolar protein localisation. In addition, PARP was needed for proper rDNA translation, pre-rRNA processing and ribosomal assembly (Boamah et al., 2012, Guetg et al., 2012). Consistent with this, ribosomal proteins have been reported to be members of the PARP1 interactome (Isabelle et al., 2010). In summary, PARP1 likely exerts a role in ribosomal biogenesis but more works needs to be done to further our understanding.

Finally, sub-cellular condensates are membrane less micron-scale biomolecular compartments in which molecules like proteins and nucleic acids are concentrated. Among other functions they are integral for the processing, transportation, and recycling of ribonucleoprotein complexes. Proteins integral for sub-cellular condensate formation are a part of the PARP1 interactome (Gibson et al., 2016; Isabelle et al., 2010) and PARP1 inhibition disrupts the formation and dynamics of these organelles (Leung, 2020). Many questions and challenges remain to further explore the role of PAR biology in sub-cellular condensate physiology and pathophysiology, but it seems likely that this is yet another way in which protein expression can be regulated by PARP.

1.2.2.3 The role of PARP1 and 2 in Metabolism and Cell death

The creation of PARP1 and PARP2 knockout mice have shown that PARP enzymes have a role in metabolism. Indeed, PARP1 and PARP2 exert a wide array of complex roles in metabolic regulation and have been associated with several metabolic disorders (P. Bai & Cantó, 2012). Additionally, hyperactivation of PARP1 results in metabolic consequences that are entwined with a type of PARP1 mediated type of cell death (discussed later). PARP mediated effects on metabolism broadly can be put into 4 categories, 1. reduced NAD+ bioavailability and the resulting biological response, 2. the accumulation of free ADP-ribose, 3. PARPs transcriptional regulation of metabolic associated genes, and 4. PARylation/interaction of metabolic proteins by/with PARP.

NAD+ is the substrate all PARP enzymes use. Hyperactivation of PARP1 dramatically decreases the amount of NAD+ available (J. Zhang et al., 1994). This has implications for other NAD+ dependant enzymes such as sitruins, CD38 and the rest of the PARP family. A notable consequence of NAD+ depletion is the requirement of NAD+ in glycolysis and reduced glycolytic rates are observed following PARP hyperactivation (Fouquerel et al., 2014). However, this is complicated by the fact that PARP1 has been shown to reduce the activity of hexokinase. Hexokinase is first enzyme in the glycolysis pathway, and it contains a PAR binding motif that upon interaction with PAR, reduces its catalytic activity, reducing the amount of glucose-6-P and the overall glycolytic flux, independent of NAD+ depletion (Fouquerel et al., 2014). Additionally, a subsequent step in glycolysis involves glyceraldehyde 3-phosphate dehydrogenase (GAPDH), which is a NAD+ dependant enzyme that is a recipient of PARP1 PARylation which restricts GAPDH catalytic activity (Du et al., 2003). Pyruvate is the final product of glycolysis. Pyruvate is then converted into lactate or utilised in gluconeogenesis or directed towards the tricarboxylic acid (TCA) cycle within the mitochondria. Subunits of the pyruvate dehydrogenase complex are PARP acceptor proteins which likely impacts pyruvate fate, potentially to the detriment of TCA supply (Hopp et al., 2019). Reduced NAD+, reduced glycolytic flux via hexokinase-PAR interactions and GAPDH

PARylation mediated inactivity and altered pyruvate fate suggest this would impact the TCA cycle. Cellular supplementation of TCA cycle substrates has been shown to rescue PARP-mediated cell death suggesting there is a deficit in TCA activity (W. Ying et al., 2002). The TCA cycle reduces NAD+ to NADH, which is required for the first step in oxidative phosphorylation and generation of ATP. Indeed, maintenance of oxidative phosphorylation is integral for cellular survival when PARP1 is hyperactivated (Murata et al., 2019) and reduced ATP pools are observed when PARP1 is hyperactivated (Berger, 1985). It is likely that a combination of direct PARylation of metabolic enzymes within the mitochondria and depletion of NAD+ regulates mitochondrial function (Lai et al., 2008; Marc Niere et al., 2008). However, the physiological regulation of this is not well understood.

As already noted, PARP can mediate cell death. Changes in ATP levels are well established to play a role in cell death. PARP-mediated cell death is called PARthanotos and is characterised by its dependence on PARP1 hyperactivation, large amounts of DNA fragmentation and nuclear shrinkage mediated by apoptosis inducing factor (AIF) nuclear translocation which proceeds independently of caspase catalytic activity (P. Huang et al., 2022). The disrupted bioenergetics discussed previously was considered initially to be responsible for contributing to cell death. Whilst this may partially be the case, the accumulation of PAR within the mitochondria is sufficient to trigger cell death (Andrabi et al., 2006). PAR acts as a death signal, and AIF possess a PAR binding motif that upon interacting with PAR, triggers AIF release from the mitochondria to the nucleus (Y. Wang et al., 2011), triggering macrophage migration inhibitory factor (MIF) mediated cleavage of DNA (Y. Wang et al., 2016). PARthanotos is typically is triggered by high levels of generalised DNA damage that occur during traumatic injury, e.g. ischemia or, myocardial infarction or in many neurodegenerative disorders each of which can lead to increased levels of DNA damage and thus PARP activation. Consistent with this, depletion of PARP protects from injury such as stoke, diabetes, heart attack and so on and PARP inhibitors have been studied as treatment in this context.

PARP1 and PARP2 have also been linked with lipid metabolism. PARP1 knockout mice display hypercholesterolaemia (Erener, Mirsaidi, et al., 2012) and altered fatty acid metabolite patterns (Kiss et al., 2015). PARP2 knockout cells exhibit altered the lipid membrane composition (Márton, Péter, et al., 2018). PARP2 deletion reduces the expression of fatty acid synthase (P. Bai et al., 2007) and increases cholesterol biosynthesis (Szántó et al., 2014). Mitochondrial fatty acid oxidation is the primary pathway responsible for fatty acid breakdown. The deletion of PARP1 or PARP2 induces it (P. Bai, Canto, et al., 2011; P. Bai, Cantó, et al., 2011). Additionally, PARP1 and PARP2 impact the expression of a range of fatty acid transporters (P. Bai et al., 2007; Erener, Hesse, et al., 2012; Kiss et al., 2015). Together these studies suggest, PARPs are involved in fatty acid biosynthesis and absorption, however, further study is required to elucidate the mechanism.

The pentose phosphate pathway is required for nucleic acid synthesis (therefore DNA replication), aromatic amino acid synthesis, NAD+ synthesis and is integral for increasing cellular biomass. The initial metabolite used in the pathway is glucose-6-phosphate, which is the resulting product of hexokinase activity using glucose which is subject to PAR mediated regulation (see above) (Fouquerel et al., 2014). This suggests PARP may regulate this facet of metabolism as well.

1.2.2.4 The role of PARP1 and 2 in inflammation

PARP1 and 2 have distinct pro-inflammatory roles. PARP1 deletion, depletion or inhibition, impacts a wide range of inflammatory processes *in vitro* and *in vivo* (Pazzaglia & Pioli, 2020). These observations are also seen with PARP2 deletion however to a lesser extent and with some non-overlapping effects (Fehr et al., 2020). The role of PARP1 and 2 in a growing list of autoimmune and inflammatory diseases is further evidence of their role within inflammation (Ke, Wang, et al., 2019). It is now known PARP1 and 2 act as cofactors that sit at the apex of a positive feedback loop that is activated in response to pro-inflammatory

signals (Rosado et al., 2013). This enables the transcription of a wide range of pro-inflammatory proteins. High free radical levels are a by-product of this feedback loop and are also a potent inducer of this pro-inflammatory cascade. The resulting damage and high PARP activity cause cellular leakage via PARP mediated necrosis. The leaked cellular debris such as PARylated high mobility group box 1 (HMGB1) (Davis et al., 2012) and PAR itself (Krukenberg et al., 2015) produces a local pro-inflammatory cellular environment that stimulates local immune cell activity and leukocyte honing. The continually expanding role of PARP1 and 2 in inflammation has yielded interest in PARP inhibition as a route for therapeutically targeting inflammatory mediated disease (Nathan A. Berger et al., 2018; Giansanti et al., 2010; Wasyluk & Zwolak, 2021). Interestingly, the ability of PARP to regulate inflammation may also have an impact on cell migration (see below).

1.2.2.5 The Role of PARP1, 2 and 3 in Migration

PARP1 depletion and overexpression, decreases and increases migration respectively in ovarian cancer using a scratch wound assay (H. Chang et al., 2022). Higher PARP1 expression is associated with increased lung metastasis in patients (E. B. Choi et al., 2016). Metastasis was attenuated via PARP1 depletion or olaparib treatment in vivo (E. B. Choi et al., 2016). AG014699 (rucaparib) or BSI-201 (iniparib) but not AZD-2281 (olaparib) reduced the migration of heptacellular carcinoma cell line HepG2 using a transwell chamber (Mao et al., 2017). These differences could be attributable varying affinities for PARP1-3 or off-target effects. Inhibition of PARP1-3 using the PARP inhibitor PJ34 has been shown to reduce migration in triple negative breast cancer cell lines using a scratch wound assay (Dutta et al., 2020).

Additional co-treatment strategies also report reductions in migration however this likely due to elevated levels of cytotoxicity. Sequential talazoparib and carboplatin treatment regimen against triple negative breast cancer (TNBC) led to reduced transwell migration in vitro and a

reduction in lung micrometastasis in vivo (Beniey et al., 2023). Talazoparib and bazedoxifene (IL-6 inhibitor) reduced scratch wound migration of ovarian cancer cells (R. Zhang et al., 2021). PJ34 and cisplatin reduced migration of cervix cancer cells in a scratch wound assay (Mann et al., 2019). Olaparib and gemcitabine exhibited greater reductions in migration of pancreatic cancer via a scratch wound assay (Quiñonero et al., 2022). ARID1A deficient gastric cancer migrated less when co-treated with Olaparib and BKM120 (PI3K inhibitor) using a transwell (Lin Yang et al., 2018).

Weigert et al., (2020) investigated the effects of niraparib or talazoparib with radiation on a panel of melanoma and healthy fibroblast cell lines. Scratch wound analysis revealed anti-migration effects for most cell lines but what is interesting is that two of the melanoma cell lines exhibited enhanced migration (Weigert et al., 2020). PMe1L and A375M in response to talazoparib or niraparib alone and PMe1L in the drug and radiation co-treatment exhibited increased rates of migration (Weigert et al., 2020). In the context of investigating PARPi resistance, it was noted a panel of TNBC cell lines developed an enhanced epithelial to mesenchymal transition (EMT) status in response to Olaparib (Ye Han et al., 2019). Furthermore, the TNBC human cell line MCF10A and mouse TNBC cell line 4T1 exhibited enhanced migration under Olaparib treatment conditions using a scratch wound assay (Ye Han et al., 2019). This was over a 24-72 hour period. Pancreatic capan-1 cancer cells treated for 214 days with Olaparib or Rabusertib (CHk1 inhibitor) individually developed enhanced migration and invasion, that was further enhanced when co-treated with a transwell assay (N. Guo et al., 2022). A greater understanding of the biological conditions that inhibit or promote migration in response to PARPi is urgently.

There are also a few reports of PARP modulating normal cell migration, which might provide insight into how PARPi could be altering migration of cancer cells. In the context of diabetes, PARP1 knockout or inhibition with PJ34, has been shown to reduce glycemia-induced vascular smooth muscle cell migration in transwell assay under high glucose conditions. This was suggested to be via changes to tissue factor pathway inhibitor 2 (TFPI2) expression and

its resultant control of matrix metalloprotease 2 (MMP2), and matrix metalloprotease 9 (MMP9) protein levels (Z. Wang et al., 2021). Conversely, PARP1 knockout or inhibition (PJ34) increased wound healing in a mouse model of excision wounding (El-Hamoly et al., 2014). Consistent with this, the authors showed that keratinocyte migration was faster following PARP inhibition in a scratch would assay. Increased wound healing was accompanied by reduced expression of inflammatory molecules and of the nitrating stress marker nitrotyrosine. Finally, knockout of PARP1 or inhibition of PARP with olaparib or talazoparib was shown to reduce leukocyte adhesion to and migration across the blood brain barrier in vitro and in mouse models (Rom et al., 2016). In this study PARP inhibition prevented activation of the integrin conformation changes involved in adhesion, reduced the ratio of F to G actin consistent with reduced migration, while in parallel reducing RhoGTPase activity (Rom et al., 2016).

These reports suggest the role PARPs play in migration is likely context dependant. Given migration is a complex cellular process and that many functions of PARP have been shown to be involved in multiple cellular processes that can each be related to migration e.g. cytoskeletal changes, inflammation, metabolism or DNA damage, isolating how PARPs may regulate migration is challenging. It is then perhaps unsurprising then that the evidence that does implicate PARP members in migration is indirect. To further complicate the issue, these processes are interconnected as well. For example, migration and cytoskeleton changes require a stable energy source and changes in the cytoskeleton can also impact metabolism (J. S. Park et al., 2020).

Above are examples of cytoskeletal changes and inflammatory changes induced by PARPi and which were coincident with changes in migration. To reiterate the complexity of defining how PARP may be involved in migration, there is a relationship between migration, DNA damage, DNA repair and the cytoskeleton, raising the possibility of yet another series of potential mechanism by which PARPi could affect migration. Constricted migration and mechanical stress have been shown to induce DNA damage primarily through nuclear

deformation, replication stress and potentially through mislocalised DNA repair factors (KU80) (Mayr et al., 2002; Pfeifer et al., 2018; Shah et al., 2021). Other studies show that once migration (constriction/mechanical stress) is over, DNA damage is repaired. Further, depletion of DNA damage response (DDR) factors was seen to impede stem cell migration to a wound site, suggesting a functional DDR is required for migration (Sahu et al., 2021). One of the gene they depleted was ataxia telangiectasia and rad3 related (ATR). ATR is activated at the nuclear envelope during mechanical stress and independantly of DNA damage. Once activated it is suggested ATR activation coordinates chromatin attachment to the nuclear envelope with nuclear envelope dynamics to protect chromatin from mechanical stress (Kumar et al., 2014). Consistent with the idea that an active DDR is required for migration, activation of the DDR modulates the expression of genes involved in the cytoskeleton and adhesion (Hall et al., 2016; J. M. Kim, 2022). Interestingly, the cytoskeleton also impacts the dynamics of repair factors at DNA damage sites suggesting reciprocal regulation (Hurst et al., 2021). It is possible that the DDR functions of PARP could contribute to changes in migration seen with PARPi via cytoskeletal changes. Alternatively, PARP hyperactivation in response to DNA damage may simply restrict cell movement through depleted NAD+ and ATP. However, the relationship between migration and DNA damage/repair is a complex recently emerging area of study and more research needs to be done.

In summary, PARP1-3 likely impact migration through a variety of complex and interconnected processes that requires further elucidation. Determining which cancer cell migration promoting pathways might be regulated by PARP, and the mechanism by which inhibition can regulate them is of vital importance, given the emerging importance PARP inhibitors are playing in cancer therapy.

1.2.3 PARP inhibitors

Many PARP inhibitors have been used in phase 3 and 4 clinical trials: veliparib, olaparib, talazoparib, niraparib and rucaparib and they have different affinities for PARP family members (Carney et al., 2018; D. Kim & Nam, 2022). The applications of PARP inhibitors in cancer will now be discussed, as well as some the limitations that have emerged in the clinic.

1.3 PARP Inhibition (PARPi): It's uses and limits in cancer

1.3.1 PARPi Sensitise to DNA Damaging Agents

Inhibition of PARP1-3 can be mediated by small molecular inhibitors that bind to the NAD+ pocket within the ART domain, acting as NAD+ competitive inhibitors, preventing ADP-ribose transferase activity (A Ruf, de Murcia, & Schulz, 1998). The characterisation of PARP1's involvement in DNA repair quickly led to the realization that inhibitors may potentiate the standard treatment modalities employed in oncology: DNA damaging chemotherapeutics and radiotherapy (Bowman, White, Golding, Griffin, & Curtin, 1998; Calabrese et al., 2004). Drug discovery pipelines eventually produced more clinically viable inhibitors with greater potency, specificity, drug solubility and bioavailability. Indeed, there are currently many clinical trials undertaken with different inhibitors of PARP in a range of cancers, namely olaparib, rucaparib, veliparib, niraparib, talazoparib (De Bono et al., 2017; Jiang, Li, Li, Bai, & Zhang, 2019; Tuli et al., 2019) and their capacity to act as chemo/radio-sensitizers is well documented (Davar, H. Beumer, Hamieh, & Tawbi, 2012).

1.3.2 PARPi is Synthetically Lethal with Defects in Homologous Recombination

An additional observation was that in cells with loss of function mutations associated with breast cancer susceptibility genes BRCA1 or 2, inhibition of PARP was synthetically lethal (Bryant et al., 2005; Farmer et al., 2005). This synthetic lethality has resulted in a paradigm shift and the search for additional promising combinations of genetic mutations and phenotypes coupled with molecular inhibition of key proteins. The mechanism of action underpinning HR deficient cells exquisite sensitivity to PARP inhibition is thought to be multifactorial. BRCA1/2 are involved in fork restart and protection, as are PARP1 and 2 (Bryant et al., 2009; Koppensteiner et al., 2014; S. Ying et al., 2012). PARP1 and 2 are involved in single strand break repair and base excision repair, intermediates which can stall or collapse replication forks if left unrepaired causing DSB formation (Ronson et al., 2018; Shiu et al., 2020). These lesions if left unrepaired without fork collision can form DSB's too. Another DNA lesion source is that PARPi causes PARP1 and 2 to become "trapped" on the DNA (Murai et al., 2012). PARPi with greater trapping ability have greater potency (Murai et al., 2014). Synthetic lethality is observed when PARP1 is depleted however the effect is greater with inhibitors (Bryant et al., 2005; Farmer et al., 2005; Murai et al., 2012) suggesting the trapping effect compounds the synthetic lethality. Consistent with the above, PARPi cause an increase in S-phase associated DNA damage (Rein et al., 2015; Simoneau et al., 2021). Collectively then, HR deficient tumours are sensitive to PARPi's because BRCA1/2 are required to resolve the increase in unrepaired DNA damage and replication associated damage that occurs in the presence of PARPi's. However, this does not necessarily translate to the clinic and the limitations of PARPi's will now be discussed.

1.3.3 Limitations of PARPi

PARP inhibition is providing positive results in the clinic. However, like any advancement made in oncology, there are some complications and limitations.

Firstly, PARP trapping by inhibitors compounds the effects of catalytically inhibiting the PARP enzyme, increasing their effects. However, different PARP inhibitors exert PARP trapping to varying degrees and it results in off target PARP trapping on the DNA of healthy tissue (Hopkins et al., 2019). Secondly, various PARP inhibitors have differential affinities for other PARP's (Carney et al., 2018). This lack of specificity could pose a challenge for therapeutic specificity. Thirdly, clinical approved inhibitors have differential off-target interactions with kinases and the therapeutic implications of this are not well understood (Antolin et al., 2020). Finally, there is the emergence of PARP inhibitor resistance within the clinic (table 1.2). Potentially underlying mechanisms have been identified using pre-clinical models. These mechanisms briefly include increased expression of drug efflux proteins, loss of PARP trapping, and restoration of HR and replication fork stabilisation (table 1.2). Given these limitations, additional drug targets that are effective against BRCA proficient and deficient tumours or indeed, even against PARP inhibitor resistant tumours, are needed. One promising target of interest is poly (ADP-ribose) glycohydrolase (PARG). PARGi also exhibits synthetic lethality in HR deficient tumours and PARPi resistant cells are sensitive to PARGi despite the adopted resistance mechanism. However, a review of the functions of the tankyrases will now be discussed.

Resistance Mechanism	Cause of Resistance	Pre-clinical and Clinical Observations	References
HR Restoration Via:	BRAC1/2 Reversion Mutations	Mutations in patient tumours and PDX models treated with PARPi	(Goodall et al., 2017; Ter Brugge et al., 2016)
	Loss of 53BP1	Low Expression and Mutations in BRCA1 deficient PDX models	(Bouwman et al., 2010; Bunting et al., 2010)
loss of resection inhibitors	Loss of Shieldin factors	Low Expression and Mutations in BRCA1 deficient PDX model	(Dev et al., 2018; Noordermeer et al., 2018)
	Loss of CTC/Pola	*In Vitro* observations that phenocopy 53BP1 loss - increased resection	(Mirman et al., 2018; Miyake et al., 2009; P. Wu et al., 2012)
(C-NHEJ downregulation)	Loss of DYNLL1/ATMIN	In Vitro reports that partially phenocopy 53BP1 loss, low expression correlates with poor progression free survival in platinum based treatment of BRCA1 mutant ovarian cancers	(He et al., 2018)

Stalled Fork Stabalization Via Impeding Nuclease Recruitment	Loss of PTIP, SLFN11 and SMARCAL1 Loss of EZH2	*In Vitro* reports of inducing PARPi resistance in BRCA1/2 deficient cells *In Vitro* reports of inducing PARPi resistance in BRCA2 deficient cells	(Chaudhuri et al., 2016; Murai et al., 2018; Taglialatela et al., 2017) (Rondinelli et al., 2017)
Decreased PARP Trapping	A reduction in trapped PARP  Loss of PARG Reduction in PARP1 Expression	Patient PARP1 mutation In vitro reports Decreases number of lesions	(Pettitt et al., 2018) (Gogola et al., 2018)
Increased Drug Efflux	ABC Transporter Upregulation	PARPi resistant In Vitro and mice models have increased expression	(Jaspers et al., 2015; Rottenberg et al., 2008; Vaidyanathan et al., 2016)

Table 1.2 **PARP inhibitor resistance mechanisms.** Summaries the mechanisms of resistance in PARP inhibitor resistant tumours, their causes, and the extent to which they have been observed clinically along with the relevant references.

1.4 Tankyrases

Tankyrase 1 (TNKS1) and Tankyrase 2 (TNKS2) form a distinct sub-family of the PARP family. TNKS1 and TNKS2 share functional redundancies and are involved in a range of functions including oncogenic signalling (S. M. A. Huang et al., 2009; N. Li et al., 2015; Mariotti et al., 2017a; Troilo et al., 2016; W. Wang et al., 2015), metabolism (N. Li et al., 2019; Hong-yi Yang et al., 2019a), mitosis (P. Chang et al., 2005, 2009; Dynek & Smith, 2004; Ozaki et al., 2012; Yeh et al., 2006), telomere stability (Canudas et al., 2007; Dynek & Smith, 2004; M. K. Kim & Smith, 2014; Xiaohong Tian, Hou, Bai, Fan, Tong, & Bai, 2014; Lu Yang et al., 2017) and the cellular stress response (Mcgurk et al., 2018). Inhibiting the catalytic activity of TNKS1/2 has been shown to impact many of these functions and several TNKS1/2 inhibitors (TNKS1/2i) have been developed and postulated as anti-cancer agents (Verma, 2021). TNKS1/2 have a wide array of interacting partners with roles in various facets of biology (table 1.3). These functions will now be discussed.

Interacting Partner	**Function**	**TNKS1 Disruption**	**TNKS2 Disruption**	**Parylates?**
TRF1	Telomere Elongation	Prevents Disassociation and impedes telomerase recruitment		Y *In vitro*
IRAP	GLUT4 Trafficking	KD of TNKS1 or IRAP attenuated vesicle translocation	Confirmed Binding partner Not characterised	Y *in vitro*
Grb14	Insulin and type 1 insulin like growth factor signalling		Interacts with TNKS2	
TAB182	Ccr4-Not Complex Component – mRNA synthesis and decay	ND	ND	Y *In vitro*
NuMA	Mitotic spindle assembly	Numa recruits TNKS1 TNKS loss results in spindle and microtubule defects	Confirmed to Bind ND	Y *In vitro* *In vivo* Mitosis

Mcl-1S	Anti-apoptotic	Overexpression reduced Mcl-1 expression	ND	N *In vitro* Inhibited PARylation of TNKS1 and TRF1
FBP17	MLL fusion partner, membrane deformation, actin polymerization	ND	*ND*	
EBV EBNA1	EBV viral replication	Upregulates replication		Y *In vitro*
Axin	Wnt signalling	Elevated Axin levels, decreased Wnt signal		Y
FANCD2	DNA Repair			Bound *In vitro* but inhibited TNKS1 autoparylation and TRF1 parylation
RNF146	E3 Ligase, degrades Axin	Prevents degradation of Axin and TNKS1		Y *In vitro*
BLZF1	Golgi Structure maintenance			Y *In vitro*
CASC3	Exon junction Complex	Stabilization		Y
HSV ICPO	HSV Replication	Reduction in viral titers		

3Bp2	Adapter protein in SRC kinase signalling	Loss of TNKS binding results in Cherubism syndrome		Y (TNKS2) *In vitro and In vivo*
Disc1				Y (TNKS2)
Striatin				Y (TNKS2)
Fat 4 C-term				Y (TNKS2)
RAD54				
BCR				Y (TNKS2)
MERIT40				Y (TNKS2)
GMD	Fructose synthesis	Unclear, GMD appears to function as an inactive stable TNKS sequester		N Inhibits activity *In vitro*
CPAP	Procentriole formation	Procentrioles abnormalities, overexpression degraded CPAP levels, cell cycle linked CPAP level regulation		Y *In vitro and In vivo*
Miki	Mitosis			
DmPI31	PI31 is a proteasome inhibitor and it binds to dmTNKS1 – human applications?	PARylation promotes 26S proteasome assembly, inhibition prevented assembly		Y *In vitro and In vivo*

PTEN	Tumour suppressor	PTEN stabilization and downregulation of AKT phosphorylation, suppressing tumour proliferation and growth		Y, PAR mediated degradation
PrxII	Required for TNKS1 to maintain B-catenin signalling, protects TNKS1 ZbM from oxidative inactivation,	Oxidative inactivation of TNKS in a PrxII deficient background - enhances Axin dependant B-catenin degradation in APC mutant colorectal cancer cells		
APC2	Part of the fly B-catenin destruction complex			Y
AMOTs	Negative YAP regulators	Supresses YAP oncogenic activity by AMOT stabilization		Y
ABRO1	Scaffold subunit of BRCC36 deubiquitin enzyme BRISC DUB	Unresolved cohesion in mitosis or loss of cohesion in S phase		Y
CD2AP	Adapter protein, kidney ultrafiltration, negatively regulates TNKS	TNKS inhibition in CD2AP deficient background increases kidney damage		

PEX14	Pexophagy	ND Overexpression decreased number/size of peroxisomes		ND
ATG9A	Autophagy and Pexophagy	ND		ND

Table 1.3 **Tankyrase Interacting Partners (TIPs)**. TIP functions, relationship with TNKS1 or TNKS2 and the consequence of their depletion/inhibition. Table also includes if there has been reported evidence of tankyrase mediated PARylation of the TIP. Information is compiled from the following references: Haikarainen, Krauss, & Lehtio (2014), Kim (2018) and Susan Smith (2015).

1.4.1 TNKS1/2 function and the effects of inhibiting TNKS1/2 in cancer

TNKS1/2 are involved in a range of cellular processes. As such, their inhibition has been observed to impact a range of different areas of biology.

1.4.1.1 The impact of TNKS1/2 inhibitors on global transcription

TNK1/2 has been shown to PARylate the axis inhibition protein (Axin) to stimulate its degradation, leading to β-catenin accumulation and thus transcription of Wnt target genes, as a consequence inhibition of TNK1/2 reduces expression of Wnt target genes (Mariotti et al., 2017a). In addition, proteomic studies of TNKS1 or 2 depleted cells demonstrate TNKS-mediated degradation of Wnt antagonists - NKD1, NKD2, and HectD1 (Bhardwaj et al., 2017).

Although TNKS1 has been reported to sequester the RNA binding protein TAR DNA binding protein 43 (TDP-43*)* in stress granules (Mcgurk et al., 2018), functions for TNKS1/2 in aspects of RNA regulation other than transcription have not been described. However, PARP1 has been reported to be involved in many aspects of RNA regulation including transcription, histone regulation, regulation of chromatin modellers, nuclear export of mRNA, RNA binding proteins, rRNA processing, initiation and elongation in the context of translation and splicing as review extensively by Eleazer & Fondufe-mittendorf, (2021). Thus, there is a clear precedent for PARylation to be involved in RNA regulation and its likely this extends to the TNKS as well.

1.4.1.2 Mitosis

TNKS1/2 have been reported to be involved in different facets of mitosis. These include telomere cohesion, spindle assembly and the centrosome (Canudas et al., 2007; P. Chang et al., 2005, 2009; W. Chang et al., 2005; Dynek & Smith, 2004; G. H. Ha et al., 2012; M. K. Kim et al., 2012; M. K. Kim & Smith, 2014; Ozaki et al., 2012; Yeh et al., 2006). Consequently, breast cancer cells treated with TE92 displayed increased incidence of IR induced aberrant spindles consistent with the loss of the mitotic functions attributed to TNKS1/2 (Gravells et al., 2018). To date all mitotic functions have been attributed to PARylation of mitotic components, promoting protein-protein interactions or via PARylation-directed targeting for protein degradation.

1.4.1.3 Glucose, Exocytosis and Metabolism

TNKS1 is reported to recruit USP25 to deubiquitinate GLUT4 ensuring it is not degraded within the GLUT4 storage vesicles when insulin is absent. Consistent with this, depletion of TNKS1 or TNKS1/2 inhibition, increases glucose uptake via GLUT4 in an insulin dependent manner in adipocytes (Chi & Lodish, 2000; H. Guo et al., 2012; Yeh et al., 2007). In muscle cells, insulin resistance resulted from treatment with the TNKS1/2 inhibitor XAV939, likely as a result of a failure to maintain the stability of GLUT4 (Su et al., 2018). Likewise in ovarian cancer cells XAV939 treatment reduced glucose uptake (Hong-yi Yang et al., 2019a). The impact of TNKS1/2 inhibitors on glucose uptake in breast cancer has not been explored. Interestingly, TNKS has been implicated in disrupting LKB1-AMPK signalling and the resulting metabolic changes increasing tumorigenesis in lung cancer (N. Li et al., 2019).

PARP1 has been implicated in affecting glycolysis and ATP levels independently of NAD+ depletion, in part by hexokinase being an acceptor protein of PARylation, reducing its catalytic activity (Fouquerel et al., 2014). The impact of TNKS1/2 inhibitors on glucose metabolism in cancer has not been extensively researched. Yang et al. (2019) did go onto

examine different aspects of metabolism and they observed a reduction in pyruvate carboxylase via western blot, a reduction in lactate secretion, a reduction in intracellular ATP and increase in cellular O_2 consumption rates in the presence of XAV939. This implicates TNKS1/2 in aerobic glycolysis although it is surprising given that glucose uptake was seemingly increased.

1.4.1.4 Apoptosis

The inhibition of TNKS1/2 and the induction of apoptosis has been observed amongst an array of cancers including bone (Stratford et al., 2013) and neuroblastoma (Xiao-hong Tian et al., 2013). Silencing of TNKS1/2 and telomerase greatly induced apoptosis in lung cancer (H. Lu et al., 2013). Silencing of TNKS1/2 enhanced ovarian cancer apoptosis when co-treated with taxane or cisplastin (Hong-yi Yang et al., 2019a). TNKS1/2 inhibition via XAV939 alone induced apoptosis in breast cancer cells but was greatly enhanced when co-treated with a PLK1 inhibitor (G.-H. Ha et al., 2018). In addition, TNKS1/2 inhibition has been reported to reduce the expression of the anti-apoptotic protein Bcl-2 (Xiao-hong Tian et al., 2013).

1.4.1.5 Migration

TNKS1/2 inhibition has been reported to exhibit an anti-migratory phenotype in lung (C. Li et al., 2018), neuroblastoma (Xiaohong Tian, Hou, Bai, Fan, Tong, & Xu, 2014), gastric (Ma et al., 2021), ovarian (Hong-yi Yang et al., 2019b) and breast cancer (Bao et al., 2012). This could be considered, at least in part, to be due to a reduction in migration persistence because of altered Arpin-TNKS1/2 interactions (Simanov et al., 2021) and altered microtubule dynamics and polarity signals (Lupo et al., 2016).

1.4.1.6 Inflammation, Immunity, and viral infection

TNKS1 deficient mice myeloid cells has been reported to develop severe systemic inflammation and TNKS1/2 function to suppress autoinflammation via reduced TLR2 signalling (Matsumoto et al., 2022). Furthermore, lymphocytic elimination of co-cultured prostate cancer cells was increased in the presence of XAV939 (Stakheev et al., 2019) and TNKS1/2 inhibition renders melanoma more sensitive to PD-1 immune checkpoint therapy in syngeneic mice (Waaler et al., 2020). Interestingly as well, it has been shown that a sub-population of colon cancer patients develop immune responses against TNKS1/2 epitopes (Shebzukhov et al., 2008). There is a small amount of literature that associates TNKS1/2 with viral infection/immunity. Human cytomegalovirus has been reported to stabilise TNKS1/2 and inhibit its PARylating catalytic activity, facilitating viral replication (Roy et al., 2016). Additionally, TNKS1/2 have been shown to PARylate VISA/MAVS, priming it for degradation upon RNA viral infection which supresses the innate antiviral immune response (Xu et al., 2022). This is likely to avoid excess damage but is an interesting consideration in the context of TNKS1/2 inhibitors being an emerging anti-cancer therapeutic.

1.5 PARG – The Primary Mediator of PAR Catabolism

1.5.1 Enzymology and Catalysis

Poly (ADP-ribose) Glycohydrolase is the primary hydrolase involved in the degradation of PAR (figure 1.4) first identified as an enzyme from a nuclear calf thymus extract (Miwa et al., 1974; Miwa & Sugimura, 1971).

PARG possesses both endo-glycohydrolase and exo-glycohydrolase activity, preferentially performing the latter by binding to the two most distal ADP-ribose residues within the PAR chain (Barkauskaite et al., 2013; Brochu et al., 1994). These different modes of catalysis produce free PAR and mono ADP-ribose moieties respectively. The free mono ADP-ribose

is then metabolised into AMP and ribose 5' phosphate by ADP-ribose pyrophosphohydrolases such as the NUDIX family (figure 1.4). AMP is utilised in ATP reformation and different metabolic and cell signalling pathways (Rodríguez-Vargas et al., 2019) while ribose 5' phosphate is a precursor to many biomolecules including DNA, RNA and ATP (Kowalik et al., 2017). Endo-glycohydrolase activity is considered to occur primarily during hyper-PARP activation where the resulting free PAR chain produced are then implicated in apoptosis acting as a death signal (Andrabi et al., 2008).

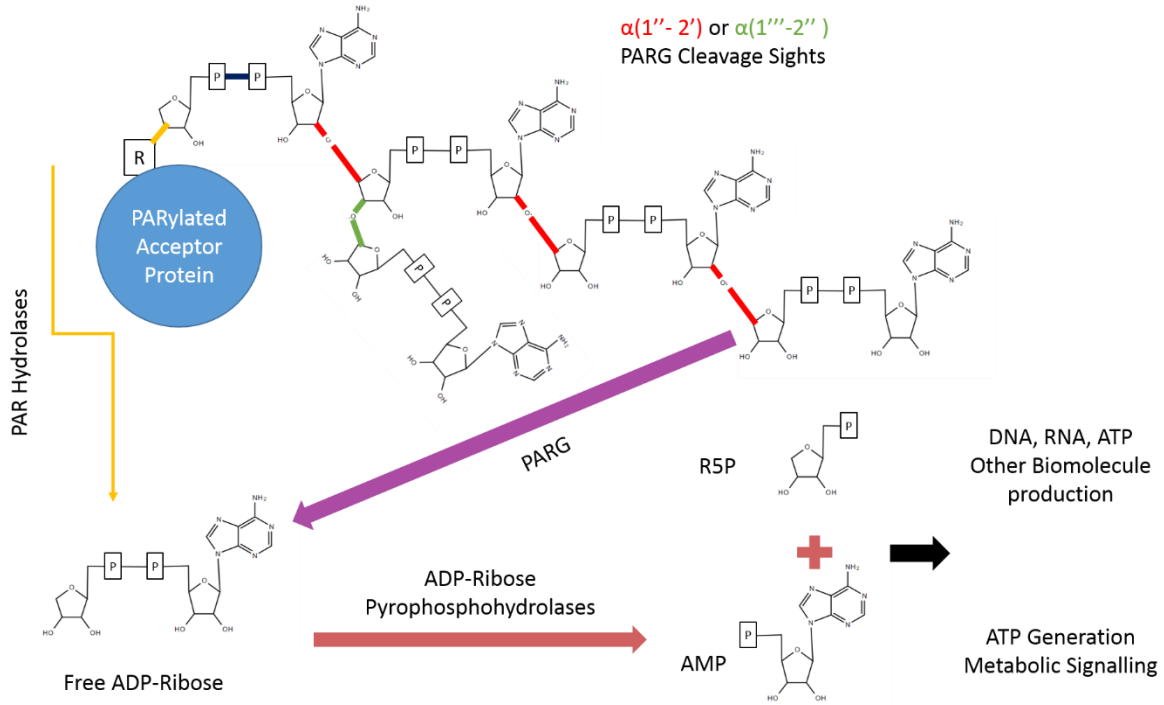

Figure 1.4. **PAR Catabolism.** PARG catalyses PAR at the depicted bonds in red and green. PARG cannot remove the most proximal ADP-ribose (yellow ester bond). R is the acceptor amino acid. Other PAR hydrolyses are responsible for breaking the ester bond. The resulting free ADP-ribose is catalysed by ADP-ribose pyrophosphohydrolases such as the NUDIX family producing ribose-5-phosphate (R5P) and Adenine-mono-phosphate (AMP). They are used in the production of biomolecules and metabolism.

PARG itself specifically catalyses the hydrolysis of α(1''- 2') or α(1'''-2'') glycosidic linkages (figure 1.4). The bonds PARG and the other PAR hydrolases cleave are depicted in figure 1.4. A more comprehensive review on the other hydrolases can be found in O'Sullivan et al., (2019).

1.5.2 The PARG isoforms – Subcellular Localization and Domain Architecture

The human PARG gene is located at a single chromosomal locus 10q11.23-21 (J Ame et al., 1999; Shimokawa et al., 1998). However, the PARG gene transcription product is subject to alternative splicing, producing different PARG isoforms (figure 1.55b) with distinct subcellular localization (figure 1.5a) (Meyer-Ficca et al., 2004).

PARG111 is the largest isoform and contains four domains: an intrinsically disordered regulatory region, a hinge domain, the PARG catalytic domain and a macrodomain (figure 1.5b). It is the primary nuclear PARG and has been reported to translocate to the cytoplasm. PARG 102 and 99 lack part of the N-terminal domain and possess a greater degree of whole cell activity. They have a cytoplasmic and perinuclear distribution and have been observed to translocate to the nucleus (Winstall et al., 1999), particularly during genotoxic insult (Haince et al., 2006). This translocation is summarised in figure 1.5a. The details of how the shuttling of different isoforms fully contributes to PAR metabolism and its significance is yet to be elucidated. Mitochondrial PARG55 and PARG60 lack catalytic activity (R. G. Meyer et al., 2007; M Niere et al., 2012; Whatcott et al., 2009). Functions have yet to be attributed to them. It could be hypothesised they may have a PAR binding/regulatory role that is independent of catalytic activity.

As the catalytic domain is conserved across all active PARG isoforms (figure 1.5b), this presents a challenge to developing an understanding of the roles PARG and its isoforms play within the cell. In addition, research was until relatively recently impeded by a lack of a PARG inhibitor. However, increasingly cell permeable PARG inhibitors are being developed with greater PARG specificity (S.-H. Chen & Yu, 2019; Houl et al., 2019; D. James et al., 2016). To date, all inhibitors inhibit all catalytically active PARG isoforms and the significance of inhibiting some or all of the PARG isoforms has yet to be explored. The functions of PARG and its therapeutic applications in cancer will now be discussed.

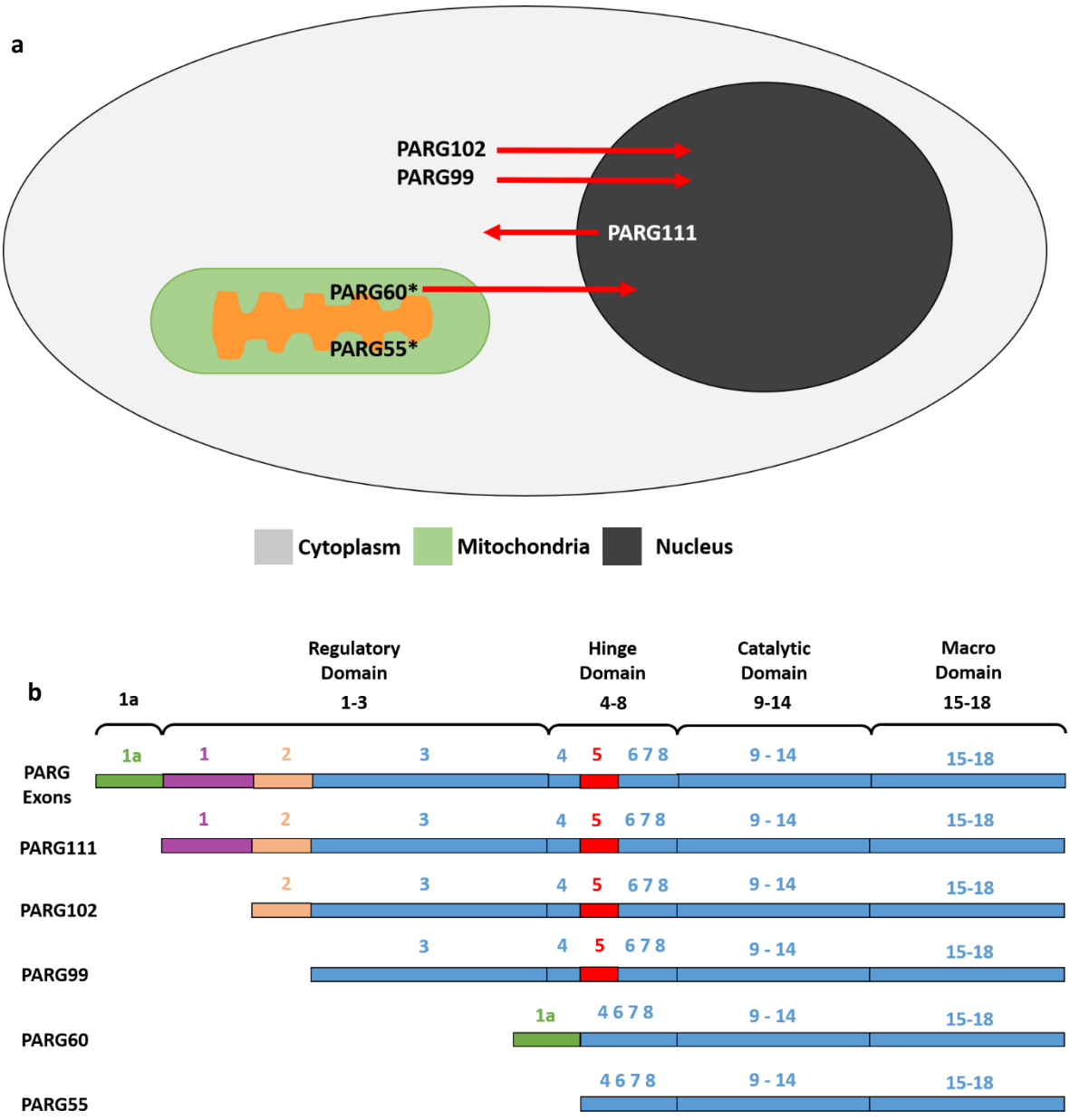

Figure 1.5. **PARG Isoforms and their subcellular locations. 1.**5a. PARG isoform subcellular locations. Red arrows indicate reported translocations during genotoxic insults. 1.5b. PARG isoforms are the product of a single gene and alternative splicing. PARG111 contains all the exons, PARG 102 lacks exon 1, and PARG99 lacks exon 1 and 2. PARG60 has exons 1a, 4 and 6-18. PARG55 is the same but lacks exon 1a. PARG60 and 55 lack exon 5 rendering them catalytically inactive.

1.5.3 PARG Functions

Deletion of the PARG gene results in embryonic lethality in mice making study of PARG by complete genetic depletion difficult (D Koh et al., 2004). Homozygous deletion of PARG in exons 2 and 3 results in a deletion of the PARG110 isoform (equivalent to human 111 isoform) and is tolerated in animals (Cortes et al., 2004). The way the rest of the exons are distributed across isoforms means other genetic manipulations, selectively removing other isoforms, is not possible. Later studies have made use of siRNA or shRNA to reduce the levels of PARG transcripts, overcoming embryonic lethality but restricted by the transient nature of depletion. Early research was also impeded by lack of a selective, potent and cell permeable PARG inhibitor (PARGi). However, the first inhibitor with these qualities was developed in 2016 (James et al., 2016) and since then a number of PARGi have been reported (S.-H. Chen & Yu, 2019; Houl et al., 2019; Jain et al., 2019).

The development of these agents has prompted a surge in publications in the last few years and there is interest in their use as therapeutic agents. Depletion of PARG with siRNA/shRNA or inhibition with a PARGi leads to enhanced sensitivity to DNA damage (table 1.4). There are three possible mechanisms by which PARG loss/depletion/inhibition could lead to sensitisation. Firstly, changes in chromatin structure due to extensive and prolonged PARylation. Histone H1, H2A and H2B are the major recipients of PAR. Due to the negative charge of PAR, PARylation relaxes the histone complex around chromatin, increasing its openness and accessibility. This may leave it more susceptible to DNA damage. In support of this, PARG null trophoblastic stem cells have been reported to keep chromatin decondensed and consequently increased the degree of intercalation by acridine orange and alkylation by MNNG and thymine base modifications into cyclobutane pyridine dimers induced by ultra violet (UV) light (David Koh, 2011; Zhou et al., 2010). A second reason for sensitisation could be to do with NAD+ consumption and depletion following DNA damage as it gets trapped in PAR (discussed later). A third reason for sensitisation could be

impaired DNA damage repair (see below). The findings associated with the manipulation of PARG will now be discussed.

Class of DNA Damage	Method of targeting PARG	Experimental System	Agent	References
Alkylating Agents	PARG 2-3/2-3 mice	*In Vivo*	MNU Streptozotocin	(Cortes et al., 2004)
	PARG -/- Mouse ES Cells	*In Vitro*	MNNG	(D Koh et al., 2004)
	PARGi	*In Vitro and In Vivo*	Temozolomide	(Tentori et al., 2005)
	PARGi GLTN	*In Vitro*	MNNG	(Keil et al., 2006)
	PARG -/- Mouse ES Cells	*In Vitro*	Dimethyl Sulfate	(Fujihara et al., 2009)
	PARG -/- trophoblast cells	*In Vitro*	MNNG Cyclo-phosphamide	(Zhou et al., 2010)
	PARG110 -/- mouse embryonic fibroblasts	*In Vitro*	MMS	(Min et al., 2010)

	PARG -/- ES Cells and SiRNA in human cancer cell lines	*In Vitro*	MMS	(H Shirai et al., 2013)
	PARGi	*In Vitro and In Vivo*	MMS Temozolomide	(Jordan et al., 2014)
	PARGi	*In Vitro*	MMS	(D. James et al., 2016)
	PARGi – COH34	*In Vitro*	Temozolomide	(S.-H. Chen & Yu, 2019)
Cross Linking Agents	PARG -/- Mouse ES	*In Vitro*	Cisplatin	(Fujihara et al., 2009)
	PARG -/- trophoblast cells	*In Vitro*	Cisplatin	(Zhou et al., 2010)
	PARG -/- ES Cells and SiRNA in human MIAPaCa2 (pancreas) and RKO (Colon) cancer cell lines	*In Vitro*	Cisplatin	(H Shirai et al., 2013)
	PARGi – COH34	*In Vitro*	Cisplatin	(S.-H. Chen & Yu, 2019)

DNA Metabolism	PARG -/- mice ES Cells	*In vitro*	Gemcitabine	(Fujihara et al., 2009)
	PARGi PDD00017273	In Vitro	Gemcitabine HU	(Pillay et al., 2019)
	PARGi - PDDX-01 shRNA	*In Vitro*	5-Fluorouracil	(Jain et al., 2019)
DNA-Protein Cross Linker	PARGi -PDDX-01 shRNA	In Vitro and In Vivo	Oxaliplatin	(Jain et al., 2019)
Intercalators	PARG Null TS	*In Vitro*	Epirubicin	(Zhou et al., 2010)
	PARPi resistant cells lines	*In Vitro*	Doxorubicin	(Chen & Yu, 2019)
Incorporated Nucleotide Analogues	PARG -/- mice ES Cells	*In vitro*	Gemcitabine	(Fujihara et al., 2009)
	Range of Ovarian cancer cell lines	*In Vitro*	Gemcitabine	(Pillay et al., 2019)
Oxidative Damage	siRNA in MEFs	*In Vitro*	Hydrogen Peroxide	(Blenn et al., 2006)
	siRNA in A549	*In Vitro*	Hydrogen Peroxide	(Fisher et al., 2007)

	PARG110-/- mice	*In Vitro*	Hydrogen Peroxide	(Min et al., 2010)
Radiation	PARG110-/- Mice	*In Vivo*	γ-Irradiation	(Cortes et al., 2004)
	PARG-/- Mouse ES cells	*In Vitro*	γ-Irradiation	(Fujihara et al., 2009)
	siRNA	*In Vitro*	X-irradiation γ-Irradiation	(J Ame et al., 2009)
	PARG-/- MES cells	*In Vitro*	γ-Irradiation	(Min et al., 2010)
	PARG-/- ES Cells	*In Vitro*	γ-Irradiation Carbon ion irradiation Fe-Ion Irradiaiton	(Hidenori Shirai et al., 2013)
	siRNA, PARGi MCF-7	*In Vitro*	γ-Irradiation	(Gravells et al., 2018)
	PARGi -	*In Vitro*	Irradiation	(Houl et al., 2019)
Topoisomerases inhibitors	PARG-/- ES cells	*In Vitro*	Camptothecin	(Fujihara et al., 2009)

	siRNA	*In Vitro*	Camptothecin	(Ray Chaudhuri et al., 2015)
	PARGi	*In Vitro*	Camptothecin	(Chen & Yu, 2019)

Table 1.4 **Classes of DNA damage PARG manipulations have been reported to sensitise or protect cells against.** References included. Red references indicate no sensitisation. Blue references indicate depletion/inhibition resulted in protection. Black indicates sensitization was observed.

1.5.3.1 The Role of PARG in DNA Repair and Replication

1.5.3.1.1 Single Strand Break Repair

PARG has been implicated in single strand break repair (SSBR) by potentiating the number of SSB (Zhou et al., 2010) and reducing repair kinetics (J Ame et al., 2009; S.-H. Chen & Yu, 2019; Fisher et al., 2007; Min et al., 2010). PARG depletion by siRNA reduced the repair kinetics of hydrogen peroxide induced SSBs (Fisher et al., 2007). Concomitant knockdown with PARP1 did not further reduce the repair kinetics (Fisher et al., 2007). This suggests PARP1 and PARG act in the same pathway to promote single strand break repair. Following induction of a SSB, PARP1 senses the damage, auto-PARylates itself and recruits XRCC1 to the damage site (figure 1.6). XRCC1 then recruits the rest of the SSBR factors finalising the repair of the lesion (figure 1.6). It has been speculated that the removal of PAR is required to promote efficient single strand break repair. In support of this, auto-modified PARP1 has been found to accumulate and persist at sites of single strand breaks for conditions where PARG has been inhibited or depleted (Gogola et al., 2018; Wei et al., 2013). Furthermore, XRRC1 has been found to be retained at sites of single strand break associated PAR for increased periods of time (Chen & Yu, 2019; Fisher et al., 2007; Wei et

al., 2013). Interestingly, mouse cells deficient of exon 2 and 3 for PARG resulted in fewer XRCC1 foci formation in response to MNNG treatment (Gao et al., 2007). This suggests there may be a relationship between the nuclear PARG isoform and XRCC1. The precise consequences of this are not clear. PAR removal has been demonstrated to facilitate XRCC1 translocation directly to the SSB (Wei et al., 2013) and if PARG activity is compromised then it may reduce the efficiency at which this can occur (figure 1.6). This may partially explain the reduced repair kinetics. It is also possible that persistence of PARP1 and XRCC1 at sites limits the availability of these molecules for repair at other sites (figure 1.6). Additionally, it is unknown if these PARGi mediated PARP1 bound complexes influence DNA replication since it is possible, they may form a barrier to replication and thus collapse or stall replication forks (figure 1.6). Support for this comes from PARG deficient -/- embryonic stem cells and PARG depleted pancreatic cancer cells (siRNA) that developed an enhanced S-phase arrest and increased levels of DNA damage visualised by gH2AX foci staining when treated with the alkylating agent MMS (H Shirai et al., 2013). Furthermore, PARG is recruited to PAR via its macrodomain and it is possible that an inhibited PARG protein may also remain bound to PAR. This has not yet been investigated.

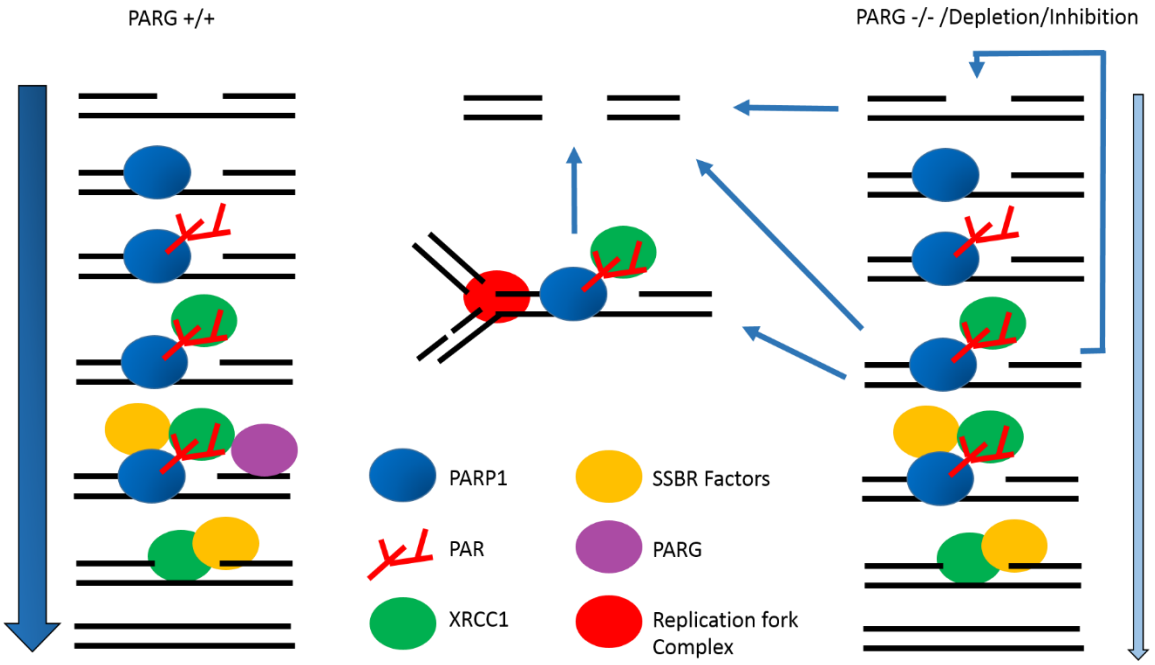

Figure 1.6. **Single strand repair in PARG proficient and deleted/depleted or inhibited cells.** Normally when PARG is functional, SSBR proceeds. An SSB is identified by PARP1, which then PARylates itself, facilitating the recruitment of XRRC1. XRCC1 then facilitates the recruitment of the rest of the SSB repair factors and PARG cleaves the PAR of PARP and they disassociate, enabling SSB to continue and repair the DNA. When PARG is compromised however, repair happens less efficiently. Auto-PARylated PARP and XRCC1 appear to remain at sites of DNA damage for longer. The unrepaired SSB may then collapse into a DSB at replication. Alternatively, a replication fork may collide with trapped PARP-PAR-XRCC1 and cause replication stalling. Finally, bound XRCC1 and PARP1 means there are less repair factors available to initiate repair elsewhere in the genome. Some unattended to SBB may then become DSB's.

1.5.3.1.2 Double Strand Break Repair and DNA replication

The relationship between PARG and DSB repair is poorly understood. PARG inhibition has been reported to reduce the repair kinetics of radiation induced DSBs (Ame et al., 2009; Chen & Yu, 2019). It is therefore likely that reversal of PARP1-3 activity by PARG is important for accurate repair of DSBs at these sites. However, problems with replication can lead to forks collapsing into DSBs, thus separating a role in DNA replication and a role in DSB repair for individual proteins is difficult. Interpretation of experiments is further compounded by the finding that a marker of homologous recombination at DSBs, RAD51,

can also be a signal for fork stabilisation and HR mediated restart of replication forks, while a marker of DSBs 53BP1 is also known to be involved in fork protection.

The first report to suggest PARG is associated with replication saw that PARG110 deficient mouse cells in the presence of the replication stress inducing agent hydroxurea had a greater number of RAD51 foci and took longer to resolve them (Min et al., 2010). Less ambiguous evidence suggesting PARG111 has a direct role in DNA replication was its association with proliferating cell nuclear antigen (PCNA), which is an integral protein involved in DNA replication (Mortusewicz et al., 2011). GFP-tagged PARG111 co-localised with PCNA throughout S-phase and the 102 and 99 PARG isoforms did not (Mortusewicz et al., 2011). Immunoprecipitation then confirmed the N-terminal residues not present in the shorter isoforms mediated an interaction. (Mortusewicz et al., 2011). Kaufmann et al., (2017) later confirmed this N-terminal sequence was indeed important for replication foci association however, the interaction was primarily mediated via the acetylation of a non-canonical PIP box in exon 3 of PARG (Kaufmann et al., 2017). This explains why co-immunoprecipitation between the PARG102/99 isoforms with PCNA was reduced relative to PARG111 yet still present (Mortusewicz et al., 2011). Perhaps the consequences of preventing PARG K409 acetylation or disrupting the protein-protein interaction with PCNA should be explored therapeutically as this maybe a way to specifically target the nuclear PARG111 isoform. It is not clear if interaction with PCNA is because PARG is integral to replication or facilities its function during replication stress.

Illuzzi et al., (2014) observed that PARG depletion via shRNA increased the levels of PAR following chronic but not transient HU-induced replication stress (Illuzzi et al., 2014). They observed an increase in PAR in a sub population of cells with reduced levels of chromatin bound and phosphorylated replication protein A (RPA) (Illuzzi et al., 2014). During perturbed replication RPA accumulates on chromatin and becomes phosphorylated and therefore it was hypothesised that excessive PAR can prevent RPA binding to collapsed but not stalled replication forks. RPA is upstream of RAD51 recruitment and consequently they observed

reduced levels of RAD51 foci in these high PAR cells (Illuzzi et al., 2014). RAD51 is required for HR repair at DSB, fork protection and fork restart. This suggests that high levels of PAR as a result compromised PARG activity may ultimately impede HR resolution of DSB at a collapsed replication fork and/or affect the degree to which replication forks are protected and can be restarted by HR. RPA is also involved in SSBR and these observations may have significance there too.

Further support for a function for PARG during replication/during the replication stress response comes from analysing single replication forks using electron microscopy and DNA fibre assays (Ray Chaudhuri et al., 2015). In this study, PARG depletion slowed forks and increased the number of reversed replication forks (Ray Chaudhuri et al., 2015). There was also an increase S-phase associated yH2AX staining, a strong ataxia-telangiectasia mutated (ATM) and ATR signal and an increase chromatin binding of RAD51 and 53BP1. However, there were no detectable DSBs by pulsed field gel electrophoresis. The recruitment of these repair proteins in a context where there were no detectable DSBs suggests that their recruitment is to facilitate their replication associated functions. This suggests that when PARG is compromised, it creates a reliance on replication fork protecting/restart factors. This may explain why PARPi resistant cells with partially restored HR activity due to 53BP1 mutations are sensitive to PARG inhibitors (Chen & Yu, 2019). Ray Chaudhuri et al., (2015) also reported an increase in post replicative single stranded gaps. This might be attributable to PARP1's recently characterised function in sensing unligated Okazaki fragments (Hanzlikova et al., 2018). PARG depletion may result in these PARylated Okazaki fragments being unresolved leading to post replicative single stranded gaps (figure 1.7). Retention of XRCC1 at SSB sites is dependent on its BRCAII domain (Wei et al., 2013). Ligase III also contains a BRCAII domain and is involved in Okazaki fragment ligation. Perhaps ligase III gets trapped at PARylated Okazaki fragments, analogous to XRCC1 at SSBs. Consistent with PARG depletion, PARG inhibition was also shown to slow forks and increase fork

stalling as shown by the DNA fibre assay, and led to increased gH2AX and RAD51 foci formation on chromatin (Gravells et al., 2017; Houl et al., 2019).

Other functions for PARG during replication/during replication stress can be proposed. RECQ1 is a replication fork associated helicase involved in replication fork restart following fork reversal at sites of stalling. PARP1 PARylates RECQ1 inhibiting its action and preventing premature fork restart and fork collapse at telomeres (Berti et al., 2013; Ray Chaudhuri et al., 2012). This suggests PAR needs to be removed in an organised manner to facilitate RECQ1 activity and thus timely fork restart. Perhaps PARG is required to remove the PAR to promote fork restart (figure 1.7). However, no direct evidence associating PARG and RECQ1 dependant fork restart has been directly reported. It could be due to another PAR degrading enzyme. The RECQ1 and PARP1 relationship is postulated to be present in non-telomere DNA but has not been confirmed. If it is true, lack of PARG during DNA replication could lead to destabilisation of reversed forks and an increased requirement for fork protection factors to prevent collapse. This may partially explain why fork protection factors are recruited to chromatin in a PARG deficient background.

Further evidence of the importance of PARG during replication stress comes from ovarian cancer cells with loss of expression of key replication proteins (e.g. Timeless, Hus1 and RFC2), led to sensitivity to PARGi. (Pillay et al., 2019). The induction of replication stress via hydroxurea/gemcitabine or preventing replication stress/DNA damage signalling pharmacologically using a CHK1 inhibitor also sensitised PARGi tolerant cells to a PARGi. Furthermore, PARGi sensitive cells displayed slowed replication forks and increased collapsed forks. Depletion of RECQ1 could phenocopy the PARGi phenotype in PARGi sensitive cells and therefore this data is consistent with the model above whereby preventing PAR reversal on RECQ1 at stalled forks leads to premature restart. The sensitisation effects were varied. This sensitivity therapeutically demonstrates a relationship between PARG and DNA replication and warrants further characterisation of the roles of PARG in DNA replication and repair. Most interestingly this study also identified a panel of ovarian cancer

cells with differential sensitivity to PARGi and PARPi. Sensitivity to PARGi was identified to be due to an underlying but uncharacterised replication vulnerability.

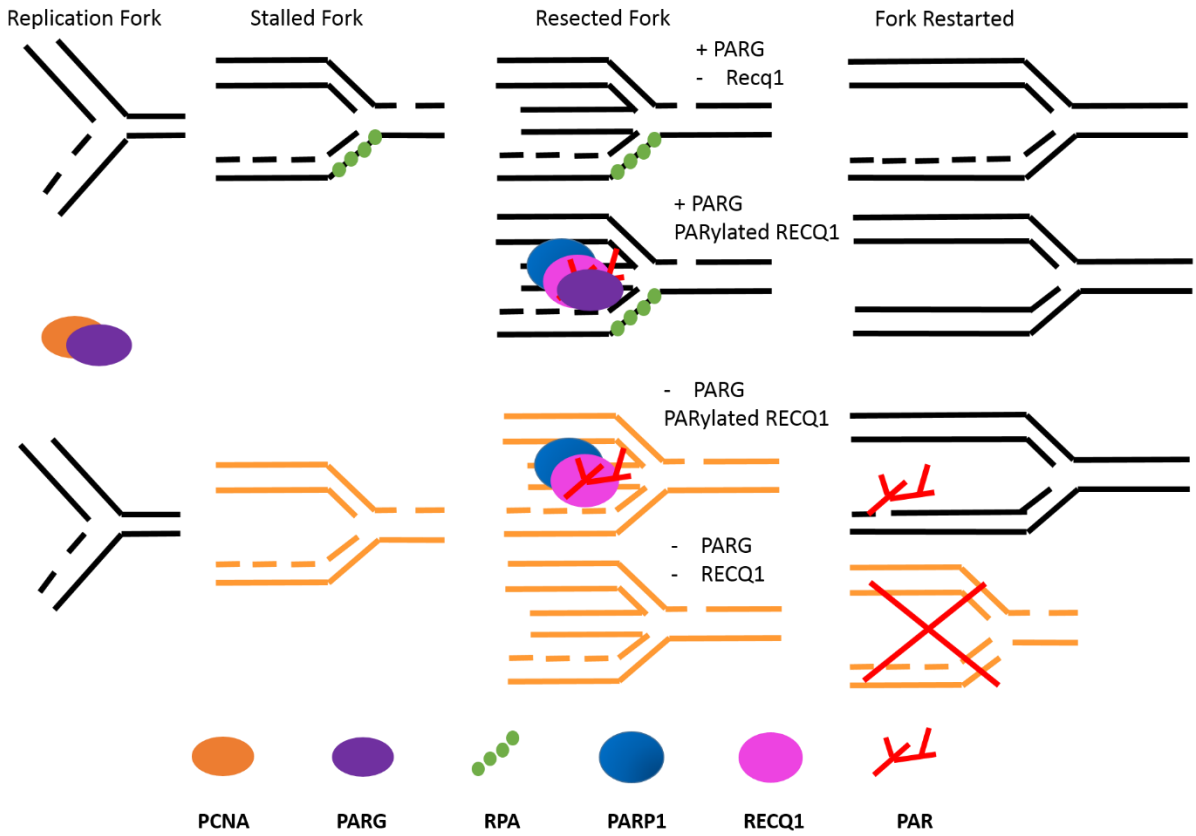

Figure 1.7 **Replication forks and the consequences of PARG Inhibition.** Replication forks proceed along the DNA tract until they come across a DNA lesion which stalls the fork. RPA is present in stabilising the fork at sights of free single strand DNA. The fork is then resected via different mechanisms, A particular mechanism involving PARP1 is the RecQ1 helicase. PARP1 PARylates RecQ1 acting as a clamp. Removal of PAR, perhaps mediated by PARG is thought to regulate the clamp. Fork resection eventually enable the fork to be restarted. PARG inhibition may compromise the fork stability by impeding RPA recruitment or other mechanisms. If RecQ1 remains unattended too the fork may collapse. The replication fork may be restarted however and increases in post replicative single strand breaks have been reported and this may be due to PAR sensing unligated Okazaki fragments being unresolved when PARG is inhibited. The orange forks indicate an increased degree of stalling and resection reported in a PARG background and potentially increased propensity for fork collapse. PARG is recruited to replication forks by PCNA.

In summary it is likely that PARG has multiple roles during replication. Repair of SSBs/BER means that damage is repaired prior to replication and prevents fork collapse but if forks do stall or collapse then PARG may also be involved in regulating the response but the exact mechanism by which it does this is still to be elucidated.

1.5.3.2 Mitosis

PARG depleted cells have evidence of mitotic defects, including fragmentation and amplification of centrosomes, multipolar spindles, chromosomal misalignment and aberrant segregation of chromosomes (J Ame et al., 2009; Min et al., 2010). PARP1 null cells exhibit centrosome dysfunction and amplification (M. Kanai et al., 2003), and PARP1 and 2 localize to centromeres interacting with CenpA, CenpB, and Bub3 (A Saxena et al., 2002). Further, PARG is enriched at spindles in Xenopus extracts (P. Chang et al., 2004). TNK1 and/or PARP3 depletion leads to spindle defects due to alteration in NuMA activity (Christian Boehler et al., 2011). Thus, PARG may co-operate with multiple PARP enzymes to regulate accurate mitosis. Consistent with this, after DNA damage PARGi led to spindle defects and the accumulation of cells at metaphase. Interestingly, TNK inhibition but not PARP1-3 inhibition, phenocopied the spindle defects (Gravells et al., 2018), highlighting the potential differences in mechanism of action of PARPi and PARGi.

1.5.4 The Therapeutic Targeting of PARG

PARG depletion/deletion and inhibition are reported to have chemo and radiosensitisation effects in addition to synthetic lethality in some contexts. These observations may be underpinned by the effects on DNA repair and replication. A review of the currently available PARGi will be performed followed by the evidence for radiosensitisaiton, chemosensitisation and synthetic lethality.

1.5.4.1 PARG inhibitors

A range of PARGi have been developed over the years, with increasing specificity (table 1.5). PDD00017273 and COH34 will used in thesis and their information is summarised in table 1.5.

Inhibitor	PARG IC50	Notes	References
Gallotannin 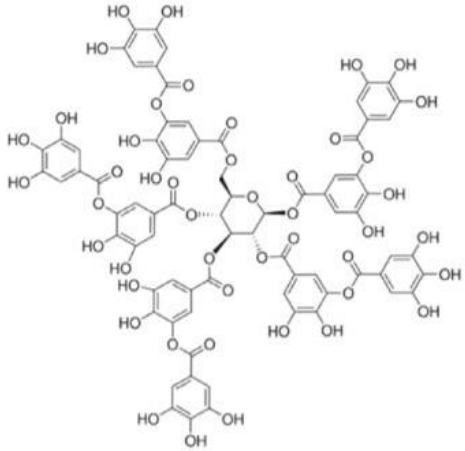	16.8 µM	Low activity, off-target effects	(Tsai et al., 1991)
Rhodanine-based inhibitors (Rhodanine scaffold shown) 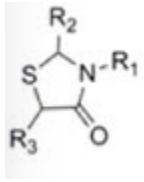	1-6 µM	Specific, not cell-permeable	(Finch et al., 2012)

GPI-16552 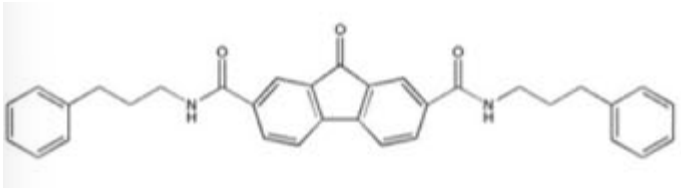	1.7 µM	Low activity, off-target effects	(X.-C. M. Lu et al., 2003)
APD-HPD 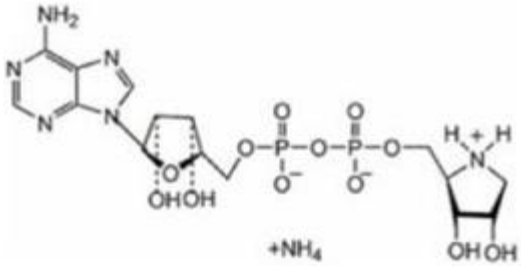	120 nM	Specific, not cell-permeable	(Slama et al., 1995)
PDD00017273 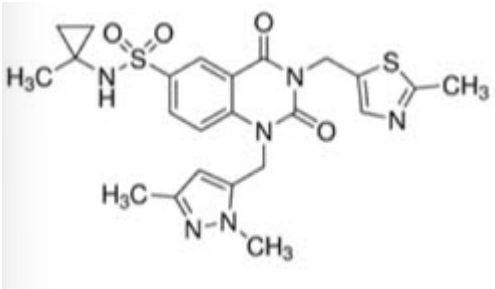	26 nM	Specific, cell-permeable, lacks bioavailability	(James et al., 2016)

COH34 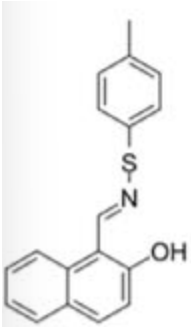	0.37 nM	Specific, potent, cell-permeable, 3.9 h half-life *in vivo*	(Chen & Yu, 2019)
JA2131 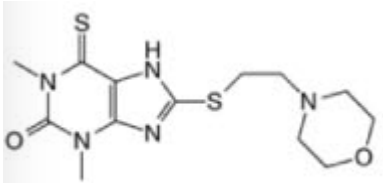	400 nM	Specific, cell-permeable, similarity to caffeine suggests bio-availability	(Houl et al., 2019)

Table 1.5 **Summary of PARG Inhibitors.** IC50, additional information and reference of origin included.

1.5.4.2 Radiosensitisation

In vitro reports in mouse embryonic stem cells and different cancer backgrounds where PARG has been silenced/depleted have consistently produced increased sensitivity to ionising radiation (IR) (J Ame et al., 2009; Min et al., 2010; Nakadate et al., 2013; Hidenori Shirai et al., 2013). This is thought to be underpinned by an increase in mitotic defects that culminate in mitotic catastrophe and cell death (Ame et al., 2009; Nakadate et al., 2013). The details of the in vitro reports are elaborated in table 1.4. These observations have been recently replicated with PARG inhibitors and the mitotic defects following IR are distinct phenotypes associated with PARG but not PARP1-3 inhibition (Gravells et al., 2018). Tankyrase inhibition partially phenocopied PARGi by promoting aberrant spindles and radiosensitisation suggesting PARG may partially mediate its effects by preventing the reversal of tankyrase activity (Gravells et al., 2018). This will need to be explored in further detail. Both PARP and PARG inhibition delayed the resolution of IR induced RAD51 foci consistent with PARG reversal of PARP activity (Gravells et al., 2018). However, PARG inhibition actually increased the speed at which yH2AX foci were resolved compared to wt cells and PARPi where repair was delayed (Gravells et al., 2018). This suggests that the DSBs or replication stress induced by radiation were resolved quicker when PARG was inhibited. A possible explanation for the increased resolution was the increased IR-induced DNA-PK foci reported under PARGi versus PARPi (Gravells et al., 2018). This increased DNA-Pk activity can be indicative of an increase in classical non-homologous end joining and would explain why the yH2AX foci were resolved quicker. Radiosensitisation by a different PARG inhibitor has been reported in a range of cancer cells confirming PARG as a viable therapeutic radiosensitising target (Houl et al., 2019).

1.5.4.3 Chemosensitisation

The reported chemosensitising effects of PARG depletion/deletion/inhibition are variable yet the majority of the reports indicate sensitisation to different classes of DNA damaging agents (table 1.4). A report suggesting protective effects in response to oxidation damage are highlighted as well. Furthermore, there has been a report of PARG deficient cells not being sensitive to gemcitabine and camptothecin (Fujihara et al., 2009). This has not been reported in any other cell system so it is possible it is an observation unique to mouse embryonic stem cells deficient in PARG but it is unclear why.

1.5.4.4 Synthetic Lethality

Synthetic lethality (SL) is the concomitant disruption of two genes that leads to cell death that individually are non-lethal. This disruption can be induced by loss of function mutations, siRNA or drug treatment such as an inhibitor. PARG has been reported to be synthetically lethal with different genes that often undergo loss of function mutations in cancer, enabling targeted cell death. Like PARPi, PARGi has been reported has been reported to be SL with XRCC1 depleted and deficient cells (Martin et al., 2018). This suggests PARGi may have efficacy in XRCC1 tumours and that PARG has unknown functions that need to be further characterised. Furthermore, PARG depletion via siRNA was reported to be SL with dual specificity phosphatase 22 (DUSP22) via suppression of the mTOR/PI3k/AKT and an increase in the expression of p53 upregulated modulator of apoptosis (PUMA), inducing increased apoptosis in lung cancer (Sasaki et al., 2019). This requires validation with an inhibitor but suggests that PARGi in tumours deficient in DUSP22 are viable targets for PARGi and other combinations of genetic targets that induce apoptosis with PARGi are worth investigating. PARG inhibition and depletion have been reported to be synthetically lethal in BRCA2 depleted or deficient breast cancer cells (Fathers et al., 2012). PARG inhibition caused an increase in yH2AX (Fathers et al., 2012). In the absence of DNA

damage, the DNA replication inhibitor aphidicolin reduced the number of yH2AX when the PARGi was present (Fathers et al., 2012). This suggests there was an increase in replication stress, fork collapse and requirement for HR to promote fork restart (Fathers et al., 2012). Accordingly, increased levels of HR were observed. Like PARPi, PARG inhibitors therefore seem to increase the reliance on HR for fork restart. This SL has also be reported with other HR related proteins: BRCA1, BRCA2, PALB2, FAM175A (ABRAXAS) and BARD1 in breast cancer cells where a more specific PARGi was used (Gravells et al., 2017). However, siRNA knockdown of PARG in BRCA1 and phosphatase and tensin homolog (PTEN) deficient/proficient cells with a different genetic background has been reported to not be synthetically lethal (Noll et al., 2016). The contradictory BRCA1 reports may be explained by sequence differences, off target effects or differences in efficiency of knockdown of PARG. The nature of the BRCA1 deficiency may also be significant. However, the BRCA/PARG siRNA result was replicated with two PARG inhibitors (Gravells et al., 2017). PTEN knockdown was not synthetically lethal according to the criteria set in the paper with siRNA PARG depletion (Gravells et al., 2017), this was surprising as PTEN deficiency leads to sensitivity to PARPi.

Interestingly, when looking for sensitivity to PARGi in ovarian cancer cell lines Pillay et al., (2019) identified cell lines that were differentially sensitive to PARG inhibition but not PARP inhibition. They identified that these cells had a replication catastrophe event upon PARGi (identified as pan-nuclear H2AX staining) which was not seen with a PARPi. This suggests that tumours with low expression of key replication factors that promote fork stabilisation may be a biomarker predictive of PARGi effectiveness. However, the siRNA library screen performed in the study did not compare PARGi to PARPi so it is unclear if the yH2AX signal is a phenotype associated with PARGi alone.

1.5.5 The Role of PARG in Cancer

The therapeutic potential of targeting PARylation using PARP or PARG inhibitors alone or in combination with other therapies has promise as an anti-cancer therapy. However genetic manipulation of PARP and PARG also suggest that PAR levels can impact tumour induction and progression too. The mechanisms by which changes in PARP expression can induce tumour formation and progression are well researched. The evidence that PARG expression can alter tumorigenesis is not as thoroughly researched and will be discussed here.

Elevated levels of PARG expression are associated with a poorer prognosis in breast cancer, particularly within HER-2 positive and triple-negative sub types (Marques et al., 2019). Additionally, PARG has been implicated in promoting tumour formation. Heterozygous PARG knockout mice +/- possessed a greater resilience to benzo(a)pyrene inhalation induced lung cancer carcinogenesis due to the lack of benzo(a)pyrene induced stabilization of Wnt ligands in the PARG(+/-) mice (Dai et al., 2019). Furthermore, overexpression of PARG increased the tumorigenic capacity of human mammary epithelial cells when co expressed with HER2 (Marques et al., 2019). Consistent with this, PARG depletion using shRNA resulted in reduced transformation of implanted MDA-MB-231 basal like breast cancer cells when transplanted in mice (Marques et al., 2019). However in contrast to the above, PARG depletion using siRNA increased uveal melanoma tumour formation when PARG depleted cells were injected into mice (Molloy-Simard et al., 2012). In summary, changes in PARG expression can promote or act as a bulwark against tumorigenesis. This is likely reflective of differences in the genetic background between cell lines. These differences and their relationship with PARG expression need to be further characterised.

There is also evidence that PARG has a role in influencing metastasis and angiogenesis. PARG depletion using shRNA reduced the invasion, migration, and adhesion capabilities of human colon carcinoma LoVo cells in vitro (Q. Li et al., 2012). Furthermore, when these cells

were injected into mice, they displayed a reduction in the number of liver metastases. PARG depletion activated the PI3K/Akt pathway which supresses' metastatic signals. An inhibitor of the PI3K/Akt pathway returned the shPARG treated conditions to non-depleted metastatic potency. This demonstrates that the PI3K/Akt pathway likely has a role in supressing metastasis when PARG is depleted. Furthermore, human umbilical vein endothelial cells (HUVEC) when co-cultured with shRNA treated PARG depleted LoVo cells exhibited a reduced migration rate (Pan et al., 2012). This was thought to be underpinned by PARG depletion resulting in reduced NF-kB activity in the LoVo cells that downregulated the release of different signalling factors. This then reduced the migratory capabilities of the HUVEC cells. Additionally, the downregulation of NF-kB also decreased the levels of different angiogenic factors released by the LoVo cells. This suggests PARG depletion may have anti-angiogenic applications as well. Furthermore, mammary epithelial cells overexpressing PARG developed increased metastatic properties in vitro (Marques et al., 2019). PARG depletion via shRNA then reduced these metastatic properties. This observation was replicated in vitro in an aggressive high PARG expressing 67NR-derived tumour cell line called 66cl4. These high expressing cells were then depleted of PARG using shRNA and injected into mice. The PARG depleted group exhibited fewer lung macro metastases and the micro metastasis were consistently reduced in number and size compared to the shControl (Marques et al., 2019).

There is also evidence that PARG has a role in influencing proliferation and differentiation. The aforementioned HUVEC cells also exhibited reduced proliferation that was thought to be mediated by reduced NF-kB activity (Pan et al., 2012). LoVo cells with PARG depleted using shRNA exhibited reduced proliferation via reduced NF-kB expression and increased Akt activity (Pan et al., 2012). Finally, PARG suppression has been linked with the differentiation and proliferation of DC and T cells (J. Wang et al., 2019). The changes in DC and T cells then produces a more favourable CD4/CD8 ratio in mice, improving immune function, reducing metastasis to the liver by colon carcinoma and increasing survival times. This was

thought to be modulated by PARG silencing decreasing PARP1 and NF-kB levels which influenced DC and T cell fate to promote a more favourable CD4/CD8 ratio.

1.5.5.1 Potential Mechanisms of PARG Mediated Tumour Induction and Progression

The effects of PARG on metastasis, angiogenesis, proliferation, and differentiation need to be validated with a PARGi in order to determine the potential of PARGi as an anti-cancer target. Furthermore, the mechanisms underlying them and PARG's tumour forming capabilities need to be investigated. PARylation has been reported to mediate a wide range of effects on transcriptional processes. Research has primarily focused on PARP, however increased or decreased PARylation because of changes in PARG expression/activity is also likely to influence transcription. For example, PARG overexpression increased dePARylation of SMAD2/3, increasing SMAD target gene transcription which was in part responsible for the metastatic phenotype observed because of PARG expression (Marques et al., 2019). Other relationships such as this are likely to exist. The upregulation of PARG has also been linked to transcriptomic changes in prostate cancer (Karpova et al., 2022a).

Genotoxic insults increase PARP1 activity to facilitate DNA repair. Consequently, sustained levels of genotoxic insult increase the levels of PAR and decrease NAD+. PAR operates as an NAD+ sink and is crucial for ATP to be replenished. Therefore prolonged PARP activity eventually results in mitochondrial membrane destabilization and the release of apoptosis inducing factors (AIF) to the nucleus (Stein & Imai, 2012; S.-W. Yu et al., 2006). AIF translocation culminates in AIF-mediated apoptosis and DNA fragmentation (S.-W. Yu, 2002). Unsurprisingly given PARG's role in PAR catabolism, loss of PARG exacerbates this form of AIF mediated, caspase independent apoptosis (Zhou et al., 2011). Increased incidence of AIF mediated-apoptosis has been reported in MNNG or UV treated PARG deficient breast cancer cell lines (Feng et al., 2012). In addition to mitochondrial membrane stability, NAD+ is a vital co-enzyme involved in glycolysis, the tricarboxylic acid cycle,

oxidative phosphorylation and serine biosynthesis, all of which sustain the survival and proliferation of rapidly dividing cancer cells. PARG overexpression may help sustain cancer survival via promoting PAR degradation and promoting NAD+ turnover. PARG inhibition however may also compromise a cancer cells ability to replenish the NAD+ as deletion of PARG decreases NAD+ levels under genotoxic stress (Min et al., 2010). Therefore, changes in NAD+ may alter metabolic signalling that influence tumour formation, transcription, behaviour, and survival.

In addition to changing NAD+ levels tumour progression may be facilitated by PARG mediated changes DNA repair dynamics that could increase genomic instability and drive cancer towards malignancy (see above). However, the long-term effects of changes in PARG expression on genomic instability have yet to be investigated.

Finally, sitruins are a class of NAD-dependant deacetylases. It is therefore conceivable that PARG inhibition results in a preservation of histone acetylation and that this dysregulation may promote the expression of genes relevant to tumour formation or suppression.

1.5.5.2 Breast Cancer, Metastasis, and the applications of PARG Inhibitors

In 2020, breast cancer became the most diagnosed cancer in the world (Sung et al., 2021). Most breast cancer originates in the lobules and ducts of breast tissue. However, the clinical presentation of breast cancer is heterogenous and to improve treatment regimens and survival outcomes, several molecular subtypes have been identified, that correlate with treatment responsiveness, tumour grade, propensity to metastasise and prognosis. Different classification systems have been refined overtime. The intrinsic subtype classification system first inspired by Perou et al., (2000) refocused clinical assessment onto the biology tumours presented with and gave rise to the classical classifications of luminal A, Luminal B, human epidermal growth factor receptor 2 (HER2) enriched and basal-like. This was further

refined by Parker et al., (2009) which incorporates gene expression signatures of 50 genes known as the PAM50 assay. Other gene expression signature assays exist. The surrogate subtype classification system uses histology and immunohistochemistry (IHC) against key protein markers. These markers include oestrogen receptor (ER), progesterone receptor (PR), HER2 and the proliferation marker Ki67. Classification is an important consideration in the clinic, to optimise the cost-benefit analysis of therapies and improve the quality of care delivered to patients. There is up to a 30% discordance rate between IHC approaches and gene-based assays, highlighting the importance of using both approaches in the clinic (Prat et al., 2015). Table 1.6 provides a simplified summary of the molecular subtypes using surrogate subtype classification system and their relative prognosis.

Table 1.6. Breast cancer subtypes

Subtype	Receptor Status	Ki67 Index	Prognosis
Luminal A-like	ER+ PR+ HER2-	Low	Good
Luminal B-like (HER2-)	ER+ PR+ (less relative to luminal A) HER2-	High	Intermediate
Non-luminal HER2 enriched	ER- PR- HER2+	High	Intermediate
Triple negative	ER- PR- HER2-	High	Poor

Luminal A-like tumours have an incidence of 60-70% and are low grade and slow growing. They respond well to endocrinal therapies that exploits their receptor status and the developments in breast cancer treatment has resulted in this subtype having the highest prognosis, however resistance to these therapies is an ongoing problem (Higgins & Stearns, 2009; Yao et al., 2020). This subtype has a relatively lower chance of remission and a relatively has the lowest chance of metastasising, with a median survival of distant metastasis of 2.2 years (Y. Guo et al., 2020; Kennecke et al., 2010).

Luminal B-like (HER2-) tumours have an incidence of 10-20% and have an intermediate prognosis. Their higher Ki67 index and pro-proliferative gene expression signatures render them more proliferative and aggressive (Raj-Kumar et al., 2019). Due to them expressing ER and PR to a reduced degree than luminal A-like, responses to endocrinal therapy are not as effective and chemotherapy is more frequently utilised against this subtype alongside endocrinal based approaches (Abraham et al., 2018). Chances of remission is slightly higher in this subtype versus luminal A as are the rates of metastasis to the liver, brain, lung and particularly bone, with a median survival of distant metastasis of 1.6 years (Kennecke et al., 2010).

HER2 positive tumours account for 10-15% of breast cancer and are more aggressive and prone to metastasis and have an intermediate prognosis. They can be luminal B-like or non-luminal. Luminal B-like (HER2+) have median survival of distant metastasis of 1.3 years (Kennecke et al., 2010). The non-luminal subtype has a distinct gene expression signature that is neither luminal nor basal (associated with triple negative breast cancer but not synonymous) but promotes a high degree of proliferation. Elevated levels of mutagenesis mediated by APOBEC3B are also reported in this subtype that likely drive its tumorigenicity (Kanu et al., 2016). These tumours have a poorer prognosis than their luminal A/B counterparts, however, with the advent of targeted therapies against HER2+ subtypes combined with chemotherapy, the clinical outcomes have improved however this subtype remains challenging (Figueroa-Magalhães et al., 2014). These tumours are associated with relatively higher levels of metastasis to the brain, liver, lung and multiple sites and are prone to higher levels of aggressive relapse. The non-luminal HER2 enriched subtype have a median survival of distant metastasis of 0.7 years (Kennecke et al., 2010).

Triple negative tumours derive their name from being devoid of all the key receptors (ER, PR and HER2). As previously stated, these tumours are sometimes described as basal-like, but this refers to their gene signatures. This subtype of tumour is very heterogenous and can be

divided along six subtypes, basal-like being one of them that is further divided into two, however the utility of this in the clinic is still being determined (Lehmann et al., 2011; D. Y. Wang et al., 2019). Triple negative breast cancer is most prevalent in younger populations <40 years of age (Plasilova et al., 2016) and is also what most commonly presents in patients with BRCA1 germline mutations (80%), with BRCA1/2 germline mutations accounting for 11-16% of all TNBC cases (Newman et al., 2015). This subtype is the most resistant to therapy (due the absence of hormone/HER2 receptors and its heterogeneity and absent effective targeted therapies), is highly prone to complex metastasis and early relapse and has a greater tendency to present in more advance stages, rendering patients with this subtype to have the poorest prognosis (X. Bai et al., 2021; Y. Guo et al., 2020; Hong Yang et al., 2020). Patients with this subtype have a median survival of distant metastasis of 0.5 years (Kennecke et al., 2010).

Metastasis accounts for approximately 90% of cancer related death (Spano et al., 2012). In the context of breast cancer, the median survival for advance stages is 2-3 years. Metastatic breast cancer is observed at presentation in 6-7% of cases and 30% of earlier stage diagnosed breast cancer patients will develop recurrent/metastatic disease. Metastasis is a complex multifaceted cascade. The focus of this thesis relates primarily to the early stages of the cascade and the processes that underlie early tumour dissemination. All cancers must overcome the same initial obstacles before going on to metastasise to secondary sites. Cancer cells undergo changes in their adhesion, de-anchoring them from neighbouring cells and the surrounding extracellular matrix (ECM) (Janiszewska et al., 2020). This enables peri-metastatic cells to migrate more freely, and changes in adhesion also help facilitate cell migration and establish themselves at secondary sites (Janiszewska et al., 2020). However, the ECM acts as a physical barrier. Invasive cancer cells remodel the ECM, which creates space to move into and resources for the cancer to repurpose (P. Lu et al., 2011). These processes require the cell to expend energy and changes in the 3D environment affect the ATP/ADP ratio of a cell (Zanotelli et al., 2018) implying metabolism is an important

consideration as well. PARP/PARG as previously discussed, impacts various areas of biology that could be linked to these processes surrounding earlier tumour dissemination and invasion. Elevated levels of PARG expression are associated with a poorer prognosis in breast cancer, particularly within HER-2 positive and triple-negative sub types (Marques et al., 2019). It's possible that PARG is involved in driving tumour formation, as discussed previously in 1.5.5.1. The depletion and overexpression of PARG has also been shown to reduce the tumorigenicity off implanted mammary human cells in mice, and increase their the metastatic potential as well, respectively (Marques et al., 2019). Migration has been reported to be perturbed in a range of other cancer backgrounds as well when PARG is depleted. It's conceivable the inhibition of PARG could impact these carefully coordinated processes that work in concert to facilitate the early stages of tumour dissemination, migration, adhesion, and invasion via the impact of inhibiting PARG on transcription and metabolism. This warrants investigating the effect of PARP and PARG inhibitors on metastasis using an in vitro approach and using both may elucidate the mechanism.

Another important area of biology related to metastasis is the epithelial to mesenchymal transition (EMT), which is a feature of normal embryological development and cellular differentiation (Z. Huang et al., 2022). It encompasses how non-migratory epithelial cells develop changes in their cell-cell adhesion and gain increased mesenchymal associated migratory and invasive capabilities. EMT is hijacked in cancer cells, further enabling migration and invasion (Z. Huang et al., 2022). In cancer, this program has a high degree of plasticity and is dynamically controlled to suit the contextual needs of cancer cells (Z. Huang et al., 2022). This is achieved in part through the downregulation of pro-epithelial protein markers (such as E-cadherin) and the upregulation of pro-mesenchymal protein markers (such as vimentin, C-MYC, YAP1 and β-catenin). PARG depletion has been reported to reduce the total protein of the pro-mesenchymal markers vimentin and snail (Marques et al., 2019). How is unclear, but it may be due to changes in transcriptional, protein signalling or proteolytic changes. Given then extensive role PARPs/PARG play in all these areas, it's

conceivable inhibition of these proteins could alter these processes and warrants further study.

1.7 Hypotheses and Aims

Subsequently, the first hypothesis of this PhD thesis is that inhibiting PARG and PARP in MDA-MB-231 cells will impact cell adhesion, migration, and invasion. PARP's require NAD+ as a substrate. Consequently, the second hypothesis of this thesis is, if PARGi impede cell migration, it may be a consequence of changes in metabolism. PARP is involved in different facets of transcriptional regulation. The third hypothesis is that PARGi will impact global transcription and some of these genes will be associated with migration/EMT.

The aims of the project are to:

1. Identify effective non-cytotoxic doses of PARP and PARG inhibitors to assess their ability to impact different facets of early-stage metastasis
2. Examine the effects of PARP and PARG inhibitors on adhesion, migration, and invasion
3. Investigate the mechanism of reduced cell migration when cells are treated with a PARGi
4. Investigate the effects of PARGi on global transcription and validate genes of interest at the mRNA and protein level

2.0 Materials and Methods
2.1 Materials

2.1.1 Lab Equipment

Table 2.1. **Lab Equipment.**

Item	**Company**
Balance MH-214	Fisher scientific
Benchtop centrifuge accuspin™ Micro	Fisher Scientific
Biological safety cabinet Class II	Walker
Criterion™ Blotter	BioRad
Colony counter	Stuart Scientific
Confocal DELTAVISION OMX SR IV 125/LF (53-851795-400) 60X Olympus plan APO N lens with a GEOMX BEAZE V4 microscope and 4 SCHOS camera	GE Healthcare UK Ltd
Eppendorf min-spin centrifuge (4ºC)	Eppendorf
Film processor SRX-101A	Konica
Haemocytometer	Neubauer
Heat block (Ori-Block)	Techne
Heraeus MegaFuge 16 Centrifuge	Thermo Scientific
Eppendorf Centrifuge 5415 R	Thermo Scientific
Hoefer™ Mighty Small™ II Mini Vertical Electrophoresis System tank	Amersham Biosciences, Hoefer
Incubator MCO-19AIC (UV)	Sanyo

Eclipse TS100-F Trinocular Inverted Phase Contrast Microscope	Nikon
Multiskan FC plate reader	Thermo Scientific
pH meter	Jenway
Pipettes	Gilson
P300 ErgoOne Multichannel Pipette	Star Lab
Power pack	BioRad
Shaking platform	Stovall Life Science
SpectraMax microplate reader	Molecular devices
Flexstation 3 Plate reader	
Vortexer	Labinco
Water Bath	Grant Instruments

2.1.2 Glassware, Plastics and Disposables

Table 2.2 **Glassware, Plastics and Disposables**	
Item	**Company**
10 cm tissue culture dish	Greiner Bio-one Cellstar
12 well Nunclon delta surface tissue culture plates	Thermo scientific
15ml Falcon tube	Starstedt
25G needles	Becton Dickinson
50ml Falcon Tube	Fisherbrand
5ml, 10ml, 25ml plastic pipettes	Fisherbrand
6 well Nunclon delta surface tissue culture plates	Thermo scientific
96 well tissue culture plates	Costar

Cell scraper	Sarstedt
Cryovials	Starstedt
Culture Inserts	Ibidi
Eppendorf	Sarstedt
Filter tips	Sarstedt
Refill pipette tips	Sarstedt
Sterile syringes	Becton Dickinson
Tissue culture T75 and T25 flasks	Starstedt
22 x 22 mm Coverslips	Epredia
13 mm Coverslips	VWR
Microscope Slides	VWR
12 x 24 well Transwell Inserts (3464)	Costar
Fibronectin Pre-coated 96 well Plates (354409)	Corning
0.2 µm-pore nitrocellulose membrane	BioRad

2.1.3 Reagents and Chemicals

Table 2.3 **Reagents and Chemicals**	
Reagent	**Company**
1X Trypsin-EDTA Solution	Sigma
30% acrylamide: 0.8% bis-acrylamide	National Diagnostics
Amersham ECL Western blotting Detection Reagent	GE Healthcare
Ammonium per sulphate (APS)	Fisher Scientific
Bovine Serum Albumin	Sigma Aldrich

DAPI D9542-5MG	Sigma Aldrich
Dimethyl sulfoxide (DMSO)	Fisher Scientific
Dulbecco's Modification of Eagle's Medium, 1X	Corning
ECL™ Western Blotting Detection Reagents RPN2209	Amersham
ECM gel from Engelbreth Hold swarm murine sarcoma (E1270)	Sigma Aldrich
Ethanol 99.8% HPLC Grade	Fisher Scientific
Fetal Calf Serum	LSP
Glucose solution (200g/L)	Sigma
Glycine	Fisher Scientific
Growth factor free Matrigel (356231)	Corning
Hydrochloric acid	Sigma-Aldrich
Industrial methylated spirit (IMS)	Fisher Scientific
Methanol 99.8% HPLC Grade	Fisher Scientific
Methylene blue	Sigma-Aldrich
Milk powder	Marvel
Non-essential amino acids	Sigma
Phalloidin 488 Conjugate sc-363791	Santa Cruz
Phenylmethanesulfonyl fluoride 1G (PMSF)	Sigma Aldirch
Precision Plus Protein™ Dual Colour Standards	Bio-Rad
Propidium iodide	Sigma Aldrich
Protease inhibitors	Sigma-Aldrich

Protein Assay Dye Reagent Concentrate #5000006	Bio-Rad
RNAse A	Sigma Aldrich
Sodium Chloride	Sigma Aldrich
Sodium dodecyl sulfate (SDS)	Sigma-Aldrich
Sodium hydroxide	Fisher Scientific
Tetramethylethylenediamine (TEMED)	VWR
Tris-HCL	Fisher Scientific
Triton-X100	Sigma Aldrich
Tween-20	Acros Organics
Universal developer	Champion Protochemistry
Universal fixer	Champion Protochemistry

2.1.4 Buffers and Solutions

Table 2.4 **Buffers and Solutions.**

Solution	**Content**
1X RIPA buffer	20 %(v/v) 5X RIPA, 1 mM PMSF, 1X protease inhibitor (Sigma), 1X phosphatase inhibitor (Roche), made up to 1 ml with ddH_2O.
5X RIPA buffer	250mM Tris (pH 8.0), 750mM NaCl, 0.5% SDS, 5.0% NP-40, 2.5% sodium deoxycholate.
PBS	8g NaCl, 0.2g KCl, 1.44g Na2HPO4, and 0.24g KH2PO4 in 800ml of ultra- pure water. pH 7.4, made up to 1L with ddH_2O. Sterilised by autoclaving.
SDS running buffer	25mM Tris base, 190mM glycine, 5g SDS, make up to 1L with ddH_2O.
TBS	20mM Tris base, 140mM NaCl, pH 7.6 (HCl), made up to 1L with ddH_2O. Sterilised by autoclaving.

TBST	0.1%(v/v) tween-20 in 1X TBS. made up to 1L with ddH_2O
Towbin transfer buffer	25mM Tris base, 190mM glycine, 20% (v/v) methanol, made up to 1L with ddH_2O.

2.1.5 Inhibitor compounds

Table 2.5 **Inhibitor compounds.**

Drug	**Origin**	**Solvent**	**Stock Concentration**	**Mechanism of action**
Olaparib	Biovision	DMSO	10 mM	PARP 1-3 Inhibitor
TE-92 Compound 14	(Nathubhai et al., 2017)	DMSO	1 mM	Tankyrases PARP 5a and 5b Inhibitor
PDD00017273	(James et al., 2016) Sigma Aldrich	DMSO	10 nM	PARG Inhibitor
LY294002	Cell Signalling Technology	DMSO	20 mM	PI3K inhibitor
COH34	MedChemExpress	DMSO	20 mM	PARG Inhibitor

2.1.6 Short interfering RNA (siRNA) and transfection Reagents

Two Individual PARG (NM_003631) ON-TARGETplus siRNA oligonucleotides were purchased from Dharmacon. ON-TARGETplus Non-targeting siRNA #1 (D-001810-01-20) was used as a negative control and was ordered from Horizon Discovery. Dharmafect 1 (T-2001-03) was ordered from Horizon Discovery.

2.1.7 PCR Assays

Table 2.6 **20X Applied Biosystems Taqman probes used to validate migration associated differentially expressed genes reported by microarray (PDD) gene list.**

Gene	Assay ID
CDK2AP2	Hs00366670_g1
CORO1A	Hs00200039_m1
MDM1	Hs01098445_m1
PRKN	Hs01038318_m1
PTK2B	Hs00169444_m1
RAPGEF3	Hs01030417_m1
RHOBTB2	Hs01598083_m1
TMSB15A	Hs00751699_s1
CC2D1B	Hs01054180_g1
E2F1	Hs00153451_m1
CDT1	Hs00368864_m1
TERT	Hs00972650_m1
ADK	Hs00417073_m1
NADSYN	Hs00216808_m1
CCL2	Hs00234140_m1
CCL24	Hs00171082_m1
GAPDH	Hs02786624_g1

2.1.8 Primary Antibodies

Table 2.7 **Primary Antibodies.**

Primary Antibody	Species	Clonality	Origin	Working Dilution (WB)/(IF)	Incubation Time
Beta-Tubulin	Mouse	Mono-clonal	Sigma Aldrich T8328	1:5000 WB	Overnight, 4ºC
E-cadherin	Rabbit	Mono-clonal	Cell signalling 24E10	1:2000 WB	Overnight, 4ºC
PAR	Mouse	Mono-clonal	Enzolifesciences ALX-804-220-R100	1:500 WB	Overnight, 4ºC
PARG	Mouse	Mono-clonal	Santa Cruz SC-398563	1:500 WB	Overnight, 4ºC
PARP1	Mouse	Mono-clonal	Santa Cruz (F-2) SC-8007	1:1000 WB	Overnight, 4ºC
Tankyrase-1/2 (E-10)	Mouse	Mono-clonal	Santa Cruz SC-365897	1:1000 WB	Overnight, 4ºC
GAPDH	Mouse	Mono-clonal	Protein Tech 60004-1-1g	1:20,000 WB	Overnight, 4ºC
YAP	Mouse	Mono-clonal	Santa Cruz Sc-376830	1:100 WB 1:1000 IF	Overnight, 4ºC
Vimentin	Mouse	Mono-clonal	Santa Cruz Sc-373717	1:10,000 WB	Overnight, 4ºC

β-Catenin	Mouse	Mono-clonal	Santa Cruz Sc-7963	1:500 WB	Overnight, 4ºC
C-MYC	Mouse	Mono-clonal	Santa Cruz Sc-40(9E10)	1:1000 WB	Overnight, 4ºC
P-AKT (p S473)	Rabbit	Mono-clonal	Abcam Ab81283	1:1000 WB	Overnight, 4ºC
T-AKT	Mouse	Mono-clonal	BD Transductions 610860	1:2000 WB	Overnight, 4ºC
Alpha-Tubulin	Mouse	Mono-clonal	A86726	1:1000 IF	Overnight, 4ºC
E2F1	Mouse	Mono-Clonal	Santa Cruz KH-95 Sc-251	1:1000 WB	Overnight, 4ºC
Lamin A	Rabbit	Mono-clonal	Abcam Ab26300	1:1000 WB/IF	Overnight, 4ºC
Lamin B1	Rabbit	Poly-clonal	Thermo Fisher 12987-1-AP	1:1000 WB	Overnight, 4ºC

2.1.9 Secondary antibodies

Table 2.8 **Secondary Antibodies.**

Secondary Antibody	**Alexa Fluor™ Conjugate**	**Species**	**Clonality**	**Origin**	**Working Dilution (WB/IF)**	**Incubation Time**
Anti-mouse	HRP	Horse	Poly-clonal	Cell Signalling 7076S	1:1000 WB	1 hr, RT
Anti-Rabbit	HRP	Goat	Poly-Clonal	Cell signalling 7074S	1:2000 WB	1 hr, RT
Anti-rabbit	488	Goat	Mono-clonal	Cell Signalling 4412S	1:200 FACS	1 hr, RT
Anti-mouse	594	Goat	Poly-clonal	Thermo-fisher A11005	1:1000 IF	1 hr, RT
Anti-rabbit	594	Goat	Poly-clonal	Thermo-fisher A11037	1:1000 IF	1 hr, RT

2.1.10 Cell Lines

Table 2.9 **Cell Lines.**

Cell Line	Cell Line Origin	Reference	Media
MCF-7	Human Breast Adenocarcinoma	ATCC	DMEM, 10% FCS
MDA-MB-231	Human Breast Adenocarcinoma	ATCC	DMEM, 10% FCS
A19	Mouse Embryonic Fibroblast	Zhao-Qi Wang (Lyon, France)	DMEM, 10% FCS
A11	Mouse Embryonic Fibroblast	Zhao-Qi Wang (Lyon, France)	DMEM, 10% FCS

2.2 Methods

2.2.1 Mammalian Cell culture

2.2.1.1 Passaging

Cell lines were cultured in a humidified incubator at 37°C and 5% CO_2. Cell passaging was routinely performed in standard T25 and T75 tissue-culture flasks. Cells were washed in PBS and incubated at 37°C with 1 ml 1X trypsin-EDTA to detach cells from flask base. Respective growth media (9ml) was then added to neutralise trypsin activity. This cell suspension was then transferred and diluted as appropriate for seeding in a new flask. MCF7 and MDA-MB-231 cells were used for no more than 30 passages, with the earliest passages of the cell lines kept in storage being 30 and 50, respectively. A11 and A19 cell lines were in storage at passage 10 or less and used for no more than 20 passages.

2.2.1.2 Freezing

Following trypsin-EDTA exposure, cells were suspended in fresh media, counted using a haemocytometer and centrifuged in 15 ml falcon tubes at 1200 rpm for 3 minutes using a Heraeus MegaFuge 16 Centrifuge. Media supernatant was discarded. Cells were then re-suspended in a freezing medium (90% media, 10% DMSO) at a density of $1x10^6$ cells per ml. This cell suspension was then aliquoted into 1 ml cryovials and stored at -80°C. As earlier passages as possible for each cell line were frozen and kept in storage and expanded to ensure enough was in reserve.

2.2.1.3 Thawing

Cells cryopreserved at -80°C were resuscitated by rapid thawing in a 37°C water bath. The thawed cell suspension was then gently diluted in 9 ml warm culture media and centrifuged at 1200 rpm for 3 minutes in a Heraeus MegaFuge 16 Centrifuge. The media supernatant was discarded. The pellet was re-suspended in 10 ml media and transferred to a T25 flask.

2.2.2 Western Blotting

2.2.2.1 Cell lysis and Protein Extraction

Cells were seeded at 1-2 million cells and treated after 4 hours. Samples were left for 18 hours overnight in the incubator. Media was then removed, and cells were washed in ice-cold PBS on ice. Cells were scraped directly into 70 µl of 1X RIPA buffer on ice, transferred to an eppendorf and vortexed every 10 minutes during a 30-minute incubation period on ice. DNA shredding was achieved by cell solution being passed through a 25G needle five times. The shredded solution was centrifuged at 13400 rpm for 10 minutes at 4°C using the eppondorf mini-spin centrifuge. The cell lysate containing supernatant was removed and stored at -20°C prior to quantification.

2.2.2.2 Protein Quantification assay

The Bradford assay was used to quantify the total cell lysate protein concentration prior to SDS-PAGE. Bovine serum albumin protein standards at 0, 1, 5, 10, 15, 20 µg/µl were made at a final volume of 800 µl. Two microliters of each cell lysate sample was added to 800 µl of ddH_2O. Each 800 µl protein standard and lysate samples then had 200 µl of Bio-Rad protein assay dye reagent added to them. Each standard and sample was briefly vortexed. A Thermo Scientific Multiskan FC was used to measure the absorbance at 595 nm (A_{595}). A standard curve was produced from the A_{595} values of the protein standards which allowed for the lysate sample proteins concentrations to be estimated. Lysates could then be diluted as appropriate to achieve equal loading in the SDS-PAGE.

2.2.2.3 SDS-PAGE

Polyacrylamide gels were produced using the reagents depicted in table 2.10 with volumes included. 10-20 µg total protein was loaded per lane. 5 µl of Precision plus Protein Standards (BioRad) was run in parallel to the samples. Protein separation by molecular weight was achieved by running the SDS-PAGE at 150V – 180V in 1X SDS-PAGE running buffer for 1 hour – 1 hour 30 minutes.

2.2.2.4 Western Blot

SDS-PAGE gels were transferred onto a 0.2 µm-pore nitrocellulose membrane (BioRad) via a BioRad Criterion Blotter for 2 hours at 100V in 1X towbin transfer buffer on ice. All membrane antibody incubations, blocking and wash steps were performed on a rocker. Membranes were blocked in TBS-T (0.1% v/v tween in 1X TBS) with 5% Marvel milk (w/v) (blocking solution) at room temperature for 1 hour. Primary antibodies were diluted in the blocking solution at dilutions shown in table 2.7. Membranes were then incubated with the diluted primary antibodies at 4°C overnight.

Table 2.10 **Reagents and their associated volumes to make each component of an SDS-PAGE gel.**

Resolving Gel (10 ml)				5% Stacking Gel (5 ml)	
(ml)	8%	10%	12%		
ddH_2O	4.6	4.0	3.3	ddH_2O	3.4
30% Acrylamide 0.8% bis Acrylamide	2.7	3.3	4.0	30% Acrylamide 0.8% bis Acrylamide	0.83
1.5 M Tris pH 8.8	2.5	2.5	2.5	1 M Tris pH 6.8	0.63
10% SDS	0.1	0.1	0.1	10% SDS	0.05
10% APS	0.1	0.1	0.1	10% APS	0.05
TEMED	0.006	0.004	0.004	TEMED	0.005

The membrane was subject to three 10-minute TBS-T washes before being incubated with the appropriate secondary antibody diluted in the blocking solution at the depicted values in table 2.8 for 1 hour. Three 10-minute TBS-T wash steps then followed.

Amersham enhanced chemiluminescence western blotting detection reagent kit contains reagent 1 and 2. They were mixed in a 1:1 ratio in a 15 ml falcon tube at a final volume of 4 ml and applied to the membrane at room temperature for 1 minute. Membrane exposure to X-ray film was performed in a dark room. The chemiluminescent signal was developed and fixed using RG Universal X-ray Developer and Fixer, respectively.

2.2.3 Clonogenic survival assays

Each cell line was seeded at 1000-2000 cells per well in a 6 well nunclon plate. After a 4-hour adhering time period, cells were treated as appropriate. Cells were left in the incubator to form colonies for 10-14 days. Once colonies had formed, the media was removed and colonies were stained with 4 g/L methylene blue in methanol. Colonies were defined using a threshold of 50 viable cells and counted. Plating efficiency was calculated by dividing the number of colonies by the number of cells seeded. The survival fraction was then calculated by dividing the plating efficiency by the untreated conditions plating efficiency. A minimum of three biological repeats was performed and the number of repeats performed is indicated in the respective figures.

2.2.4 Trypan Blue Exclusion Assay – Proliferation Assay

Each cell line was seeded at 50,000 cells per well in 6-well dishes with a final volume of 2 ml. Four hours later they were drugged accordingly with drugs at indicated doses or DMSO in the negative control. Every 24 hours cells were washed, and new media containing drugs/control added. At the 48-, 96- and 144-hour time point cells were trypsinised and re-suspended in media. Cells were pipetted to ensure they were homogenous then mixed in a

1:1 with 20 µl of trypan blue and counted using a haemocytometer. Raw cell counts were then plotted over time. A minimum of two biological repeats were performed and the number of repeats performed is indicated in the respective figures.

2.2.5 Fluorescence-activated Cell Sorting – Cell Cycle Analysis

2.2.5.1 Cell Harvesting

1 x 10^6 cells were seed per 10 cm dish and after 4 hours treated as appropriate. Cells were harvested for FACS analysis 24 hours post drugging by two PBS washes and 1 ml of trypsin. Cells that washed off were pooled with samples into 50 ml Falcon tubes containing 10 ml ice cold PBS. Cells were pelleted at 1200 RPM using a Heraeus MegaFuge 16 Centrifuge for three minutes and washed twice before being transferred to a 15 ml falcon tube and fixed in 100% ice cold methanol. Sample was then vortexed and left in the freezer (-20ºC) for 24 hours prior to staining.

2.2.5.2 Propidium iodide (PI) and S10 p-Histone 3 Co-staining

Fixed samples were removed from the -20ºC and pelleted at 1200 RPM using a Heraeus MegaFuge 16 Centrifuge for three minutes. The methanol was removed, and the pellet was resuspended in 5 ml of ice-cold PBS twice with the same centrifugation conditions. The PBS was removed, and samples were resuspended and incubated in PBS with 100 µl 0.5% BSA and 0.25% Triton-X100 for 15 minutes on ice. Secondary antibody only controls were obtained by the removal of 30 µl of DMSO condition and it being pipetted into a separate 15 ml falcon tube. Cells were pelleted at 1200 RPM using a Heraeus MegaFuge 16 Centrifuge and the supernatant removed. The pellet was resuspended in 100 µl 0.5% BSA and 0.25% Triton-X100 containing a 1:500 dilution of S10 p-Histone 3 (ab5176 Abcam) primary antibody for 1 hour at room temperature. The secondary antibody only control was suspended in 100 µl 0.5% BSA and 0.25% Triton-X100. Cells were then washed twice with 200 µl of PBS with

0.25% Triton-X100 via two centrifugal rounds at 1200 RPM for 3 minutes and supernatant removal. Cells were then suspended in 100 µl of PBS with 1% BSA containing 1:200 dilution of Anti-rabbit Alexa flour 488 (4412S Cell Signalling). Cells were incubated for 30 minutes in the dark at room temperature. Cells were then centrifuged at 1200 RPM for 3 minutes and the supernatant removed twice. Cells were then resuspended in 200 µl of PI/RNAse A solution (18 µg/ml PI and 8 µl RNAse A) in the dark at 4ºC for 1.5 hours prior to being analysed on the LSRII.

2.2.5.3 Analysis

Analysis was performed using FlowJo. Single cells were isolated by plotting the PI signal (Blue 660_20) area vs the width (figure 2.1A). The circled population are single cells and this population was isolated to exclude cell doublets and other debris (figure 2.1A). Histogram vs PI Area was then plotted, using a minimum of 10,000 cells (figure 2.1B). This produced two peaks connected by a less prominent bridge (figure 2.1B). The area prior to the first peak was defined as sub G1(figure 2.1B). The first peak was defined as G1 (figure 2.1B). The bridge connecting the two peaks was defined as s-phase (figure 2.1B). The second peak was defined as G2/M (figure 2.1B). The mitotic population was isolated from the rest of the G2 fraction by plotting Blue 530_30 height vs the PI area (figure 2.1C). This produced two discrete populations with and without p-H3 staining (figure 2.1C). Discrete populations that weren't present on the no primary antibody control group that were higher up along the Blue 530_20 -H axis was classified as mitotic cells. Once cell cycle stages were defined, they were applied to all conditions within a biological repeat. The number of cells within each stage, based on the total number of single cells, allowed for the percentages to be quantified. A minimum of three biological repeats was performed.

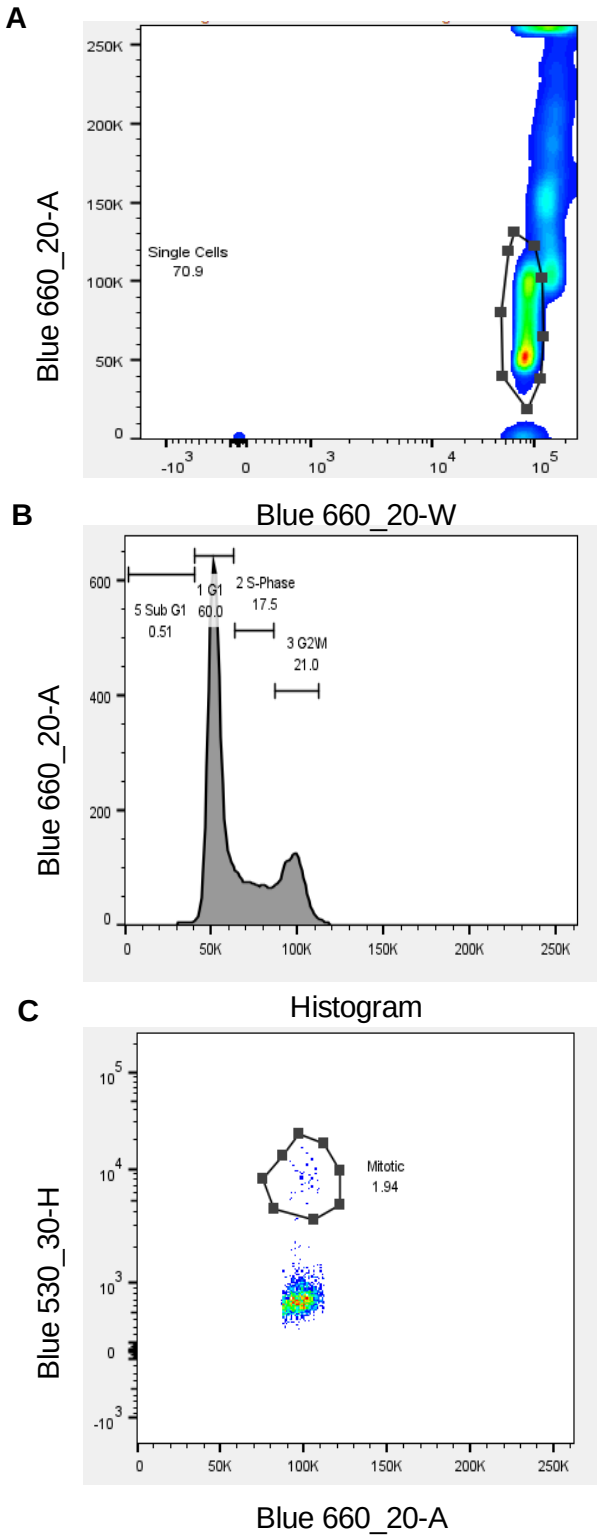

Figure 2.1. **FACS Gating Strategy using Flowjo.** (A) Single cell isolation by plotting Blue 660-22-A vs Blue 660-22-W. (B) Identifying the number of cells with each cell cycle stage based on propidium iodide content by blotting Blue 660-22-A as a histogram and labelling the appropriate cell cycle stages. (C) Identifying which cells within the G2/M fraction are mitotic based on pH3 labelling, which is indicated by the signal strength along the Blue 530-20-H axis. A no pH3 primary antibody control was also used. Once all cell cycle groupings were defined, they were applied to all conditions within a biological repeat and the percentage of cells within each stage of the cell cycle as a percentage of the total number of single cells, were calculated.

2.2.6 Static Adhesion Assay

2.2.6.1 Fibronectin Static Adhesion Assay

Fibronectin pre-coated plates were purchased and stored at 4ºC. On the day of the experiment, plates were placed at 37 degrees for 30 minutes prior to use. To prevent evaporation, 100 µl of PBS was pipetted into the surplus wells. Subsequently, 100 µl of media containing media, 0.2% DMSO or drugs of interest at 2x the intended final concentration were added into the wells. Then 100 µl of a range of cell concentrations indicated in the appropriate figure was added to the wells. Each drug and cell concentration had 3 technical repeats. The plate was left in the incubator at 37 degrees for two hours to allow for the cells to adhere. Subsequently, the media was removed and 3 x 100 µl PBS washes were performed using a multichannel pipette. The cells were then fixed with 100 µl of 4% paraformaldehyde in PBS for 15 minutes. The cells were then washed with 100 µl PBS. The cells were then stained with 0.1% crystal violet in 20% methanol for 15 minutes using 100 µl per well. The cells were then washed with 200 µl of deionised water. The remaining crystal violet was solubilised in 100 µl of 1% SDS. The absorbance at 540 nM was then recorded using the FC multiscan plate reader. A minimum of three biological repeats was performed and the number of repeats performed is indicated in the respective figures.

2.2.6.2 Matrigel Static Adhesion Assay

Ninety-six well plates were coated with ECM gel (E1270) diluted 1 in 50 in cell media. 35 µl was then applied to each well and left to set in the incubator for 30 minutes. To prevent evaporation, 100 µl of PBS was pipetted into the surplus wells. Subsequently, 100 µl of media containing media, 0.2% DMSO or drugs of interests at 2x the intended final concentration were added into the wells. Then 100 µl of a range of cell concentrations as indicated was added to the wells. Each drug and cell concentration had 3 technical repeats. The plate was left in the incubator for two hours to allow for the cells to adhere.

Subsequently, the media was removed and 3 x 100 µl PBS washes were performed using a multichannel pipette. The cells were then fixed with 100 µl of 4% paraformaldehyde in PBS for 15 minutes. The cells were then washed with 100 µl PBS. The cells were then stained with 0.1% crystal violet in 20% methanol for 15 minutes using 100 µl per well. The cells were then washed with 200 µl of deionised water. The remaining crystal violet was solubilised in 100 µl of 1% SDS. The absorbance at 540 nM was then recorded using the FC multiscan plate reader. A minimum of three biological repeats was performed and the number of repeats performed is indicated in the respective figures.

2.2.7 Invasion Assay

Transwell inserts were coated with 150 µl of serum free media with Matrigel diluted in a 1:31 ratio (0.213 ug/ml). This equated to approximately 30 µg of Matrigel per transwell. These were left to set overnight at room temperature. 1.5 $x10^6$ MDA-MB-231 cells were seeded into two 10 cm dishes and left overnight in the incubator. Twenty-four hours later, each plate either received 10 µl of DMSO or 0.3 mM PDD for two hours. Plates were then washed in PBS twice and trypsinised and resuspended in serum free DMEM. Two rounds of centrifugation at 1200 RPM (Heraeus MegaFuge 16 Centrifuge) for 3 minutes and pellet resuspension in 2 ml serum free media was then performed. The bottom chamber had 600 µl of complete media carefully pipetted into it. Cells were then counted and volume equating to 250,000 cells was pipetted into the top chamber of a coated or untreated transwell. The DMSO or drug treated cells were introduced to the transwell upper chambers. Each test condition was performed in duplicate. The transwells were then placed in the incubator for 16 hours after which the media from the upper chamber was carefully removed. One transwell from each pair was then swabbed with a cotton bud 10 times clockwise. All transwells then had 0.1 ml of 20% methanol with 0.1% crystal violet added to the top chamber and 0.6 ml of added to the bottom chamber. Each transwell was then dipped gently

into water and the excess poured off three times. The transwell were left to dry overnight at room temperature. The membrane was then removed with tweezers and solubilised in 400 ul 0.1 M sodium citrate and 50% ethanol in a 96 well plate. The plate was left on the rocker for 5 minutes. The absorbance was then recorded the FC multiscan at 595 nm. The following formula was then used to calculate the percentage of cells that invaded: (swabbed absorbance reading/unswabbed absorbance reading) x 100. These relative differences between conditions were then assessed for. A minimum of three biological repeats was performed and the number of repeats performed is indicated in the respective figures.

2.2.8 Culture Well Inserts – Bi-Directional Cell Migration Assay

MDA-MB-231 cells were detached using trypsin-EDTA and counted using a haemocytometer. Culture wells placed in the bottom of wells of a nunclon 6 well plate. A cell solution with 300,000 cells per ml was produced and 70 µl was extracted from this solution and pipetted into both sides of the culture well. Therefore, approximately 21,000 cells were within in each side of the culture well. Two millilitres of media were then carefully added to the surrounding well to prevent the culture well drying out. Plates were left to incubate overnight. Subsequently, each culture well was carefully removed, and the cells were washed twice gently with PBS and 2 ml 0.5% FCS media was added carefully to each well. Cells were then treated with the appropriate inhibitors or vehicle control. Live bright field images were then taken using the Nikon TE200 inverted fluorescent microscope using NIS-elements 5 BR 20.01 software at 10X magnification. This acted as the 0-hour time point and plates were returned to the incubator and then imaged as needed over time. The area between each population of cells was calculated using the polygon tool to eliminate gaps in the cell walls. Threshold was then applied, and the magic wand tool selected the area between the two population of cells and the and measure tool recorded the area in imageJ. A minimum of three biological repeats was performed and the number of repeats performed is indicated in the respective figures.

2.2.9 Live Cell - Single Cell Random Non-Directional Migration Assay

All live experiments were performed in 24 well plates with 20,000 cells seeded into each well at a final volume of 2 ml. Drugging occurred 4 hours after initial cell seeding and imaging 14 hours after drugging. Experiments that utilised β-nicomononucleotide were pretreated with 6.6 µl of 150 mM stock equating to 500 µM an hour prior to drugging and four hours after cell seeding. Transfected cells were seeded at 20,000 cells and left 4 hours prior to drugging (see transfection section). Experiments that utilised COH34 were treated with β-nicomononucleotide 1 hour before they were treated with COH34 and after 1 hour were subject to live cell analysis. This was done so that 18 hours after initial seeding all live cell experiments were performed by 21 hours after initial seeding.

Live cell experiments were performed on a Leica AF6000LX microscope at 5% CO_2 and 37ºC. Brightfield images were captured. Every well had 3 field of visions (FOV) and images were taken every 15 minutes for 2.5 hours producing 11 images per FOV. Ten Cells per FOV were tracked in the XY plane over time using the manual tracking tool in imageJ fiji. Every biological repeat therefore had 30 cells per condition, unless otherwise stated. The manual tracking tool was used to produce the trajectory plots and each cells accumulated distance, euclidean distance, directionality and velocity were recorded. A minimum of three biological repeats was performed and the number of repeats performed is indicated in the respective figures.

2.2.10 NAD+/NADH Quantification Assay

NAD/NADH quantification was performed by following the manufacturer's instructions using the ab65348 kit from abcam with some amendments and repeated steps for optimisation. Briefly, 2 $x10^6$ MDA-MB-231 cells were seeded initially into 10 cm dishes and after 24 hours they were drugged and/or treated with β-nicomononucleotide an hour prior to drugging where appropriate. After 18 hours in the incubator, samples were prepared as described in

the protocol. Cells were scraped and resuspended in ice cold PBS. During cell washes in PBS, cell counts for each condition were obtained to factor in during the final analysis. Cells were centrifuged at 2000 RPM (Heraeus MegaFuge 16 Centrifuge) for 5 minutes and the pellet was resuspended in 400 µl of NAD/NADH extraction buffer. Cells were then subjected to two freeze/thaw cycles on dry ice lasting 20 minutes with 10 minutes at room temperature. Extracted samples were vortexed for 10 seconds. Samples were then centrifuged three times at 4ºC at top speed (16.1 RCF) for 5 minutes. The insoluble pellet was separated from the supernatant with a pipette. This was transferred to a new Eppendorf tube and kept on ice. Samples were then filtered for removal of NAD/NADH degrading enzymes by centrifuging samples in a 10 kDa spin column (ab93349) at 10,000 RCF for 20 minutes at 4ºC. The filtrate for each sample was collected and split into two Eppendorf tubes. One was heated to 60ºC for 30 minutes on a heating block, decomposing all NAD+ whilst NADH remained intact. The other unheated sample was left on ice. This produced an NAD/NADH (NAD+ total) and NADH sample for each condition. Sample and standards with background controls were performed as indicated in the protocol in duplicate. For NAD+ total sample and background wells, 5 µl of the neat filtrate was used. For NADH sample and background wells, 10 µl of the neat filtrate was used. Once all the reagents were placed into the wells of a 96 well plate, the reaction was left to catalyse for 1 hour at room temp. The optical density at 450 nM was recorded using a flexstation 3 plate reader. Means were calculated and the mean of the blank standard was subtracted from all conditions. Background samples were subtracted from samples. The trendline from the NADH standards was plotted and sample readings were read off using the equation Y=MX+C. The volume added into each well was accounted for and given that the volume of each sample was recorded, and the concentration of cells was known, the relative differences in NADH per million cells could be calculated. Additionally, NAD+ could be calculated by subtracting the NADH value from the NAD+ total value. This allowed the NAD+/NADH ratio to be determined. One biological repeat was performed.

2.2.11 ATP Quantification Assay

ATP quantification was performed according to the manufacturer's instructions using ab83355 (abcam). Briefly, 2 x10^6 MDA-MB-231 cells were seeded into 10 cm dishes and after 24 hours they were drugged and/or pre-treated with β-nicomononucleotide pre-treatments an hour prior to drugging where appropriate. After 18 hours in the incubator, cells were scraped and resuspended in ice cold PBS. During the cell wash in PBS, cell counts for each condition were obtained to factor in during the final analysis. Cells were centrifuged at 1200 RPM for 3 minutes and the pellet was resuspended in 100 µl of ATP assay buffer. The volume of each sample was also recorded. Cells were pipetted eight times to homogenize them. Cells were then centrifuged for 5 minutes at 4ºC at 13000g. The supernatant was collected and transferred to a new tube and deproteinated using the TCA deproteinization sample preparation kit (ab204798 – abcam). To prepare the standard, a 0.01 mM stock of ATP was used, giving a standard curve of 0-100 pmol/well. Sample and background controls used 20 µl per condition per well. All standards, samples and background controls were performed in duplicate in a 96-well plate. After reaction mixes were added to samples and standards, the plate was left for 30 minutes in the dark at room temperature. The average Ex/Em 535/587 nM was recorded using a flexstation 3 plate reader. Averages were recorded and the mean of the blank standard was subtracted from all averaged conditions. Average background samples were subtracted from samples. The trendline from the ATP standards was plotted and sample readings were read off using the equation Y=MX+C. The volume added into each well and the dilution following deproteinization was accounted for. Given that the volume of each sample was recorded, and the concentration of cells was known, the relative differences in ATP per million cells could be calculated. One biological repeat was performed.

2.2.12 Cell Morphology

Cell morphology was determined using the freehand tool in image-J. The perimeter of cells was manually drawn and the area, circularity and aspect ratio were then determined. Analysis was performed on bright field live cell images. One hundred cells were analysed per biological repeat and a minimum of three biological repeats was performed.

2.2.13 Immunofluorescence

2.2.13.1 Alpha-Tubulin and Actin

2.2.13.1.1 Alpha-Tubulin and Actin staining

Rounded coverslips (13 mm) were sterilised in 70% IMS and stood in 24 well plates to dry. Once dry, they were laid flat and 20,000 MDA-MB-231 cells were seeded on top in 2 ml media. After four hours in the incubator, cells were treated with 2 µl of DMSO or 0.3 mM PDD. After 16 hours in the incubator, the media was removed and two PBS washes were performed. Cells were then fixed for 15 minutes using 4% paraformaldehyde. Cells were subject to two more PBS washes. Cells were then permeabilised using 0.5% Triton-X100 in PBS for five minutes. Cells were then blocked in 3% BSA in PBS for 30 minutes at room temperature. Coverslips were then flipped and placed into 100 µl of 3% BSA PBS with 1:1000 dilution of anti-mouse alpha-tubulin (A86726) overnight in the fridge at 4ºC in a humidified chamber. Coverslips were then flipped facing up and received three 5-minute PBS washes. Coverslips were then placed facedown and placed into 100 µl of 3% BSA containing 1:500 anti-mouse 594, 1:1000 dilution of 1 mg/ml DAPI and 1:1000 488 Phalloidin for 1 hour in the dark at room temperature. Coverslips were flipped upwards and received two 5-minute washes. Coverslips were then dipped in ultra-pure deionised water and inverted facedown onto labelled slides with immunomount applied. After drying at room temperature overnight, slides were stored in the fridge at 4ºC. Images of 50 cells were then

captured at 100x magnification using oil immersion on a Nikon TE200 inverted fluorescent microscope using NIS-elements 5 BR 20.01 software. One repeat was performed.

2.2.13.1.2 Alpha Tubulin Analysis

Images were imported into ImageJ and the whole cell alpha tubulin integrated density (594 nm) was measured using the threshold and magic wand tool. To measure alpha tubulin nuclear integrated density, the nuclear area was determined from the DAPI signal using threshold and magic wand tools, this area was then transferred to the 594 nm channel and the measurement of integrated area in the nucleus was determined. The cytoplasmic integrated density was recorded by subtracting the nuclear integrated density from the whole cell integrated density. Additionally, images were inspected for abnormalities of the microtubule organising centre. Representative images of normal and abnormal staining are presented.

2.2.13.1.3 Actin Analysis

Whole cell integrated density of actin (488 nm) was also determined in imageJ using the threshold and magic wand tool and nuclear and cytoplasmic areas determined as above. Additionally, filopodia were examined by manually drawing along the length of filopodia that emanated outwards from the cell periphery using the free hand and measure tool to record the length and number per cell. Representative images of cells with stress fibres are presented. The percentage of cells with visible stress fibres was calculated. Representative images of cells displaying podosomes are presented and the number of podosomes per cell was determined by manual counting.

2.2.13.2 YAP

22 x 22 mm coverslips were sterilised in 70% IMS and stood upright in 6 well plates to dry. Once dry, they were laid flat and 300,000 cells were seeded into each well with a final volume of 2 ml. Cells were placed in the incubator for 4 hours. After four hours, cells were drugged appropriately. After 18 hours, the media was removed, and coverslips were washed in PBS and fixed in 4% paraformaldehyde in PBS for 10 minutes at room temperature. Coverslips were then washed twice with PBS for 5 minutes. Cells were then blocked and permeabilised with 0.1% Triton-X100 with 1% BSA in PBS for 10 minutes. Coverslips were then washed 3 times with PBS for 5 minutes. Coverlslips were then inverted into 100 µl of 1% BSA with 1:100 diluted YAP primary antibody (Sc-154-07) overnight at 4ºC in a humidified chamber. Coverslips were then flipped and washed 3 times in PBS for 10 minutes. Coverslips were the flipped facing down into 100 µl with 1:1000 dilution of Alexa flour 594 anti-mouse with 1:1000 of 1 mg/ml DAPI at room temperature in the dark. Coverslips were then flipped facing upwards and washed three times in PBS for 5 minutes. Coverslips were then dipped in ultra-pure deionised water and inverted facedown onto labelled slides with immunomount applied. After drying at room temperature overnight, slides were stored at 4ºC.

Images of 100 cells per condition were then captured at 60x magnification using oil immersion on a Nikon TE200 inverted fluorescent microscope using NIS-elements 5 BR 20.01 software.

2.2.13.3 Lamin A

Cells were seeded onto dried 70% IMS sterilised 22 x 22 mm coverslips with 300,000 cells per well in a 6 well plate and placed into an incubator. After four hours cells were drugged and left to incubate for 18 hours. The media was removed, and coverslips were washed in PBS and fixed in 4% paraformaldehyde in PBS for 10 minutes at room temperature.

Coverslips were then washed twice with PBS for 5 minutes. Cells were permeabilised using 0.2% TritonX-100 in PBS for 10 and then washed 3 times in PBS for 5 minutes. Cells were then blocked with 3% BSA in PBS for 1 hour at room temperature. Coverslips were inverted and placed into 100 µl of 1% BSA with 1:1000 diluted Lamin A primary antibody overnight in a humidified chamber at 4ºC. Coverslips were placed facing up and washed 3 times in PBS for 5 minutes. Coverslips were inverted and placed into 100 µl of 1% BSA in PBS with 1:1000 diluted alexa-flour 594 anti-rabbit secondary with 1:1000 of 1mg/ml DAPI at room temperature in the dark for 1 hour. Coverslips were then flipped facing upwards and washed two times in PBS. Coverslips were then dipped in ultra-pure deionised water and inverted facedown onto labelled slides with immunomount applied. After drying at room temperature overnight, slides were stored at 4ºC.

Confocal imaging was performed using a 60X Olympus plan APO N lens with a GEOMX BEAZE V4 microscope and 4 SCHOS camera to perform OMX deconvolution with the startsoftworx V7.0 software. Twenty cells per condition were imaged with 0.25 µ M spacing and 7 µM thickness rendering each image to have 29 optical spaces. Deconvolution and OMX alignment was then applied to each image using the tasks of the same name built into the software. Images were captured using the DAPI and 569 nm channels and imageJ, nuclear abnormalities were observed and scored in imageJ and representative images presented.

2.2.14 Microarray

Cells were trypsinised and 180,000 MDA-MB-231 cells were seeded into 6 wells of a 6 well plate. After 4 hours in the incubator, cells were treated with DMSO, PDD or TE92. Two wells were used for each condition. Cells were left in the incubator for 18 hours. The RNA was then purified using the RNAeasy kit (Qiagen) according to the manufacturer's instructions and submitted for in house Affymetrix microarray analysis. Due to COVID-19, RNA integrity

analysis (Agilent 2100 Bioanalyser), reactions and hybridisation to the arrays was carried out by Paul Heath.

The raw CEL files were sent to me and were inputted into transcriptome analysis console 4.0 (Applied biosystems). Each conditions biological repeats were grouped, and a comparison was performed allowing for differential expression to be observed between all three groups, as well as the quality control status of every condition submitted for each biological repeat.

2.2.14.1 Bioinformatics

The differentially expressed genes retrieved by comparing PDD vs DMSO were interrogated further for statistical enrichment of biological processes and KEGG pathways. Several methods were employed. The differentially expressed genes were plugged into the R package *Cluster profiler* and the following command functions were used to interrogate them and the results were retrieved: enrichGO, gseGO, enrichKEGG and gseKEGG. The commands with GO suffixes assessed for enrichment of gene ontologies. The commands with KEGG suffixes assessed for enrichment of KEGG pathways. The distinction between the “enrich” and “gse” prefixes in the command function is that the ”gse” command factored in gene fold change directionality in the analysis. The differentially expressed genes were plugged into the database for annotation, visualization and integrated discovery (DAVID) and the gene ontology and KEGG was retrieved. The over representation test was performed in PANTHER and the results were retrieved.

2.2.15 Differential Expressed Genes – RT-qPCR

MDA-MB-231 cells were seeded in 6 well plates at 180,000 cells per well. Each condition was performed in duplicate. Cells were left to incubate for four hours and subsequently drugged. After the appropriate time, cells were harvested and suspended in media, centrifuged at 1500 RPM for 3 minutes and the pellet was resuspended in ice cold PBS. The centrifugation conditions were repeated and the pellet was resuspended in 1 ml ice cold PBS and transferred to a 1.5 ml Eppendorf tube. This was centrifuged at 5000 RPM for 5 minutes at 4ºC and the supernatant was removed. The pellet was stored at -80ºC prior to RNA extraction.

2.2.15.1 Total RNA Extraction

RNA was extracted from each sample pellet using the RNAeasy Kit (Qiagen) and supplied reagents according to the manufacturer's instructions. This produced a final elusion of 20 µl. A Nanodrop (ThermoFisher) was used to determine the RNA concentration as per standard protocol. An A_{260}/A_{280} ratio of equal to or greater than 2.0 was used to assess RNA purity. RNA was reverse transcribed to cDNA immediately after extraction (see below) and the excess was stored at -80ºC.

2.2.15.2 Reverse Transcription: cDNA synthesis from Total RNA

RNA samples were diluted in nuclease-free water to a concentration of 0.039 µg/µl in a final volume of 10 µl giving 390 ng of RNA total per reaction. RNA was then reversed transcribed into cDNA using a high-capacity RNA to cDNA kit (Applied biosystems – 4368814) according to the manufacturer's instructions (see table 2.11).

Table 2.11 **Applied Biosystems high-capacity RNA to cDNA kit (4368814) RNA reverse transcription reaction mixture recommended conditions.**		
Reagent	**Volume per 20 µl Reaction (µl)**	**Final Reaction Mixture Concentration**
10X RT Buffer	2.0	1X
100 mM dNTP Mix	0.8	4 mM
10X Random Primers	2.0	1X
Multiscribe Reverse Transcriptase (50U/µl)	1.0	50U
Nuclease-free Water	4.2	-
Total RNA 0.039 µg/µl	10	390 ng

The reaction was run on a Geneamp PCR system 2700 (Applied Biosystems) using standard thermal cycling conditions (see table 2.12).

Table 2.12 **Recommended thermal cycling conditions for RNA to cDNA reverse transcription reactions.**	
Temp (ºC)	**Time (min)**
25	10
37	120
85	5
4	∞

2.2.15.3 Taqman qPCR

Taqman probes select against a range of differentially expressed genes were purchased from thermofisher (see table 2.6). In addition, GAPDH mRNA expression was determined for each cDNA sample. The relative expression of each gene of interest compared to GAPDH and subsequent normalisation allowed for comparisons between conditions to be made.

Each gene to be tested had a Taqman qPCR reaction master mix made such that the final volume per well in the 384 well plates (Applied Biosystems – 4309849) was 10 µl (table 2.13). cDNA samples were diluted in RNase free water to give a final concentration of 100 ng/µl. and 300 ng of cDNA was used in the reaction. Plates were sealed with optical adhesive covers (Applied Biosystems – 4360954) and centrifuged at 1000 RPM for 1 minute. A quantstudio™ 7 Flex Real-Time PCR system (Thermofisher) was used to perform the real

time qPCR. The fluorescent signal from the PCR product was monitored over 40 amplifications and the recommended thermal cycling conditions for Taqman qPCR reactions were used (table 2.14).

All real-time qPCR reactions were carried out in triplicate using samples from three biological repeats with three technical plates per probe. A reaction with no cDNA was ran in parallel with all probes to assesses for DNA contamination.

Table 2.13 **The components within a 10 µl Taqman qPCR reaction per well.**

Reagent	Volume of Reagent per 10 µl Reaction (µl)	Final Reaction Mixture Concentration
2X Taqman Universal PCR master mix	5.0	1X
20X Taqman gene expression assay probe	0.5	1X
RNAse free water	1.5	-
0.1 µg/µl cDNA	3	300 ng

Table 2.14 **The recommended thermal cycling conditions for Taqman RT-qPCR probes.**

Temp (°C)	Time (min)	No. of Cycles
95	10.00	1
95	0.25	40
60	1.00	

2.2.15.4 qPCR Analysis

The Quantstudio (v1.3) software produced amplification plots that tracked the fluorescent signal over cycles. The software selected a mutually amicable threshold within the log phase of each probes PCR product. The Ct value was then recorded (the number of cycles take to reach the fluorescent threshold). These data were then exported to manually calculate the $2^{-\Delta\Delta Ct}$. The average Ct of each probe within each condition was recorded. Each respective conditions GAPDH average Ct values were then subtracted from each probes average Ct values producing the ΔCt. The probe of interest within each condition under investigation had the respected probe within the DMSO untreated conditions ΔCt subtracted from it's ΔCt,

producing the ΔΔCt. This value was then inserted into $2^{-\Delta\Delta Ct}$. Values below 1 were downregulated and values above 1 were upregulated. These values were then exported to GraphPad prism.

2.2.16 Statistical Analysis

When single data points were derived from individual experiments, the data was expressed as means -/+ the standard deviation. If data from biological repeats were pooled, then data was expressed with a line depicting the median. If experiments included technical repeats, the resulting mean of means was recorded as mean-/+ the standard error of the mean. Statistical differences between means were performed using an unpaired two-tailed t-test. If more than two means were compared statistically, then a one-way ANOVA was performed. Normality testing was done by the Shapiro-Wilk test. Pooled data was not normally distributed and when two means were being compared, a Mann-Whitney was performed. In instances where more than two means were compared statistically, pooled data was assessed using the Kruskal-Wallis method. GraphPad Prism was used for all statistical calculations, with $p=\leq 0.05$ being the assumed cut-off for statistical significance.

Chapter 3.0 Results: Evaluation of PARP and PARG inhibitors as anti-metastatic agents in Breast Cancer *in vitro*

3.1 Introduction, aims and hypotheses

There is some limited evidence to suggest that the depletion of PARG *in vitro* exerts an anti-metastatic phenotype (Q. Li et al., 2012; Marques et al., 2019; Pan et al., 2012). Depletion of PARG in the colon cancer cell line LoVo reduced migration of co-cultured HUVEC cells (Pan et al., 2012). Overexpression of PARG increased tumorigenesis and cell migration of normal mammary epithelial cells and depletion of PARG lead to reduced tumour growth and metastasis of TNBC cells *in vivo* (Marques et al., 2019). In addition, PARG depletion reduced migration and invasion in hepatocellular carcinoma (HCC) cell lines and PARGi using COH34, reduced tumorigenesis in *in vivo* models of HCC (Mincheng Yu et al., 2022). One study i*n vitro* has explored pharmacological inhibition of PARG, where PDD00017273 reduced migration of two ovarian cancer cell lines (Matanes et al., 2021). However, these data were limited by the high cytotoxic doses used (2 µM and 5 µM).

The hypothesis of this chapter is that PARylation has a role in metastatic progression.

Considering that PARG overexpression is reported oncogenic in breast cancer (Marques et al., 2019) and that PARP and PARG function are well studied in breast cancer, triple negative breast cancer cells, MDA-MB-231, were chosen here as a model to study the metastatic effect function of PARylation. A range of inhibitors selective against different PARylators will be used to try and delineate function and will be validated using siRNA.

The aim of this chapter is therefore to examine if PARylation impacts different facets of the metastatic cascade. Specifically, I will:

1. Determine the effective, non-cytotoxic doses of PARP and PARG inhibitors
2. Determine if inhibitors of PARP and PARG affect cell adhesion
3. Determine if PARG inhibitors impact invasion

4. Determine if inhibitors of PARP and PARG affect migration
5. Validate migration results using siRNA against PARG

3.2 Results

3.2.1 Clonogenic Survival to PARP, Tankyrase and PARG inhibition in MDA-MB-231 and MCF7 Cell Lines

Before starting to investigate effects on metastatic phenotypes, it was important to establish the optimum dose and cellular consequences of these doses in MDA-MD-231 cells. MCF-7 cells were also used in these initial studies as they have been used widely in Bryant lab and effective non-toxic does of both PARP and PARG inhibitors are known for these cells.

To establish toxicity, MDA-MB-231 and MCF7 cells were treated with increasing doses of the PARP1-3 inhibitor Olaparib (PARPi), the Tankyrase inhibitor TE92 (TNKSi) or the PARG inhibitor PDD00017273 (PDD or PARGi) (Figure 3.1). The MCF7 cell line was more sensitive than MDA-MB-231 to PDD (mean survival fraction at 1 µM 0.68 cf. 0.95, figure 3.1 A&B). In contrast, sensitivity to Olaparib was similar in both cell lines (Figure 3.1C&D), while MDA-MB-231 cells were more sensitive to TE92 at 1 µM compared to MCF7 (mean survival fraction at 1 µM 0.55 cf. 0.68, figure 3.1 E&F).

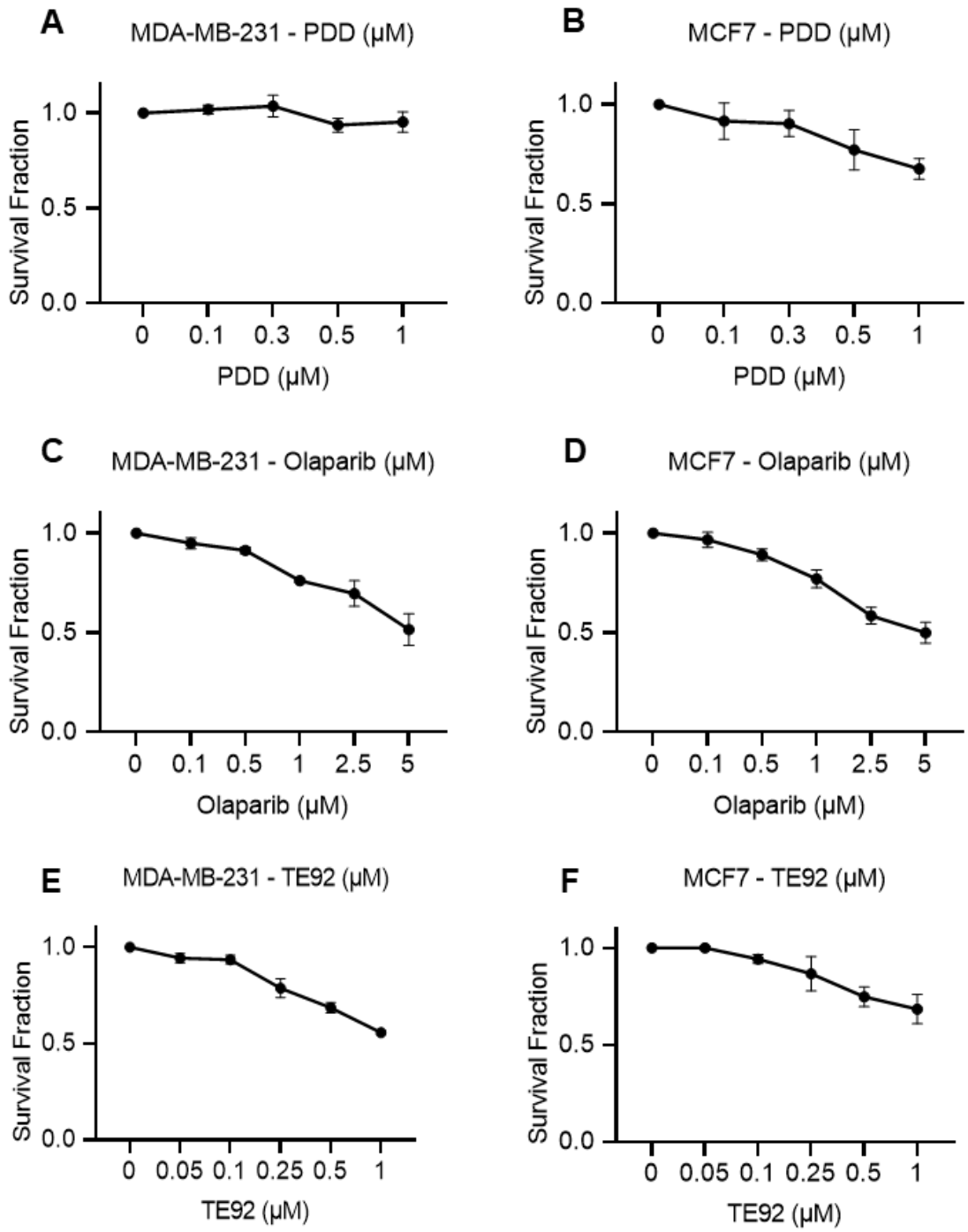

Figure 3.1. **Survival Fraction (SF) of MDA-MB-231 and MCF7 cell lines to PARPi, TNKSi or PARGi.** (A) MDA-MB-231 SF in response to PARGi PDD (0-1μM). (B) MCF7 SF in response to PARGi PDD (0-1 μM). (C) MDA-MB-231 SF in response to PARPi Olaparib (0-5 μM). (D) MCF7 SF in response to PARPi Olaparib (0-5 μM). (E) MDA-MB-231 SF in response to TNKSi TE92 (0-1 μM). (F) MCF7 SF in response to TNKSi TE92 (0-1 μM).

3.2.2 Inhibition of PARP1-3, Tankyrase and PARG with respective inhibitors in MDA-MB-231 Cells

Having determined doses of each inhibitor that have limited toxicity in cells, inhibition of enzymatic activity was confirmed by western blotting. At 0.3 μM, PDD increased PAR signal relative to the DMSO control (Figure 3.2). In contrast, 0.5 μM Olaparib reduced the PAR signal (Figure 3.2). TE92 (0.1 μM) did not alter the levels of PAR (Figure 3.2), however it did result in the stabilization of TNKS1 and TNKS2 compared to the DMSO control (Figure 3.2). This stabilisation has been associated with changes in Tankyrase activity previously reported (Bhardwaj et al., 2017). PARP and PARG levels remained unchanged in the presence of all the drugs relative to the DMSO control (Figure 3.2A), demonstrating that the changes in PAR seen were due to inhibition rather than changes in total protein levels.

Having confirmed the toxicity and inhibitory action of the drugs at these doses, the effect on proliferation and cell cycle profiles were then examined.

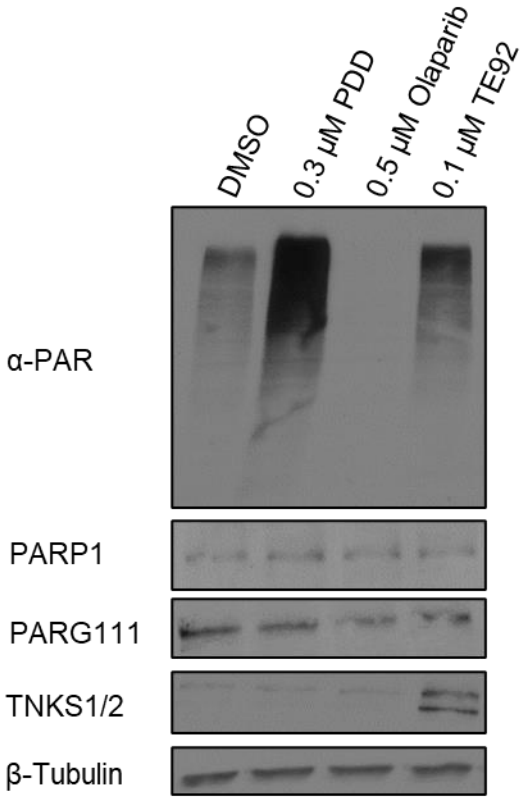

Figure 3.2. **Effective non-cytotoxic inhibitory doses of PARPi, TNKSi and PARGi in MDA-MB-231 cells.** Legend overleaf.

Figure 3.2. **Effective non-cytotoxic inhibitory doses of PARPi, TNKSi and PARGi in MDA-MB-231 cells.** PARGi PDD (0.3 µM) increased α-PAR signal relative to DMSO. PARPi Olaparib (0.5 µM) decreased α-PAR signal relative to DMSO. TNKSi TE92 (0.1 µM) did not impact α-PAR signal relative to DMSO. Total PARP1 and PARG110 levels remain unchanged in response to each drug. TE92 stabilised TNKS1/2 protein whereas PDD and Olaparib did not. β-Tubulin served as a loading control.

3.2.3 Proliferation of MDA-MB-231 and MCF7 cells treated with PARP1-3, Tankyrase and PARG inhibitors

The effects of these drug doses on cell proliferation were determined. Cells were dosed every 24 hours (by replacing media containing fresh drug) and counted every 48 hours by trypan blue exclusion. At 48 hours PDD, Olaparib and TE92 had little effect on MDA-MB-231 cell proliferation (consistent with survival data) (Figure 3.3A), however, by 144 hours proliferation was reduced by PDD, Olaparib and TE92 in MDA-MB-231 cells (Figure 3.3A), although only 2 biological repeats were performed at this time point so statistical analysis was not possible. Similarly, only two biological repeats were obtained for MCF7's (Figure 3.3B). However, the result appears to be broadly consistent with findings in MDA-MB-231.

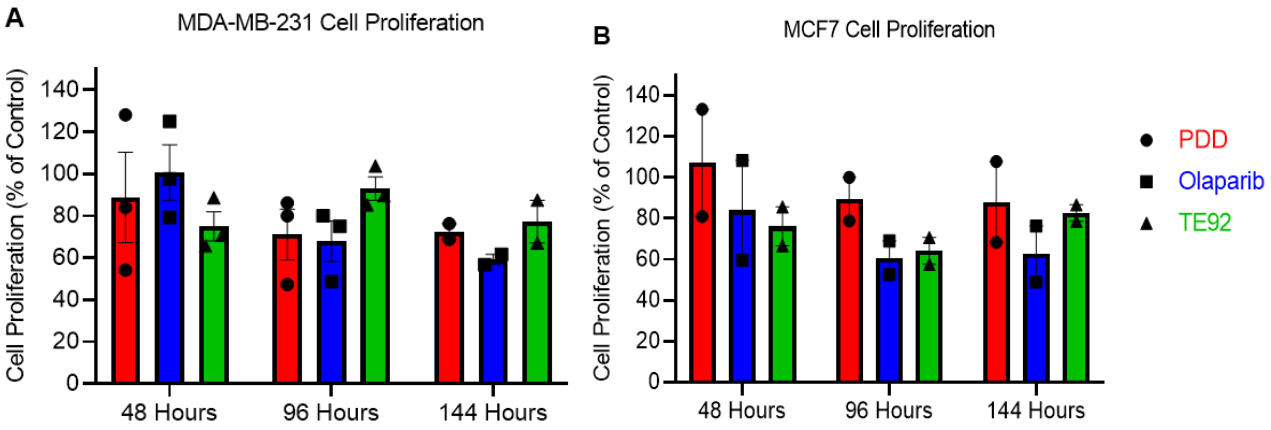

Figure 3.3. **Proliferation of MDA-MB-231 and MCF7 cells treated with PARP1-3, Tankyrase and PARG inhibitors.** (A) MDA-MB-231 cell proliferation as a % of the DMSO control over time using daily doses of PARPi, TNKSi or PARGi. (B) MCF7 cell proliferation as a % of the DMSO control over time using daily doses of PARPi, TNKSi or PARGi. Each dot reflects a biological repeat. Proliferation determined using trypan blue exclusion. A one-way anova was performed on the MDA-MB-231 48 and 96 hour conditions relative to normalised DMSO control. The P-values were 0.88, >0.99 and 0.44 (48 hour) and 0.09, 0.06 and 0.88 (96 hour) for PDD, Olaparib and TE92 respectively. Statistical analysis was not performed on the rest of the conditions due to N=2.

3.2.4 Cell cycle profiles of MDA-MB-231 and MCF7 cells treated with PARP1-3, Tankyrase and PARG inhibitors

The cell cycle profiles of MDA-MB-231 and MCF7 cells treated with PDD, Olaparib or TE92 for 24 hours was assessed using fluorescence assisted cell sorting and PI/p-H3 staining to differentiate between the different cell cycle fractions. A no primary control was used to assess for nonspecific binding of the secondary antibody to p-H3. There was no statistically significant difference between any of the phases of the cell cycle with any drug in either cell line (Figure 3.4A-D).

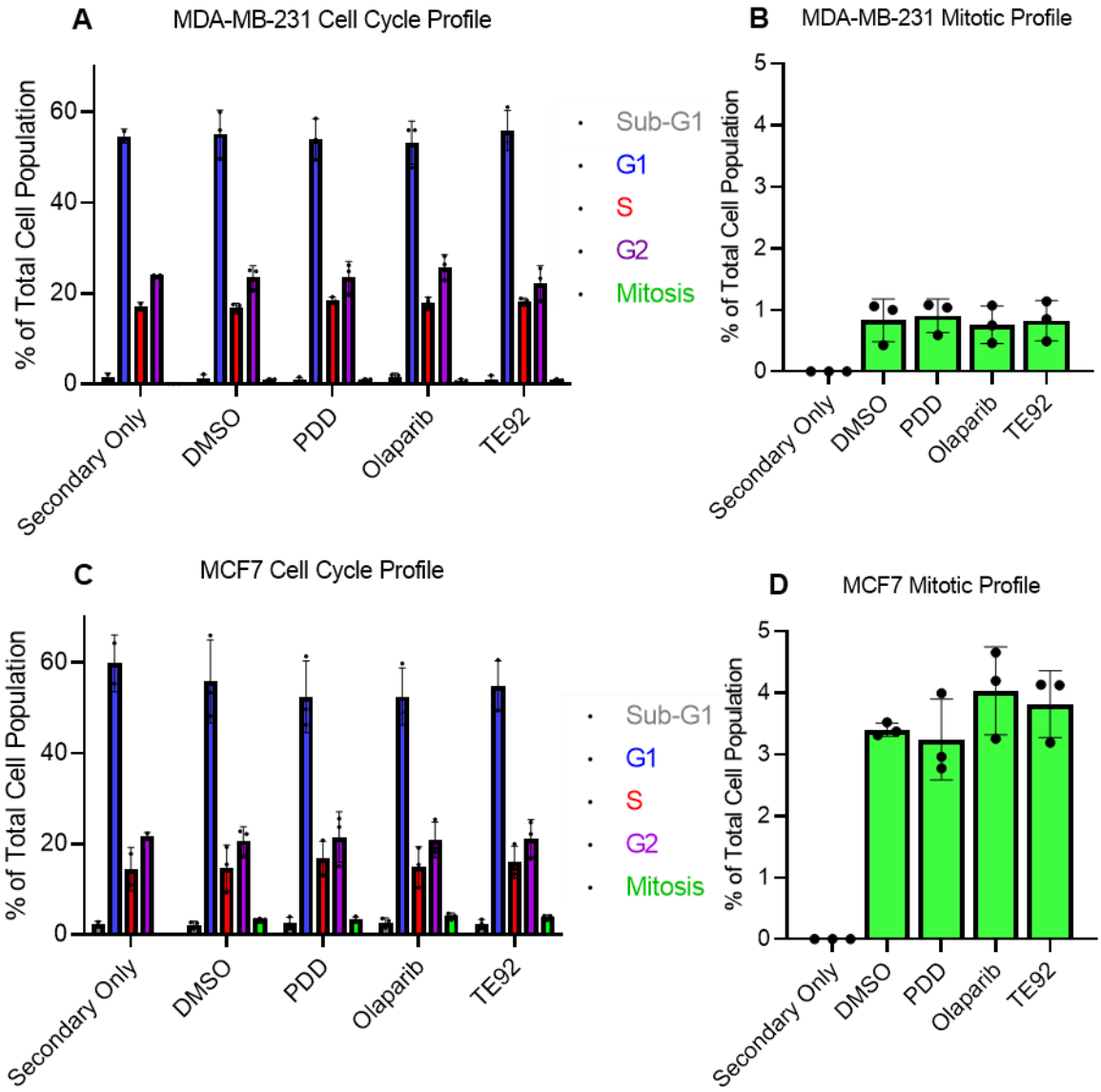

Figure 3.4 **Cell cycle profiles of MDA-MB-231 and MCF7 cells treated with PARP1-3, Tankyrase or PARG inhibitors.** Legend overleaf.

Figure 3.4. **Cell cycle profiles of MDA-MB-231 and MCF7 cells treated with PARP1-3, Tankyrase or PARG inhibitors.** (A) FACS PI/p-H3 staining of MDA-MB-231 cells after 24 hours treated with a PARPi, TNKSi or PARGi. (B) Enlarged mitotic MDA-MB-231 prolife derived from figure 3.4A. (C) FACS PI/p-H3 staining of MCF7 cells after 24 hours treated with a PARPi, TNKSi or PARGi. (B) Enlarged mitotic MCF7 profile derived from figure 3.4A. An one-way ANOVA was performed comparing the respective cell cycle phases with the DMSO control. No statistical significance was observed. The NS P-values for the MDA-MB-231 data was 0.97, 0.93, 0.99 (Sub-G1), 0.98, 0.92, 0.99 (G1), 0.22, 0.45, 0.26 (S), >0.99, 0.72, 0.94 (G2) and 0.98, 0.99 and >0.99 (M) for PDD, Olaparib and TE92 respectively. The NS P-values for the MCF7 data was 0.95, 0.88, 0.99 (sub-G1), 0.89, 0.9, >0.99 (G1), 0.89, >0.99, 0.97 (S), >0.99, >0.99, >0.99 (G2) and 0.97, 0.42 and 0.7 (M) for PDD, Olaparib and TE92 respectively.

Taking together all these data 0.3 μM PDD, 0.5 μM Olaparib and 0.1 μM TE92 were taken forward as non-toxic, effective doses of their respective inhibitors with few proliferative consequences following short-term (24-48 h) treatments.

3.2.5 Inhibition of PARP1-3, PARG or Tankyrase had no effect on static adhesion of MDA-MB-231 cells to fibronectin

Fibronectin is a commonly cancer associated extracellular matrix component implicated in tumour malignancy that is frequently investigated in adhesion studies, particularly with MDA-MB-231 cells. Static adhesion assays are a common method of assessing the impact of agents on adhesion. Cells are seeded onto a coated surface and left to adhere for a selected period. The cells are then subject rounds of washes to remove potential loose cells and stained and solubilised to assess for differences in relative cell numbers. Figure 3.5A demonstrates that there is a linear relationship between solubilised crystal violet-stained MDA-MB-231 cell number treated with 0.1% DMSO (equivalent of drugged conditions) and absorbance at 540 nM with an R^2 value of 0.9678 providing evidence of sensitivity. Two hours is the most common time frame these types of adhesion assays are performed in the literature. A range of cell numbers: 5,000, 10,000 and 25,000 were seeded on drugged pre-coated plates and left to adhere for two hours. Statistical analysis could not be performed on the 5,000-cell number condition as there was only two biological repeats (Figure 3.5B). There was no statistically significant difference with any of the drug treatments relative to the DMSO control at 10,000 or 25,000 cell number conditions (Figure 3.5B).

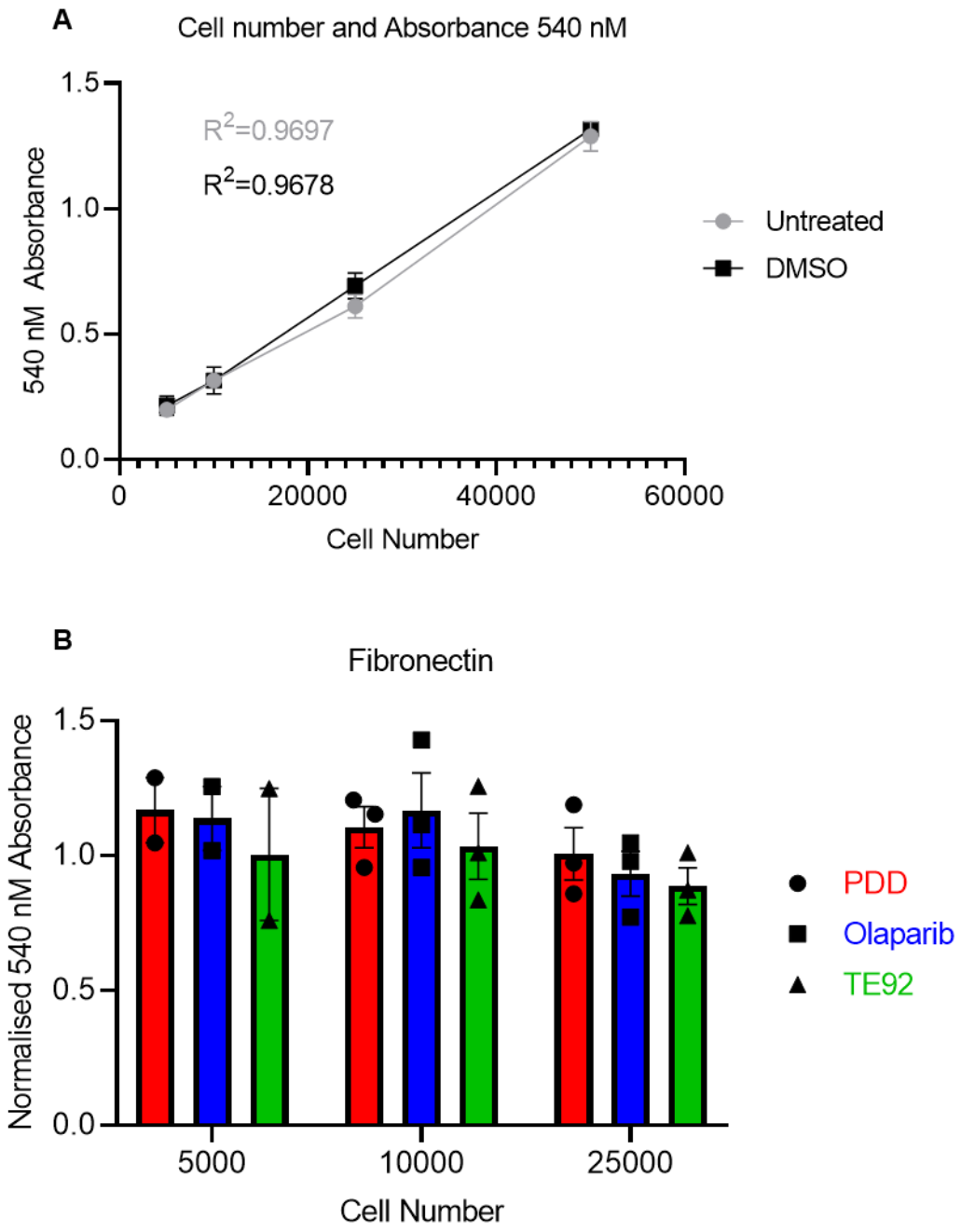

Figure 3.5. **Inhibition of PARP1-3, PARG or Tankyrase has no effect on static adhesion of MDA-MB-231 cells to fibronectin.** (A) Cell number and crystal violet absorbance (540 nM) have a linear relationship (R^2 = 0.97) demonstrating assay sensitivity. (B) 540 nM absorbance of a range of crystal violet-stained cell values relative to the DMSO control seeded on fibronectin in the presence of a PARPi (Olaparib), PARGi (PDD) or TNKSi (TE92). An one-way ANOVA was performed to assess for statistical differences between the treatment conditions and the respective cell numbers relative DMSO control. No statistical significance was observed. Statistical analysis was only performed when N=3. The P-values were 0.8, 0.54 and 0.99 (10,000 cell number) and for 0.99, 0.85 and 0.57 (25,000 cell number) for PDD, Olaparib and TE92, respectively.

3.2.6 Inhibition of PARP1-3, PARG or Tankyrase had no effect on static adhesion of MDA-MB-231 cells to Matrigel

Matrigel is a heterogenous mixture of extracellular matrix protein including laminin, collagen IV and entactin as its primary constituents and it is used as an alternative to pure fibronectin in some adhesion assays and may more closely resemble the ECM in real tumours. We therefore wanted to assess if any of the inhibitors could affect MDA-MB-231 adhesion to this matrix. An optimal concentration of Matrigel to coat the plates was determined (Figure 3.6A).

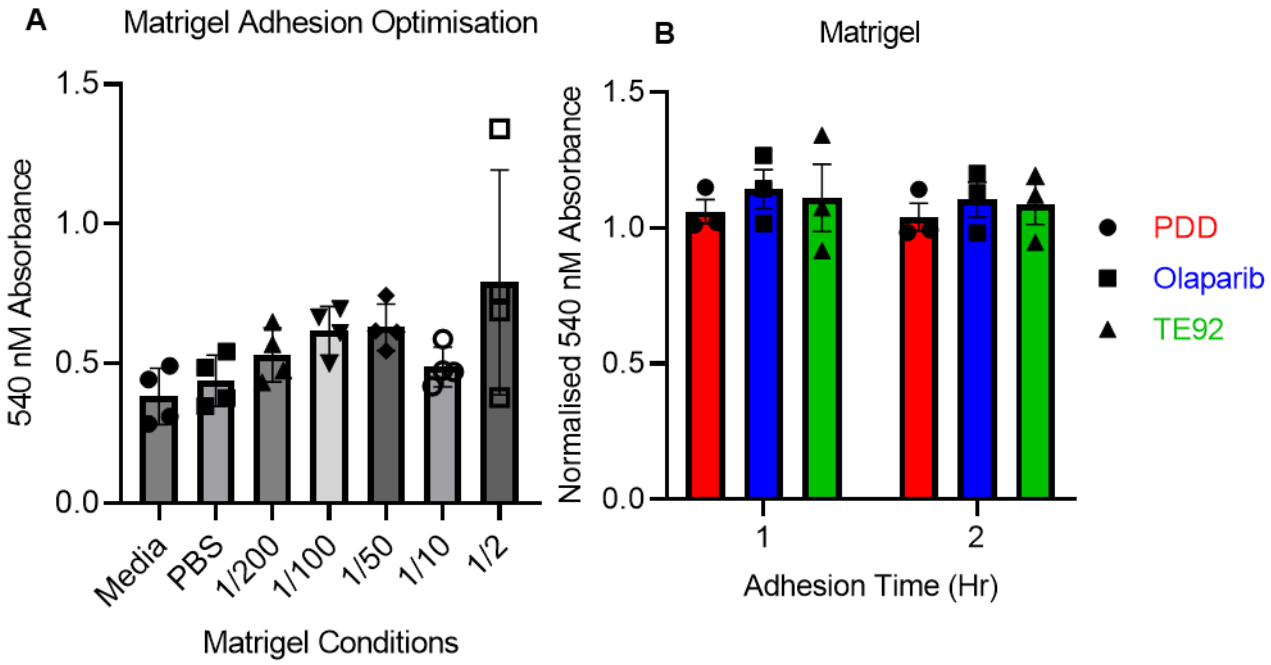

Figure 3.6. **Inhibition of PARP1-3, PARG or Tankyrase had no effect on static adhesion of MDA-MB-231 cells to Matrigel.** (A) Matrigel static adhesion optimisation displaying a range of Matrigel dilutions. A 1/50 dilution achieved the strongest and most consistent signal (Mean -/+ SD) and was used to experimentally assess the impact of the drugs on static adhesion to Matrigel. N=4. (B) 540 nM absorbance of crystal violet-stained cells (10,000) at 1-2 hour time points relative to the DMSO control seeded on Matrigel in the presence of a PARPi (Olaparib), PARGi (PDD) or TNKSi (TE92). An one-way ANOVA was performed to assess for statistical differences between the treatment conditions and the respective time points DMSO control. No statistical significance was observed. The p-values were 0.9, 0.44 and 0.62 (1 Hr) and 0.92, 0.45 and 0.57 (2 Hr) for PDD, Olaparib and TE92 respectively.

A one in fifty dilution achieved the highest absorption with the most consistency and was used experimentally to assess the impact of the drugs on adhesion. The relative number of cells remaining (based on solubilised crystal violet absorption at 540 nM), compared to the DMSO control after one and two hours was investigated (Figure 3.6B). However, consistent with fibronectin, no drug at either time point yielded a statistically significant difference in adhesion (Figure 3.6B).

3.2.7 Inhibition of PARG reduced invasion of MDA-MB-231 cells through Matrigel

An important part of the metastatic cascade is that a sub-population of the tumour's cells develop the ability to degrade the surrounding extracellular matrix for resources and invade/migrate into that new territory. We wanted to assess the impact of all three inhibitors on this facet of metastasis, however, due to issues with scalability and time spent optimising the assay, only the PARG inhibitor (PDD) was assessed. The matrix at the bottom of the upper chambers of the transwell inserts was coated with Matrigel and left to set. The lower chambers were then supplemented with complete media and pre-treated MDA-MB-231 cells were resuspended in low FCS media and seeded on top of the Matrigel. The chemotactic gradient incentivises the cells to move down through the Matrigel and transwell matrix. Each condition was performed in duplicate to assess for the number of cells added relative to the number of cells that invaded (Figure 3.7A). Figure 3.7B shows that 48% of the DMSO treated cells reached the transwell matrix when there was no coating present, this represents migration as there is no barrier present. In comparison, 37% of the DMSO treated cells reached the transwell matrix in the presence of Matrigel, which represents invasion (Figure 3.7B). PDD caused a statistically significant reduction in the number of cells that invaded through the Matrigel compared to DMSO - 27 % vs 37 % (Figure 3.7B).

These data suggest that inhibition of PARG by PDD can reduce the invasiveness of MDA-MB-231 cells and that by implication that PARG plays an important role in invasion.

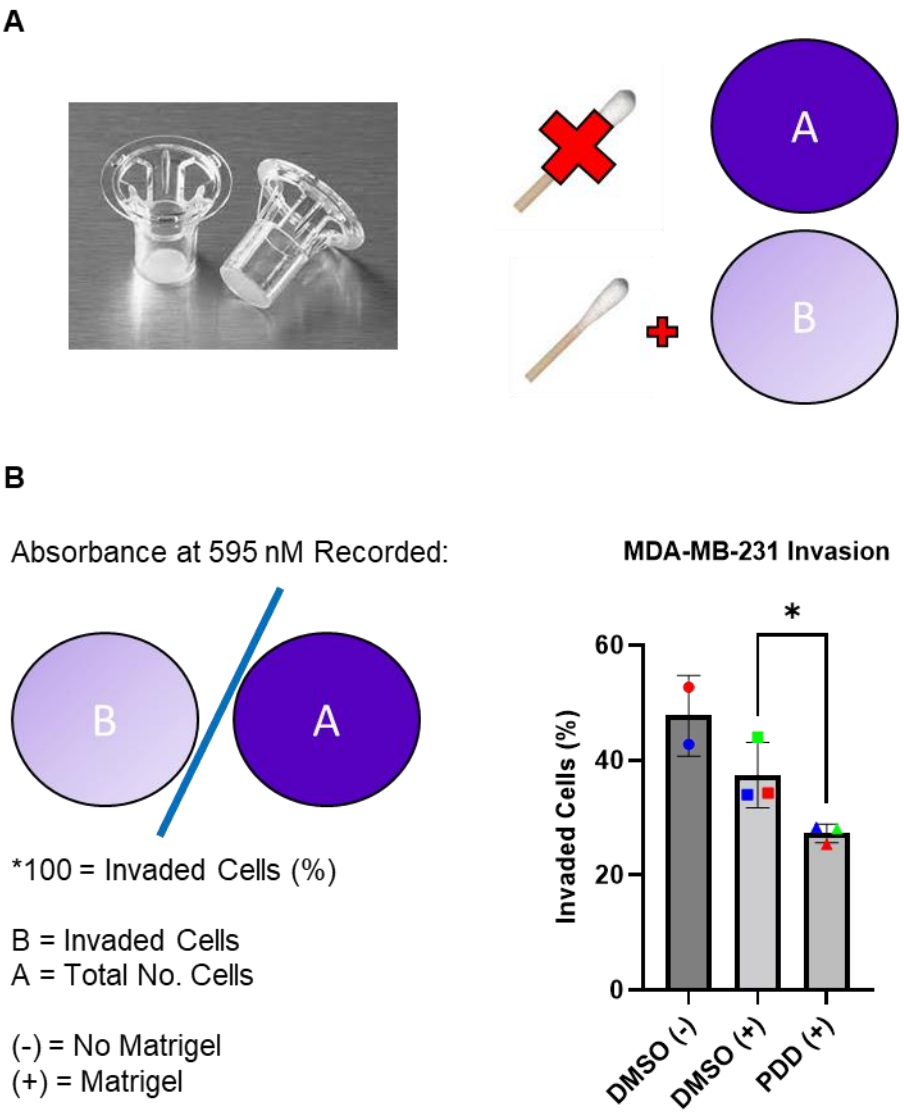

Figure 3.7. **PARGi (PDD) reduces MDA-MB-231 invasion through Matrigel.** (A) Schematic diagram showing the principal of the method used to assay the impact of PDD on MDA-MB-231 invasion. Briefly, experimental conditions were performed in duplicate and one of the transwells had the upper layer of cells swabbed with a cotton bud. The swabbed transwell served as a way of measuring the number of invaded cells. The unswabbed transwell served as a way of measuring the total number of cells. Cells in each transwell were stained with crystal violet and the membrane was removed from the plastic and solubilised in 0.1% sodium deoxycholate. (B) The solubilised crystal violets absorbance was recorded (595 nM) and the percentage of invaded cells was calculated. "-" denotes no Matrigel in the transwell. "+" denotes Matrigel is in the transwell. The DMSO (-) condition had a higher % of cells that had "invaded" however no membrane was present. Therefore, this denotes the number of migrated cells. Less cells invaded in the DMSO (+) condition relative to the DMSO (-) condition suggesting the Matrigel acted as a barrier to MDA-MB-231 cells. Normality was not tested for as three biological repeats were obtained. An unpaired t-test reported a statistically significant reduction in the percentage of invaded cells in the PARGi (PDD +) condition relative to the DMSO (+) condition. * denotes p=≤0.05. Mean -/+ SD is depicted in the graph.

3.2.8 Inhibition/depletion of PARG reduces migration of MDA-MB-231 cells

3.2.8.1 Migration into a Bilateral Cell Free Area

Culture well inserts were used to create a cell free exclusion zone and as a proxy for cell movement the relative cell free area remaining after 18 hours was recorded. The greater the gap that remained, the less the cells had migrated (Figure 3.8A). Figure 3.8B displays representative images of brightfield and analysed images under each condition at 0 hours and 18 hours. After 18 hours, DMSO treated MDA-MB-231 cells left a cell free gap of 34% whereas PDD treated cells had a larger gap that remained (67%), suggesting cell migration was reduced by PDD ($p<0.01$) (Figure 3.8C).

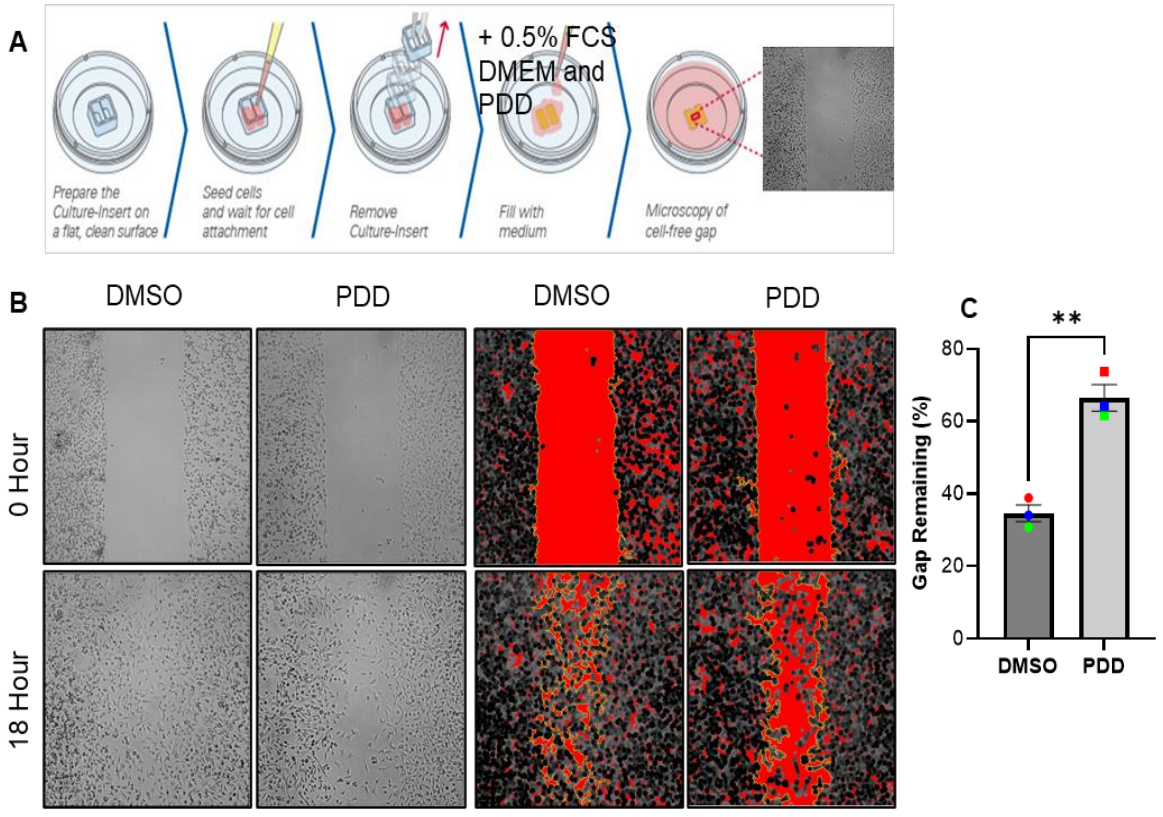

Figure 3.8. **PARGi (PDD) reduces bilateral migration of MDA-MB-231 cells into a cell free area.** Legend overleaf.

Figure 3.8 **PARGi (PDD) reduces bilateral migration of MDA-MB-231 cells into a cell free area.** (A) schematic diagram depicting the principal of the assay from Ibidi. Briefly, the culture well insert was placed into a 6 well dish. Cells were seeded and left to adhere. Culture well was removed. Media was replaced with 0.5% FCS DMEM and 0.3 µM PDD. Images at the 0-hour time point were captured along the length of the cell free gap. This was repeated after 18 hours. An average area that remained was recorded using imagej and the % of the gap that remained after 18 hours relative to the 0-hour time point was calculated. (B) Representative images of DMSO or PDD treated cells at 0 or 18 hours with or without (brightfield) the ImageJ analysis performed to record the area. (C) The percentage of the gap that remained after 18 hours when cells were treated with DMSO or PDD (0.3 µM). An unpaired t-test reported a statistically significant increase in the gap that remained when cells were treated with the PARGi (PDD). This suggests migration was impaired. ** denotes p=≤0.01. Mean -/+ SEM.

3.2.8.2 Random Non-Directional Single Cell Migration

Live cell imaging was performed to assess individual MDA-MB-231 random cell movement over a 2.5-hour period with images taken every 15 minutes. Within each biological repeat, 30 cells were monitored equating to 90 cells across three biological repeats. The trajectory plots show 30 representative routes taken by cells under DMSO or PDD treated conditions over 2.5 hours (Figure 3.9A).

The accumulated distance (AD) is the total distance travelled by a cell along the whole length of the black line depicted within the trajectory plots. When all the cells from each biological repeat were pooled, control DMSO treated cells had an average AD of 46.75 µm (Figure 3.9B). A statistically significant reduction in AD was observed when MDA-MB-231 cells were treated with PDD which possessed an average AD of 18.66 µm (Figure 3.9B). The average AD of each biological repeat has also been plotted and was statistically different (Figure 3.9C).

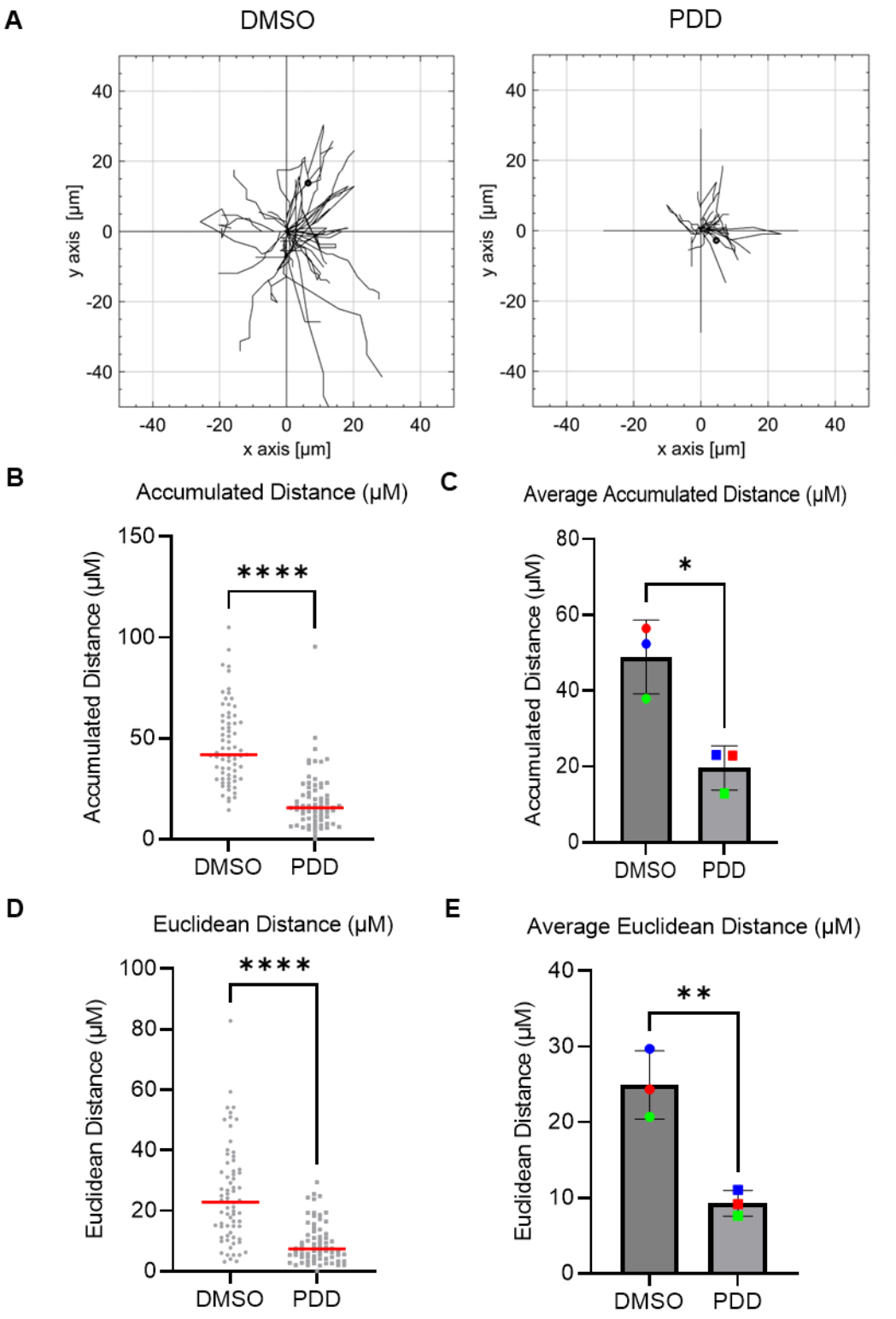

Figure 3.9. **PARGi (PDD) impedes random non-directional MDA-MB-231 cell migration by live cell analysis.** Legend overleaf.

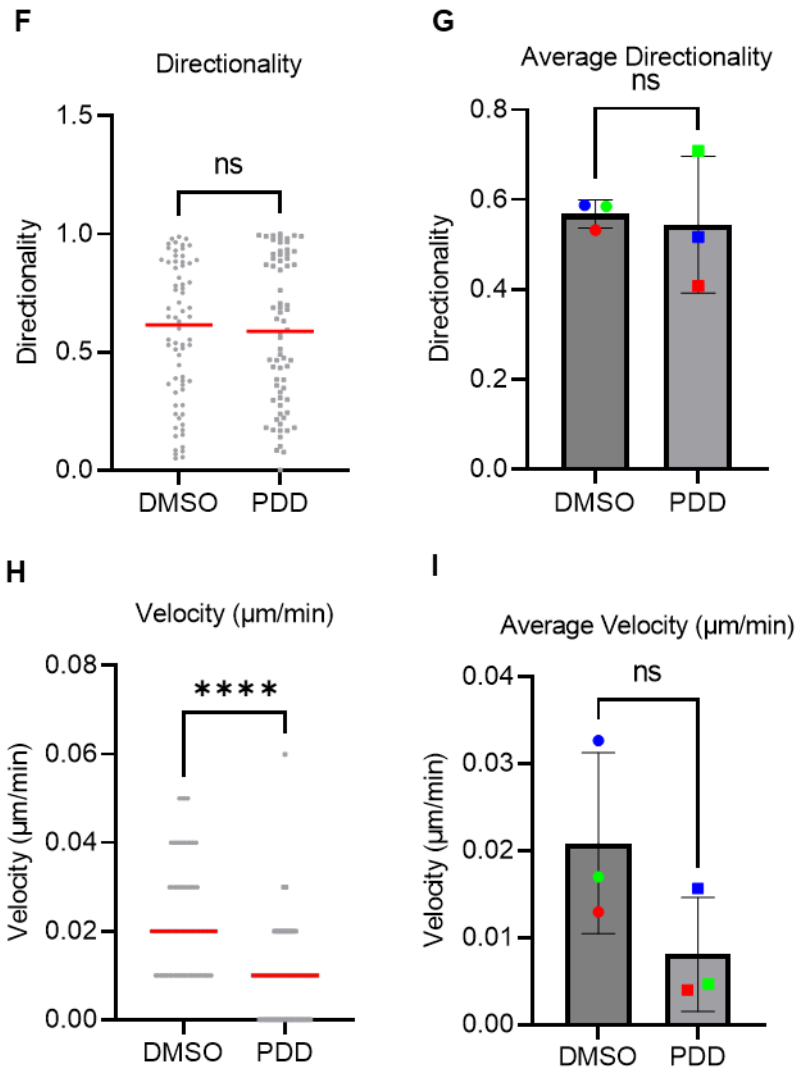

Figure 3.9 **PARGi (PDD) impedes random non-directional MDA-MB-231 cell migration by live cell analysis.** (A) Trajectory plots that tracks individual cell movement of 30 cells within one biological repeat when cells were treated with DMSO or PDD. (B) Pooled data from 3 independent biological repeats of accumulated distance (µm). (C) Average accumulated distance (µm) of each biological repeat. (D) Pooled data from 3 independent biological repeats of euclidean distance (µm). (E) Average euclidean distance (µm) of each biological repeat. (F) Pooled data from 3 independent biological repeats of directionality. (G) Average directionality of each biological repeat. (H) Pooled data from 3 independent biological repeats of cell velocity (µm). (I) Average cell velocity (µm) of each biological repeat. Pooled data depicts the median. Average data depicts mean -/+ SD. Statistical testing was by Mann-Whitney for pooled data and unpaired t-test for averages. **** denotes p=≤0.0001, ** denotes p=≤0.01, * denotes p=≤0.05, NS denotes no statistical significance. The NS P-values were 0.77 (F), 0.8 (G) and 0.15 (I).

The Euclidean distance (ED) is the direct distance between the start and end point of a cells AD. When all the cells from each biological repeat were pooled, control DMSO treated MDA-MB-231 cells had an average ED of 25.09 µm and PDD treated cells exhibited a statistically significant reduction in ED with an average of 9.3 µm (Figure 3.9D). The average ED of each biological repeat has also been plotted and was statistically different (Figure 3.9E).

The directionality is the ratio of the AD and ED. The greater the concordance, the greater degree of linearity a cell will exhibit in its migration pattern i.e. a ratio of 1 will translate to a cell having moved in a completely straight line. When all the cells from each biological repeat were pooled, control DMSO treated MDA-MB-231 cells had an average directionality of 0.57 and PDD treated cells had an average directionality of 0.58 (Figure 3.9F). There was no statistical difference (Figure 3.9F). The average of each biological repeat's directionality is also depicted (Figure 3.9G) and interestingly, the standard error of the mean was greater in the PDD condition compared to the DMSO. This was not seen in other measures of migration (AD, ED) and a lack of statistical difference may have been observed due to how little distance was travelled in PDD treated cells.

The velocity of the pooled DMSO data set on average was 0.023 µm/min (Figure 3.9H). The velocity of the pooled PDD data set was on average 0.009 µm/min (Figure 3.9H). PDD pooled velocity was reduced statistically significantly compared to the pooled DMSO data set (Figure 3.9H). The averages of each biological repeat were also plotted (Figure 3.9I) and in this case here, there was no statistical difference (Figure 3.9I).

3.2.8.3 Depletion of PARG reduces migration of MDA-MB-231 cells and in this context PARG inhibition cannot further reduce migration

To confirm the on-target effects of PDD, the impact of siRNA mediated PARG depletion on migration was investigated using live cell imaging. Depletion of PARG was confirmed by western blotting (Figure 3.10A&B).

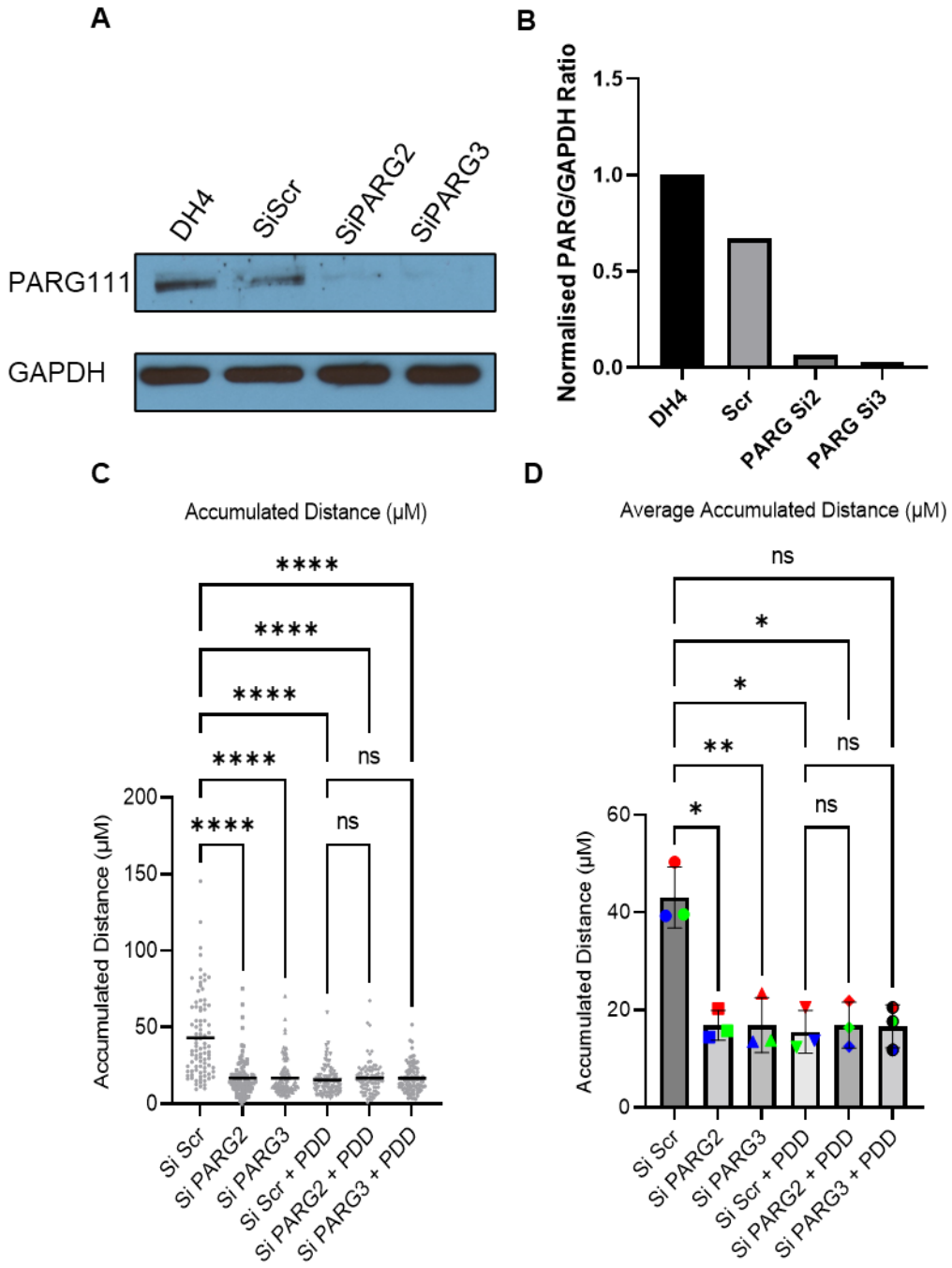

Figure 3.10. **Depletion of PARG reduces MDA-MB-231 cell migration and is not enhanced with a PARGi.** Legend overleaf.

Figure 3.10 **Depletion of PARG reduces MDA-MB-231 cell migration and is not enhanced with a PARGi.** (A) Western blot confirming depletion of PARG with two separate PARG targeting siRNA (siPARG2 and siPARG3). (B) Densitometry plot quantifying the relative differences in PARG adjusted for GAPDH loading. (C) Pooled data from 3 independent biological repeats of accumulated distance (µm). siPARG2 and siPARG3 relative to siScr was statistically reduced. SiScr + PDD was statistically reduced relative to siScr, as was siPARG2+PDD and siPARG3+PDD. Notably however, the medians of all test conditions were similar and siPARG2+PDD and siPARG3+PDD was not significant relative to siScr+PDD. (D) Average accumulated distance (µm) of each biological repeat under each test condition. Same comparisons as described above apply however siScr vs siPARG3+PDD was not statistically significant. . Pooled data depicts the median. Average data depicts mean -/+ SD. Statistical testing was by Kruskal-Wallis test for pooled data and 1-way ANOVA for averages. **** denotes p=≤0.0001,** denotes p=≤0.01, * denotes p=≤0.05, NS denotes no statistical significance. The NS P-values for Si Scr+PDD relative to SiPARG 2 and SiPARG3 were both >0.99 (C) and 0.99 (D).

To demonstrate that depletion of PARG phenocopied PARG inhibition, PARG was depleted for 24 hours prior to re-seeding at low density and live cell imaging as performed previously. When all biological repeats were pooled together, cells treated with control Scrambled siRNA had an average AD of 43.14 µm, consistent with DMSO treated cells above and suggesting control siRNA has no effect on migration (Figure 3.10C). Two separate PARG targeting siRNA (SiPARG2 and siPARG3) transfected cells had an average AD of 16.84 and 16.9 µm respectively, which was statistically different and reduced relative to the control condition (Figure 3.10C).

Furthermore, all transfection conditions were treated with PDD in parallel. As expected in the control cells (scrambled siRNA) cells, treatment with PDD significantly reduced the AD from 43.14 µm to 15.53 µm (Figure 3.10C). In contrast, PDD did not significantly alter the AD in PARG depleted cells ((AD of 16.84 vs. 16.93 and 16.9 µm vs 16.67 µm in PARG2 siRNA and PARG3 siRNA transfected cells respectively) (Figure 3.10C)). The average accumulated distance of each biological repeat is also displayed (Figure 3.10D). Thus, the reduction of migration induced by PARG depletion is not enhanced by PARG inhibition.

Taken together, the data above (3.2.8) suggest that low levels of PARG or inhibition of PARG can reduce the migration of MDA-MB-231 cells and by implication that PARG plays an important role in promoting migration.

3.2.9 Inhibition of PARP1-3 or Tankyrase reduces migration of MDA-MB-231 cells

The two types of migration assay used to assess the effects of PARG inhibition/deletion were repeated with Olaparib and TE92. In each case, the same conditions as for PDD were used.

In culture well assays DMSO treated MDA-MB-231 cells had a cell free gap of 44 % (Figure 3.11). In comparison, olaparib and TE92 treated cells retained gap sizes of 72 % and 68 % respectively (Figure 3.11). This suggests olaparib and TE92 reduced cell migration and by implication, PARP1-3 and TNKS1/2 have roles in promoting migration.

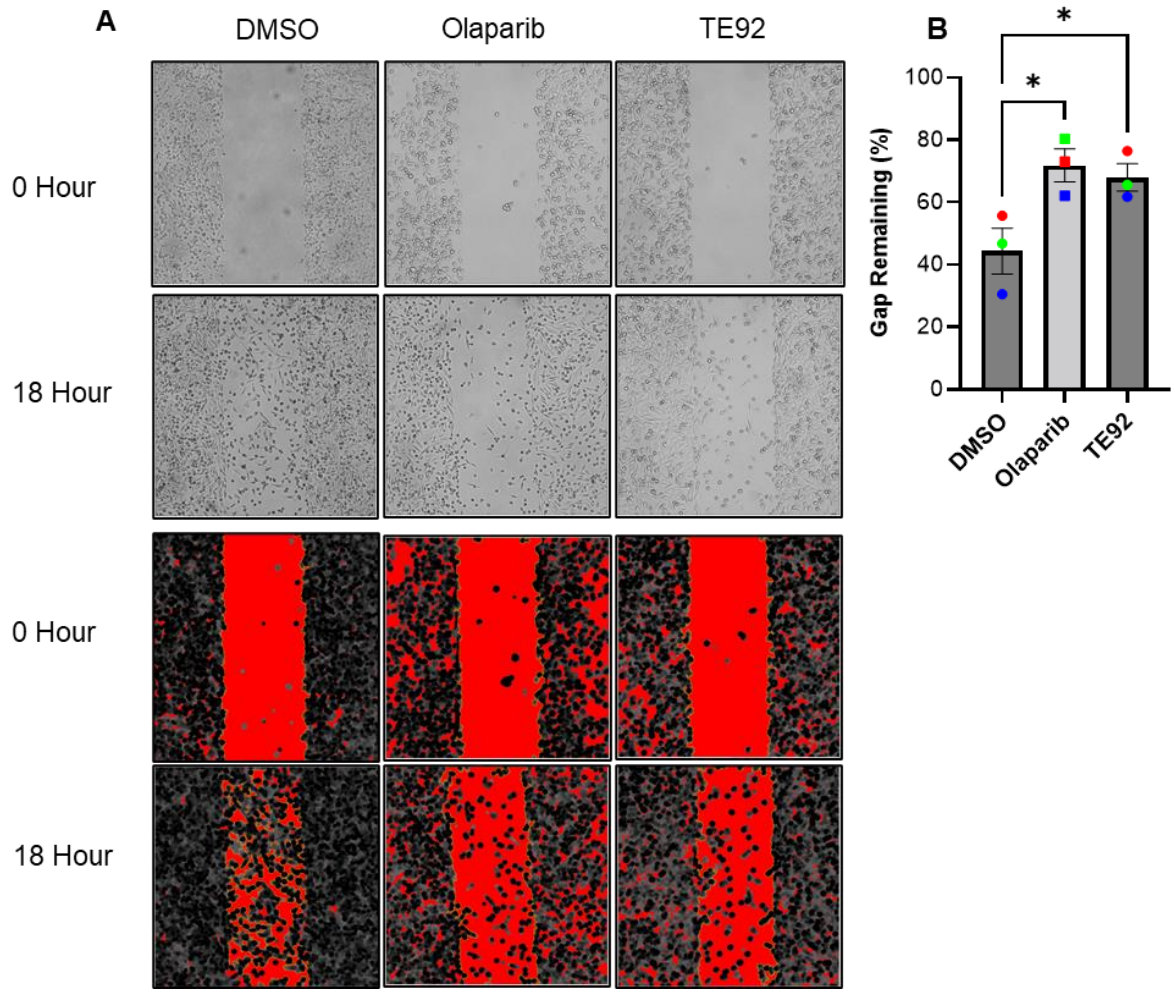

Figure 3.11. **PARP1-3i and TNKSi reduces bilateral migration of MDA-MB-231 cells into a cell free area.** Legend overleaf.

Figure 3.11 **PARP1-3i and TNKSi reduces bilateral migration of MDA-MB-231 cells into a cell free area.** (A) Representative images of DMSO or treated cells at 0 or 18 hours with or without (brightfield) the imagej analysis performed to record the area. (B) The percentage of the gap that remained after 18 hours when cells were treated with DMSO, Olaparib (0.5 µM) or TE92 (0.1 µM). An one-way ANOVA reported a statistically significant increase in the gap that remained when cells were treated with Olaparib and TE92. This suggests Olaparib and TE92 impair MDA-MB-231 migration. * denotes p=≤0.05. Mean -/+ SD.

In live cell imaging AD was significantly reduced with olaparib and TE92 compared to DMSO control (19.38 and 17.88 µm compared to 46.75 µm respectively in pooled data) (Figure 3.12A&B). The average AD of each biological repeat has also been plotted and showed a significant difference (Figure 3.12C). Likewise, ED was significantly reduced by either inhibitor, olaparib or TE92 (pooled data - 11.95 and 9.7 µm respectively compared to 25.09 µm) (Figure 3.12D). The average ED of each biological repeat has also been plotted and was also significantly different to DMSO control (Figure 3.12E). There was no statistical difference in directionality between DMSO and either olaparib or TE92 (Figure 3.12F), although in each of the biological repeats there was a small increase in average directionality compared to DMSO control (Figure 3.12G).

The velocity of the pooled DMSO data set on average was 0.023 µm/min (Figure 3.12H). The velocity of the pooled olaparib and TE92 data set was on average 0.01 and 0.008 µm/min respectively (Figure 3.12H). Olaparib and TE92 pooled velocity was statistically significantly different compared to the pooled DMSO data set (Figure 3.12H). The averages of each biological repeat were also plotted (Figure 3.12I). The average of the velocity for the DMSO data set was 0.02 µm/min (Figure 3.12I). For olaparib and TE92, it was 0.009 and 0.007 µm/min respectively (Figure 3.12I). They were not statistically different compared to the DMSO condition (Figure 3.12I).

Taken together, the data suggests that low levels of PARP1-3 or TNKS1/2 activity can reduce the migration of MDA-MB-231 cells and by implication that PARP1-3 and TNKS1/2 play an important role in promoting migration.

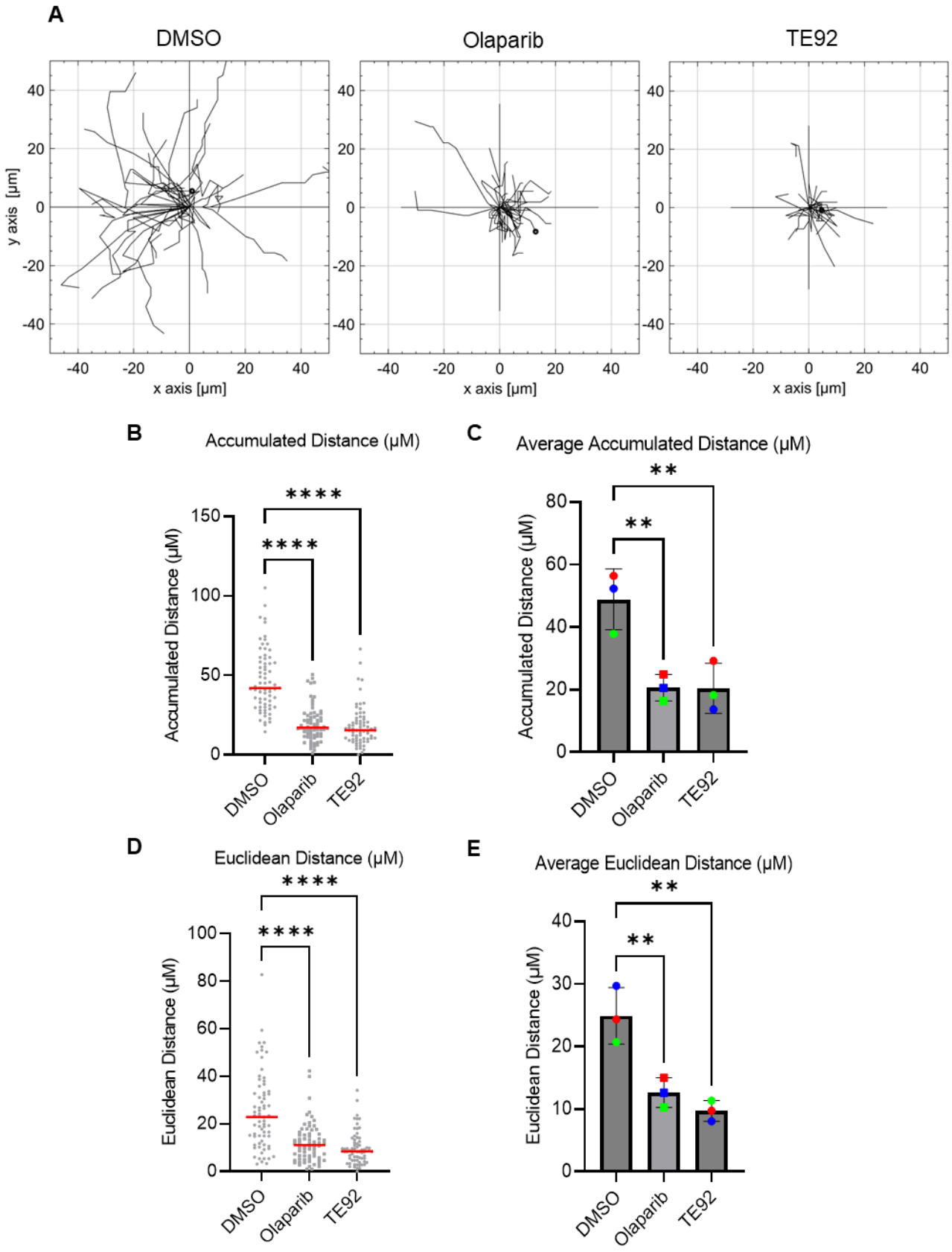

Figure 3.12. **PARP1-3i and TNKSi impedes random non-directional MDA-MB-231 cell migration by live cell analysis.** Legend overleaf.

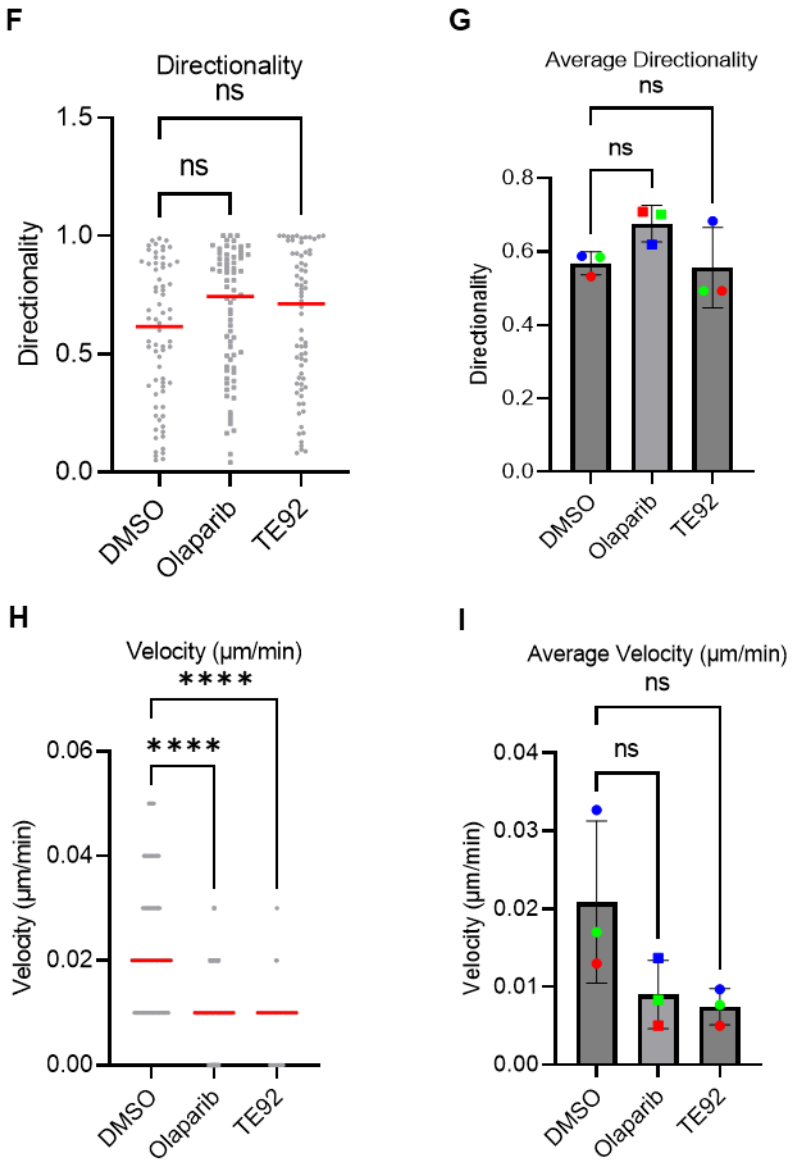

Figure 3.12 **PARP1-3i and TNKSi impedes random non-directional MDA-MB-231 cell migration by live cell analysis.** (A) Trajectory plots that tracks individual cell movement of 30 cells within one biological repeat when cells were treated with DMSO, Olaparib or TE92. (B) Pooled data from 3 independent biological repeats of accumulated distance (µm). (C) Average accumulated distance (µm) of each biological repeat. (D) Pooled data from 3 independent biological repeats of euclidean distance (µm). (E) Average euclidean distance (µm) of each biological repeat. (F) Pooled data from 3 independent biological repeats of directionality. (G) Average directionality of each biological repeat. (H) Pooled data from 3 independent biological repeats of cell velocity (µm). (I) Average cell velocity (µm) of each biological repeat. Pooled data depicts the median. Average data depicts mean -/+ SD. Statistical testing was by Kruskal-Wallis test for pooled data and 1-way ANOVA for averages. **** denotes p=≤0.0001, ** denotes p=≤0.01, NS denotes no statistical significance. The NS P-values were 0.18 and 0.33 (F), 0.19 and 0.97 (G) and 0.12 and 0.08 (I) for Olaparib and TE92 respectively.

3.3 Discussion

In this chapter, we present evidence that PARPi, TNKSi and PARGi do not impact MDA-MB-231 adhesion to fibronectin and Matrigel. We also showed that PARGi reduces MDA-MB-231 cells capacity to invade through Matrigel. Finally, we also demonstrated that PARPi, TNKSi and PARGi reduce MDA-MB-231 migration – single cell random migration and bi-directional migration to fill a cell free area. The anti-migration phenotype of PARGi was validated with 2 siRNA against PARG using the live cell single cell random migration.

3.3.1 Inhibiting PARP1-3 Reduces MDA-MB-231 Migratory Capabilities

Olaparib (0.5 μM) reduced migration of MDA-MB-231 cells *in vitro* after 18 hours using a culture well insert to create a gap that the cells could bi-directionally fill. Olaparib at this dose did not impact the cell cycle or proliferation during the duration of the migration assay. Additionally, a dose with 0.9< survival fraction was used, and the dose was sufficient to deplete α-PAR signal via western blot and total levels of PARP1 and PARG111 were unaffected. This suggests the observed anti-migratory effects are not artifacts of cytotoxicity or proliferation but a consequence of PARP1-3 inhibition. Dutta et al., (2020) reported a reduction in cell migration of MDA-MB-231 cells using the PARPi PJ34 (20 μM) and a scratch wound assay after 10 hours. Proliferation was unlikely to be affected during this time frame, however PJ34 at 20 μM is cytotoxic and causes off-target anti-mitotic effects so it's difficult to conclude if it was the inhibition of PARP1-3 that caused the reduction in migration (Madison et al., 2011). Increasing doses of Olaparib were administered to capan-1 pancreatic cells over 214 days (Ye Han et al., 2019). They acquired a resistance to PARPi and exhibited enhanced migratory capability. They monitored migration using an uncoated transwell assay with a chemotactic gradient. Whilst the chemotactic variant is a confounding variable, it would be interesting to observe the same experiment performed in a breast cancer setting. We observed a reduction in random single cell migration using live cell

analysis. Live cell analysis examining the effects of Olaparib on MDA-MB-231 migration has not been performed. Whilst a statistically significant reduction in AD, ED and velocity was observed with Olaparib, directionality was not statistically different. However, the directionality increases in the treatment condition and follows the same trend across each biological repeat. If the experiment was performed for longer or there was a chemotactic gradient driving migration, perhaps a statistically significant difference could be observed. The impact of PARPi on cancer polarity signalling is not well studied and warrants further research. The previously published data and our data imply that PARP1-3 play a role in migration that can be attenuated by PARPi.

3.3.2 Inhibiting TNKS1/2 Reduces MDA-MB-231 Migratory Capabilities

TE92 is a recently developed highly potent inhibitor that has dual activity against TNKS1/2 (Nathubhai et al., 2017). TE92 (0.1 µM) reduced bi-directional migration of MDA-MB-231 cells into a cell free gap. Live cell imaging confirmed anti-migratory effects of TE92. TE92 at this dose did not alter cell cycle progression or proliferation. Additionally, a dose with >0.9 survival fraction was used, although α-PAR signal was not altered, the dose was sufficient to stabilise TNKS1/2. Total levels of PARP1 and PARG111 were unaffected. We choose to use TNKS1/2 stabilization as a marker for drug activity as tankyrase autoPARylation targets it for proteasomal degradation (Callow et al., 2011). This suggests the observed anti-migratory effects are not artifacts of cytotoxicity or proliferation but a consequence of TNKS1/2 inhibition. As well as revealing a potential therapeutic outlet for TNKSi, the data suggest that TNK1/2 likely play a role in promoting cell migration. We can speculate that TNK1/2 regulates migration via one of its TIP's. Particularly those with known roles in migration, such as β-catenin for example.

TE92 has not previously been investigated for its anti-migratory applications. However, consistent with our findings, the TNKSi XAV939 (5 µM) reduced MDA-MB-231 Wnt3a

mediated cell migration in a scratch wound assay (Bao et al., 2012). In our model, we did not use Wnt3a complemented media and despite this, we observed the same anti-migratory effect with a different TNKSi. Possible explanations for this include genetic drift between cell line batches or the presence of death signals and cell debris that is formed during the act of creating a cell free area with a scratch wound assay. Another possibility is differences in off-target effects between TE92 and XAV939. In addition, compared to our data, the dose of XAV939 used was reported cytotoxic resulting in approximately 50% survival (Bao et al., 2012). Nevertheless, the previously published data and our data imply that TNKS1/2 play a role in migration, warranting further study and justifies further elucidating the relationship between TNKS1/2 and migration and the role Wnt ligands play in this context.

3.3.3 Inhibiting PARG Reduces MDA-MB-231 Migratory and Invasion Capabilities

PDD00017273 (PDD) is a recently developed specific, cell permeable PARG inhibitor that is not suitable for in vivo work due to its low bioavailability (D. I. James et al., 2016). Here we demonstrate that PDD can reduce migration of MDA-MB-231 cells into a cell free gap and reduce single cell migration using live cell imaging. We used a dose of PDD (0.3 µM) that does not impact cell cycle progression or proliferation and allows ≥90% survival. We confirmed this was an effective dose of PARGi by observing increased α-PAR signal on western blots. Total levels of PARP1 and PARG111 were unaffected. This is consistent with the effective non-toxic inhibitory dose reported by Gravells et al., (2018). This suggests the observed anti-migratory effects seen here are not artifacts of cytotoxicity or proliferation but a consequence of PARG inhibition. One other study has explored cell migration following pharmacological inhibition of PARG (Matanes et al., 2021). They also saw reduced migration, however high cytotoxic doses were used (2 µM and 5 µM), making it difficult to conclude whether the anti-migratory effect was due to the inhibition of PARG per se or due to cytotoxicity or other off-target effects. We also validated the migratory effects of PARGi by depleting MDA-MB-231 cells of PARG111. Pleasingly, PARG depletion also reduced migration. Addition of PDD to PARG depleted cells did not further reduce migration

compared to depletion alone implying the effect of PDD was via inhibition of PARG111. Our data is consistent with another study where migration was inhibited when PARG111 was depleted in MD-MB-231, this time using shRNA (Marques et al., 2019). It is also consistent with PARG depletion reducing cell migration and invasion in colon cancer cells (Fauzee et al., 2012; Q. Li et al., 2012) and HCC cell lines (Mincheng Yu et al., 2022) *in vitro*. Our data is the first reported investigation of PARGi in the context of invasion, however the result is consistent with depletion of PARG reducing MDA-MB-231 invasion through Matrigel (Marques et al., 2019). It should be noted however since a PDD Matrigel free condition was not performed in parallel, the results could be a consequence of the anti-migratory effects of inhibiting PARG using PDD.

The discussed published data and our data, provide evidence of PARG being a viable drug target and that by implication, inhibiting PARG can attenuate PARG's role in driving migration and invasion.

3.3.4 Limitations

The adhesion studies were not performed with a negative wash control or a positive control. Therefore, it's possible the washes were not vigorous enough to dislodge the cells hence why differences were not observed. Scratch wounds assay leave behind cellular debris and activate death signalling pathways and the release of cytokines. Culture wells do not have these confounding variables, but performing both in parallel can provide additional insights into drug function. Furthermore, our live cell analysis was performed without a chemokine gradient, so the cells are said to be moving randomly. Absent the gradient to compare along an axis and in instances where migration is reduced, longer experimental time frames maybe required to examine the effects of the drugs on cell directionality. The invasion assay requires a PDD matrigel free condition to account for the anti-migratory effects of the drug. If it was performed, the percentage of cells whose migration was reduced could be factored into the analysis providing a more accurate insight into the effects of PDD on invasion.

Chapter 4.0 Results: Evaluation of PARG inhibitions anti-migratory phenotype mechanism in vitro

4.1 Introductions, aims and hypotheses

Chapter 3 demonstrated that both PARGi and PARPi disrupted cell migration. Here we set out to understand how PARGi is altering migration. Understanding the mechanism by which PARG inhibition reduces cellular migration is important for a few reasons. Metastasis accounts for approximately 90% of cancer related death (Spano et al., 2012) and is an underutilised facet of combating tumour biology (Anderson et al., 2019). Effective therapies against metastasis are urgently needed. Refining our understanding of how PARG inhibition impedes migration may lead to exploitable biomarkers within tumour sub-populations. Furthermore, metastasis is a complex multifaceted process. Developing multifaceted treatment regimens are thus likely required. Insight into PARG inhibitions cellular effects could lead to rationalized combination strategies with the goal of improving effectiveness. This second results chapter will address some of these mechanisms using MDA-MB-231 cells as a model cell line.

The hypothesis of this chapter is PARGi will affect multiple migration associated areas of biology.

The aims of this chapter are to:

1. Establish if the anti-migratory effects of PARG inhibition are contingent on PARP1-3/Tankyrase activity
2. Determine the significance of metabolism in PARG inhibitions anti-migratory effects
3. Visualise and semi-quantify the effect of PARG inhibition on the cytoskeleton and nuclear envelope
4. Understand the effect of PARG inhibition on mechano-sensing pathways
5. Examine the effect of PARG inhibition on expression of migration promoting proteins

4.2 Results

4.2.1 β-NMN supplementation or co-treatment with PARP or Tankyrase inhibitors, restores MDA-MB-231 cell movement following PARG inhibition with PDD.

The accumulated distance (AD) of MDA-MB-231 cells was recorded using live cell imaging as described in chapter 3. Initially, the effect β-NMN in combination with either PDD or Ola was tested (Figure 4.1). Cells were pre-treated with β-NMN for 1 hour after which PDD or Ola were added. As seen previously both PDD and Ola significantly reduced the AD compared to DMSO control. Supplementation of PDD with β-NMN restored cell migration to control levels while it had no effect in cells treated with Olaparib. β-NMN alone had no effect on AD.

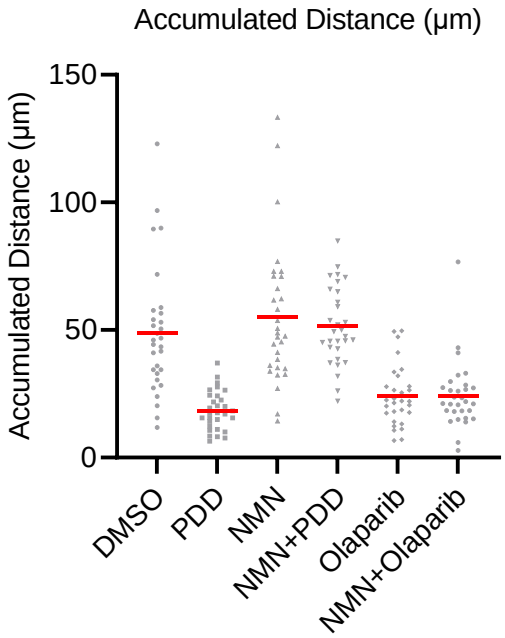

Figure 4.1. **β-NMN rescues PARGi but not PARPi anti-migration phenotype.** MDA-MB-231 cells were imaged for 2.5 hour following treatment as indicated and where cells were supplemented with NMN pre-incubation, it was for 1 hour. This was one biological repeat and consists of 30 cells. Due to sample size and lack of repeats, no statistical analysis was performed.

After this preliminary experiment, 3 independent repeats of the β-NMN + PDD experiment were performed (figure 4.2 A/B). In addition, the effects of combinations of Ola+PDD and TE92+PDD were tested in parallel (Figure 4.2 A/C/D).

There was no statistical difference between any conditions in the averaged data (figure 4.2A). However, there was statistical differences in the pooled data and for simplicity, the three observations have been split into three separate graphs but the statistics depicted are derived from testing done in parallel (figure 4.2 B/C/D).

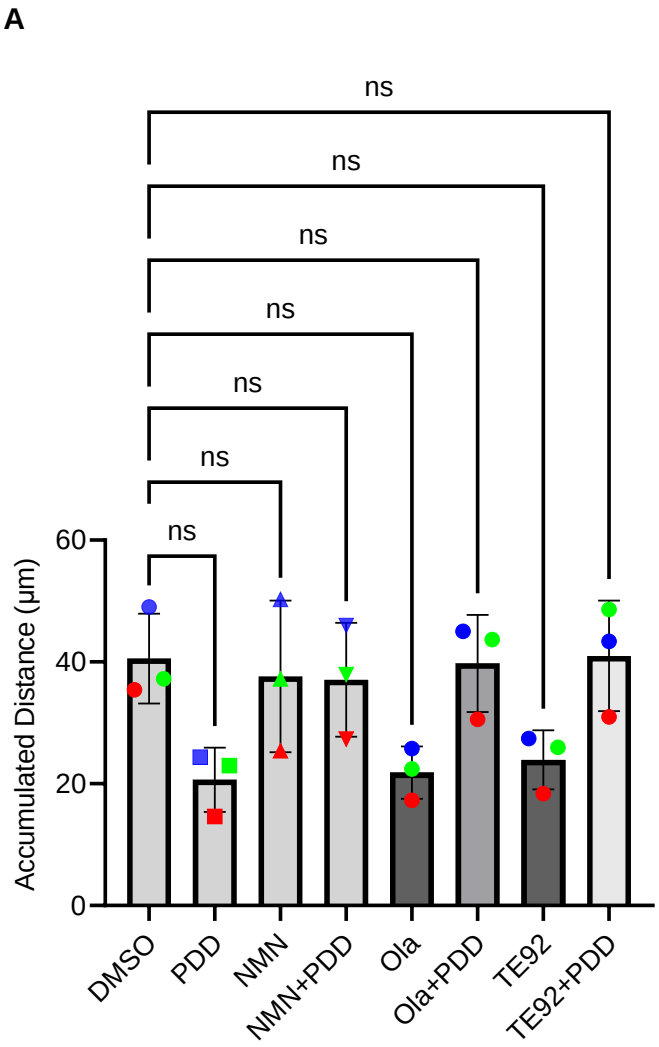

Figure 4.2. **Anti-migration effects of PARGi (PDD), PARPi (Ola) and TNKSi (TE92) are rescuable.** Legend overleaf plus one.

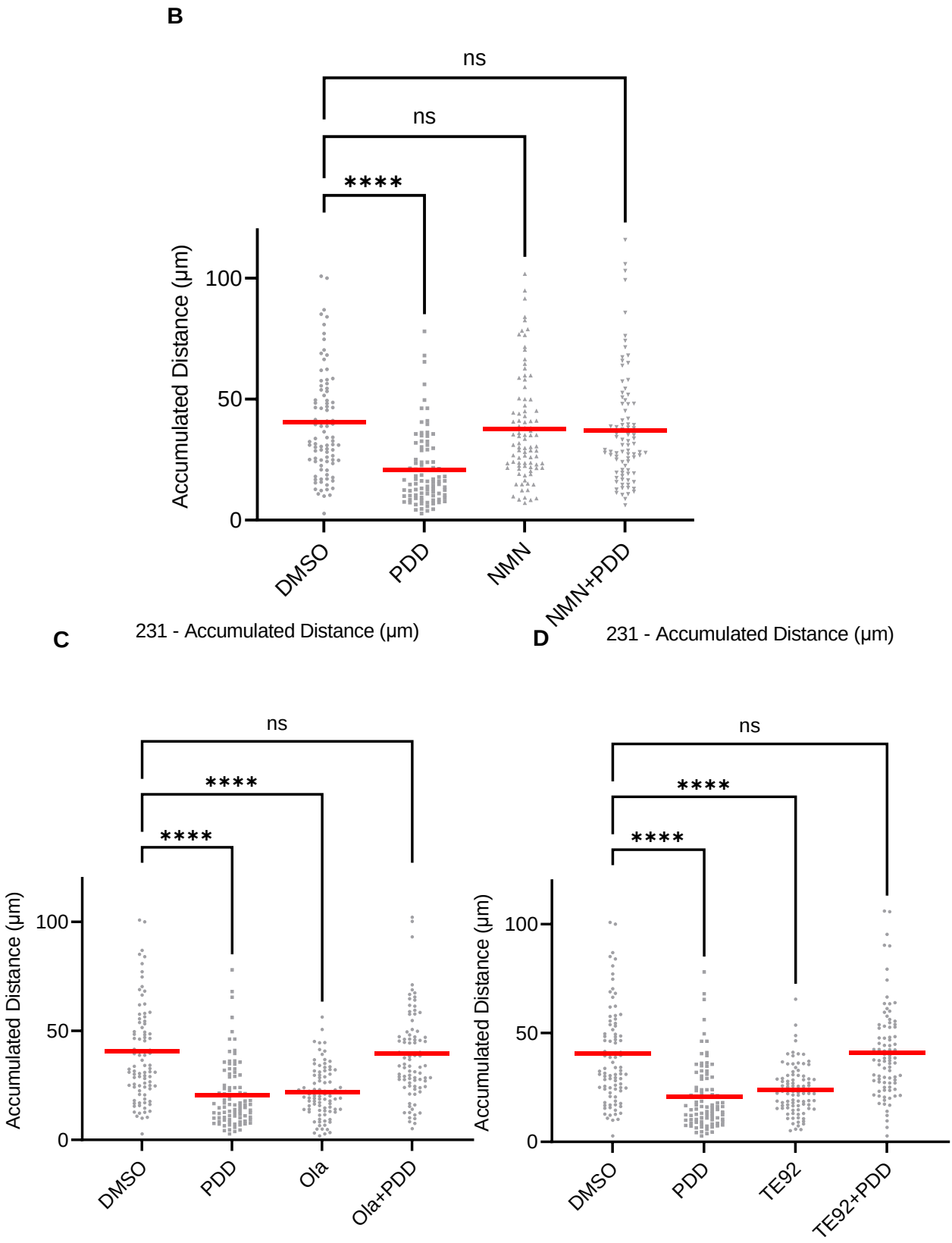

Figure 4.2. **Anti-migration effects of PARGi (PDD), PARPi (Ola) and TNKSi (TE92) are rescuable.** Legend overleaf.

Figure 4.2 **Anti-migration effects of PARGi (PDD), PARPi (Ola) and TNKSi (TE92) are rescuable.** MDA-MB-231 cells were imaged for 2.5 hour following treatment as indicated, where cells were supplemented with NMN pre-incubation, it was for 1 hour, while combinations of inhibitors were added simultaneously and imaged. For each independent biological repeat 30 cells were imaged. (A) Average of each biological repeat under all conditions. The same data but pooled is depicted in three separate graphs to aid comparisons. Statistical significance observed when test in parallel depicted. (B) Pooled data showing the effects of β-NMN supplementation rescuing the anti-migration effects of PARGi via PDD. (C) Co-treatment of MDA-MB-231 cells with PDD and Olaparib restores migration. (D) Co-treatment of MDA-MB-231 cells with PDD and TE92 restores migration. For pooled data the line represents the median. For averages mean and SD are shown. Statistical testing was by Kruskal-Wallis test for pooled data and an one-way ANOVA for averages, **** denotes p=≤ 0.0001. NS denotes no statistical significance. The NS P-values were 0.15, 0.99, 0.92, 0.11, >0.99, 0.2 and >0.99 for the respective conditions (A), both >0.99 (B), >0.99 (C) and >0.99 (D).

The β-NMN supplementation assay yielded the same results as the preliminary result above. Control DMSO treated cells had an average AD of 40.97 µm (figure 4.2B). Addition of PDD caused a statistically significant reduction in AD, which on average had an AD of 21.02 µm. β-NMN alone (average AD of 38.02 µm) had no effect on AD compared to DMSO control and β-NMN+PDD resulted in an average AD of 37.25 µm which was also non-significant when compared to the control. These data indicate that supplementation with β-NMN can rescue PDD induced inhibition of cell movement but has no effect on Olaparib induced inhibition of cell movement.

PDD, Olaparib and TE92 alone treated conditions exhibited a statistically significant reduction in AD when compared to the DMSO control (21.02 µm, 22.29 µm and 23.34 µm respectively) (Figure 4.2C/D). However, Olaparib+PDD and TE92+PDD did not exhibit a statistically significant reduction in AD when compared to the DMSO control (39.37 µm and 41.08 µm respectively), suggesting that cell migration had been restored (Figure 4.2C/D). This suggests that a ratio between PARP/TNKS and PARG activity is required to facilitate efficient cell movement and an imbalance in that ratio can impede cell movement.

4.2.2 The anti-migratory effects of the *in vivo* PARG inhibitor COH34 are rescued with β-NMN pre-treatment in MDA-MB-231 cells

COH34 is a recently developed PARG inhibitor suitable for *in vivo* use (S.-H. Chen & Yu, 2019). Clonogenic survival assays determined the toxicity of COH34 (Figure 4.3A), with doses up to 10 nM resulting in ≥0.9 survival fraction. Western blotting demonstrated that 0.1, 1 and 10 nM COH34 produced an increase in PAR signal relative to the DMSO control (Figure 4.3B), however this was modest compared to the standard PDD dose used in this thesis. Olaparib was also used as a control and as expected, it decreased the PAR signal relative to the DMSO control. From these data, doses of 0.1, 1 and 10 nM were chosen to investigate cell migration.

These doses were used in live cell analysis, with paired β-NMN pre-treatment conditions (figure 4.3C/D). The DMSO average AD was 42.07 μm and the β-NMN alone average AD was 38.61 μm and was not significantly different compared to the DMSO control (figure 4.3C). All three COH34 doses used in figure 4.3C reduced the AD relative to the DMSO control and were statistically significant. β-NMN pre-treatment followed by the corresponding COH34 dose 1 hr later were not statistically different from the DMSO control (figure 4.3C).

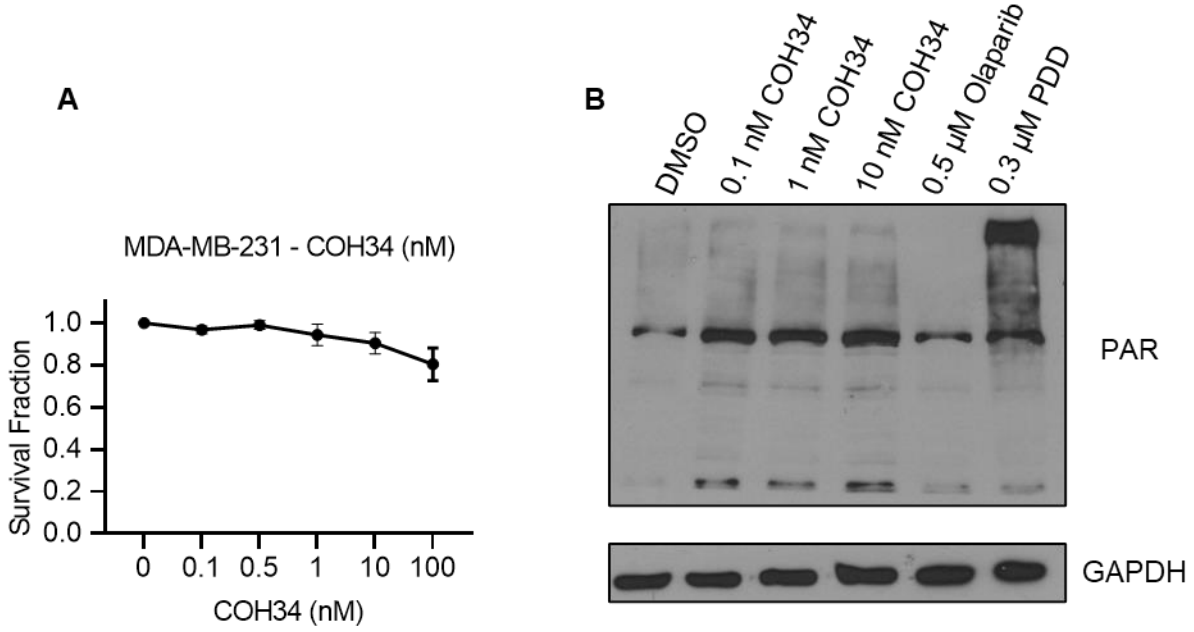

Figure 4.3. **The anti-migration effects of inhibiting PARG and it being rescuable with NMN pre-treatment are observed with the *in vivo* PARGi COH34.** Legend overleaf.

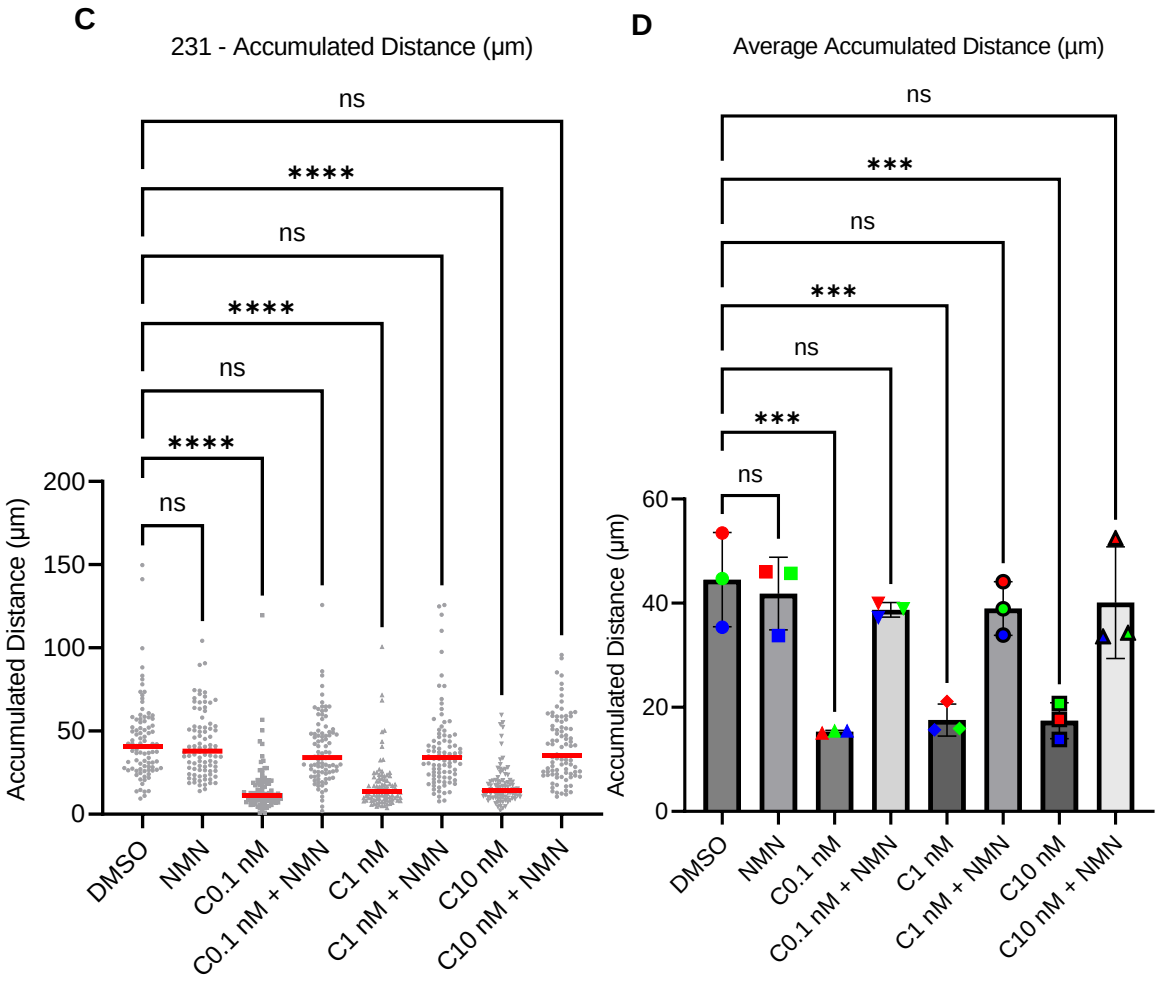

Figure 4.3. **The anti-migration effects of inhibiting PARG and it being rescuable with NMN pre-treatment are observed with the *in vivo* PARGi COH34.** (A) Clonogenic survival assay displaying the relative survival fraction with increasing doses of COH34. (B) PAR Western blot with increasing non-cytotoxic doses of COH34 with Olaparib and PDD as western blot controls. (C) MDA-MB-231 cells were imaged for 2.5 hour following treatment as indicated, where cells were supplemented with NMN pre-incubation, for 1 hour prior to the addition of COH34. For each independent biological repeat 30 cells were imaged. (C) Pooled data from 3 independent repeats of accumulated distance (µm) under all conditions (D) Average of each biological repeat under all conditions. For pooled data the line represents the median. For averages mean and SD are shown. Statistical testing was by Kruskal-Wallis test for pooled data and one-way ANOVA for averages, **** denotes p=≤ 0.0001, *** denotes p=≤ 0.001. NS denotes no statistical significance. The NS P-values were >0.99, >0.99, 0.49 and >0.99 (C) and 0.99, 0.88 0.9 and 0.97 (D) for the NMN, C0.1 nM+NMN, C1 nM+NMN and C10 nM+NMN conditions respectively.

The averaged data of each biological repeat, shows the same trend (figure 4.3D). Thus, the results obtained with PDD were reproduced with a second PARGi and β-NMN supplementation seems to reverse the effects of PARGi on the accumulated distance that MDA-MB-231 cells have travelled.

4.2.3 PARP1 defective mouse embryonic fibroblasts migration behaviour is different in response to PARG, PARP1-3 and Tankyrase inhibitors and β-NMN pre-treatment

PARP1 is generally considered the major PARylation activity in cells. To examine whether the anti-migratory effects seen were PARP1 dependent, we repeated the migration assay with *A19* (WT) and *A11* (PARP-1$^{-/-}$) mouse embryonic fibroblasts (*MEFs)*. Figure 4.4A confirms the PARP1 status of A19 and A11. Unexpectedly, PARG110 was not detected in A11 (figure 4.4A).

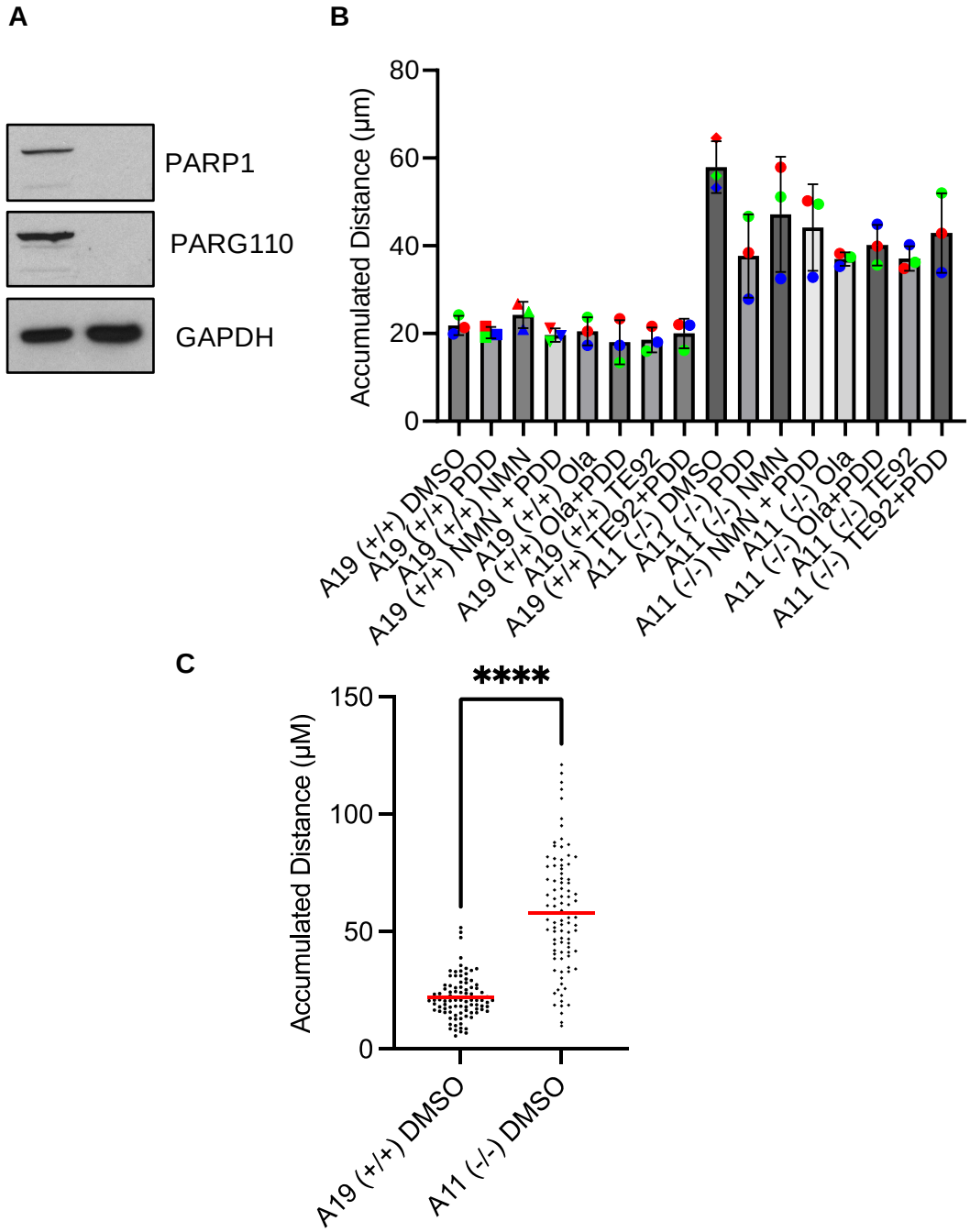

Figure 4.4 **PARP1 defective mouse embryonic fibroblasts migration behaviour is different in response to PARG, PARP1-3 and Tankyrase inhibitors and β-NMN pre-treatment.** Legend overleaf plus one.

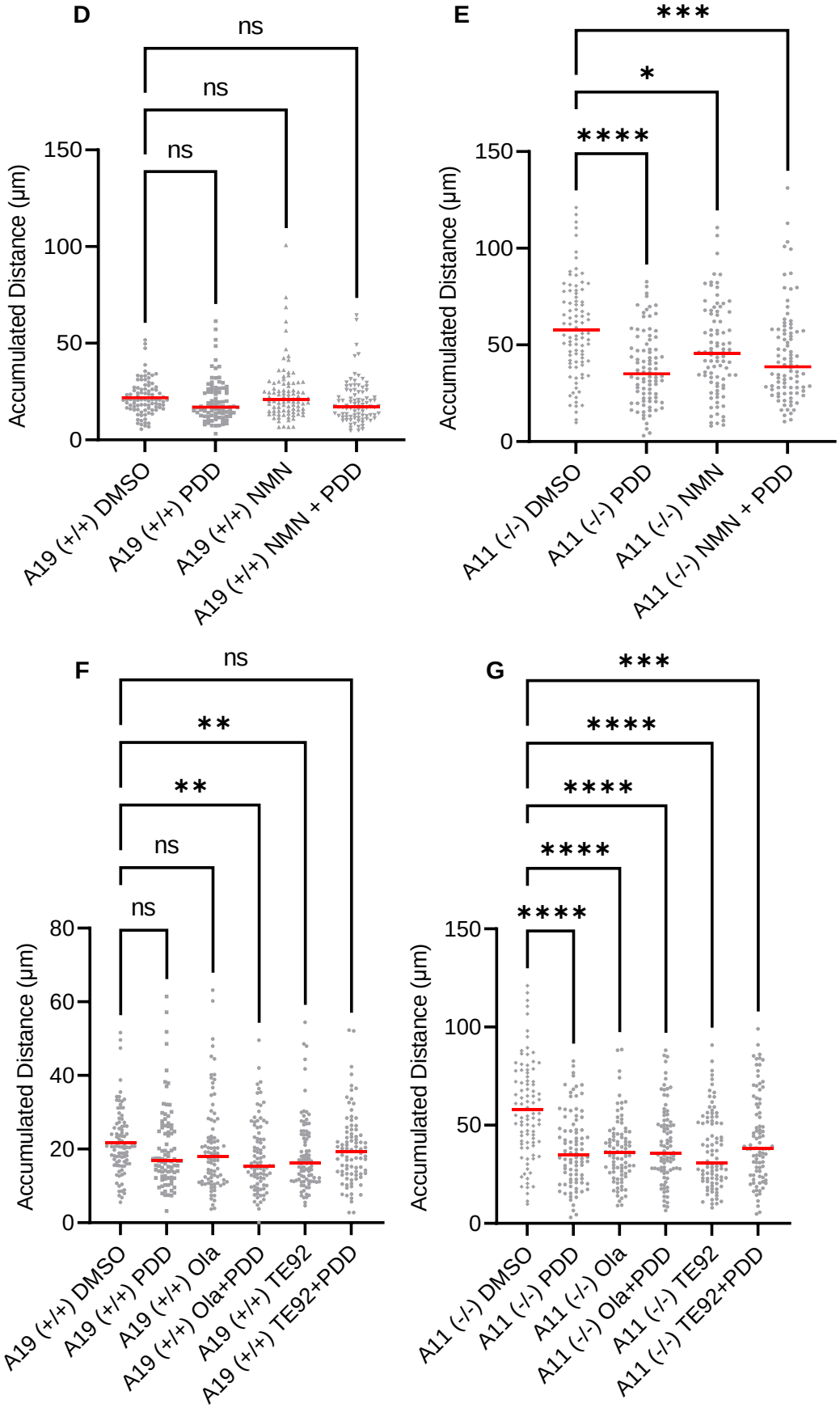

Figure 4.4 **PARP1 defective mouse embryonic fibroblasts migration behaviour is different in response to PARG, PARP1-3 and Tankyrase inhibitors and β-NMN pre-treatment.** Legend overleaf.

Figure 4.4 **PARP1 defective mouse embryonic fibroblasts migration behaviour is different in response to PARG, PARP1-3 and Tankyrase inhibitors and β-NMN pre-treatment.** A19 and A11 cells were imaged for 2.5 hour following treatment as indicated, where cells were supplemented with NMN pre-incubation, it was for 1 hour, while combinations of inhibitors were added simultaneously and imaged. For each independent biological repeat 30 cells were imaged. (A) Confirmation of PARP1 Status of A19 and A11. PARG110 was not detected in the A11 cell line. (B) Average of each biological repeat under all conditions. The rest of the graphs are pooled data from 3 independent repeats of accumulated distance (μm) split up to allow for easier comparisons (C) Untreated A19 and A11 accumulated distance (μm) (D & E) A selection of A19 and A11 NMN and PDD relevant conditions, respectively. (F & G) A selection of A19 and A11 drug combination relevant conditions, respectively. For pooled data the line represents the median. For averages mean and SD are shown. Statistical testing was by Kruskal-Wallis test for pooled data and one-way ANOVA for averages, **** denotes p=≤ 0.0001, *** denotes p=≤ 0.001, ** denotes p=≤ 0.01, * denotes p=≤ 0.05. NS denotes no statistical significance. The NS P-values were 0.12, >0.99 and 0.05 (D) and 0.21, 0.15 and 0.56 (F) for the respective conditions NS was reported.

Figure 4.4B displays all the conditions tested for in parallel using the average of each biological repeat and statistically significant differences were observed. Figure 4.4C-G displays all the conditions tested for in parallel and are pooled from three biological repeats of live cell analysis but split to aid comparison between the relevant conditions.

Unexpectedly A11 (PARP-/-) MEFs migrated faster than A19 (PARP+/+) MEFs which had an average AD 58.7 μm vs. 22.09 μm respectively ($p<0.0001$) (Figure 4.4C). Addition of PDD in wildtype cells did not induce a statistically significant difference in A19 migration (figure 4.4D), although there was a trend for reduced AD, consistent with the finding in MDA-MB-231 cells. Likewise, addition of NMN did not statistically alter migration however β-NMN+PDD did not rescue the migration statistically or as a trend (figure 4.4D). It is possible that the result is not statistically significant due to the very small distances travelled by A19 cells.

Figure 4.4E examines the effect of PDD, with and without β-NMN, on A11 migration. Addition of PDD or NMN alone reduced AD, compared to DMSO control, while supplementation with NMN did not rescue PDD effects. These results differ when the same conditions were performed in A19 and MDA-MB-231 cells.

Figure 4.4F&G examines the effect of Ola or TE92 alone, plus the effect of each had when combined with PARG inhibitor in A19 and A11 cell lines respectively. In wildtype (A19) cells, Ola+PDD combination and TE92 alone statistically significantly reduced AD compared to DMSO control (figure 4.4F). PDD and Olaparib alone did not statistically significantly reduce the AD relative to the DMSO control, and only the TE92+PDD co-treatment condition restored migration. In PARP-/- (A11) cells, PDD, Ola and TE92 significantly reduced AD compared to DMSO control (figure 4.4G), suggesting PARP-1 in A19/A11 cells acts as bulwark against the anti-migratory effects of PDD and Olaparib. When examining combination treatments, AD was not restored. Perhaps this is reflective of the fact this model is not human and cancerous in nature but it does warrant repeating in a more relevant model where the levels of PARG can be maintained as it is difficulty to conclude the meaning of these results given the surprising reduction in total PARG110 levels.

4.2.4 The effect of PARG inhibition and β-NMN on NAD+/NADH levels in MDA-MB-231 cells

As β-NMN pre-treatment was capable of rescuing MDA-MB-231 cells from the anti-migratory effects of the PARG inhibitor PDD, we wanted to assess the levels of NAD+ and NADH in response PDD treated cells. A commercial kit for measuring NAD/NADH was used (Figure 4.5A). Cellular levels are calculated relative to a standard curve (Figure 4.5B). Figure 4.5C displays the amount of NAD+ in pmol per $1x10^6$ cells across each of the treatment conditions. DMSO alone produced a NAD+ reading of 405.526 pmol/$1x10^6$cells. PDD treatment produced a similar NAD+ reading of 436.182 pmol/$1x10^6$ cells. β-NMN treatment alone or 1 hour before addition of PDD increased NAD+ to 700.803 pmol/$1x10^6$cells and 731.182 pmol/$1x10^6$ cells respectively. One repeat was obtained so statistical analysis could not be performed.

Figure 4.5D displays the amount of NADH in pmol per $1x10^6$ cells across each of the treatment conditions. DMSO alone produced a NADH reading of 154.338 pmol/$1x10^6$cells, whereas the addition of PDD produced a much lower NADH reading (65.927 pmol/$1x10^6$cells). β-NMN alone produced a NADH reading of 153.478 pmol/$1x10^6$cells which was consistent with the DMSO reading. The β-NMN+PDD produced a NADH reading of 225.113 pmol/$1x10^6$cells, which was the highest reading amongst all groups tested. One repeat was obtained so statistical analysis was not performed.

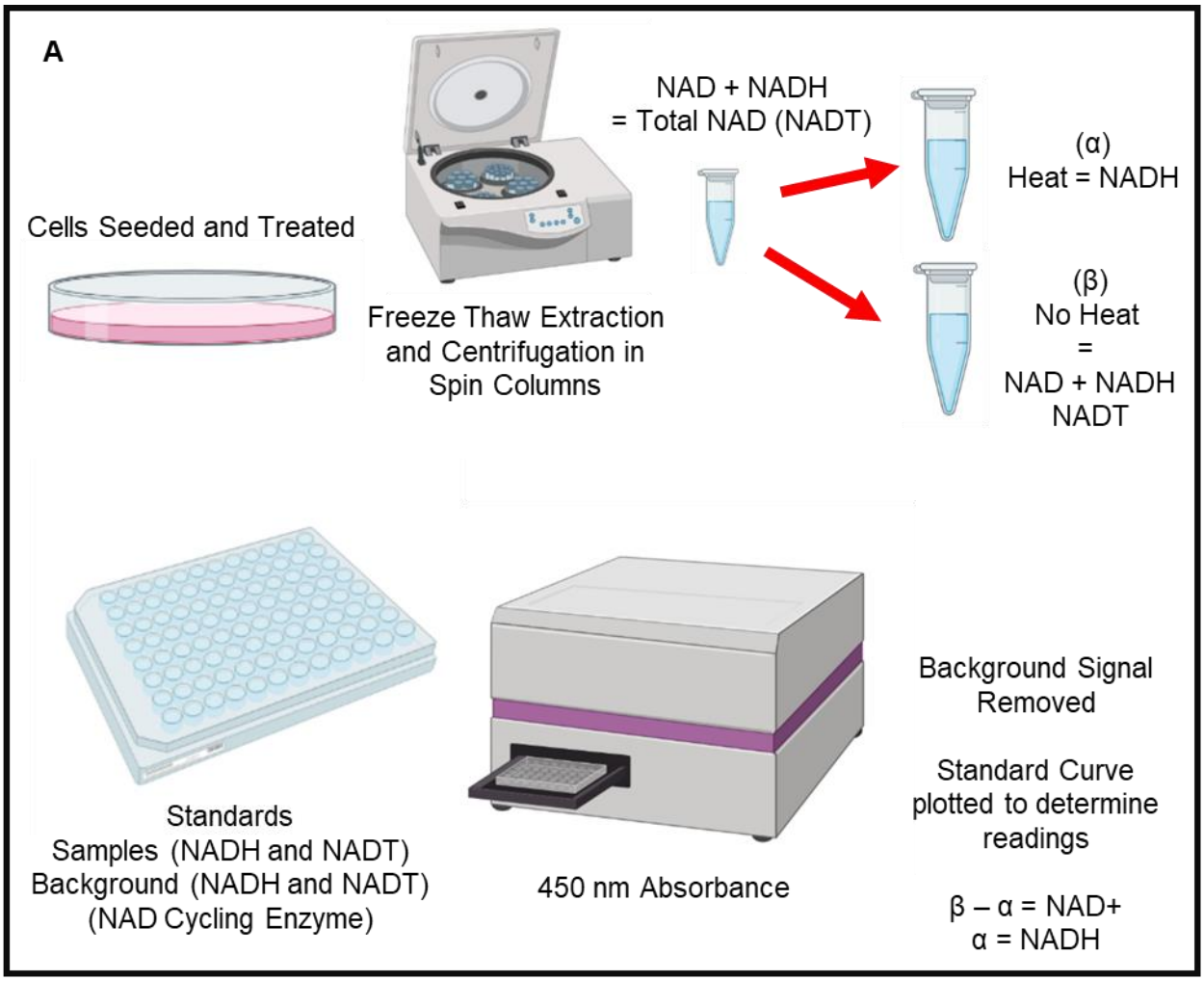

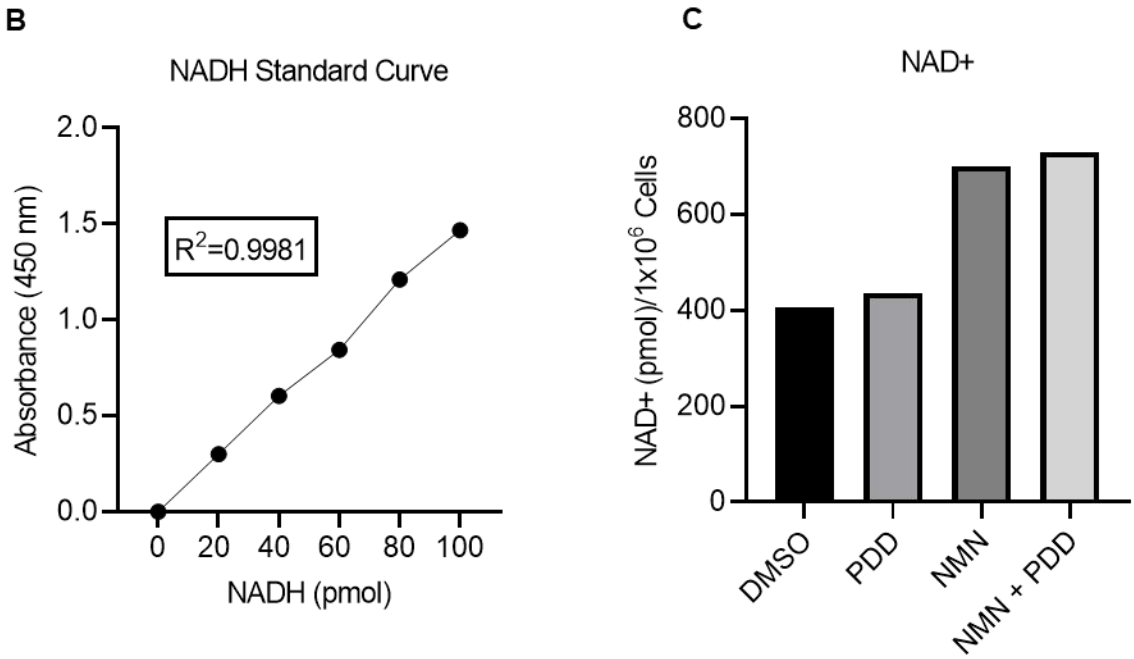

Figure 4.5. **The impact of PARGi and NMN-pre-treatment on NAD+/NADH levels.** Legend overleaf.

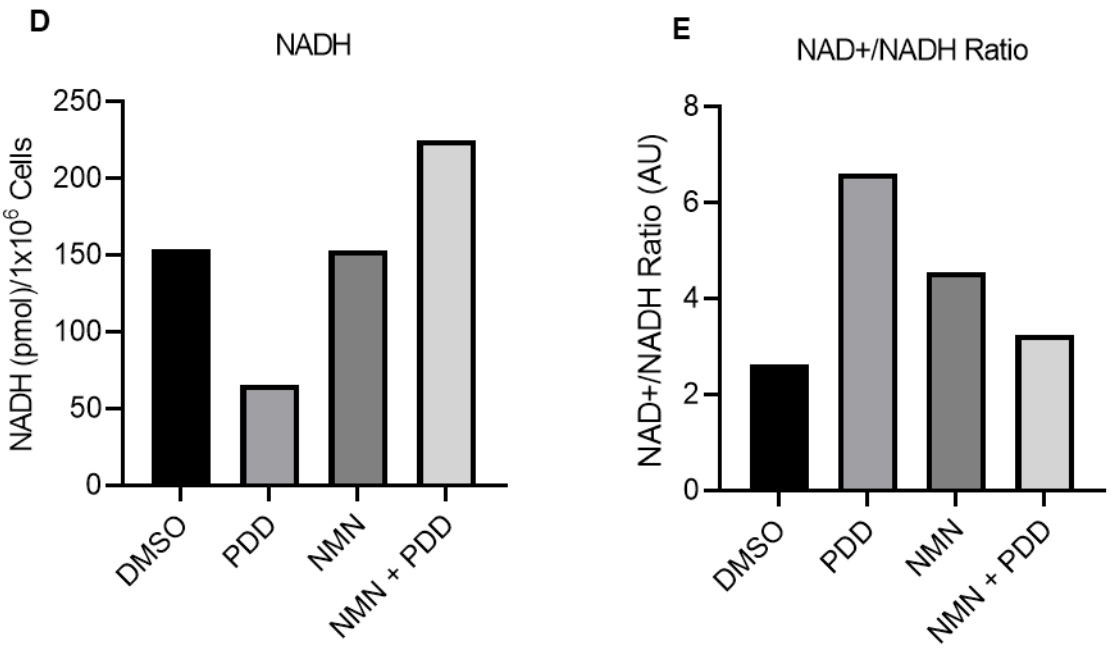

Figure 4.5. **The impact of PARGi and NMN-pre-treatment on NAD+/NADH levels.** (A) Schematic diagram summarising the protocol. Briefly, cells were seeded and treated as per the conditions in the live cell experiment in figure 4.11. Cells were then subject to freeze thawing and centrifugation steps using spins columns to isolate the total NAD (NADT = NAD+ and NADH). A fraction of the sample was heated which degraded the NAD+ leaving only the NADH. Standards along with samples from heated and unheated conditions were mixed with reaction agents as per the standard manufacturer's instructions in duplicate. Samples were left for 1 hour in the dark and the 450 nM absorbance was recorded. Average background signal based was subtracted from the average of the technical repeats. Samples were then read off the standard curve and adjusted for based on total sample volume, volume used in the reaction mixture and the average total number of cells recorded prior to freeze thawing and NADT isolation. (B) NADH (pmol) standard curve in relation to 450 nm absorbance. (C) Total NAD+ per 10X10^6 cells in pmol within each condition. (D) Total NADH per 1X10^6 cells in pmol within each condition. (E) The ratio of NAD+/NADH within each condition. N=1 so no statistical analysis was performed.

Figure 4.5E displays the ratio of NAD+ to NADH and is derived from the readings in figure 4.5C and 4.5D respectively. The DMSO control NAD+/NADH ratio was 2.627, whereas PDD produced a much higher NAD+/NADH ratio of 6.616 and was highest amongst all conditions. The β-NMN alone had a slightly higher NAD+NADH ratio of 4.566 which was the second highest ratio recorded. The combination condition had a NAD+NADH ratio of 3.248, which most closely resembled the DMSO reading. One repeat was obtained, so statistical analysis was not performed.

These data together suggest PDD does not deplete cells of NAD+, rather the effect is on NADH at least over the time course of the experiment. The net result of this is an alteration in NAD+/NADH ratio, which can be rescued by addition of β-NMN. Thus, the anti-migratory effect of PDD maybe due to changes in NAD+/NADH ratio.

4.2.5 The effect of PARG inhibition and β-NMN on ATP levels in MDA-MB-231 cells

Given that β-NMN pre-treatment was capable of rescuing MDA-MB-231 cells from the anti-migratory effects of the PARG inhibitor PDD and NADH was possibly reduced in response to PARG inhibition, we wanted to assess MDA-MB-231 levels of ATP in response to PDD and β-NMN. Figure 4.6A provides a summary of the standard protocol used. Figure 4.6B displays the standard curved that was produced as per the manufacturer's instructions.

Figure 4.6C displays the ATP µmol/1x10^6cells across each of the treatment conditions. PDD had a lower ATP µmol/1x10^6cells (4.086) versus the DMSO control (4.430). The addition of β-NMN alone and with PDD increased the ATP µmol/1x10^6cells readings. Figure 4.6D is re-formatted from the data in figure 4.6C but reformatted as percentage change in ATP relative to the DMSO. PDD reduced ATP/1x10^6cells by 7.75% and is consistent with a reduction in NADH levels. β-NMN alone increased ATP /1x10^6cells by 17.34% despite NADH readings being similar to DMSO. β-NMN with PDD increased ATP /1x10^6cells by 41.18% and is consistent with the increase NADH readings we observed. No statistical analysis was performed as one repeat was obtained.

These data together suggest PDD reduces ATP levels, consistent with a reduction in NADH and that pre-treatment with β-NMN, increases the ATP levels and is enhanced when cells are treated with a PARG inhibitor. This increase in ATP provides insight into how β-NMN may be rescuing the cells from their perturbed migration in the presence of PDD.

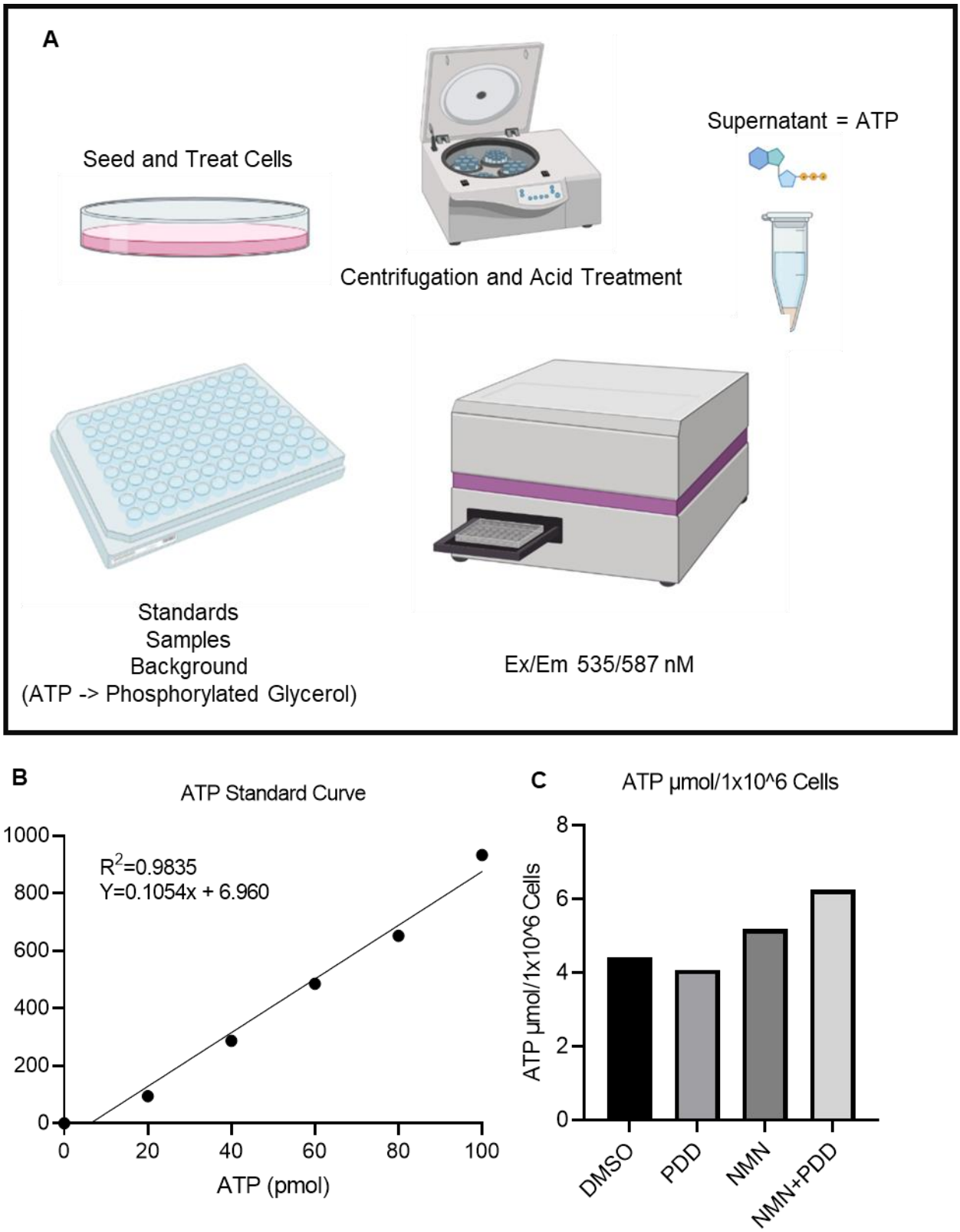

Figure 4.6 **The impact of PARGi and NMN-pre-treatment on ATP levels.** Legend overleaf.

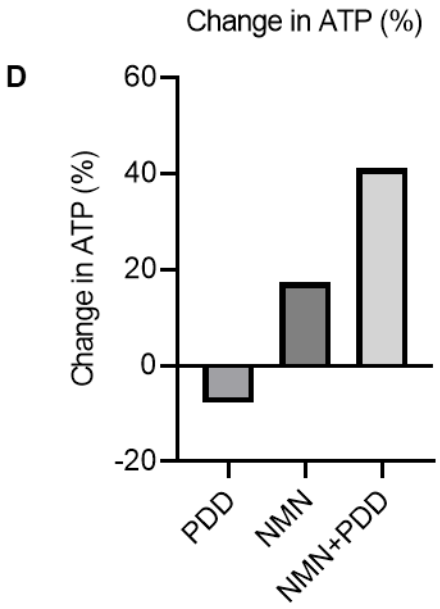

Figure 4.6 **The impact of PARGi and NMN-pre-treatment on ATP levels.** (A) Schematic diagram summarising the protocol. Briefly, cells were seeded and treated as per the conditions in the live cell experiment in figure 4.11. Cells were then subject to centrifugation and acid treatments to isolate the ATP. Standards, samples and sample background were mixed with reaction agents as per the manufacturer's instructions in duplicate. Samples were left in the dark for 1 hour. The fluorometric signal using Ex/Em 535/587 nm was recorded for each condition. The Average relevant background signals were subtracted from the average standard and average sample readings. Samples were then read off the standard curve and adjusted for based on total sample volume, volume used in the reaction mixture and the average total number of cells recorded prior to centrifugation and acid treatments. (B) ATP (pmol) standard curve relative to Ex/Em 535/587 nm. (C) Total ATP (µmol) per 1x10^6 cells across each condition. (D) The percentage change in ATP levels relative to DMSO control. N=1 so no statistical analysis was performed.

4.2.6 PARG inhibition alters MDA-MB-231 morphology and potentially its cytoskeleton and associated sub-structures

4.2.6.1 PARG inhibition alters MDA-MB-231 cellular morphology

During analysis of MDA-MB-231 live cell data, we noted differences in the cell morphology. Using the live cell image stills, the cell area, circularity, and roundness were measured by manually drawing around the cell perimeter in image J. Figures 4.7G and H show representative stills of cells under DMSO or PDD treatment respectively. Three biological repeats were obtained and 99 cells per biological repeat were included in the analysis.

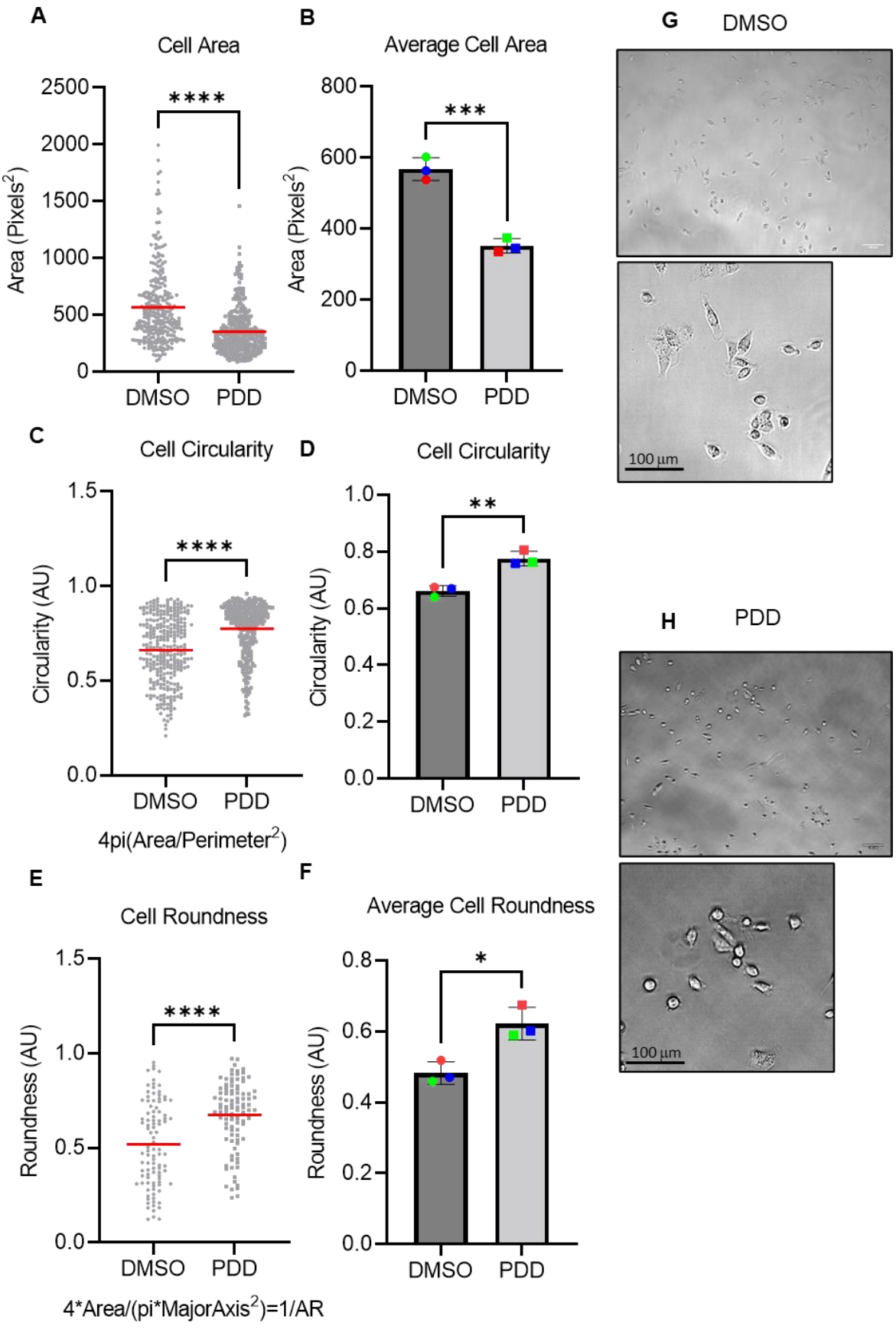

Figure 4.7 **PARGi impacts MDA-MB-231 cell morphology based on live cell images.** Legend overleaf.

Figure 4.7 **PARGi impacts MDA-MB-231 cell morphology based on live cell images.** Quantification is from live cell imaging. 99 cells per biological repeat. (A) Cell area (pixels^2). (B) Average cell area (pixels^2) across each biological repeat. (C) Cell Circularity (AU) (D) Average cell circularity (AU) across each biological repeat. (E) Cell roundness (AU). (F) Average cell roundness (AU) across each biological repeat. (G) Representative image of DMSO live cell image displaying morphologies. (H) Representative image of PDD live cell image displaying morphologies. For pooled data the line represents the median. For averages mean and SD are shown. Statistical testing was by Mann-Whitney for pooled data and unpaired t test for average. **** denotes p=≤ 0.0001, *** denotes p=≤ 0.001, ** denotes p=≤ 0.01, * denotes p=≤ 0.05, NS denotes not statistically significant.

Figures 4.6A, C and E are pooled data for the respective metrics. Figures 4.6B, D and F are the averages of each biological repeat, respectively for each metric.

PARGi treated cells had a statistically significant reduction in cell area (figure 4.7A&B). PARGi treated cells had a statistically significant increase in cell circularity (figure 4.7C&D). PARGi treated cells had a statisitically significant increase in cell roundness (figure 4.7E & F).

This suggests PARGi affect the morphology of MDA-MB-231 cells and make them smaller, more circular and rounder.

4.2.6.2 PARG inhibition increases F-actin levels in MDA-MB-231 cells

Given the change in cell morphology, we wanted to investigate the effect of PDD on MDA-MB-231 cytoskeleton. Integrated density (intden) is a method of quantifying fluorescent intensity whilst factoring in size. We used phalloidin 488 to stain for total cell F-actin and co-staining for DAPI allowed us to define the nuclear area and thus determine the nuclear integrated density of F-actin. By then subtracting the 488 nuclear integrated density from the whole cell 488 integrated density, we could calculate cytoplasmic integrated density of F-action. PDD increased the integrated density of total, nuclear and cytoplasmic F-actin (Figure 4.8A & C & E). Figure 4.8B & D include representative images. All results were

derived from one repeat so statistical analysis was not performed and approximately 30 cells were used for each condition.

This suggests that PARGi increases MDA-MB-231 F-actin levels across the cytoplasm and around the nucleus.

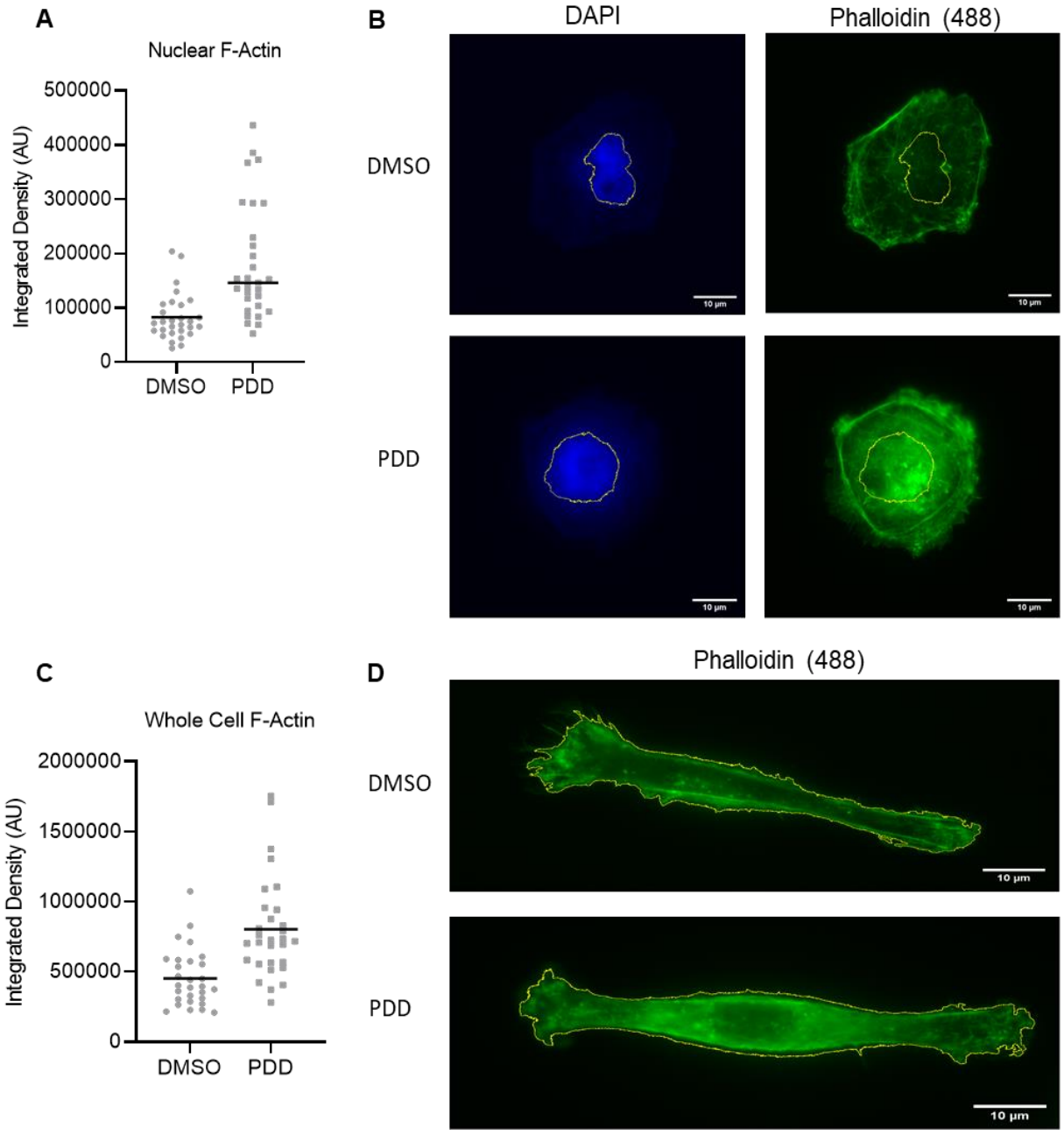

Figure 4.8 **PDD impacts MDA-MB-231 F-actin signal by immunofluorescence.** Legend overleaf.

E

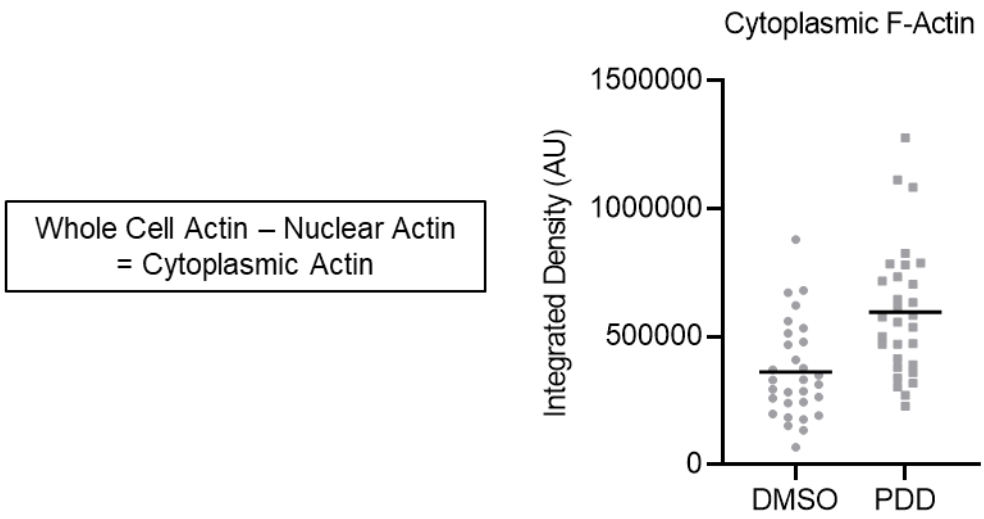

Figure 4.8 **PDD impacts MDA-MB-231 F-actin signal by immunofluorescence.** (A) Integrated density (AU) of nuclear actin signal defined by DAPI threshold. (B) Representative images of Nuclear actin integrated density (AU). (C) Integrated density (AU) of whole cell actin defined by 488 channel threshold. (D) Representative images of whole cell actin integrated density (AU). (E) Cytoplasmic actin integrated density defined by the integrated signal density of the nuclear actin being subtracted from the corresponding whole cell actin integrated density (AU). N=1. Approximately 30 cells per condition. No statistical analysis performed.

4.2.6.3 PARG inhibition increases the number of podosomes per cell in MDA-MB-231

Podosomes are actin rich conical substructures situated on the ventral surface of cells and aid migration (functioning as attachment sites) and invasion (enabling localised delivery of extracellular matrix degrading enzymes). We noted an increase in the number of highly fluorescent dots in cells, indicative of podosomes, and counted the number of visible dots per cell from the same data set analysed for F-actin above (figure 4.8). Representative images included (figure 4.9A & B). There was an average of 15.9 and 24 podosomes per cell for the DMSO and PDD treatment conditions respectively (figure 4.9). All results were derived from one repeat so statistical analysis was not performed and approximately 30 cells were used for each condition.

This suggests that PARGi impact podosome dynamics.

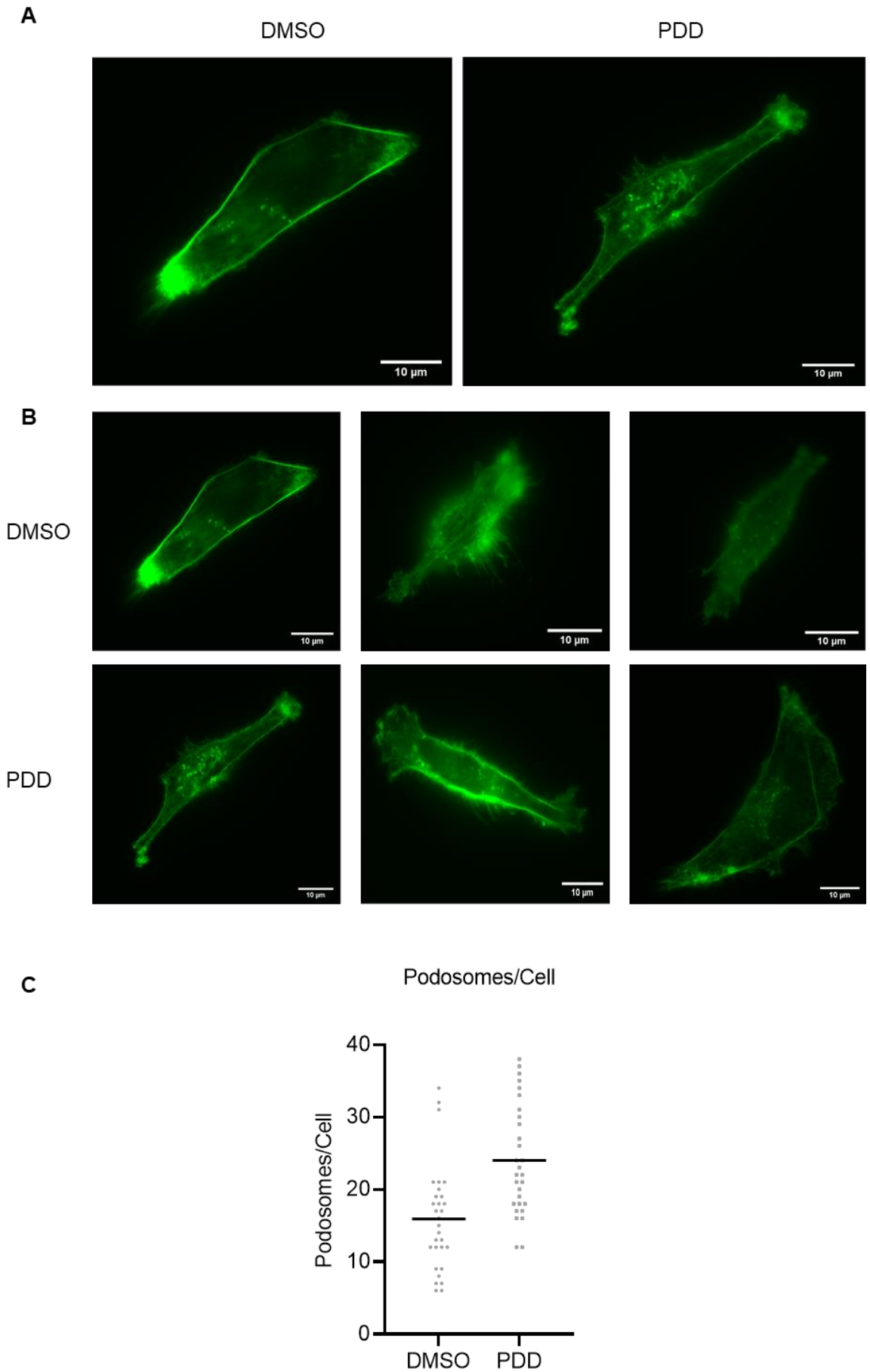

Figure 4.9 **PDD impacts podosome dynamics.** Legend overleaf.

Figure 4.9 **PDD impacts podosome dynamics.** (A) Larger representative images to aid visualization. The bright dots are possible indications of podosome structures. (B) More examples (C) Number of podosomes manually counted per cell. N=1. Approximately 30 cells per condition. No statistical analysis was performed.

4.2.6.4 PARG inhibition increases stress fibre formation in MDA-MB-231 cells

Stress fibres are actomyosin (rich in actin) contractile bundles that form during migration and facilitate the movement of non-muscle cells and are also involved in adhesion and mechanosensing. Following PDD treatment, we noted an increase in the number of cells where stress fibres were visible in the F-actin-stained cells set analysed above.

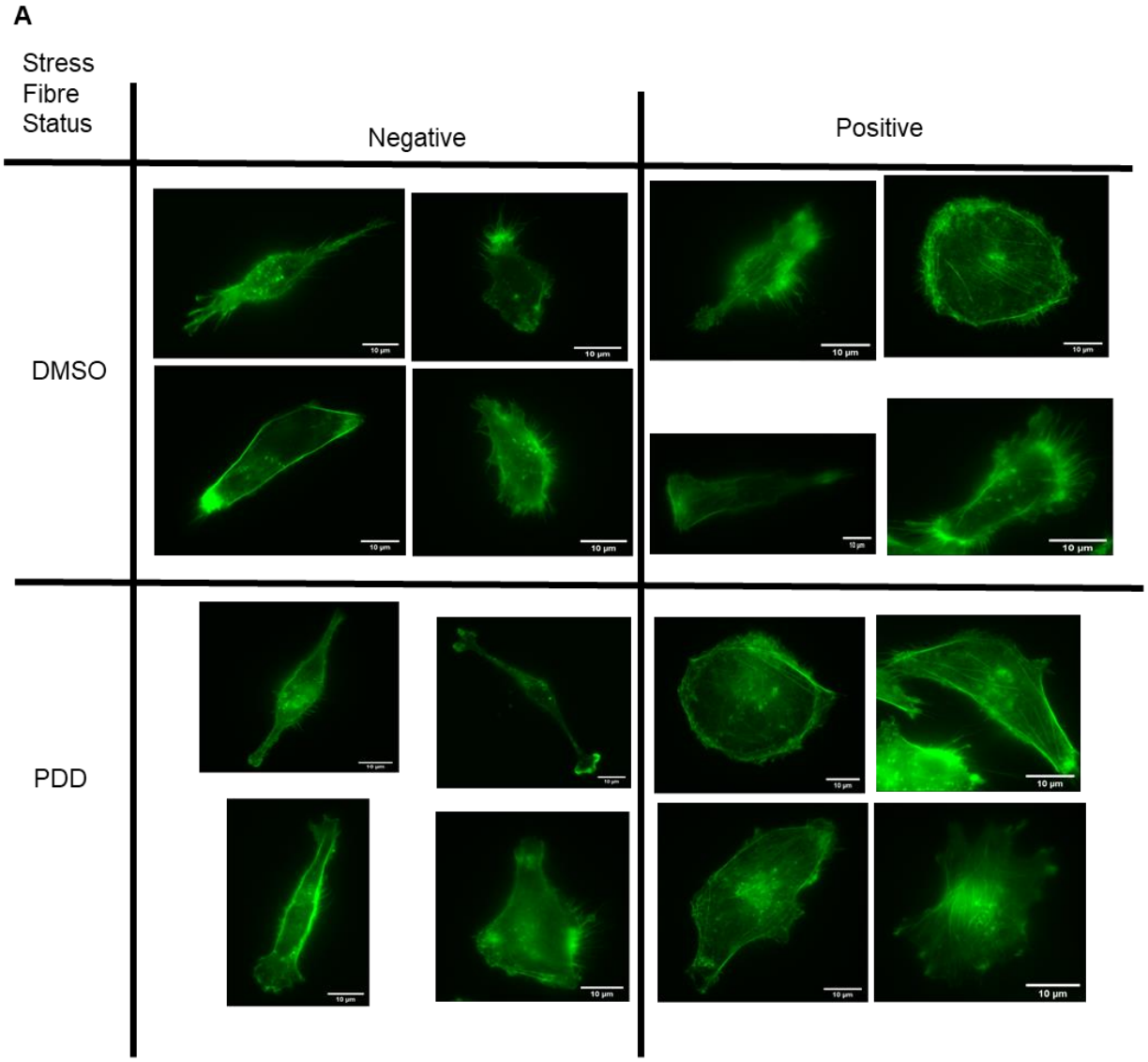

Figure 4.10 **PDD impacts stress fibre dynamics.** Legend overleaf.

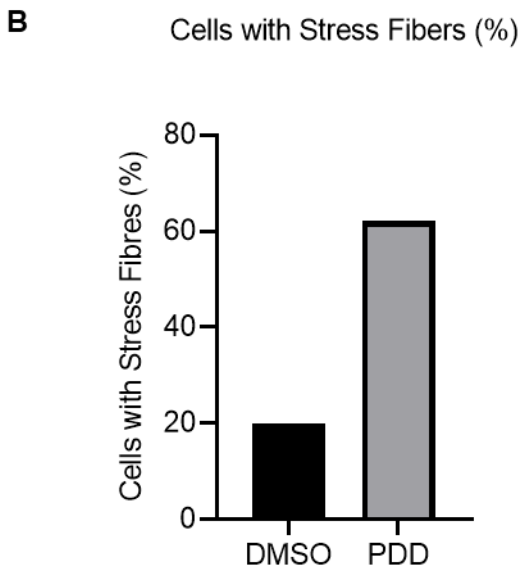

Figure 4.10 **PDD impacts stress fibre dynamics.** (A) Representative images of cells categorised as stress fibre negative or positive treated with DMSO or PDD. (B) The percentage of cells that exhibited visible stress fibres. N=1, approximately 30 cells per condition. No statistical analysis was performed.

When cells were classified as positive or negative for stress fibres (figure 4.10A), 62.07% of PDD treated versus 20% in the DMSO control were classified positive (figure 4.10B). All results were derived from one repeat so statistical analysis was not performed and approximately 30 cells were used for each condition.

This implicates PARG in supressing stress fibre formation.

4.2.6.5 PARG inhibition reduces the number and length of filopodia in elongated MDA-MB-231 elongated

Filopodia are thin, actin-rich components of the cytoskeleton that protrude through the plasma membrane, aiding in environmental sensing and facilitating cellular movement. Using the same F-actin-stained cells (figure 4.8), the length of the filopodia was determined by manually drawing along their length in imagej. Figure 4.11A displays representative images of untreated and PDD treated cells. The number of filopodia per cell and average filopodia length per cell was also calculated. The cells displayed a wide array of morphologies so to reduce the variability, we focused on elongated cells that we assumed were in the process of migrating. The average filopodia length of DMSO treated cells was 2.042 µm, which was reduced to 1.766 µm in PDD treated cells (figure 4.11B). In addition, the average number of filopodia per cell also reduced from 33.38 in the DMSO treated cells to 20.6 in PDD treated cells (figure 4.11C). Consistent with these data, the average filopodia length per cell was also reduced in PDD treated cells (figure 4.11D). The results were derived from one repeat so statistical analysis was not performed and approximately 15-20 cells were used for each condition.

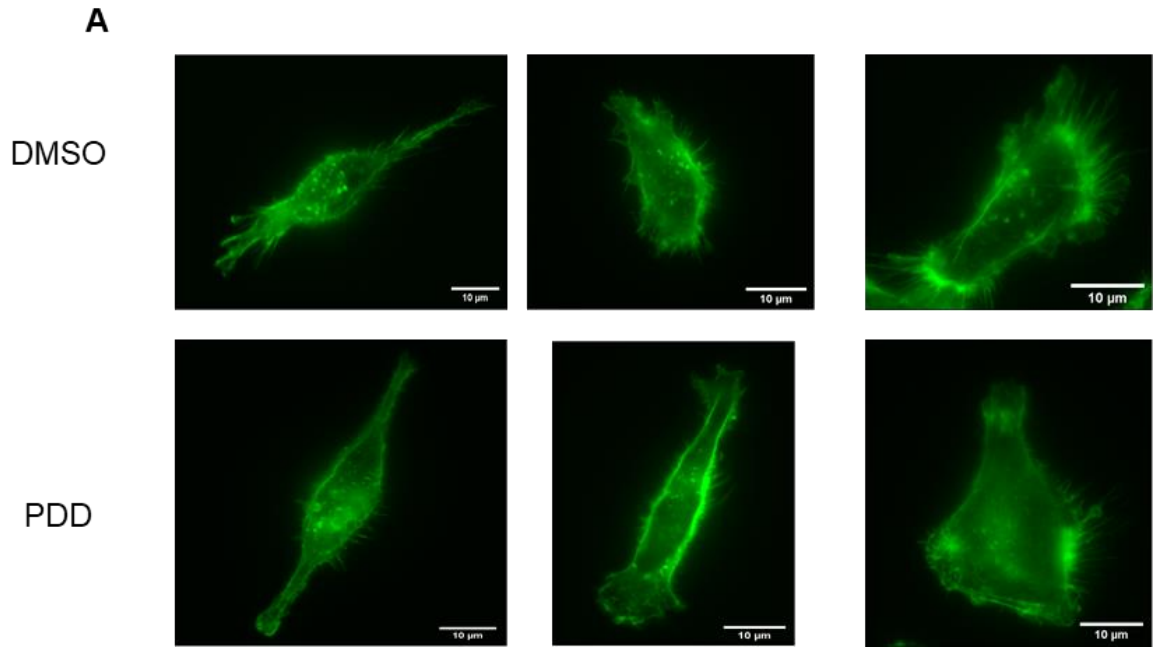

Figure 4.11 **PDD impacts filopodia dynamics in elongated cells.** Legend overleaf.

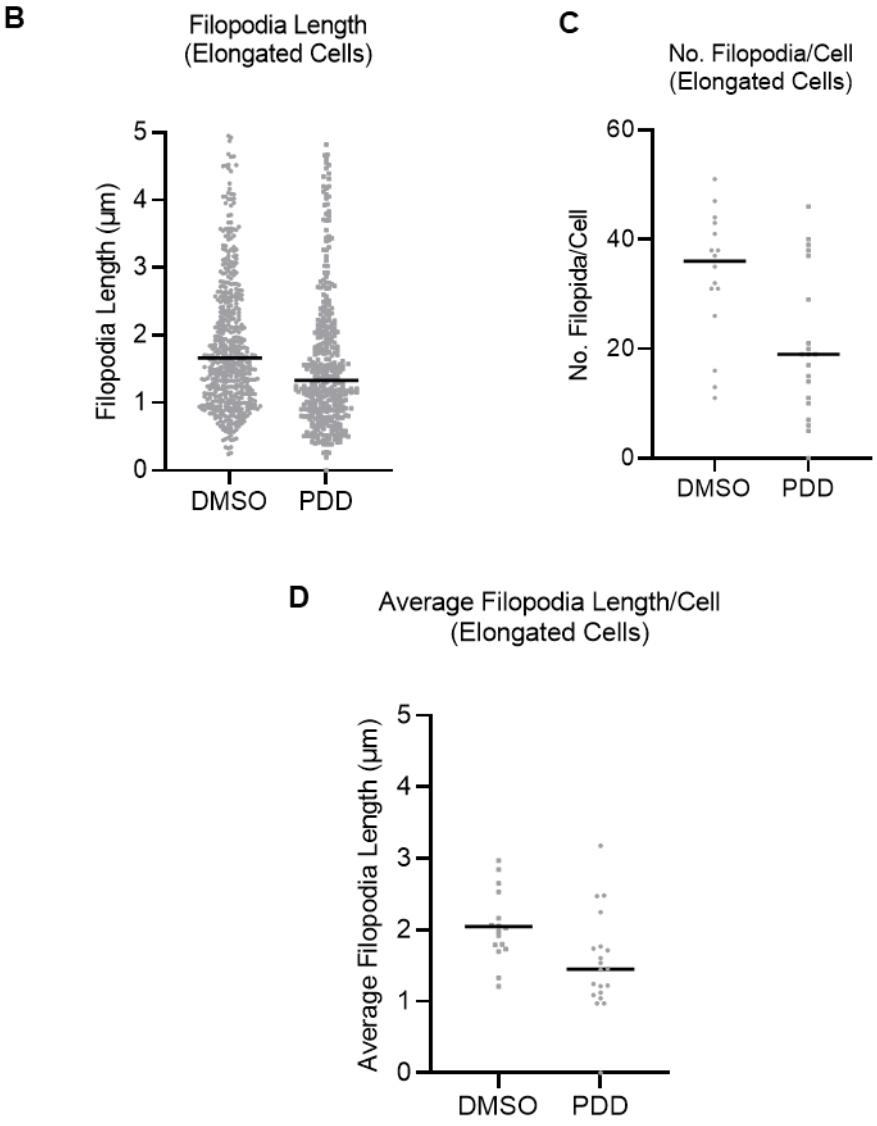

Figure 4.11 **PDD impacts filopodia dynamics in elongated cells.** (A) Representative images of DMSO or PDD treated elongated cells with visualisable examples of the trends depicted in figures 4.10B, C and D. (B) Filopodia length (µm) in elongated cells. (B) Number of filopodia per elongated cell. (C) Average Filopodia length (µm) per elongated cell. Given the anti-migratory effects we have reported, elongated cells were focused on for the filopodia quantification as we reasoned a disruption in a cell actively attempting to migrate would be more pronounced. N=1, 15-20 cells per condition. No statistical analysis was performed.

The decrease in filopodia length and reduction in the number of filopodia per cell, suggest that PARGi can impact filopodia formation and polymerisation in elongated cells and suggest PARG has a role in filopodia dynamics.

4.2.6.6 PARG inhibition increases α-tubulin in MDA-MB-231 cells

The F-actin stained cells were also co-stained with α-tubulin and a 594 conjugated secondary antibody and the same intden analysis was performed.

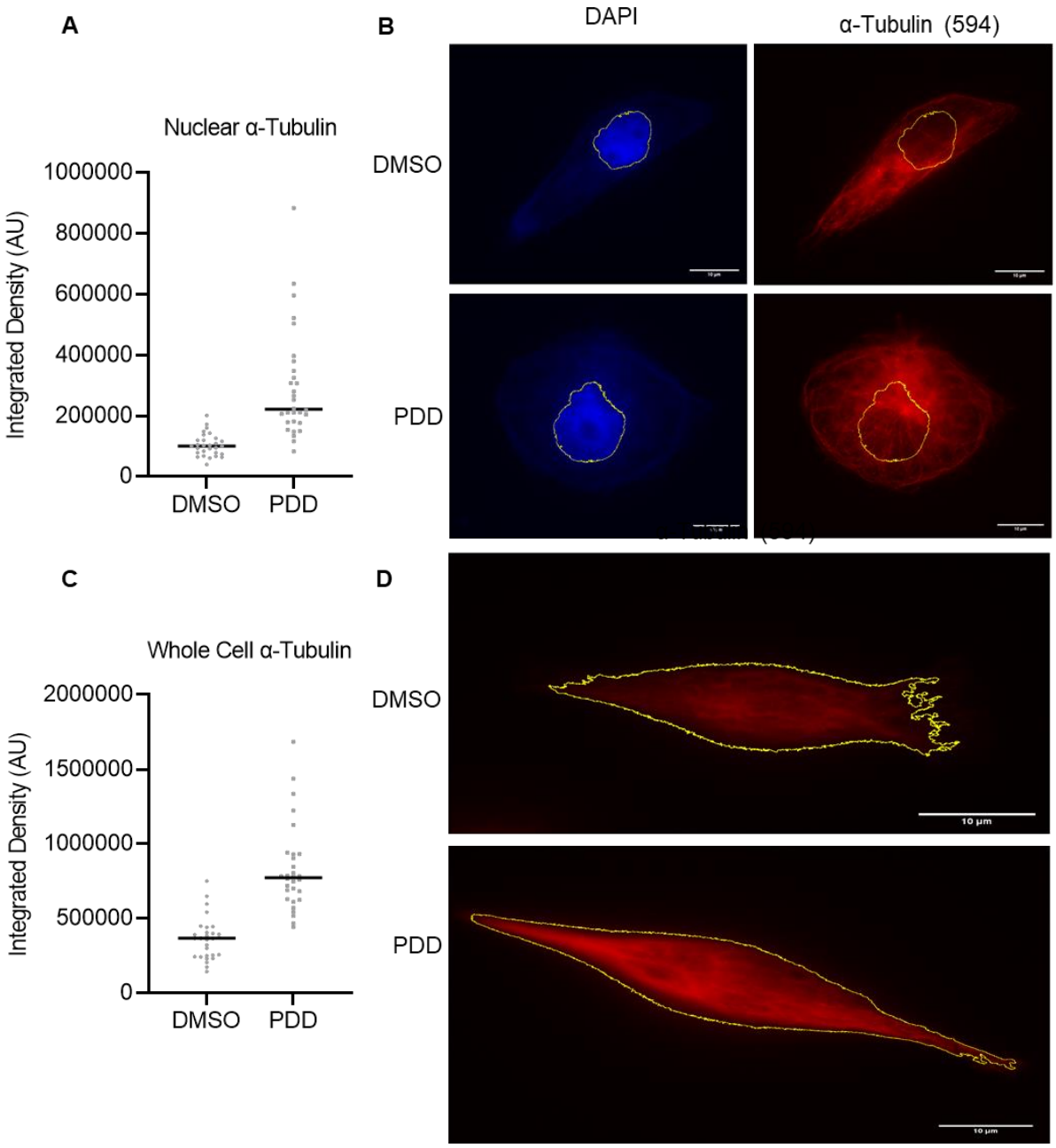

Figure 4.12 **PDD impacts MDA-MB-231 α-tubulin signal by immunofluorescence.** Legend overleaf.

E

Whole Cell α-Tubulin – Nuclear α-Tubulin = Cytoplasmic α-Tubulin

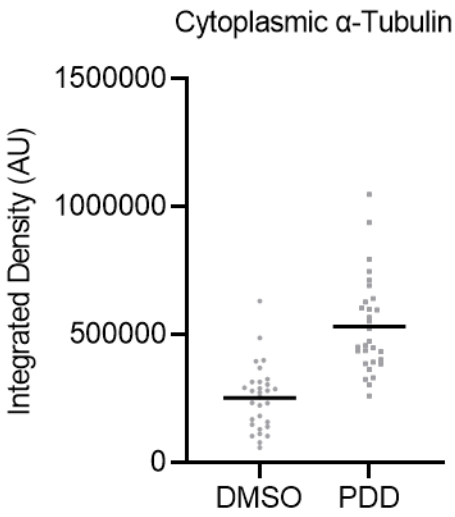

Figure 4.12 **PDD impacts MDA-MB-231 α-tubulin signal by immunofluorescence.** (A) Integrated density (AU) of nuclear α-tubulin signal defined by DAPI threshold. (B) Representative images of Nuclear α-tubulin integrated density (AU). (C) Integrated density (AU) of whole cell α-tubulin defined by 594 channel threshold. (D) Representative images of whole cell α-tubulin integrated density (AU). (E) Cytoplasmic α-tubulin integrated density defined by the integrated density signal of the nuclear α-tubulin being subtracted from the corresponding whole cell α-tubulin integrated density (AU). N=1. Approximately 30 cells per condition. No statistical analysis performed.

Representative images of nuclear and whole cell α-tubulin are included (figure 4.12B & D). Integrated density analysis demonstrated that PDD increased the total, nuclear and cytoplasmic levels of α-tubulin (figure 4.12A & C & E). The trend was consistent with the F-actin results. All results were derived from one repeat so statistical analysis was not performed and approximately 30 cells were used for each condition.

This suggests that PARGi increases MDA-MB-231 α-tubulin across the cytoplasm and around the nucleus.

4.2.7 MDA-MB-231 cells but not MCF7 exhibit altered nuclear morphology in response to PARG inhibition

Given that we observed an increase in nuclear cytoskeletal signal, when MDA-MB-231 cells were treated with a PARG inhibitor, we considered the possibility this could impact nuclear morphology. Using DAPI stained fixed cells, the nuclear area and circularity of MDA-MB-231 nuclei were measured in imagej. We also examined MCF7 nuclear morphology. One hundred nuclei were measured per biological repeat and three biological repeats were performed.

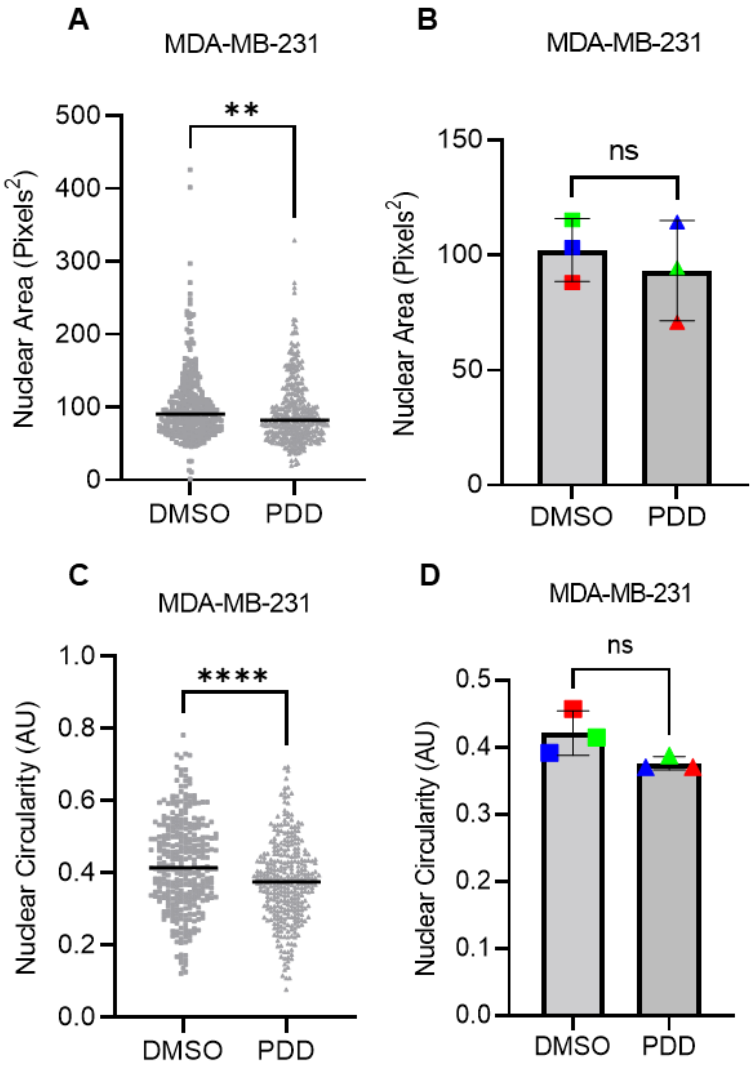

Figure 4.13 **PDD impacts MDA-231-MB but not MCF7 nuclear morphology based on 2D immunofluorescent images of DAPI stained nucleus.** Legend overleaf.

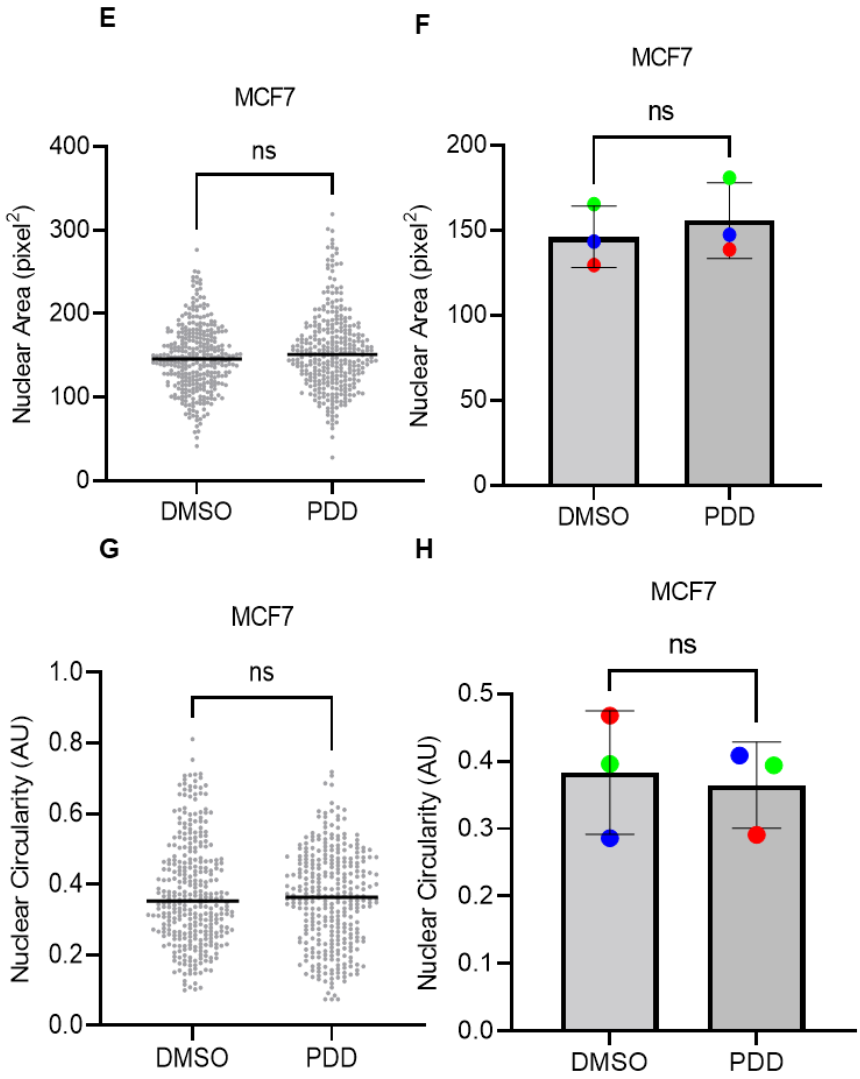

Figure 4.13 **PDD impacts MDA-231-MB but not MCF7 nuclear morphology based on 2D immunofluorescent images of DAPI stained nucleus.** (A) MDA-MB-231 Nuclear Area (pixel^2) (B) Average MDA-MB-231 nuclear area (pixel^2) across each biological repeat. (C) MDA-MB-231 nuclear circularity (AU) (D) Average MDA-MB-231 nuclear circularity (AU) across each biological repeat. (E) MCF7 Nuclear Area (pixel^2) (F) Average MCF7 nuclear area (pixel^2) across each biological repeat. (G) MCF7 nuclear circularity (AU) (H) Average MCF7 nuclear circularity (AU) across each biological repeat. N=3, 100 nucleus per biological repeat. For pooled data the line represents the median. For averages mean and SD are shown. Statistical testing was by Mann-Whitney for pooled data and unpaired t test for average. **** denotes p=≤ 0.0001, ** denotes p=≤ 0.01, NS denotes no statistical significance. The NS P-values were 0.7 (B), 0.1 (D), 0.07 (E), 0.7 (F), 0.53 (G) and >0.99 (H).

PDD statistically reduced the nuclear area and circularity of MDA-MB-231 nuclei when repeats were pooled (figure 4.13A &C) but did the same metrics did not statistically differ using the average data (figure 4.13B & D). The average area data of PDD treated MDA-MB-

231 nuclei had a larger standard deviation, whereas the average circularity data had a smaller standard deviation, compared to the DMSO control. MCF7 nuclear area (figure 4.13E & F) and circularity (figure 4.13G & H) were unaltered when treated with PDD.

This suggests PARGi can impact nuclear morphology in a cell line and cancer subtype dependant manner.

4.2.8 PARG inhibition alters the nuclear envelope of MDA-MB-231 cells

Given the differences in nuclear area and circularity observed in MDA-MB-231 cells when treated with a PARG inhibitor, we wanted to assess if there were changes to the nuclear envelope. DAPI and lamin A were detected by immunofluorescent labelling and confocal images were taken. Cells with lamin irregularities were split into 3 categories: those with gaps in lamin A staining, (likely indicating gaps in the nuclear envelope), those containing lamin A dots (likely nuclear invaginations) and those where the lamin A appeared to bulge out from the regular envelope shape (likely nuclear blebs) (figure 4.14A and B). PDD treated cells exhibited a greater number of gaps in their lamin A staining (70.97%) compared to 27.27% of DMSO treated cells as a percentage of cells analysed (Figure 4.14C). PDD treated cells exhibited a greater number of nuclear invaginations (64.52%) versus 9.091% of DMSO treated cells as a percentage of cells analysed (Figure 4.14D). PDD treated cells exhibited nuclear blebs a greater number of nuclear blebs (70.97%) versus 27.27% of DMSO treated cells as a percentage of cells analysed (Figure 4.14E). One biological repeat was performed so statistical analysis was not done. Approximately 30 cells per condition were analysed.

These data suggest that PARG inhibition can alter the integrity of the nuclear membrane and increase the incidence of nuclear rupture, nuclear invaginations, and nuclear blebs.

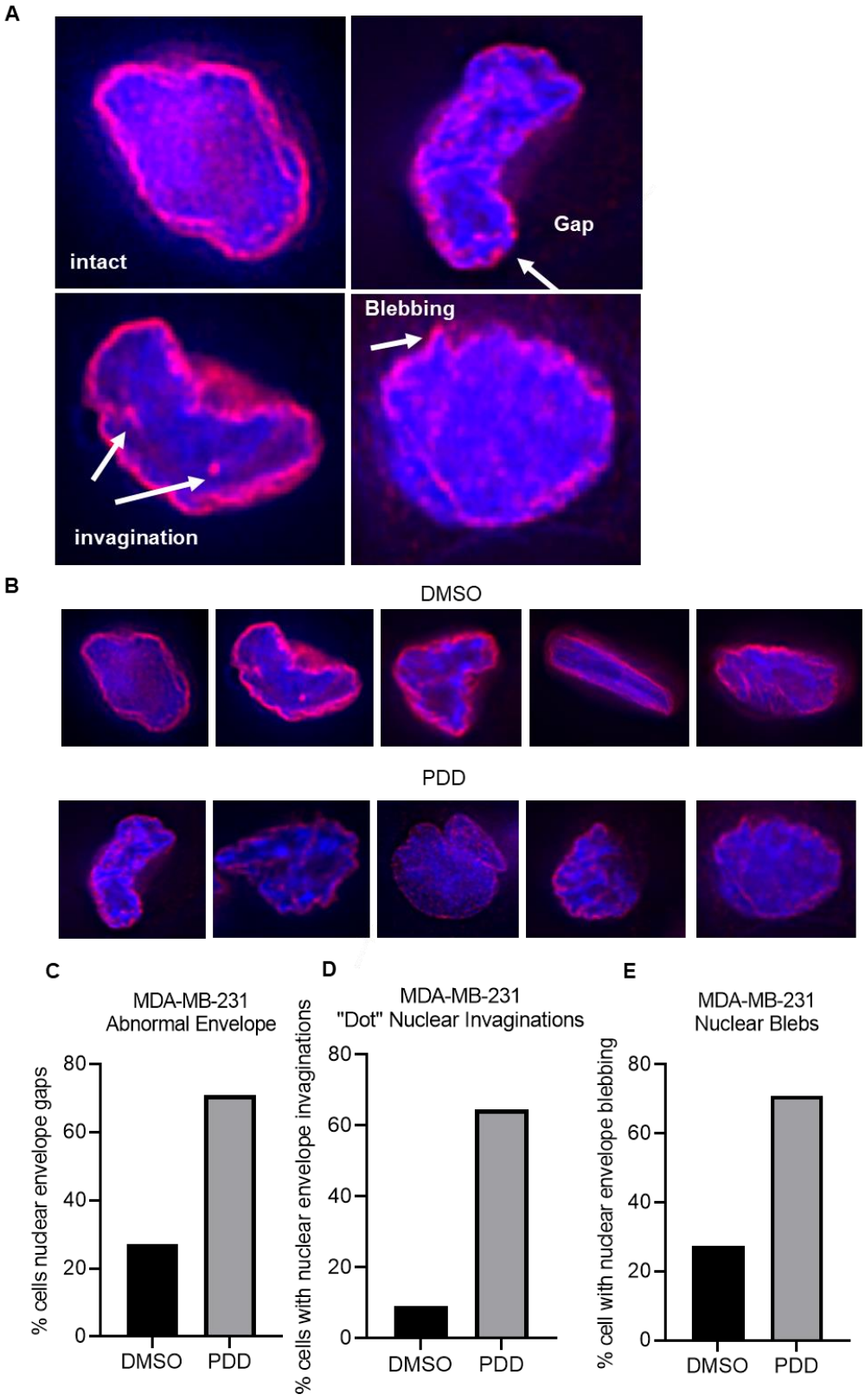

Figure 4.14 **PDD disrupts nuclear envelope structures of MDA-MB-231 cells.** (A) Representative images of abnormalities, (B) representative images of cells under DMSO or PDD treatment. (C-E quantification of % cells displaying these phenotypes. N=1, approximately 30 cells per condition. No statistical analysis was performed.

4.2.9 PARG inhibition does not effect total protein levels of Lamin A/C or B1 in MDA-MB-231 cells

Given that PDD treated MDA-MB-231 cells exhibited differences in their nuclear envelope, we examined expression of total whole cell lamin A and lamin B1 proteins by western blotting. However, no statistical difference in total protein was observed between DMSO and PDD treated cells for either protein (figure 4.15A & B). This suggests PARGi does not impact the total protein levels of lamin A or B1.

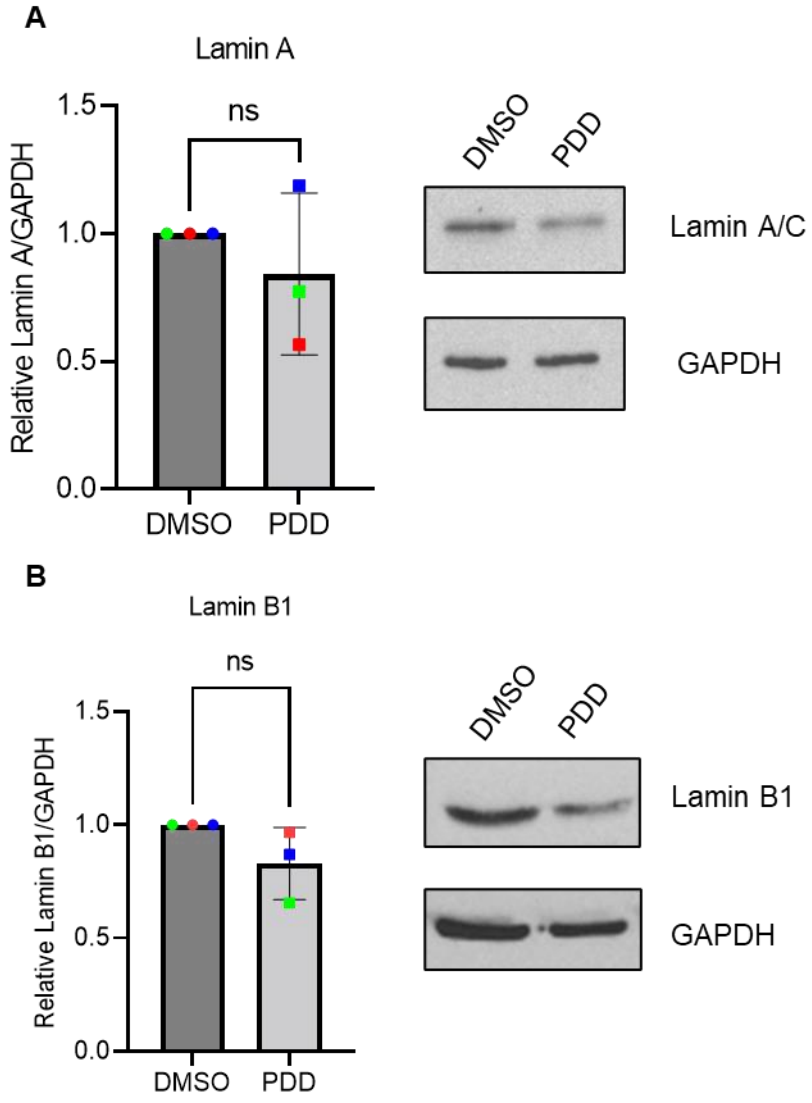

Figure 4.15 **PDD does not alter MDA-MB-231 total lamin A or Lamin B1 protein levels.** (A) Densitometry plots of normalised Lamin A adjusted for using GAPDH loading control. Included is a representative western blot. (B) Densitometry plots of normalised Lamin B1 adjusted for using GAPDH loading control. Included is a representative western blot. N=3. An unpaired t-test was performed however both results were not statistically significant (NS). The NS P-values were 0.44 (A) and 0.14 (B).

4.2.10 Reduced total YAP1 protein and reduced YAP1 nuclear localisation is observed in PARG inhibitor treated MDA-MB-231 cells

Yes-associated protein 1 (YAP1) is a transcriptional co-regulator that is translocated to the nucleus via the activation of the hippo signalling pathway. However, it also functions as a cell stiffness sensor and is involved in signalling mechanotransduction independantly of the hippo pathway (Dupont et al., 2011). YAP1 typically gets translocated to the nucleus in stiffer conditions, and we reasoned if PDD induces cytoskeletal changes then it could alter nuclear translocation of YAP1. YAP1 was visualised by immunofluorescent staining and the nuclear area was defined by the DAPI co-stain and the integrated density of nuclear YAP was then measured. PDD reduced the median integrated density of nuclear YAP from 125,595 (AU) to 88,045 (Figure 4.16B). Pooled data and averages of 3 independent biological repeats are shown and in each case the result is statistically significant. Total YAP1 protein levels were assessed via western blotting. There was a statistically significant reduction in total YAP1 protein levels in the presence of PDD relative to the DMSO control (figure 4.16D). This suggests that PARGi reduces nuclear YAP1, possibly as a side effect PARGi reducing YAP1 total protein.

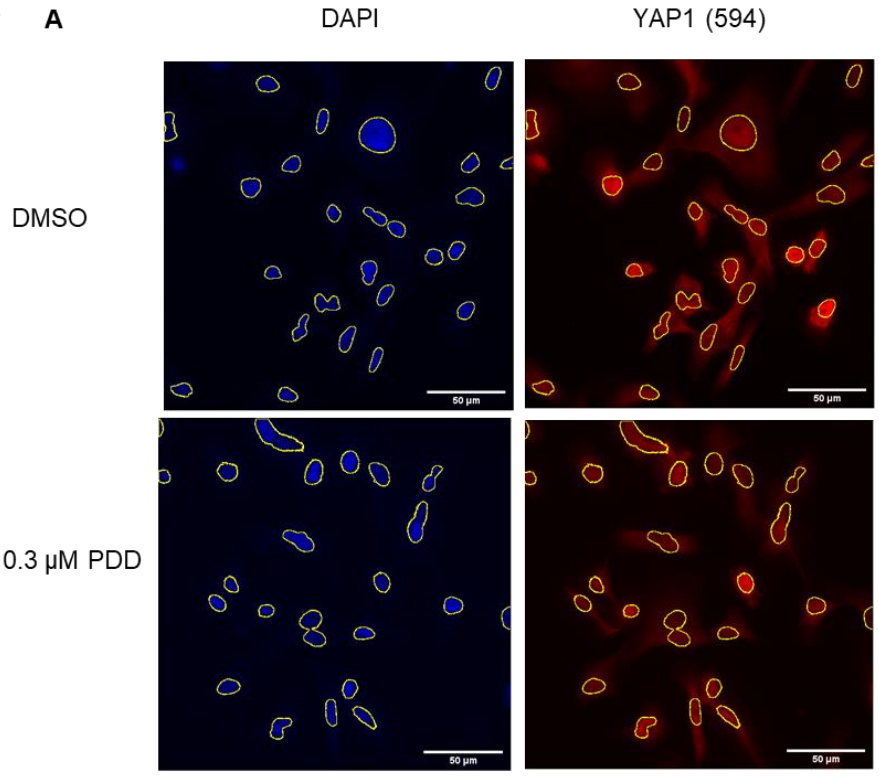

Figure 4.16 **PDD reduces MDA-MB-231 YAP1 nuclear localisation possibly due to reduced total YAP1 protein levels.** Legend overleaf.

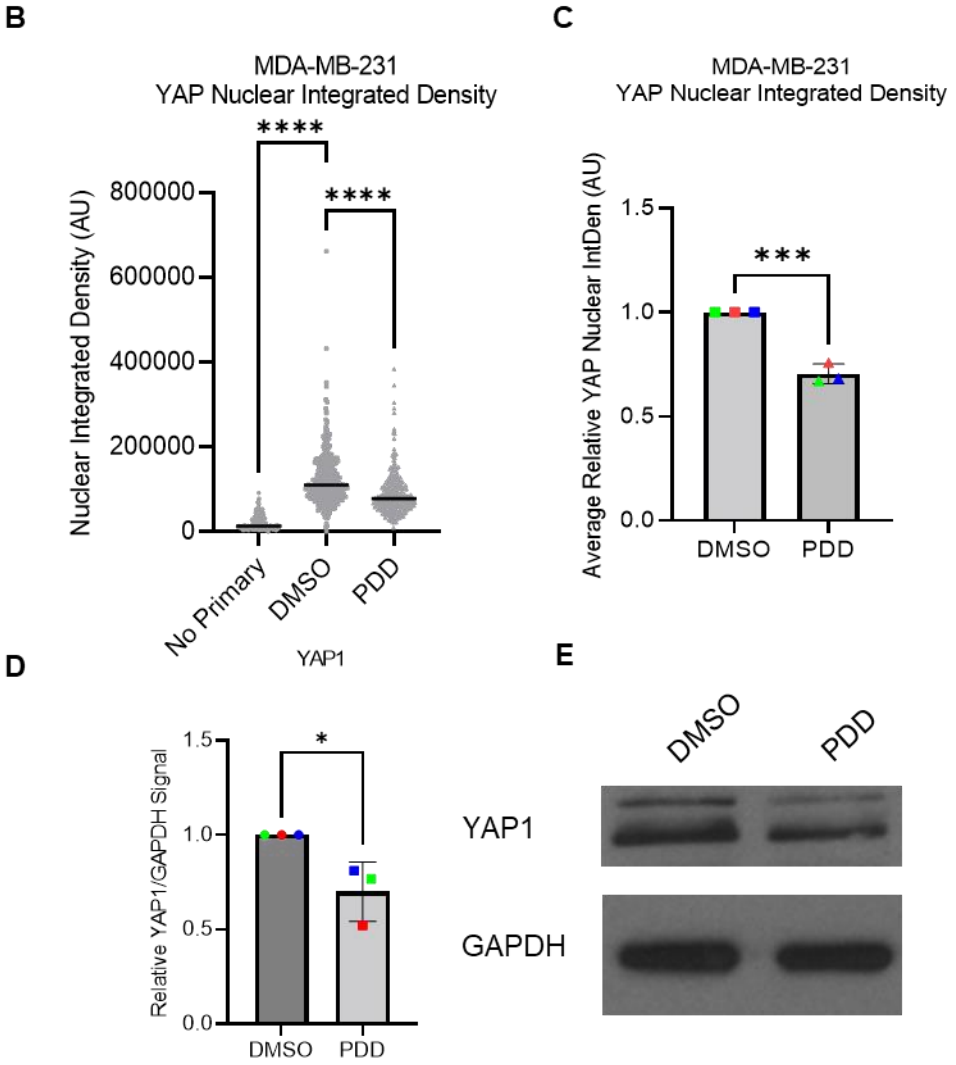

Figure 4.16 **PDD reduces MDA-MB-231 YAP1 nuclear localisation possibly due to reduced total YAP1 protein levels.** (A) Representative image of DMSO or PDD treated cells with the DAPI and YAP1 594 channels. The nuclear area was selected using the DAPI threshold and copied onto the 594 channel (B) DMSO or PDD treated cells nuclear integrated density of the YAP1 594 signal. 100 cells per repeat. N=3. (C) Average integrated density of YAP1 594 signal across each biological repeat. N=3. (D) Densitometry plots of normalised YAP1 adjusted for using GAPDH loading control. Included is a representative western blot. N=3. An unpaired t-test was performed to assess for statistical significance. For pooled data the line represents the median. For averages mean and SD are shown. Statistical testing was by Mann-Whitney for pooled data and unpaired t test for average and western densitometry data. **** denotes p= ≤0.0001, *** denotes p= ≤ 0.001, * denotes p= ≤ 0.05, NS denotes no statistical significance.

4.2.11 PARG inhibition reduces the total protein levels of β-catenin, C-MYC and Vimentin but not E-cadherin in MDA-MB-231 cells

PARP1 is involved in regulating vimentin and C-MYC (Chu et al., 2007; Mostocotto et al., 2014). The tankyrases PARylate Axin, preventing the destruction complex from degrading β-catenin (Mariotti et al., 2017b). We therefore wanted to assess the ability of PARG inhibition to alter the total protein levels of these mesenchymal and pro-migration markers. There was a statistically significant reduction in total β-catenin, C-MYC and vimentin protein levels in the presence of PDD relative to the DMSO control (figure 4.17A-C). Increases in E-cadherin are indicative of a reversion of EMT. E-cadherin was undetectable in MDA-MB-231 cells therefore establishing if changes in the total protein level occurred in the presence of PDD could not be determined (figure 4.17D). This suggest PARGi can reduce the total protein of the tested mesenchymal markers and that PARG may a role in regulating these proteins.

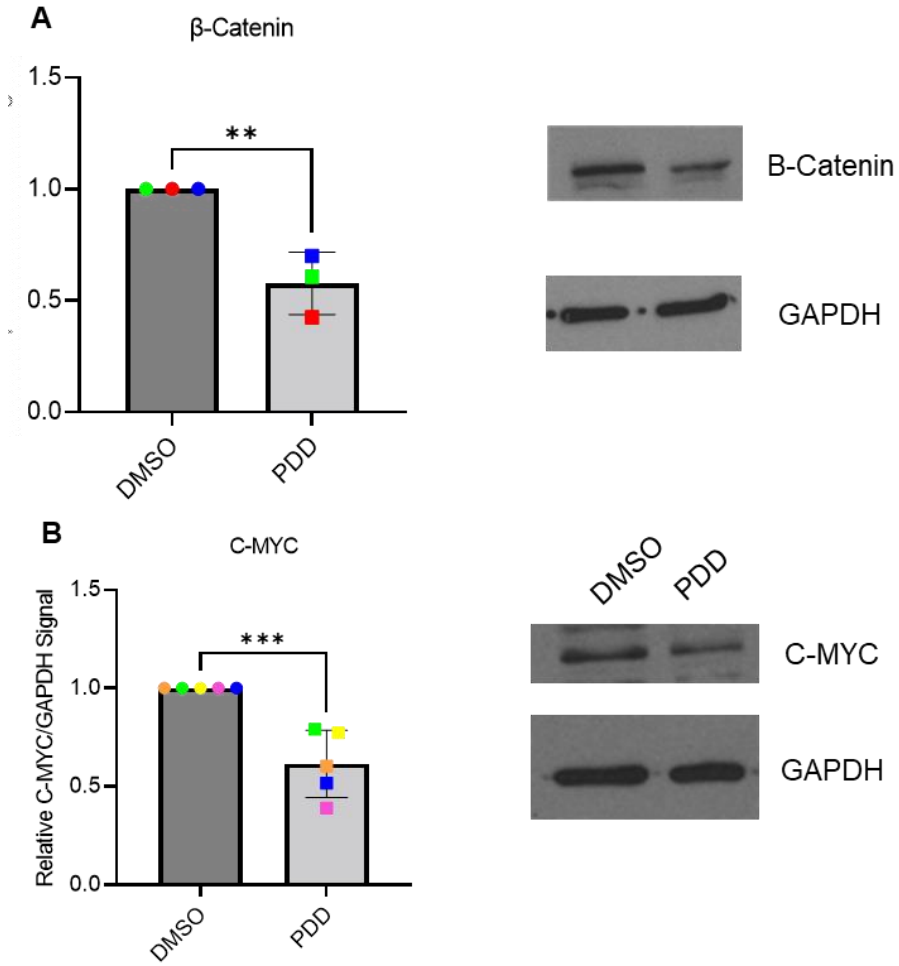

Figure 4.17 **PDD reduces the total protein levels of β-catenin, C-MYC and Vimentin but not E-cadherin in MDA-MB-231 cells.** Legend overleaf.

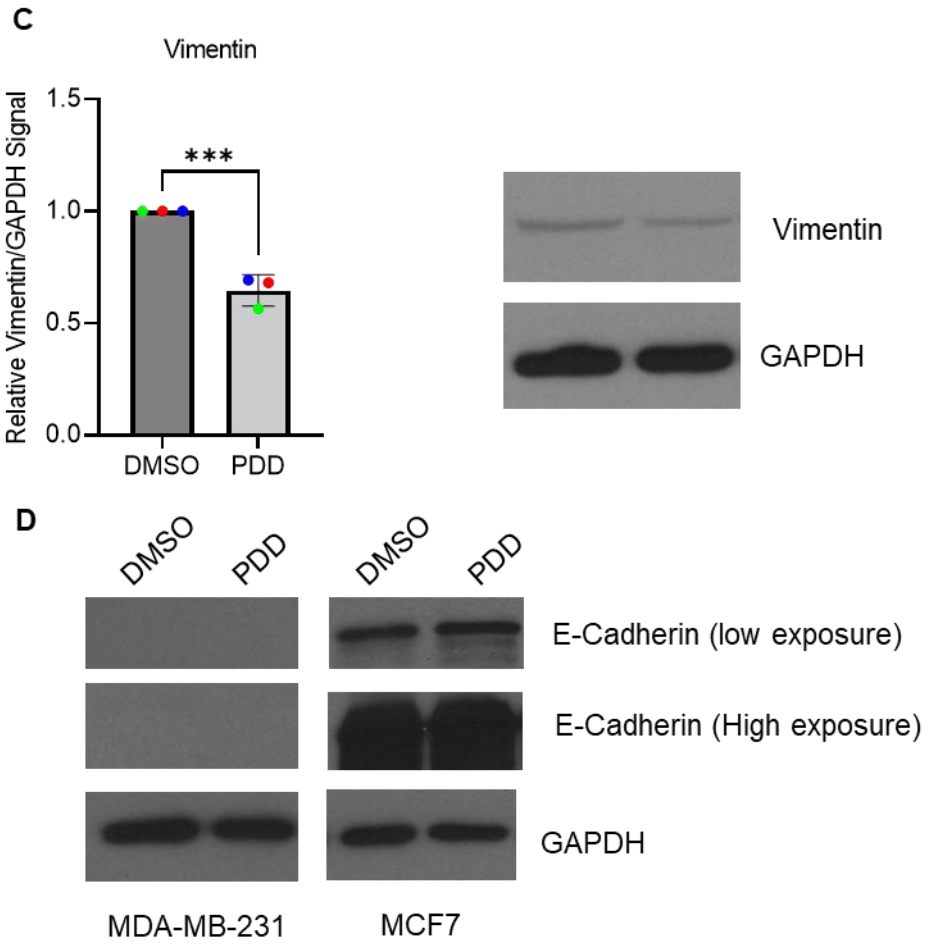

Figure 4.17 **PDD reduces the total protein levels of β-catenin, C-MYC and Vimentin but not E-cadherin in MDA-MB-231 cells.** (A) Densitometry plots of normalised β-catenin adjusted for using GAPDH loading control. (B) Densitometry plots of normalised C-MYC adjusted for using GAPDH loading control. (C) Densitometry plots of normalised Vimentin adjusted for using GAPDH loading control. Representative western blots included. (D) Representative western blot of E-Cadherin protein levels with an MCF7 blot to confirm the antibody is working. N=3-5. An unpaired t-test was performed to assess for statistical significance. *** denotes p= ≤ 0.001, ** denotes p= ≤ 0.01.

4.2.12 PARG inhibition does not impact P-AKT (S473) or Total AKT protein levels

PARG depletion has been reported to increase P-AKT (S473) signalling in colon carcinoma (Fauzee et al., 2012; Q. Li et al., 2012). Therefore, we wanted to assess AKT signalling in the presence of a PARGi. There were no statistical changes in P-AKT (S473), total AKT or the ratio of P-AKT to total AKT when MDA-MB-231 cells were treated with a PARG inhibitor

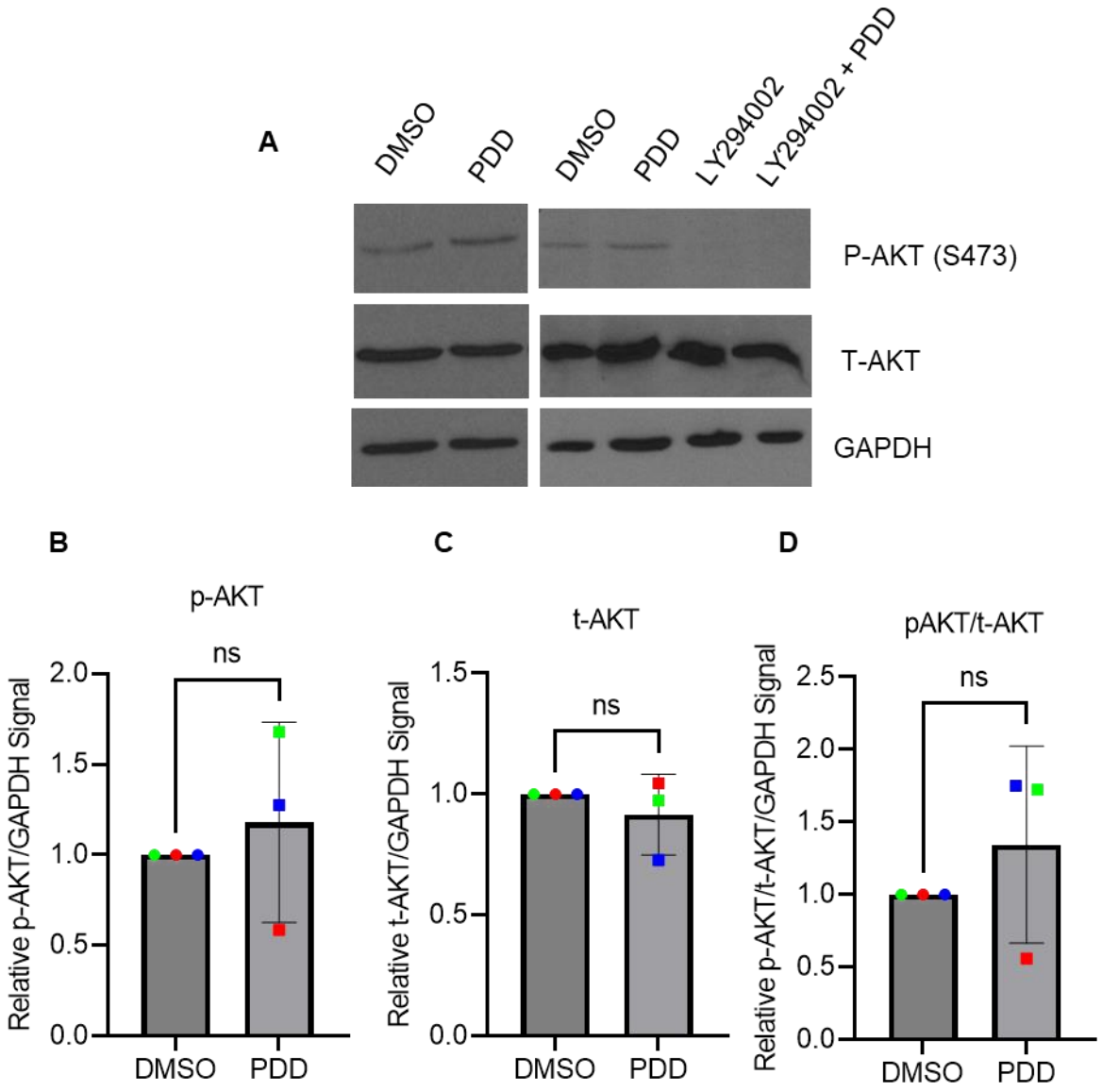

Figure 4.18. **PARGi does not impact p-AKT or total AKT protein levels.** (A) Representative western blots for P/T-AKT densitometry and confirmation of P-AKT (S473) antibody specificity using the P-AKT inhibitor LY294002. (B) Densitometry plots of normalised P-AKT (S473) adjusted for using GAPDH loading control. (C) Densitometry plots of normalised T-AKT adjusted for using GAPDH loading control. (D) Densitometry plots of the ratio of P-AKT to T-AKT adjusted for using GAPDH loading control. N=3. An unpaired t-test was performed to assess for statistical significance. NS denotes no statistical significance. The NS P-vales were 0.6 (A), 0.43 (B) and 0.43 (C).

(figure 4.18A-D). To confirm the specificity of the P-AKT (473) antibody against the phosphorylated epitope, we used the P-AKT inhibitor LY294002 and a reduction in P-AKT (S473) signal was observed (figure 4.17A). This suggests that inhibiting PARG does not impact AKT (S473) phosphorylation in breast cancer.

4.3 Discussion

In this chapter, we aimed to explore the mechanism of PARG inhibitions anti-migratory phenotype. We present evidence that the anti-migratory effects of PARGi is due to metabolic changes and is rescuable with β-NMN pre-treatment. Furthermore, we also present evidence that co-treatment of MDA-MB-231 with a PARGi and PARPi or TNKSi rescued the anti-migration phenotype observed with all treatments individually. We also provide evidence that PARGi impacts the cell morphology, the cytoskeleton, YAP1 localisation and total protein, the nuclear envelope, and reduces total protein of mesenchymal markers that drive migration.

4.3.1 The anti-migratory effects of PARGi are a result of metabolic changes

Pre-treatment with β-NMN, a precursor to NAD+, rescued the anti-migratory effect of PARGi treated but not PARPi treated cells. This suggests that a mechanism underpinning PARGi anti-migratory phenotype is due to metabolic changes. To further investigate this, we quantified the levels of NAD+/NADH and ATP when in the presence of PDD and β-NMN+PDD. β-NMN functioned as a positive control. Surprisingly, NAD+ levels were not impacted by PDD alone, but were increased by β-NMN and β-NMN+PDD. We did however observe a reduction in NADH when MDA-MB-231 cells were treated with PDD. The impact of PARGi in breast cancer on NAD+/NADH has not been reported. PARGi cytotoxicity was enhanced by increasing NAD+ level in glioma cells (J. Li et al., 2021), and is enhanced in IDH1 mutants (Nagashima et al., 2021), when treated with alkylating agents. They did not report the impact of PARGi on NAD+ levels alone. Here, we did not induce DNA damage and enhance PARP activity. However, it's possible β-NMN enhanced PARP activity as elevated NAD+ has been reported to increase α-PAR signal on a western blot (J. Li et al., 2021). The surprising NAD+/NADH ratio seen here could be reflective of heterogeneity within altered metabolic pathways in cancer. NAD+ and NADH can be converted into each

other. Establishing how other breast cancer cells respond and further elucidating these differences could provide insight into which tumours will respond to PARGi and its anti-migratory effects. NADH is required for ATP generation, however only a modest reduction in ATP was observed with PDD.

COH34 is a recently derived highly specific, potent, cell-permable PARG inhibitor that is suitable for in vivo work (S.-H. Chen & Yu, 2019). This is the first time COH34 has been investigated for its role in affecting cell migration. A range of noncytotoxic doses (survival fraction >0.9) that induced a modest increase in α-PAR, reduced the AD of MDA-MB-231 cells. This was also rescued with β-NMN pre-treatment. This observation with two different PARG inhibitors increases the reliability of the result.

4.3.2 The anti-migratory effects of PARGi are contingent on the catalytic activity of PARP/TNKS and their relative protein ratios

Co-treatment of MDA-MB-231 with a PARGi and PARPi or TNKSi rescued the anti-migration phenotype observed with all treatments individually. The AD in co-treatment conditions was similar to the DMSO control. This suggests that the anti-migratory effect of each drug is mediated by the ratio of PARylation vs dePARylation. This is analogous to a mechanism of PARPi resistance, namely reduced PARG expression, increasing the PARP signal (Noordermeer & Van Attikum, 2019). This ratio likely has implications for tumour formation. For example, upregulation of PARG has been reported to suppress PARP driven prostate cancer malignancy (Karpova et al., 2022b). This potentially extends to TNKS as well however has not been experimentally investigated.

4.3.3 The effects of PARGi in A19 (PARP1+/+) and A11 (PARP1-/-) are inconclusive

We wanted to investigate the drug combinations (including β-NMN) in a paired cell line proficient and deficient in PARP1. Interestingly, PARP1 deletion increases the MEF A11 AD. Loss of PARP1 has been reported to promote EMT which drives migration (Pu et al., 2014).

The AD of PARP1 wildtype A19 cells was too low to record differences in drug conditions. Therefore, conclusions about the effects of the drugs and drug combinations in a PARP1 deficient context cannot be made. PARG110 (mouse isoform of human nuclear PARG111) unexpectedly had no detectable levels of PARG110 in the A11 (PARP1-/-) cell line. PARG depletion has been reported to reduce PARP1 expression (Uchiumi, 2013). Perhaps the inverse is also true given that PARP inhibitors can lead to reduced PARG expression (Noordermeer & Van Attikum, 2019). Mouse embryonic fibroblasts metabolically may not be able to tolerate the endogenous β-NMN, as they are not cancer cells, and this may explain why β-NMN alone reduced A11 migration.

4.3.4 PARGi alters MDA-MB-231 cell morphology, the cytoskeleton and decreases the total levels of mesenchymal proteins but does not impact P-AKT (S473)

We noted the PARGi treated MDA-MB-231 cells in the live cell analysis tended to be rounder. When quantified, PDD treated cells had a smaller area, and increased circularity and roundness. Pleasingly, depletion of PARG111 in MDA-MB-231 cells has also been reported to produce a consistent effect on MDA-MB-231 morphology (Marques et al., 2019). MDA-MB-231 cells are mesenchymal, and changes in the cytoskeleton and/or reversal of EMT could explain the change in cell morphology. We observed changes in both.

We observed that when MDA-MB-231 cells were treated with PDD, they exhibited a greater phalloidin F-actin stained integrated density signal in the nucleus, whole cell and cytoplasm. If the total proteins levels were unchanged, differences in the signal could be attributable to changes in the 3D confirmation of F-actin and α-tubulin. This could be confirmed with atomic force microscopy to investigate the stiffness of cells and further explored by examining cytoskeletal cross linkers using confocal microscopy. Consistent with the idea of cytoskeletal crosslinkers being changed, PARGi also increased the number of cells with visible stress fibres. Stress fibres are comprised of actin-myosin and crosslinking rich proteins that typically drive migration. Vimentin has been reported to reduce the assembly of contractile

stress fibres (Jiu et al., 2017). Our data suggests that PDD reduced vimentin total protein levels in MDA-MB-231 cells. Why stress fibres would be present in cells with reduced migration is not intuitive but perhaps is related to the fact migration requires coordination between actin, microtubules, and intermediate filaments. Additionally, we also observed PDD treated MDA-MB-231 cells exhibited a greater α-tubulin stained integrated density signal of the nucleus, whole cell and cytoplasm. It would be interesting to further examine other crosslinking proteins that interact with actin and α-tubulin.

An increase in the number podosomes per cell were also observed. Podosomes aid migration and invasion and their assembly and dynamics are controlled in many ways. A decrease in filipodia length, number of filopodia per cell and average filopodia length per cell was also observed in PDD treated cells. Arp2/3 is a TIP that is required to generate the actin core of podosomes and also controls filopodia formation (Johnston et al., 2008; Linder et al., 2023; Simanov et al., 2021). The effects of TNKSi or PARGi on Arp2/3 have not been investigated but warrants investigation as this could explain the reported changes in filopodia and podosomes.

As previously discussed, YAP1 is controlled by the activation of the hippo pathway and mechanosensing. The changes in cytoskeleton could explain why we observed a reduction in nuclear YAP1 integrated density in PDD treated MDA-MB-231 cells. If the cell stiffness is altered, reduced nuclear YAP1 would imply its less stiff. However, atomic force microscopy would have to be performed to determine this. An alternative and more likely explanation for the reduction in nuclear YAP1, is the reduction of total YAP1 protein which we observed on a western blot. This suggests PARGi either reduces YAP1 expression at a transcriptional or translation level and/or promotes its degradation via the activation of the hippo pathway and/or increases the activity of the E3 ubiquitin ligase SCF(β-TRCP) that targets YAP1 for proteasomal degradation (B. Zhao et al., 2010). Given the large number of roles PARP1-3 and TNKS1/2 are involved in, it's conceivable that inhibiting PARG could impact any of these processes. Probing for p-127 of YAP1 would rule out if hippo signalling is altered. Inhibiting

TNKS1/2 has been reported to stabilise AMOT, suppressing YAP1. If PARG reverses TNKS1/2 PARylation of AMOT, then PARGi could reduce AMOT levels. However, this would not account for the decrease in total YAP1 protein we observed. Perhaps co-treating cells with a PARPi or TNKSi and a PARGi and monitoring for YAP1 nuclear localisation and total protein levels could provide insight how PARGi is affecting YAP1.

We observed a reduction in EMT markers when MDA-MB-231 cells were treated with a PARGi. We observed a reduction in total protein levels of β-catenin, C-MYC and vimentin. This suggests PARGi can partially promote MET or reduce the mesenchymal markers at the protein level. PARG +/- mice treated with the carcinogen bezno(a)pyrene, have been reported to reduce the expression of Wnt ligands, stabilise Axin by increased PARylation and increase the phosphorylation of proteins within the DC (Dai et al., 2019). The model presented describes how a reduction in PARG could stabilise the DC, hence the reduction in β-catenin protein levels that they reported. It's conceivable this occurs with a PARGi. PARGi has been reported to reduce the accumulation of PARP1-DNA complexes (Gogola et al., 2018). PARP1 is associated with the C-MYC promoter, driving chromatin decondensation and C-MYC expression (Mostocotto et al., 2014). PARP inhibition prevents this from occurring (Mostocotto et al., 2014). It is unknown if PARG plays a role in this PARP1-C-MYC axis but it is possible PARGi prevents efficient transcription of C-MYC if the number of PARP1-DNA complexes are altered as a result PARGi (Gogola et al., 2018). The catalytic activity of PARP1 is required to drive C-MYC expression (Mostocotto et al., 2014). Perhaps ADP-riboslyated PARP is unable to bind to the C-MYC promoter. PARP1 also binds to promoter of vimentin and drives vimentin expression, independently of PARP1's catalytic activity (Chu et al., 2007). PARGi may also prevent ADP-ribosylated PARP1 from binding the vimentin promoter.

Finally, the depletion of PARG has been reported to increase P-AKT (S473) signalling in colon carcinoma (Fauzee et al., 2012; Q. Li et al., 2012). We observed no changes in P-AKT,

T-AKT or in the ratio of the two when adjusted for GAPDH loading control. This could be due to it being a different tumour background or it being a feature of depleting the PARG protein.

4.4.5 PARGi alters MDA-MB-231 nuclear morphology and the nuclear envelope

We observed that the DAPI stained nucleus of MDA-MB-231 cells treated with PDD had a lower nuclear area and circularity. This is the first time PARGi has been reported to impact the morphology of the nucleus. MCF7 nuclear morphology was unaffected. Consequently, we wanted to explore if the nuclear envelope of MDA-MB-231 cells treated with PDD was altered. We performed analysis of confocal images of DAPI and Lamin A stained cells. PDD treated MDA-MB-231 exhibited an increase in nuclear envelope gaps, invaginations, and blebs, as a percentage of cells analysed.

Nuclear gaps or ruptures are attributable to changes in nuclear lamina organisation, mechanical stress, chromatin bridge resolution and improper nuclear envelope formation and repair (Hatch, 2018; Maclejowski & Hatch, 2020). These observations were not due to changes in the total protein levels of Lamin A or Lamin B1. Changes in total protein are usually associated with altered nuclear lamina organisation and nuclear rupture (Hatch, 2018). No evidence exists for PARylation affecting lamin B2. The cytoskeletal changes we have reported could increase the mechanical stress on the nucleus. Chromatin bridges form because of sister chromatid telomeric fusion however PARG depletion in Hela cells has been reported to reduce sister chromatid telomere fusion (J Ame et al., 2009). Only PARP8/11/16 have been implicated in nuclear envelope formation (Richard et al., 2022) and no PARylator has been implicated in resolving nuclear envelope damage.

Nuclear invaginations facilitate nuclear import/export and are associated with chromatin remodelling as well as localising around sites of DNA repair (Schoen et al., 2017). Their formation is believed to be mechanically mediated as a result pushing and pulling forces (Schoen et al., 2017). An example of pushing forces on the nuclear envelope would be

generated by the polymerization of cytoskeletal components. An example of pulling forces on the nuclear envelope would chromosomal rearrangements pulling on lamin anchored to the nuclear envelope. The elevated levels of F-actin and α-tubulin we observed in response to PDD treatment imply there is an increase in polymerisation or a decrease in depolymerisation. It's unclear which, but it would provide support for the pushing forces. The role of PARP1 in transcription, chromatin remodelling, DNA replication and repair and the potential role PARG plays in these processes could also account for the pushing forces and may explain why increased nuclear invaginations were observed when cells were treated with a PARGi.

Nuclear blebs are abnormal nuclear protrusions that arise because of lamin and chromatin alterations or intranuclear pressure from perinuclear actomyosin (Shah et al., 2017; Stephens et al., 2018). Softer nucleus are more likely to exhibit nuclear blebs. PARP1 PARylates histones leading to chromatin relaxation, regulates other histone modifications and regulates the 3D organisation of chromatin in conjunction with CTCF. The impact of PARGi on nuclear stiffness has not been explored but given the roles of PARP1, it's conceivable inhibiting PARG would have consequences for nuclear stiffness but needs to be investigated experimentally. Bleb formation has been reported to be induced because of changes in the ratios of Lamins. The impact of PARGi on Lamin B2 is unknown so this possibility cannot be ruled out. Our cytoskeletal observations could account for the nuclear blebs as well if they are increasing the intranuclear pressure.

In summary, we observed reduced cellular migration in PDD treated cells, that can be rescued with β-NMN supplementation and changes in the NAD+/NADH ratio and decreased levels of ATP may underpin the reduced migration. Additionally, co-treatment with a PARP/TNKSi and PARGi can restore cellular migration, suggesting the ratio between PARylation and dePARylation must be maintained to promote migration. We also observed increases in F-actin and α-tubulin, with changes in the dynamics of actin sub-structures such as stress fibres, podosomes and filopodia in the presence of a PARGi. PDD treated cell

nuclei also exhibited increases in nuclear ruptures, invaginations and blebs and were smaller in area and circularity and that this was not due to changes in the total protein levels of Lamin A and B1. We observed a reduction in nuclear and total YAP1 protein levels in PDD treated cells, as well as a reduction in mesenchymal markers. Surprisingly, P-AKT (S473) levels in the presence of PDD remained unchanged. All these observations provide insight into how PARGi may be reducing cellular migration, however require further validation before causality can be claimed.

4.4.6 Limitations

Except for the β-NMN and NADH data, almost all the data is correlational and requires further study to demonstrate that these observations are contributing to the reduced migration observed in PDD treated MDA-MB-231 cells. The same could be said for the changes in cytoskeleton and the observations surrounding the nucleus morphology and envelope abnormalities. The use of β-NMN is also partially limiting as other NAD+ precursors could have been used and exploring what the rescue effect would be with different NAD+ precursor involved in different NAD+ generating pathways would have provided additional insight. Additionally, the attempts to gauge whether our observations were dependant on PARP1 are limited by the fact that the A19 wild type cells barely migrated, making comparisons and conclusions difficult.

Chapter 5.0 Results: Evaluation of PARG Inhibitors on Global Transcription in MDA-MB-231 cells

5.1 Introduction, aims and hypothesis

The PARP protein family has a wide range of mechanisms by which they alter transcription: modulating chromatin structure ((Krishnakumar et al., 2008), functioning as transcription factors themselves ((Akiyama et al., 2001; K. Huang et al., 2004), or impacting the recruitment of transcription factors and other regulatory elements to DNA (Lin et al., 2011; Simbulan-Rosenthal et al., 2003), as well as affecting post transcriptional processes such as mRNA stability (Di Giammartino et al., 2013) and impacting RNA binding (Isabelle et al., 2010; Jungmichel et al., 2013; Teloni & Altmeyer, 2016). However, the consequence of PARG inhibition on global transcription has not been investigated. Here we investigate the transcriptional changes induced by a non-cytotoxic dose (0.3 µM) of the PARG inhibitor PDD00017273 (PARGi) on the triple negative breast cancer cell line MDA-MB-231. This model was chosen because extensive research regarding the PARP family has been performed in breast cancer, including transcriptional profiling of PARPi treated and PARP depleted MDA-MB-231 cells (Dutta et al., 2020; Parra, 2012). In addition PARG is highly expressed in breast cancer where higher expression correlates with poorer survival (Marques et al., 2019) and depletion/inhibition of PARG in breast cancer has shown therapeutic promise *in vitro* and *in vivo* (Gravells et al., 2018; Marques et al., 2019), meaning that any changes in gene expression seen might be of translational relevance or provide insight into how PARGi may work therapeutically.

The hypothesis of this chapter are:

1. PARG inhibition will Impact global transcription
2. These identified differentially expressed genes will provide potential insight into PARG function

3. These identified differentially expressed genes will provide insights into potential novel applications for PARGi's

The aim of this chapter are therefore as follows:

1. Identify differentially expressed genes
2. Interrogate the differentially expressed genes for functional enrichment with a range of bioinformatic approaches
3. Highlight the top differentially expressed genes in terms of fold change and statistically significance and explore their function and significance on breast cancer prognosis
4. Relate these results to known PARG function and consequences of inhibition

Figure 5.1 depicts the workflow of this chapter. Chapter 5.2.2 discusses the rational for using different pathways of analysis.

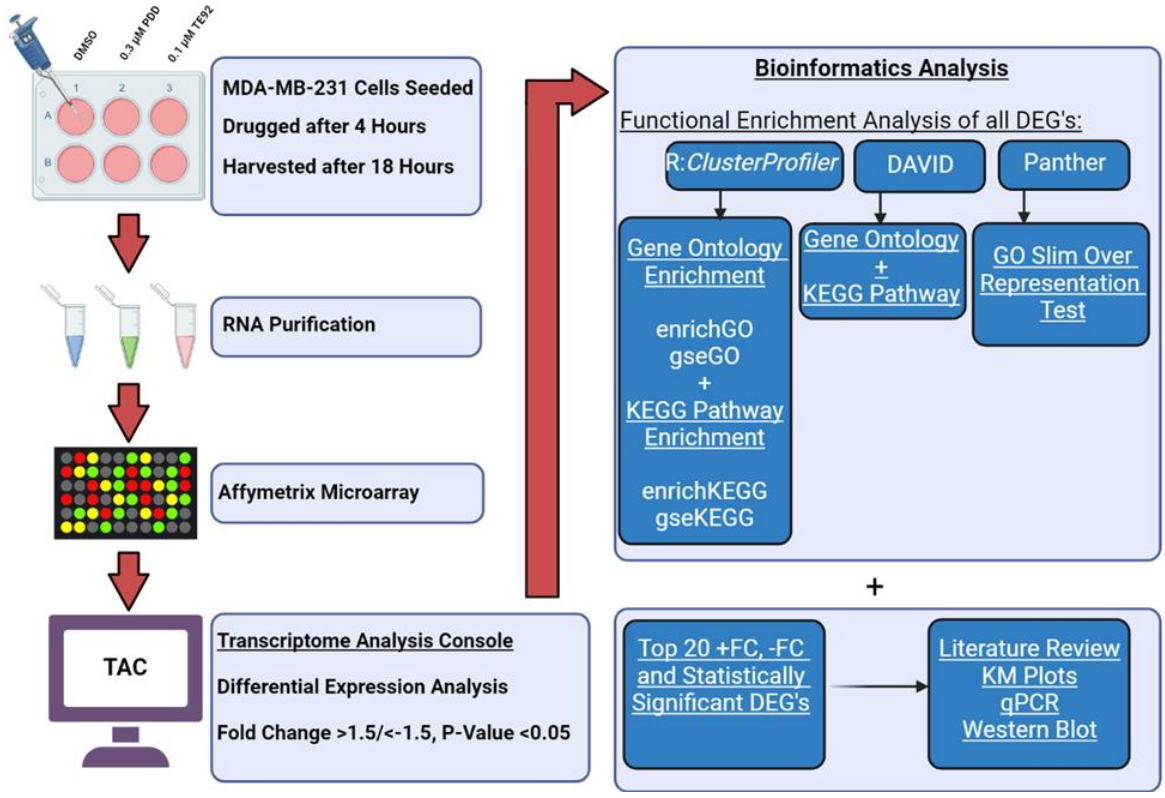

Figure 5.1. **Summary of workflow investigating PARGi induced changes in global Transcription.** Legend overleaf.

Figure 5.1 **Summary of work flow investigating PARGi induced changes in global Transcription.** MDA-MB-231 cells were seeded and drugged as per the migration protocol. The RNA was purified and submitted for Affymetrix microarray analysis and was performed by Paul Heath. Differentially expressed genes were identified using the transcriptome analysis console with a fold change threshold of -/+1.5 and p=≤0.05 (thermofisher). This produced 139 genes that were interrogated for bioinformatics analysis. The R package cluster profiler was used to performed gene ontology enrichment using the enrichGO and gseGO functions and KEGG pathway enrichment using the enrichKEGG and gseKEGG functions (Yu, et al. 2012, Wu, et al. 2021). The gene list was also inputted into DAVID and the gene ontologies of biological processes was investigated, as was enriched KEGG pathways (Huang, et al. 2009, Sherman, et al. 2022). A gene ontology slim over representation test was also performed in panther (Mi, et al. 2019, Thomas, et al. 2022). Additionally, a review of the functions of the top 20 differentially expressed genes in terms of -/+ fold change and statistical significance was performed. These same genes were also assessed for their expression levels prognostication on breast cancer (Lanczky & Gyorffy, 2021) and a sub population of them were validated by qPCR and western blot.

5.2 Results

5.2.1 Microarray Quality Controls

Following extraction of RNA, quality controls, RNA integrity analysis and the Affymetrix microarray were all performed in house by Dr Paul Heath. Figure 5.2 shows the microarray labelling controls (figure 5.2A), hybridization controls (figure 5.2B) and the positive versus negative area under the curve (figure 5.2C). In every instance, each condition within each biological condition passed quality control. The principal component analysis (PCA) is depicted in figure 5.2D. There is greater variation amongst the PDD biological repeats versus DMSO along the PCA axis', suggesting greater variation amongst the PDD treated transcriptomic data.

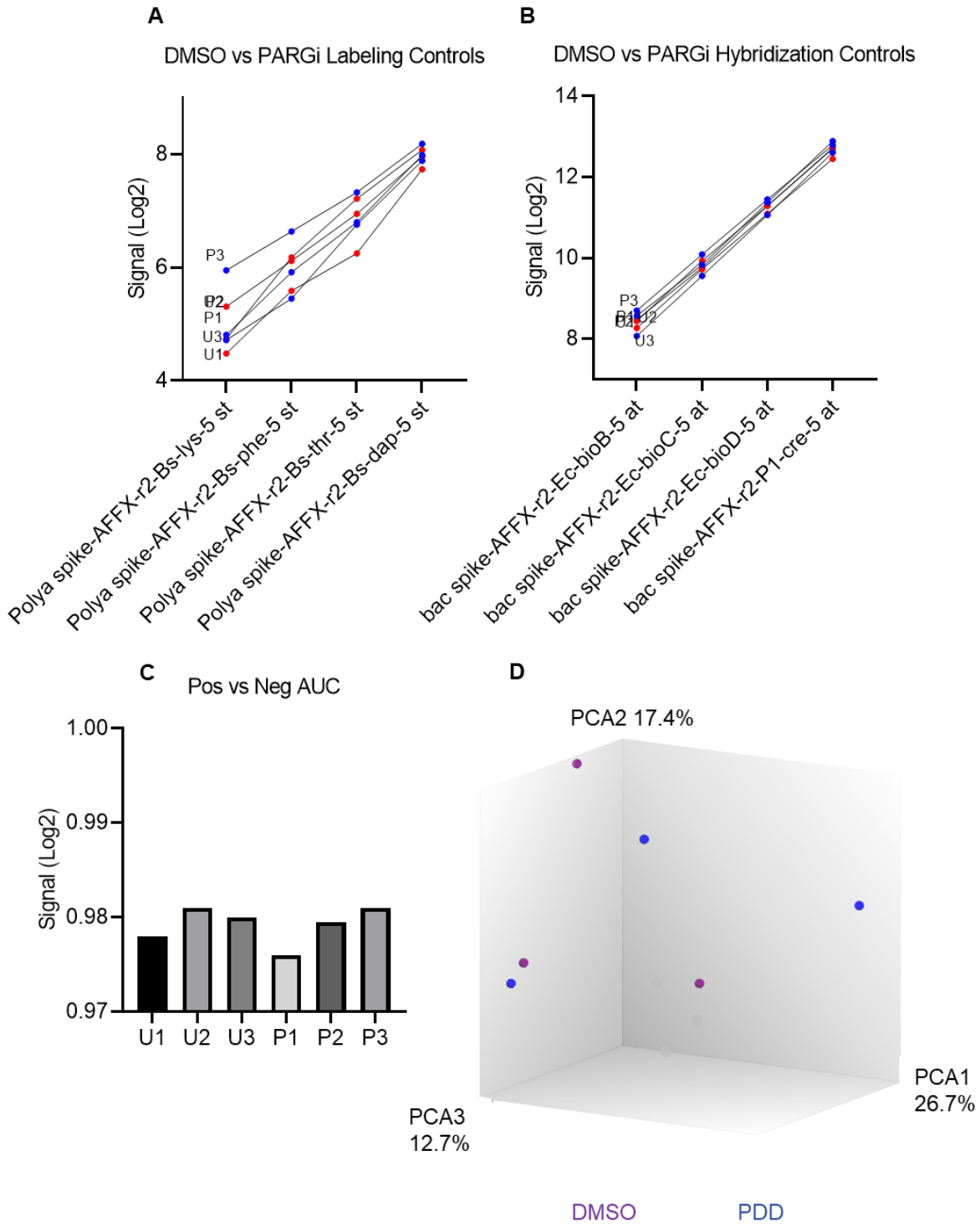

Figure 5.2. **Microarray Quality Controls of each biological repeat within each condition.** (A) Labelling Controls (B) Hybridization controls (C) Positive vs Negative Area under the curve (D) PCA of DMSO and PDD treatment conditions for each biological repeat.

5.2.2 Identification of Differentially Expressed Genes

Differentially expressed genes (DEGs) were identified using the Transcriptome Analysis console (TAC) version 4.0.1. In brief, following the treatment of MDA-MB-231 cells, RNA was purified and submitted for Affymetrix Microarray analysis. The resulting Clarion_S_Human .CEL files were imported into TAC. A p-value of less than 0.05 and fold change greater than 1.5 or less than -1.5 was used as a cut off for significance (figure 5.3). These criteria produced a gene list consisting of 139 genes (Figure 5.4).

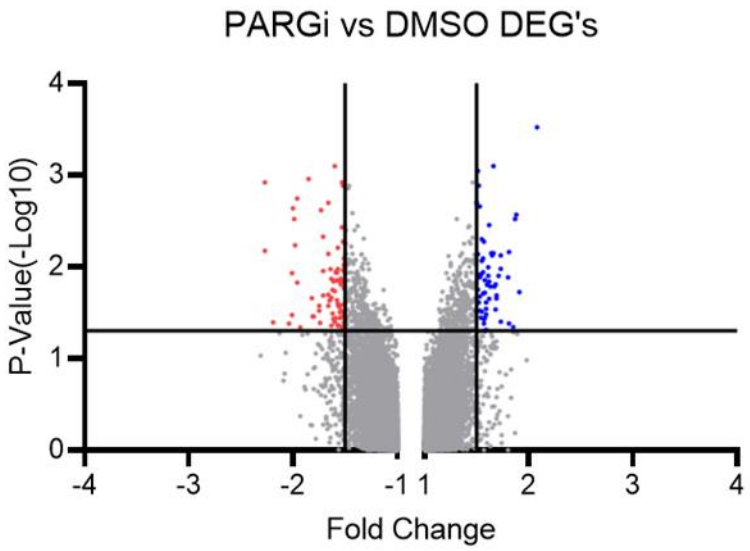

Figure 5.3 **Treatment with PARG inhibitor results in 139 statistically significant differentially expressed genes (DEG).** –log10 p-value of 1.3 (p-value ≤0.05) and -/+ 1.5 fold change threshold allowing for visualisation of all 139 differentially expressed genes amongst all genes probed for in the microarray (21448).

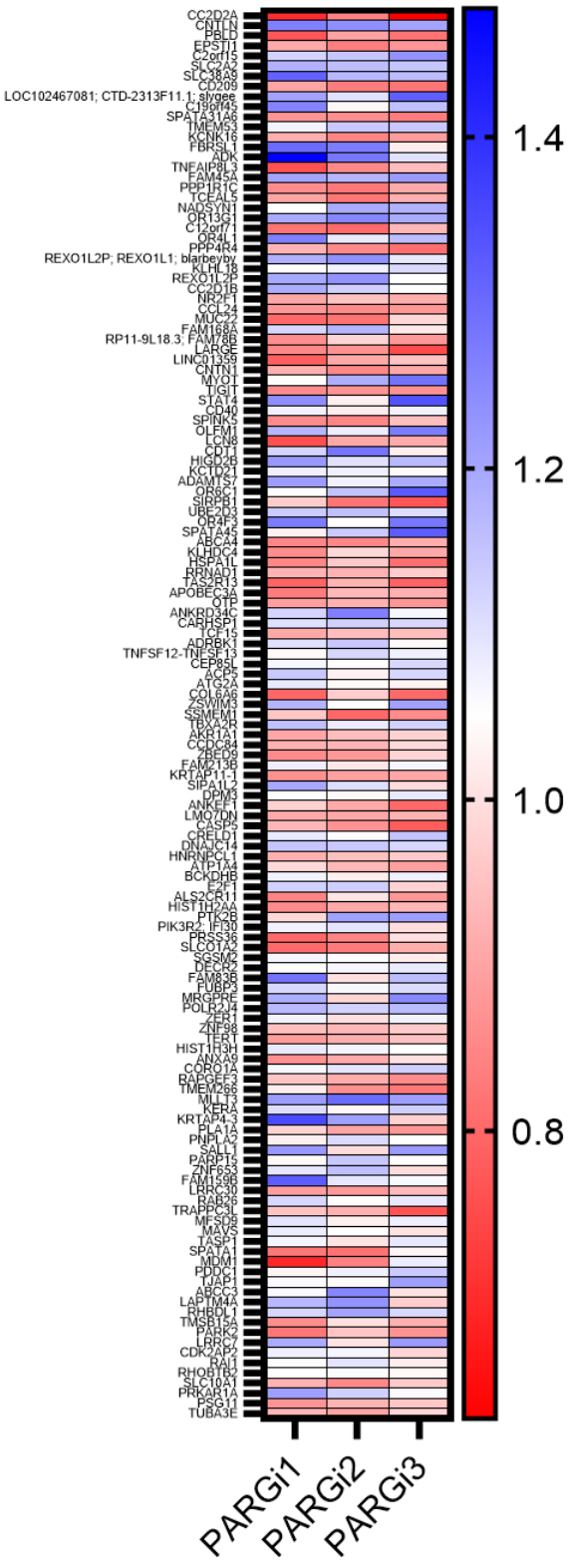

Figure 5.4 **Differentially expressed genes directionality is consistent across biological repeats.** These are the 139 differentially expressed genes, rank ordered by p-value (ebayes method). The axis depicts the relative log2 fluorescent signal of differentially expressed genes in PDD treatment conditions adjusted with the respective biological repeats DMSO signal (DMSO/PDD signal). Red denotes downregulation and blue denotes upregulation.

5.2.3 Functional Enrichment using Cluster Profiler

Having identified the DEG's, Gene Ontology Enrichment analysis (GOEA) and KEGG pathway enrichment analysis (KPEA) were both used to explore functional enrichment. Gene ontology is a hierarchy of classification based on the ascribed biological processes (BP), Molecular Functions (MF) and Cellular components (CC) the genes have been implicated in. Each hierarchy is split into levels and the higher the level, the greater degree of specificity there is within that ontological domain. Kyoto Encyclopaedia of Genes and Genomes (KEGG) is a collection of databases used to explore largescale datasets and is useful for pathway visualisation. Both GOEA and KPEA within the Clusterprofiler package have two means of assessing enrichment: Gene set enrichment (GSE) and enrichment. GSE allows for greater sensitivity as it factors fold change into the analysis, i.e. It's conceivable that even if only a small number of genes in a particular pathway are altered if the fold change of each is altered drastically this could have a significant biological effect. Enrichment simply factors in the ontological term/KEGG pathway and whether it is overrepresented versus the background gene list. Consequently, these yield different outputs, and the results of both will be depicted for each type of enrichment analysis. Additional enrichment tests were performed, namely DAVID and PANTHER, as each uses different databases, with different gene annotations, along with different background lists and thresholds for significance. This provides greater confidence in reliably observed hits and allows for wider insight into enriched terms.

5.2.3.1 Enriched Gene ontology Terms

The Entrez ID's of the 139 DEGs were imported (without fold change) into R and GO enrichment was performed using the Clusterprofiler enrichGO function. This retrieved 266 biological processes that were statistically enriched following PARGi. The top 20 were rank ordered by p-value (Figure 5.5A). The genes count ranged from 1-4.

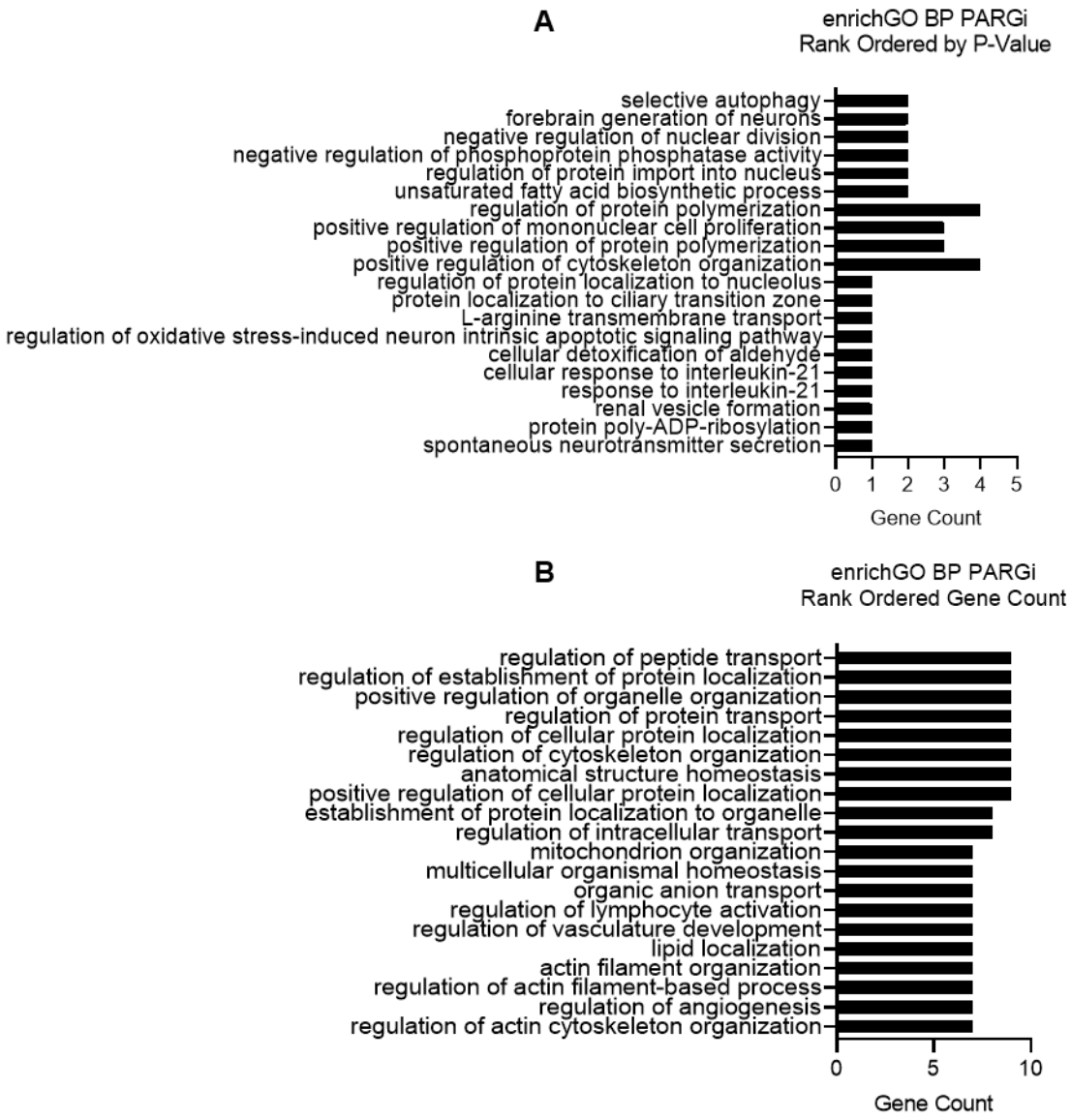

Figure 5.5 **Statistically significant biological processes (<0.05 P-value) retrieved by the *enrichGO* function in the R package Clusterprofiler.** (A) Top 20 Rank ordered by p-value (B) Top 20 Rank ordered by gene count

A broad range of biological processes were retrieved and are summarised in figure 5.5. Of note with respect to migration is the positive regulation of protein polymerization and positive regulation of cytoskeleton organization.

The top 20 biological processes were also rank ordered based on gene count (Figure 5.5B). In this case the gene counts ranged from 7-9. A broad range of biological processes were retrieved and are summarised in figure 5.5. Of note with respect to migration include:

organelle organization, regulation of cytoskeleton organization, mitochondrion organization, actin filament organization, regulation of actin filament-based process and regulation of actin cytoskeleton organization.

5.2.3.2 Gene set enrichment of Gene Ontology Terms

The Entrez ID's with the associated fold changes of the 139 DEGs were imported into R and gene ontology (GO) gene set enrichment was performed using the Clusterprofiler gseGO function (figure 5.6). Only 6 biological processes were statistically significant so statistically significant hits in terms of molecular function and cellular compartment were also included. This produced 11 terms which were rank ordered by p-value (Figure 5.6). The enrichment scores ranged from -0.88 to 0.70. Semantically similar hits have been omitted. The enriched terms were endosome/late endosome, regulation of cellular catabolic process, zinc ion binding, enzyme binding, cellular biosynthetic process, transition metal ion binding, anatomical structure homeostasis and catabolic process.

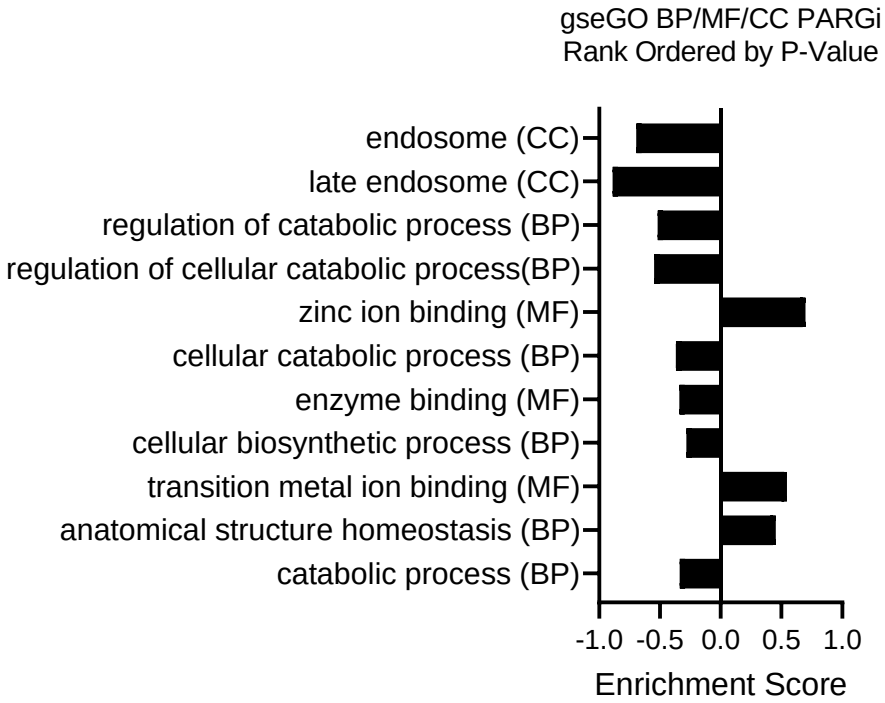

Figure 5.6 **All Statistically significant biological processes (BP), molecular functions (MF), and cellular compartments (CC) (<0.05 P-value) retrieved by the *gseGO* function in the R package Clusterprofiler rank ordered by p-value.**

5.2.3.3 KEGG Pathway Enrichment Analysis

The Entrez ID's with the associated fold changes of the 139 DEGs were imported into R and KEGG Pathway enrichment was performed using the Clusterprofiler enrichKEGG function. The gene counts ranged from 2 – 6 (figure 5.7). The statistically significant KEGG pathways included hepatitis B, bile secretion, carbohydrate digestion and absorption, measles, aldosterone-regulated sodium reabsorption, ABC transporters, type II diabetes mellitus, chemokine signalling pathway and leukocyte transendothelial migration (figure 5.7).

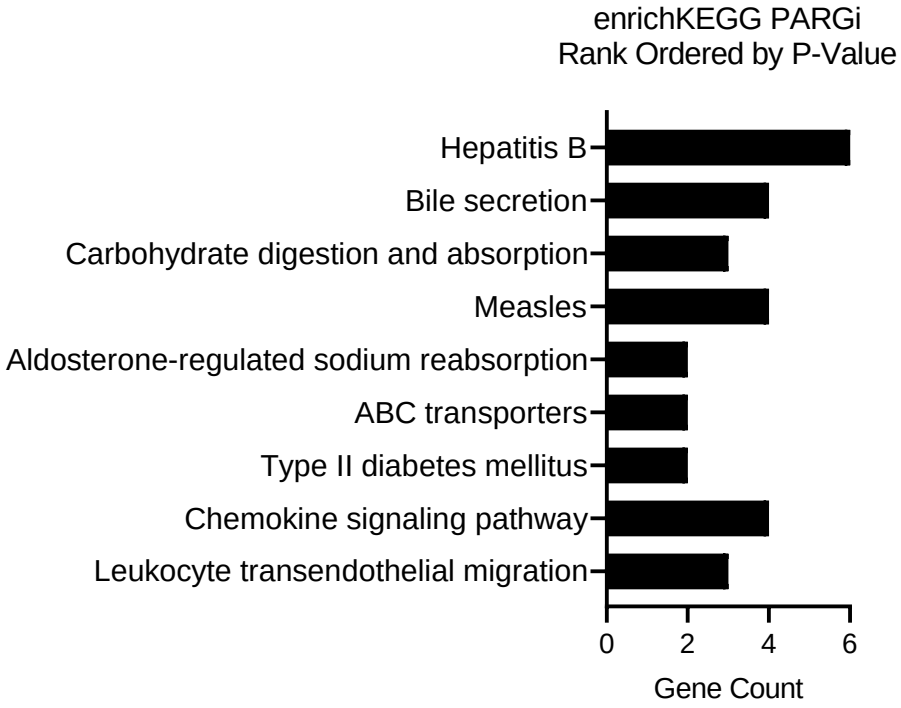

Figure 5.7 **All Statistically significant KEGG pathways (<0.05 P-value) retrieved by the *enrichKEGG* function in the R package Clusterprofiler rank ordered by p-value.**

5.2.3.4 Gene Set enrichment of KEGG Pathways

The Entrez ID's with the associated fold changes of the 139 DEGs were imported into R and KEGG Pathway enrichment was performed using the Clusterprofiler gseKEGG function. The only retrieved term with an enrichment score of -0.72 was hepatitis C (figure 5.8).

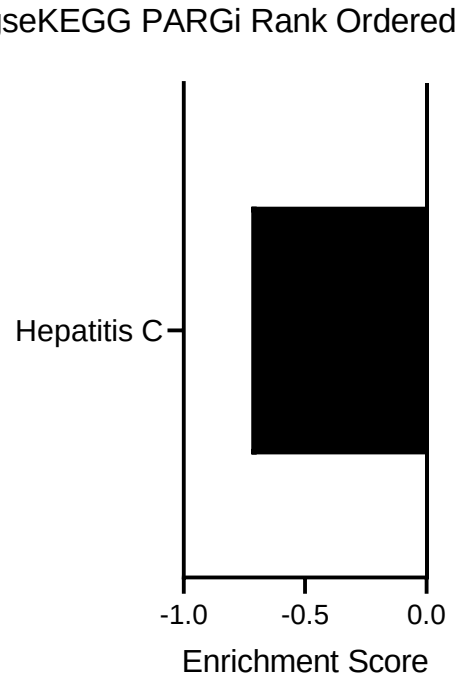

Figure 5.8 **Statistically significant KEGG pathways (<0.05 P-value) retrieved by the *gseKEGG* function in the R package Clusterprofiler.**

5.2.4 Functional Enrichment using DAVID

The official gene symbols without the associated fold changes of the 139 DEGs were imported into DAVID – The database for annotation, visualization, and integrated discovery to assess for functional annotation (D. W. Huang et al., 2009; Sherman et al., 2022). DAVID recognised 126 of the DEG. The database regarding the gene ontologies related to biological processes was only able to retrieve annotations for 104 of those 139 genes. The Threshold settings of count 2 and EASE 0.2 were used and it retrieved 23 significant biological processes (figure 5.9A). The gene counts ranged from 2 - 11. A range of biological processes were retrieved. With respect to migration, these included regulation of cell shape, positive regulation of GTPase activity, regulation of actin cytoskeleton reorganization, actin

filament organization and regulation of actin filament polymerization. Encouragingly, several PARG associated signalling pathways were included i.e. positive regulation of PI3K, cellular response to tumour necrosis factor and positive regulation of Wnt signalling pathway.

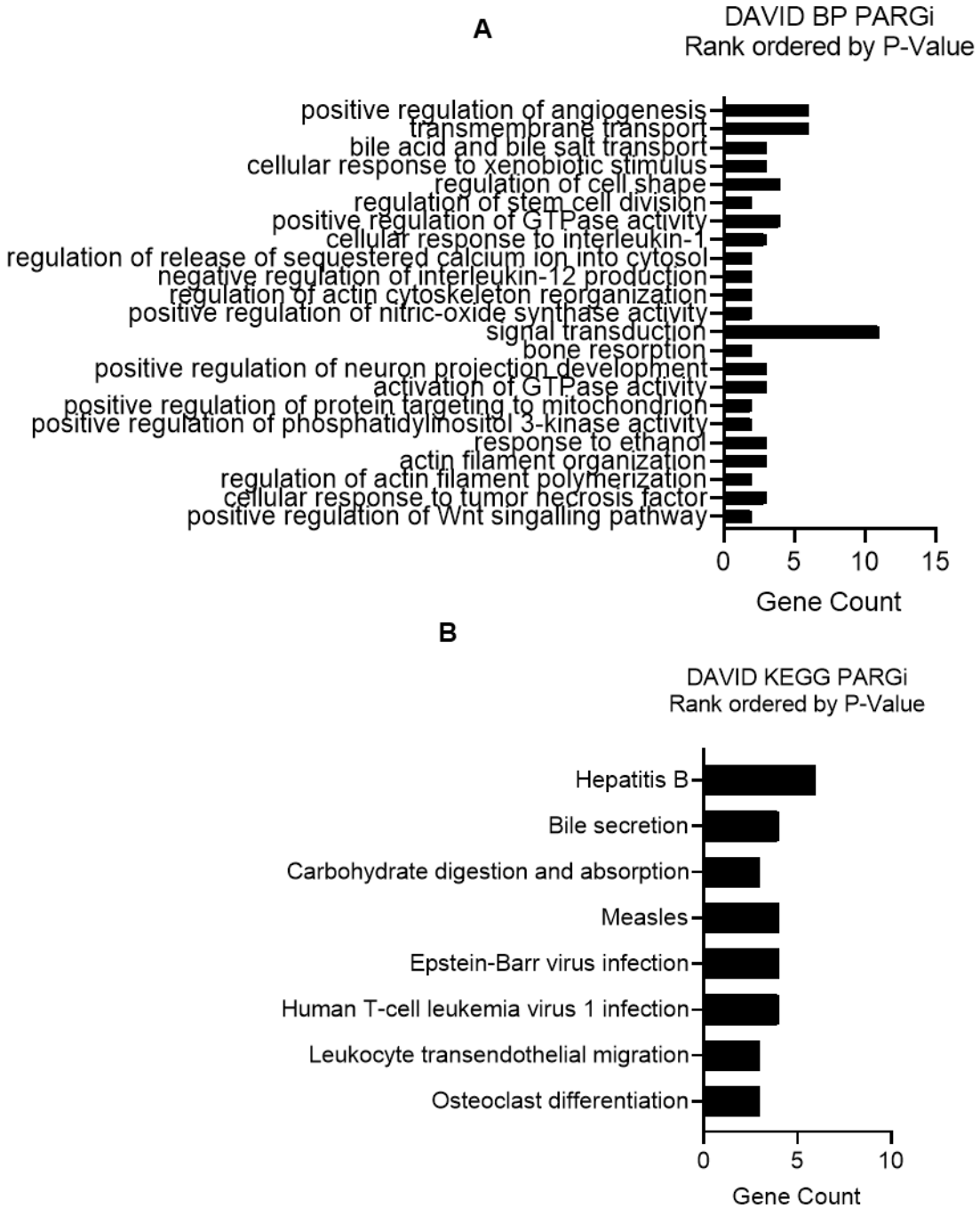

Figure 5.9 **DAVID Functional Enrichment.** (A) Statistically significant biological processes (<0.05 P-value) retrieved by DAVID rank ordered by p-value (B) Statistically significant KEGG pathways retrieved DAVID KEGG pathway analysis (<0.05 P-value).

KEGG pathway analysis was also performed in DAVID. The gene count ranged from 3 -6. Figure 5.9 rank orders the enriched KEGG pathways by p-value. The pathways retrieved included hepatitis B, bile secretion, carbohydrate and absorption, measles, Epstein-barr virus infection, human T-cell leukaemia virus 1 infection, leukocyte transendothelial migration and osteoclast differentiation (figure 5.9).

5.2.5 Functional Enrichment using PANTHER

The official gene symbols without the associated fold changes of the 139 DEGs were imported into PANTHER – Protein analysis through evolutionary relationships (Mi et al., 2016; Thomas & Mushayahama, 2022). To reduce the number of annotations that were semantically similar, a statistical over representation test was performed using the PANTHER GO slim biological processes. Of the 139 genes, PANTHER was able to perform the analysis on 125. There were 50 statistically significant results retrieved. The top 20 biological processes retrieved were rank ordered by p-value (Figure 5.10A). The gene counts ranged from 1-5. A wide range of biological processes were retrieved (figure 5.10A). Migration relevant terms include: regulation DNA metabolic process, positive regulation GTPase activity, cell-cell adhesion, positive regulation of cytokine production. The top 20 biological processes rank ordered by gene count (range 2-5) were also listed (figure 5.10B). The migration relevant terms from 5.10B overlapped with the relevant terms in figure 5.10A.

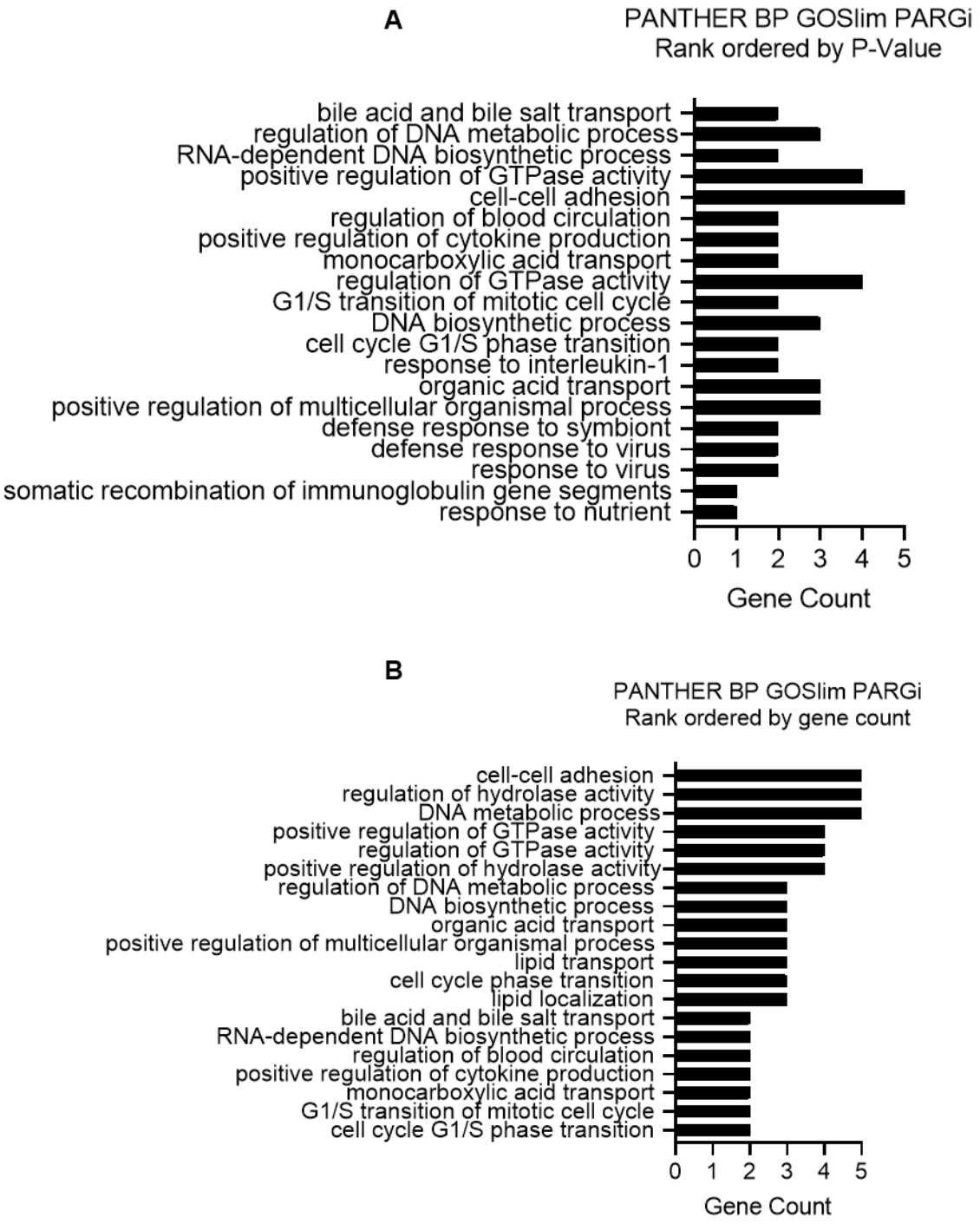

Figure 5.10 **Panther Biological Process Gene Ontology Slim Over representation test.** (A) Top 20 statistically significant (<0.05 P-value) GO slim biological processes retrieved by PANTHER rank ordered by p-value (B)Top 20 statistically significant (<0.05 P-value) GO slim biological processes retrieved by PANTHER rank ordered by gene count.

5.2.6 Exploring the most significant differentially expressed genes by fold change or statistical significance

The bioinformatics approach deployed so far determines the ontologies and pathways which are statistically enriched. Whilst useful, particularly with large data sets, it doesn't necessarily capture the potential nuance of biology. A term/pathway may not be enriched but a single gene in a pathway in a particular biological context can still exert a notable effect. For example, PARG deletion/inhibition is linked to phenotypic changes in mitosis and while mitotic related processes were not enriched in our analysis, there were some DEGs in the list that are associated with mitosis, and these may be relevant to understanding of PAR biology and PARG inhibition in the context of mitosis. Therefore, expression of individual DEGs was considered. The top 20 DEGs were determined both by fold change and by statistical significance, producing a list of 50 distinct genes, with 25 being upregulated and 25 being downregulated (figure 5.11).

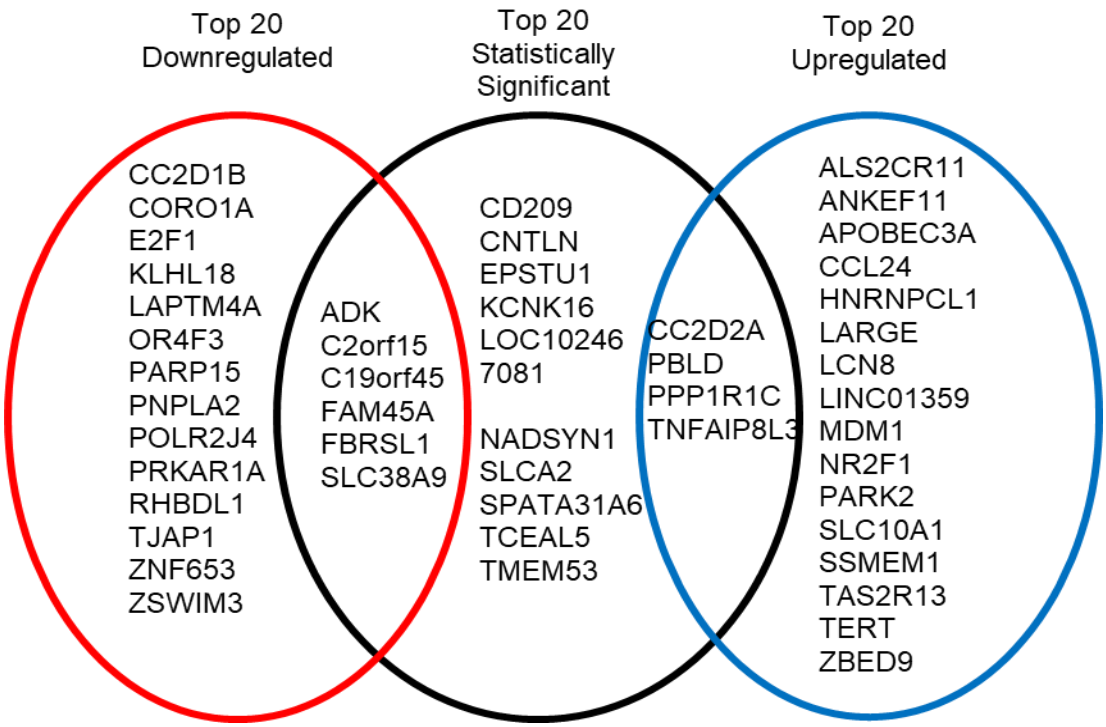

Figure 5.11 **Top 20 differentially expressed genes by -/+ 1.5 fold change and statistical significance.** Highlights which group each gene belongs to and equates to 50 genes total.

PARG inhibition downregulated expression of genes involved in nuclear envelope repair, transport, proteolysis, metabolism, RNA/DNA/protein binding, transcription, actin regulation, centrosome cohesion and cancer associated pathway modulation. In depth details on each gene are provided in figure 5.12A/B. In contrast, PARG inhibition upregulated genes involved in cilliogenesis, cell protrusion, lipid transfer, apoptosis, transport, proteolysis, cytidine deamination, receptors, microtubule stabilization, nucleosome assembly, fertility, telomeres, chemotaxis, polarization, metabolism, differentiation, transcription, and the modulation of cancer associated pathways. In depths details on each gene are provided in figure 5.12C/D.

A

Gene Name	Fold Change	P-Value	Gene Information
CC2D1B	-2.27	0.0067	Nuclear Envelope Rupture and repair during cancer cell migration, mitotic NE, TF
SLC38A9	-2.27	0.0012	Lysosomal amino acid transporter, upstream of mTORC1
TJAP1	-2.19	0.0403	Golgi Regulation and Cellular tight junctions
RHBDL1	-2.04	0.0414	Proteolysis, EFGR pathway?
OR4F3	-2.01	0.0117	Olfactory Receptor
PNPLA2	-2.01	0.0336	Triglyceride Hydrolysis, pro BRCA microenvironment
FBRSL1	-2	0.0023	RNA Binding
FAM45A	-1.99	0.003	Endocytic pathway Homeostasis
KLHL18	-1.98	0.0058	E3 Ligase – mitotic progression and cytokinesis
C19orf45	-1.96	0.0018	Testis Associated
ZSWIM3	-1.96	0.0149	DNA Binding and Protein Interactions
PRKAR1A	-1.93	0.046	cAMP-dependant protein kinase regulation – MAK, PI3k/AKT, JAK/STAT, Wnt beta-catenin
C2orf15	-1.85	0.0011	Protein and RNA Binding
E2F1	-1.82	0.0219	Multifunctional Transcription Factor
PARP15	-1.81	0.0347	Mono-ADP-Ribosylator, negatively regulates transcription
ZNF653	-1.8	0.0348	Transcriptional Repressor
CORO1A	-1.75	0.03	Actin and Locomotion
POLR2J4	-1.75	0.0267	Pseudogene
LAPTM4A	-1.74	0.0409	Nucleoside Transportation
ADK	-1.73	0.0024	ATP dependant AMP Biosynthesis
TMEM53	-1.66	0.002	Part of a Tumour Suppressor/Oncogene Family
CNTLN	-1.6	0.0008	Centrosome cohesion and CEP68 recruitment
SLC2A2	-1.53	0.0012	Glucose Transporter
NADSYN1	-1.53	0.0037	Final Step of NAD+ de novo synthesis pathway
LOC102467081	-1.52	0.0013	LncRNA

Figure 5.12 **Top hits are involved in a wide array of biological processes.** Legend overleaf plus three.

B

Gene Name	Fold Change	P-Value	Gene Information
CNTLN	-1.6	0.0008	Centrosome cohesion and CEP68 recruitment
C2orf15	-1.85	0.0011	Protein and RNA Binding
SLC38A9	-2.27	0.0012	Lysosomal amino acid transporter, upstream of mTORC1
SLC2A2	-1.53	0.0012	Glucose Transporter
LOC102467081	-1.52	0.0013	LncRNA
C19orf45	-1.96	0.0018	Testis Associated
TMEM53	-1.66	0.002	Part of a Tumour Suppressor/Oncogene Family
FBRSL1	-2	0.0023	RNA Binding
ADK	-1.73	0.0024	ATP dependant AMP Biosynthesis
FAM45A	-1.99	0.003	Endocytic pathway Homeostasis
NADSYN1	-1.53	0.0037	Final Step of NAD+ de novo synthesis pathway
KLHL18	-1.98	0.0058	E3 Ligase – mitotic progression and cytokinesis
CC2D1B	-2.27	0.0067	Nuclear Envelope Rupture and repair during cancer cell migration, mitotic NE, TF
OR4F3	-2.01	0.0117	Olfactory Receptor
ZSWIM3	-1.96	0.0149	DNA Binding and Protein Interactions
E2F1	-1.82	0.0219	Multifunctional Transcription Factor
POLR2J4	-1.75	0.0267	Pseudogene
CORO1A	-1.75	0.03	Actin and Locomotion
PNPLA2	-2.01	0.0336	Triglyceride Hydrolysis, pro BRCA microenvironment
PARP15	-1.81	0.0347	Mono-ADP-Ribosylator, negatively regulates transcription
ZNF653	-1.8	0.0348	Transcriptional Repressor
TJAP1	-2.19	0.0403	Golgi Regulation and Cellular tight junctions
LAPTM4A	-1.74	0.0409	Nucleoside Transportation
RHBDL1	-2.04	0.0414	Proteolysis, EFGR pathway?
PRKAR1A	-1.93	0.046	cAMP-dependant protein kinase regulation – MAK, PI3k/AKT, JAK/STAT, Wnt beta-catenin

Figure 5.12 **Top hits are involved in a wide array of biological processes.** Legend overleaf plus two.

C

Gene Name	Fold Change	P-Value	Gene Information
CC2D2A	2.08	0.0003	Ciligoenesis and Sonic Hedgehog signalling
ANKEF1	1.91	0.0189	Protocadherin-mediated cell protrusion and adhesion (Xenopus laevis)
TNFAIP8L3	1.88	0.0027	Lipid transfer, may be involved in PI3K-AKT and MEK-ERK Pathways
PPP1R1C	1.87	0.003	Phosphatase inhibitor of PP1
SLC10A1	1.85	0.0454	Sodium dependant transport channel
NR2F1	1.81	0.0069	Transcription Factor
PARK2	1.81	0.0416	E3 Ligase that binds to many substrates (actin, beta-catenin, hsp70)
APOBEC3A	1.8	0.013	Cytidine deaminase, anti-viral, genomic instability
LCN8	1.73	0.0105	Retinoid Carrier
LINC01359	1.73	0.0075	lncRNA
MDM1	1.73	0.0397	Microtubule stabalising Binding protein that negatively regulates centriole duplication
TAS2R13	1.71	0.0125	Gustatory Receptor
ALS2CR11	1.69	0.0221	Amytrophic Lateral Sclerosis 2
HNRNPCL1	1.69	0.0205	Nucleosome Assembly
SSMEM1	1.68	0.0156	Fertility
TERT	1.68	0.0291	Telomeres
ZBED9	1.67	0.0164	NSCLC Oncogene
CCL24	1.66	0.0071	Chemotactic (migration, ERK, Cell Shape, Angio)
PBLD	1.66	0.0008	Supressses Nf kb, Migration, EMT, SMAD
LARGE	1.65	0.0075	Biosynthesis of phosphorylated O-mannosyl trisaccharide important for DAG1 – interesting functions
TCEAL5	1.62	0.0035	Transcriptional Regulation, family implicated in cancer
KCNK16	1.53	0.0022	Potassium Channel
CD209	1.52	0.0013	Pathogen Recognition Receptor
EPSTI1	1.51	0.0009	Macrophage Polarization
SPATA31A6	1.5	0.002	Spermatogenesis and Differentiation

Figure 5.12 **Top hits are involved in a wide array of biological processes.** Legend overleaf plus one.

D

Gene Name	Fold Change	P-Value	Gene Information
CC2D2A	2.08	0.0003	Ciligoenesis and Sonic Hedgehog signalling
PBLD	1.66	0.0008	Supressses Nf kb, Migration, EMT, SMAD
EPSTI1	1.51	0.0009	Macrophage Polarization
CD209	1.52	0.0013	Pathogen Recognition Receptor
SPATA31A6	1.5	0.002	Spermatogenesis and Differentiation
KCNK16	1.53	0.0022	Potassium Channel
TNFAIP8L3	1.88	0.0027	Lipid transfer, may be involved in PI3K-AKT and MEK-ERK Pathways
PPP1R1C	1.87	0.003	Phosphatase, may increase TNF-induced apoptosis
TCEAL5	1.62	0.0035	Transcriptional Regulation, family implicated in cancer
NR2F1	1.81	0.0069	Transcription Factor
CCL24	1.66	0.0071	Chemotactic (migration, ERK, Cell Shape, Angio)
LINC01359	1.73	0.0075	lncRNA
LARGE	1.65	0.0075	Biosynthesis of phosphorylated O-mannosyl trisaccharide important for DAG1 – interesting functions
LCN8	1.73	0.0105	Retinoid Carrier
TAS2R13	1.71	0.0125	Gustatory Receptor
APOBEC3A	1.8	0.013	Cytidine deaminase, anti-viral, genomic instability
SSMEM1	1.68	0.0156	Fertility
ZBED9	1.67	0.0164	NSCLC Oncogene
ANKEF1	1.91	0.0189	Protocadherin-mediated cell protrusion and adhesion (Xenopus laevis)
HNRNPCL1	1.69	0.0205	Nucleosome Assembly
ALS2CR11	1.69	0.0221	Amytrophic Lateral Sclerosis 2
TERT	1.68	0.0291	Telomeres
MDM1	1.73	0.0397	Microtubule stabalising Binding protein that negatively regulates centriole duplication
PARK2	1.81	0.0416	E3 Ligase that binds to many substrates (actin, beta-catenin, hsp70)
SLC10A1	1.85	0.0454	Sodium dependant transport channel

Figure 5.12 **Top hits are involved in a wide array of biological processes.** Legend overleaf.

Figure 5.12 **Top hits are involved in a wide array of biological processes.** Genes are compiled from figure 5.11 and includes information relating to their reported function/role. (A) Top downregulated genes rank ordered by negative fold change. (B) Top downregulated genes rank ordered by statistical significance. (C) Top upregulated genes rank ordered by positive fold change. (D) Top upregulated genes rank ordered by statistical significance.

5.2.7 Relating DEG to breast cancer prognosis

PARG expression is altered in some cancers, however, the effects of high or low expression and its association with tumorigenesis or prognosis varies amongst cancers. In breast cancer, elevated PARG expression is associated with poorer prognosis and has oncogenic or pro-tumour effects (Marques et al., 2019). Here wanted to test whether any of the genes differentially expressed following treatment with PARGi, were associated with overall survival outcome in breast cancer. The rational was that if high expression of a particular gene in breast cancer is associated with worse prognosis and PARGi downregulates that same gene, then some weight can be added to the argument that PARGi could be of therapeutic value. Likewise, the opposite could be argued that low expression of a gene being associated with worse prognosis in combination with PARGi causing up regulation of that gene would support potential theraputic use.

The 50 differentially expressed genes were imported into KMplotter using the standard settings and the RNA-Seq breast cancer data set (Lanczky & Gyorffy, 2021). Of the 25 genes whose expression was downregulated by PARGi, high expression of 7 were associated with poor surivival - RHDBL1, ZSWIM3, E2F1, POLR2J4, LAPTM4A, ADK, TMEM53, SLC2A2 and NADSYN1 (figure 5.13).

Gene Name	High/Low Expression associated with poor prognosis	Directionality following PARGi	Potential Biomarker for PARGi
CC2D1B	Low	Down	No
SLC38A9	Not SS	Down	Not SS
TJAP1	Low	Down	No
RHBDL1	High	Down	Yes
OR4F3	N/A	Down	N/A
PNPLA2	Not SS	Down	Not SS
FBRSL1	Low	Down	No
FAM45A	N/A	Down	N/A
KLHL18	Low	Down	No
C19orf45	N/A	Down	N/A
ZSWIM3	High	Down	Yes
PRKAR1A	Not SS	Down	No
C2orf15	Low	Down	No
E2F1	High	Down	Yes
PARP15	Low	Down	No
ZNF653	Not SS	Down	Not SS
CORO1A	Not SS	Down	Not SS
POLR2J4	High	Down	Yes
LAPTM4A	High	Down	Yes
ADK	High	Down	Yes
TMEM53	High	Down	Yes
CNTLN	Low	Down	No
SLC2A2	High	Down	Yes
NADSYN1	High	Down	Yes
LOC102467081	N/A	Down	N/A

Figure 5.13**. Summary of Kmplot results derived from Lanczky & Gyorffy, (2021) using RNA-Seq data in breast cancer with downregulated differentially expressed genes.** Legend overleaf plus one.

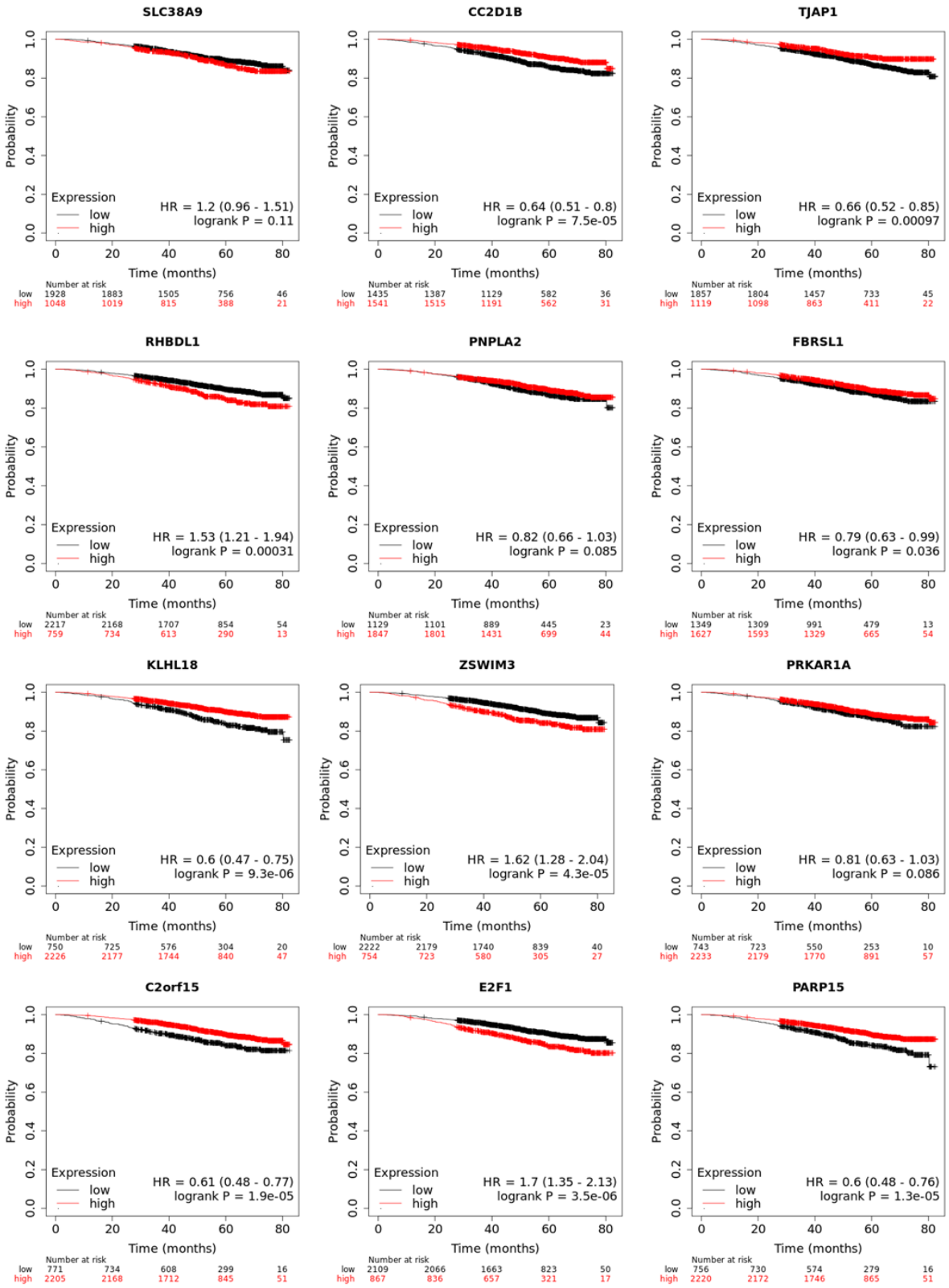

Figure 5.13 Summary of Kmplot results derived from Lanczky & Gyorffy, (2021) using RNA-Seq data in breast cancer with downregulated differentially expressed genes. Legend overleaf.

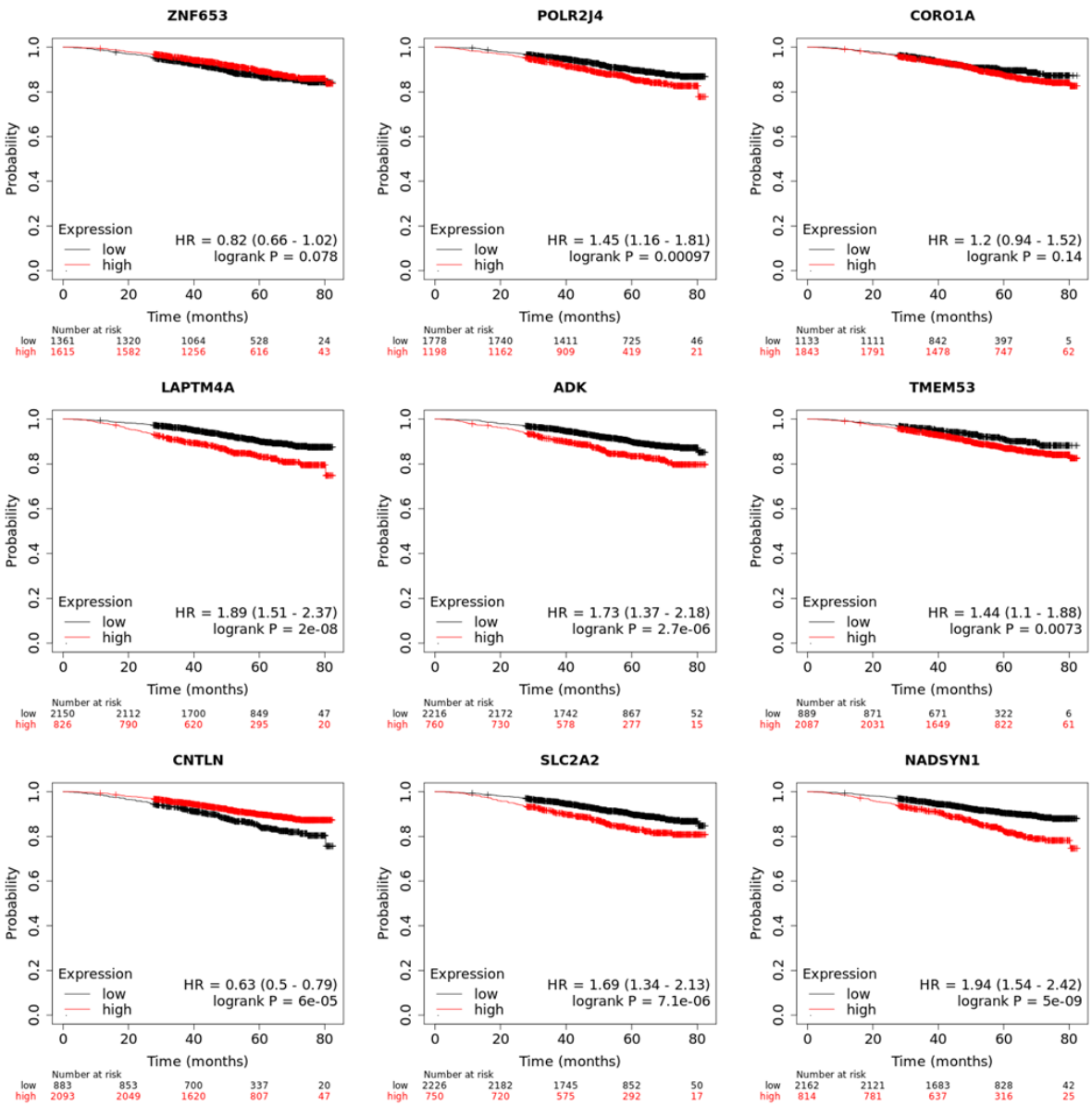

Figure 5.13 Summary of Kmplot results derived from Lanczky & Gyorffy, (2021) using RNA-Seq data in breast cancer with downregulated differentially expressed genes. Kmplots included. No indicates the genes directionality observed in the microarray does not correspond to a more favourable prognosis. Yes indicates the genes directionality observed in the microarray does correspond to a more favourable prognosis. Not SS indicates that high or low expression did not statistically correlate with survival. N/A indicates the gene was not in the database so a Kmplot could not be produced.

Conversely of the 25 genes whose expression was upregulated by PARGi, low expression of 10 were associated with poor survival - CC2D2A, ANKEF1, PPP1R1C, NR2F1, HNRNPCL1, TERT, TCEAL5, KCNK16, CD209 and EPSTI1 (figure 5.14). Expression of these genes may indicate a potential therapeutic use for PARGi in the relevant patient groups. However, there were also genes for which low expression was associated with poor survival and that PARGi downregulated and for which high expression was associated with poor survival and PARGi upregulation, cautioning the use of PARGi.

Gene Name	High/Low Expression associated with poor prognosis	Directionality following PARGi	Potential Biomarker for PARGi
CC2D2A	Low	Up	Yes
ANKEF1	Low	Up	Yes
TNFAIP8L3	High	Up	No
PPP1R1C	Low	Up	Yes
SLC10A1	Not SS	Up	Not SS
NR2F1	Low	Up	Yes
PARK2	N/A	Up	N/A
APOBEC3A	High	Up	No
LCN8	Not SS	Up	Not SS
LINC01359	N/A	Up	N/A
MDM1	Not SS	Up	Not SS
TAS2R13	Not SS	Up	Not SS
ALS2CR11	N/A	Up	N/A
HNRNPCL1	Low	Up	Yes
SSMEM1	Not SS	Up	Not SS
TERT	Low	Up	Yes
ZBED9	N/A	Up	N/A
CCL24	Not SS	Up	Not SS
PBLD	Not SS	Up	Not SS
LARGE	N/A	Up	N/A
TCEAL5	Low	Up	Yes
KCNK16	Low	Up	Yes
CD209	Low	Up	Yes
EPSTI1	Low	Up	Yes
SPATA31A6	Not SS	Up	Not SS

Figure 5.14 **Summary of Kmplot results derived from Lanczky & Gyorffy, (2021) using RNA-Seq data in breast cancer with upregulated differentially expressed genes.** Legend overleaf plus one.

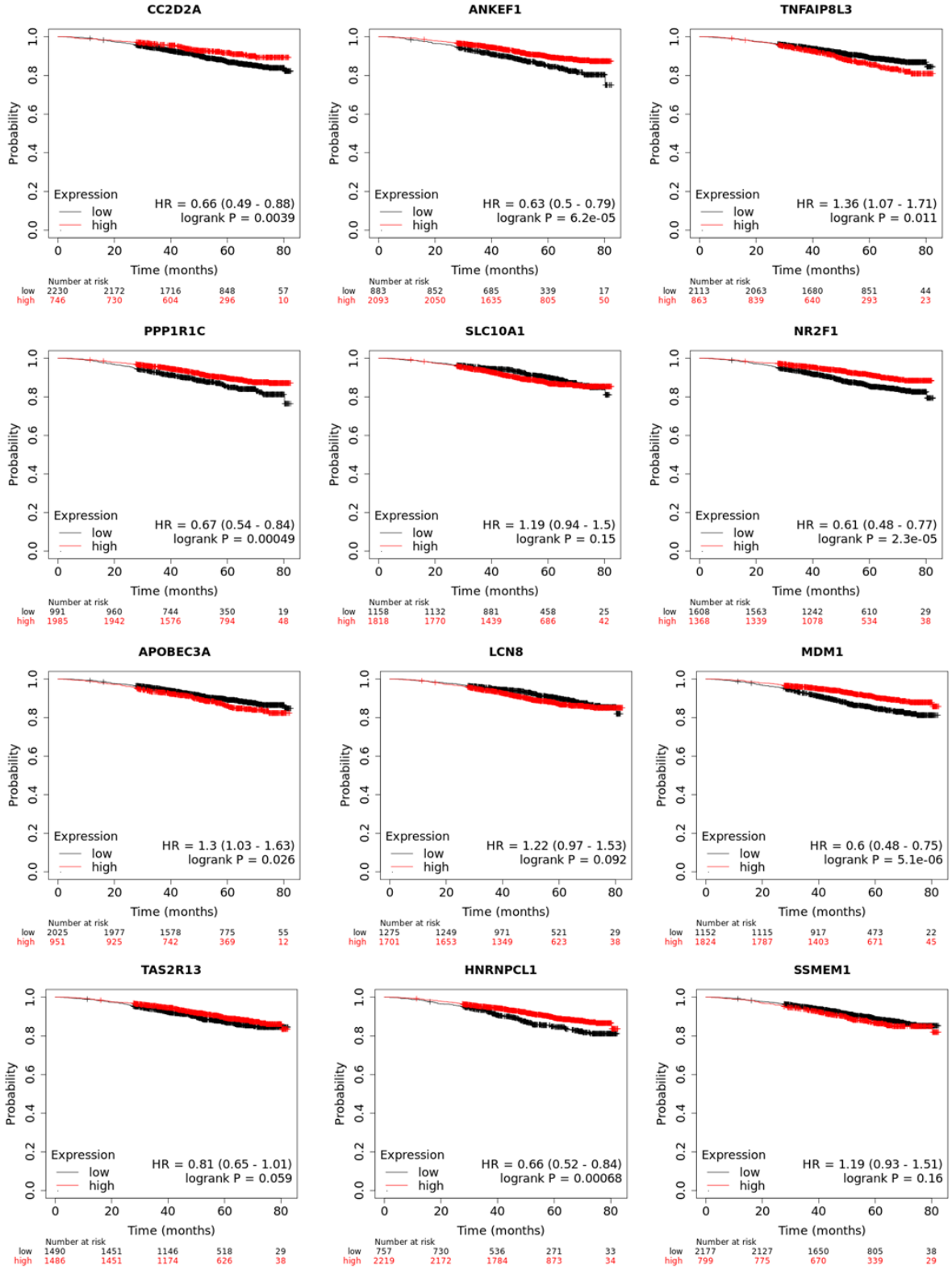

Figure 5.14 **Summary of Kmplot results derived from Lanczky & Gyorffy, (2021) using RNA-Seq data in breast cancer with upregulated differentially expressed genes.** Legend overleaf.

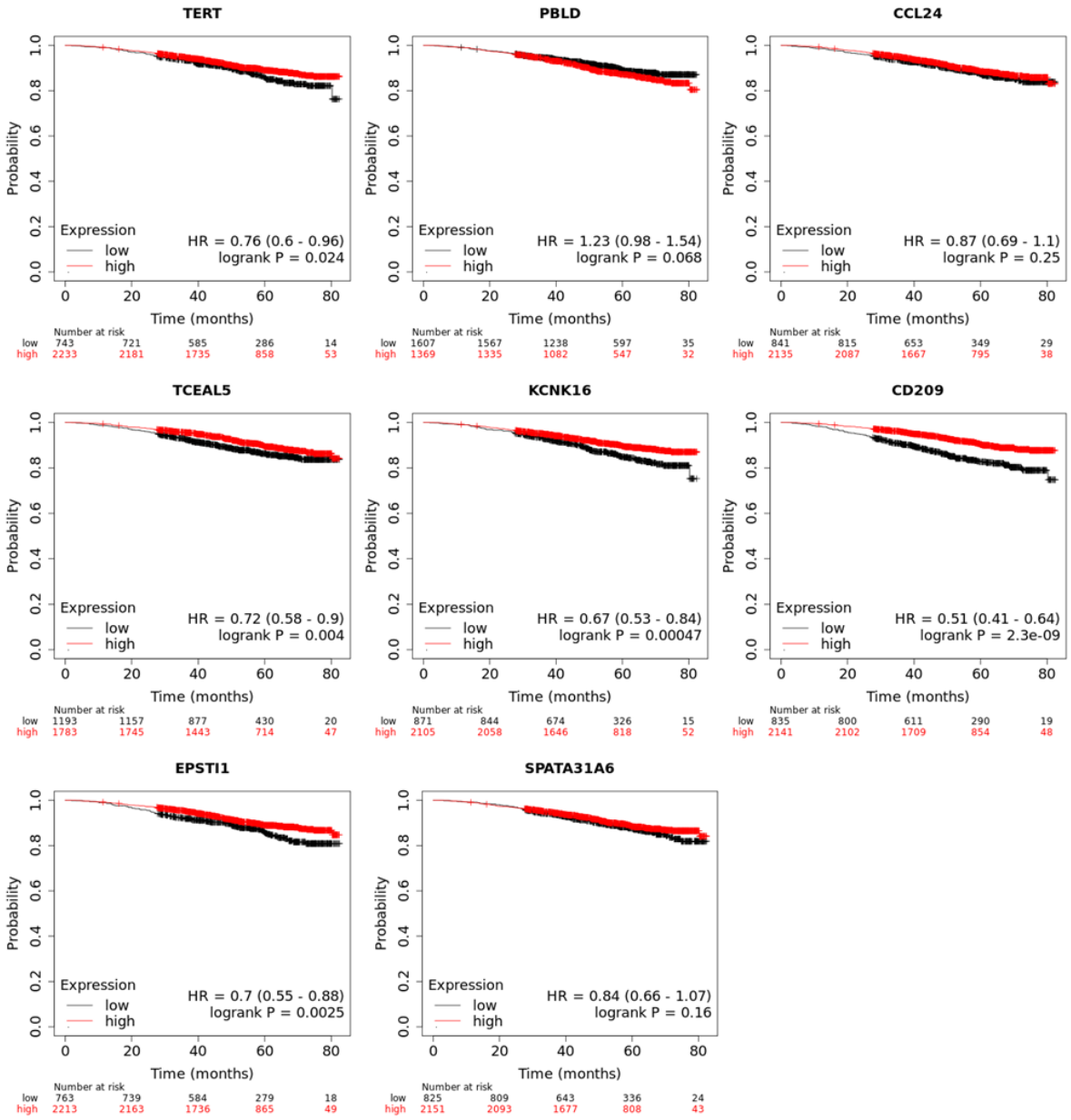

Figure 5.14 **Summary of Kmplot results derived from Lanczky & Gyorffy, (2021) using RNA-Seq data in breast cancer with upregulated differentially expressed genes.** Kmplots included. No indicates the genes directionality observed in the microarray does not correspond to a more favourable prognosis. Yes indicates the genes directionality observed in the microarray does correspond to a more favourable prognosis. Not SS indicates that high or low expression did not statistically correlate with survival. N/A indicates the gene was not the in database so a Kmplot could not be produced.

5.2.8 q-PCR validation of differentially expressed genes is inconclusive

To validate the changes in expression a subset of DEG were selected. The first set of genes PARK2, MDM1, RHOBT2, RAPGEF3, CORO1A, CDK2AP2, and CCL24 are each involved in cytoskeletal organization and are therefore of interest because PARGi induced changes in expression could drive altered migration observed in chapter 3. In addition, CCL2 was of particular interest as PARP1 inhibition has been demonstrated to increase its expression (Dutta et al., 2020). Further, E2F1, TERT and CDT1 (which are under the transcriptional control of E2F1) were investigated. These were chosen because PARP1 is suggested to function as a transcriptional co- regulator of E2F1 (Simbulan-Rosenthal et al., 1999, 2003), although there is no evidence that PARP1 can alter the transcription of E2F1 itself. Finally, ADK and NADSYN1 were investigated as they are associated with ATP/NAD metabolism respectively and it is interesting to consider how changes in PARG activity may be related to NAD+ metabolism.

To extend the transcriptional study from DMSO vs PDD, PARPi, TNKi, COH34, β-NMN pre-treatment and combinations of these treatments were also carried out and RNA was extracted, the cDNA was transcribed and RT-PCR performed. In this way, it was hoped that changes in expression seen could be related to the phenotypes observed in chapter 3.

Figure 5.15 summarises all the selected differentially expressed genes probed for under each respective condition. Unfortunately, the data were highly variable across multiple repeats and no conclusions could be drawn.

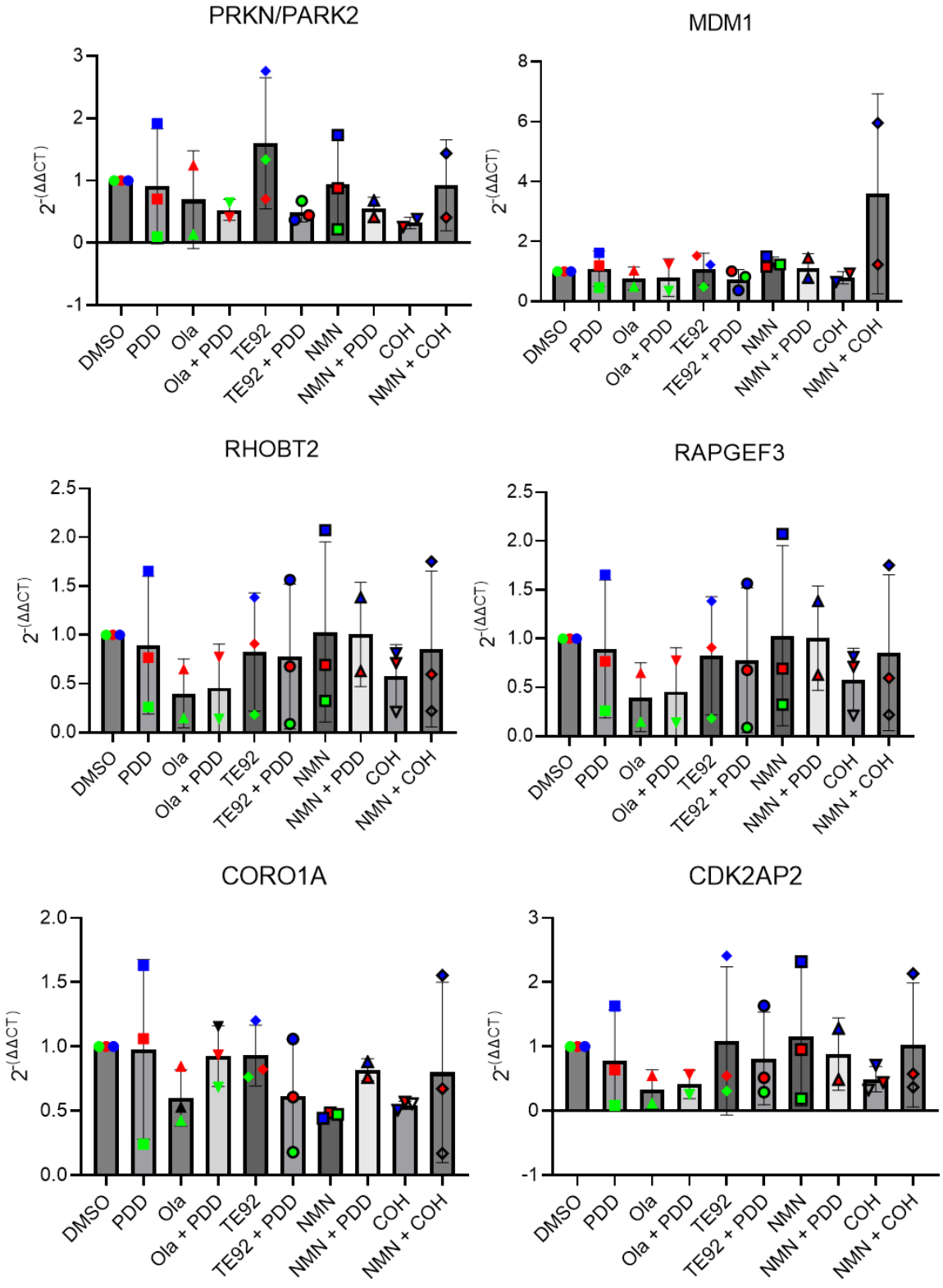

Figure 5.15 **Relative gene expression of differentially expressed genes across tested conditions in MDA-MB-231 cells.** Legend overleaf plus one.

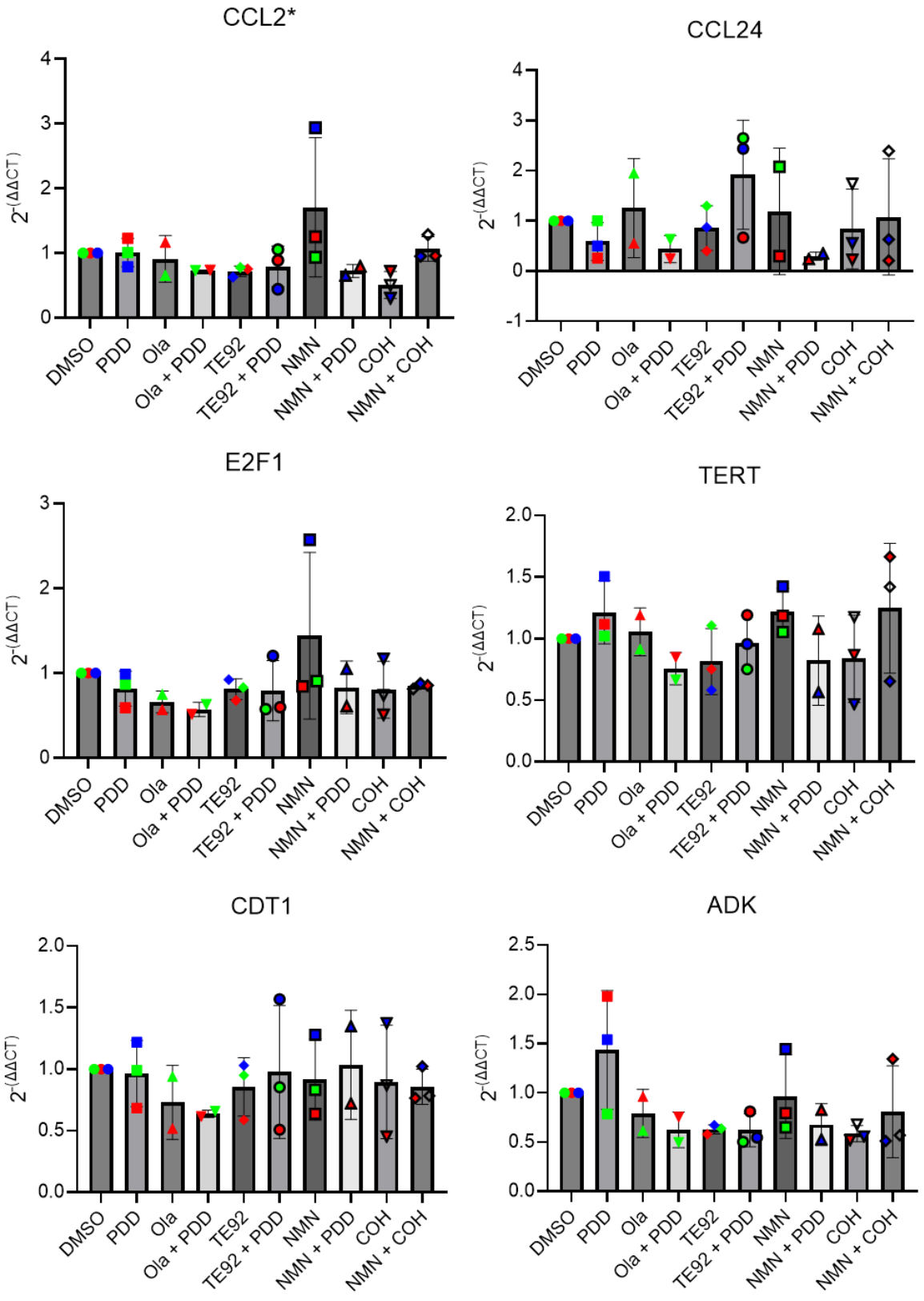

Figure 5.15 **Relative gene expression of differentially expressed genes across tested conditions in MDA-MB-231 cells.** Legend overleaf.

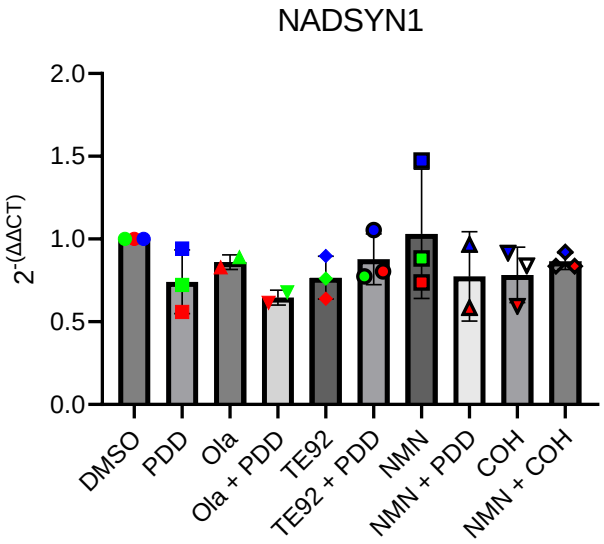

Figure 5.15 **Relative gene expression of differentially expressed genes across tested conditions in MDA-MB-231 cells.** For each condition, RNA was extracted, cDNA transcribed, and RT-PCR performed using primers for each respective differentially expressed gene. Expression was calculated using the 2-(ΔΔCT) method. N=3. An one-way ANOVA was performed. No results were statistically significant. PDD = PARGi, Ola =PARP1-3i, TE92 =TNKS1/2i, NMN = β-NMN, COH = COH34 (PARGi).

5.2.9 Validation of Differentially Expressed Gene E2F1 via Western Blot

To investigate if changes occurred at the protein level, a western blot was performed probing for E2F1. Figures 5.16A and 5.16B demonstrate there is a statistically significant reduction in total E2F1 protein following PARGi. PARPi and TNKSi treatment conditions did not have a statistically significant effect on total E2F1 protein levels. This suggests PARGi downregulate E2F1 and implies PARG is involved in maintaining E2F1 protein levels.

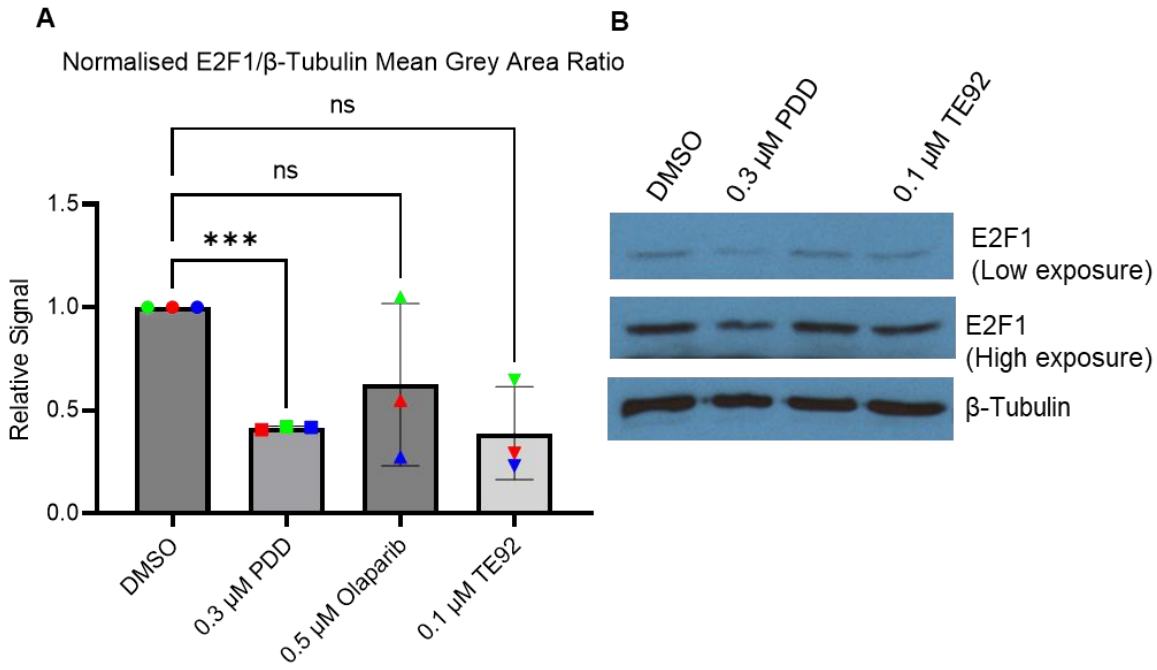

Figure 5.16 **E2F1 total protein levels following 18 h treatment with PARGi (0.3 uM PDD), PARPi (0.5 uM Olaparib) or TNKSi (0.1uM TE92) in MDA-MB-231 cells**. (A) E2F1 protein expression relative to DMSO control after normalisation to β-tubulin. N=3. An one-way ANOVA relative to the DMSO control was performed using P ≤0.05 as a threshold (B) Representative western blot. *** denotes p=≤0.001. NS denotes not statistically significant.

5.3 Discussion

We wanted to explore the effect of PARGi of MDA-MB-231 global transcription. An Affymetrix microarray was performed and the DEG's were retrieved. Bioinformatics analysis revealed that a range of biological processes and KEGG pathways are changed by PARGi. Validation of DEG's by qPCR was inconclusive but consistent with microarray data E2F1 total protein levels were reduced.

5.3.1 PARGi DEG's retrieve a wide range of overrepresented biological processes and KEGG pathways

Inputting the 139 PARGi associated DEG's into Cluster profiler, DAVID, and PANTHER retrieved a wide range of overrepresented biological processes and KEGG pathways. Terms of note relevant to migration include cytoskeleton organisation and polymerisation, response

to interleukin-21, carbohydrate digestion and absorption, chemokine signalling, leukocyte transendothelial migration, positive regulation of GTPase activity, regulation of cell shape and positive regulation of Wnt signalling pathway. The genes attached to these terms may provide further insight into how PAR biology regulates these cellular processes and how PARGi affects migration with further experimental validation.

5.3.2 PARGi promotes the expression of favourable prognostic markers in breast cancer

Of the 25 genes whose expression was downregulated by PARGi, high expression of 7 were associated with poor survival in breast cancer - RHDBL1, ZSWIM3, E2F1, POLR2J4, LAPTM4A, ADK, TMEM53, SLC2A2 and NADSYN1. Expression of these genes may indicate patient groups that could benefit from PARGi treatment. RHDBL1 is a golgi associated member of the rhomboid family that regulate EGFR signalling (Bergbold & Lemberg, 2013). No substrates to date have been reported and its role in cancer has not been investigated. ZSWIM3 has been reported to enhanced inflammation once methylated by DNMT3b in liver injured by alcohol (H.-D. Li et al., 2020). It's inflammatory role in cancer has not been investigated. E2F1 is a transcription factor and PARP1 functions as a co-activator of E2F1 (Simbulan-Rosenthal et al., 1999, 2003). E2F1 is involved in promoting breast cancer migration and is localised at sites of DNA damage and increases the expression of HR genes (E. H. Choi & Kim, 2019; Hollern et al., 2019). POLR2J4 is a lncRNA and high expression POLR2J4 has been linked to promoting breast metastasis to the bone (S. B. Park et al., 2020). POLR2J4 has been implicated in regulating m6A methylation of mRNA (W. J. Wu et al., 2023) however, its unknown how this function impacts metastasis. LAPTM4a is a lysosomal transporter and is associated with drug resistance in colon cancer (Fekete & Győrffy, 2023). ADK is a kinase responsible for the conversion of ATP into AMP. Knockdown of ADK isoforms in MDA-MB-231 cells reduces their migration and invasiveness (Shamloo et al., 2019). TMEM53 is a nuclear envelope transmembrane

protein and its function in cancer has not been investigated. SLC2A2 (GLUT2) is a glucose transporter and sensor and its functional role in cancer has not been explored however elevated expression is poor prognostic factor in hepatocellular carcinoma (Joo et al., 2020). Given the extensive role TNKS play in glucose transportation by regulating GLUT4, perhaps research exploring whether there is a relationship between TNKS and GLUT2 is warranted as well. NADSYN1 is an enzyme that catalyses the last step in the Preiss-Handler Pathway (PH-pathway), converting nicotinic acid-adenine dinucleotide (NAAD) to NAD+ (Navas & Carnero, 2021). Different cancers exhibit different gene amplifications within the PH-pathway, including NADSYN1 (Chowdhry et al., 2019). This implies that some tumours can become addicted to the PH-pathway and the resulting increase in NAD+ (Chowdhry et al., 2019). Functional studies manipulating the levels of NADSYN1 in cancer have not been performed. Perhaps a downregulation of NADSYN1 is a metabolic response to the persistent poly(ADP-Ribose) that occurs in the presence of a PARGi. It would be interesting to determine how different NAD+ generating pathways respond to PARGi.

Conversely of the 25 genes whose expression was upregulated by PARGi, low expression of 10 were associated with poor breast cancer survival - CC2D2A, ANKEF1, PPP1R1C, NR2F1, HNRNPCL1, TERT, TCEAL5, KCNK16, CD209 and EPSTI1. CC2D2A is involved in cilia formation and CC2D2A -/- neuronal cells exhibited perturbed sonic hedgehog signalling however the significance of this in the context of cancer is unknown (Gorden et al., 2008). ANKEF1 function is cancer is unknown however it has been implicated in cilia formation and protocadherin-mediated cell protrusion and adhesion (Daniel & Panizzi, 2019). PPP1R1C is a regulatory inhibitor of the serine/threonine protein phosphatase 1 (PP1). PP1 has been implicated in promoting tumorigenesis (Felgueiras et al., 2020) however, the role of PPP1R1C in cancer has not been extensively studied investigated. MicroRNA-182 has been reported to target PPP1R1C, reducing its expression and protein levels, consequently reducing invasion and migration of glioblastoma cell lines in vitro (L. Liu et al., 2017). NR2F1 is a nuclear hormone receptor that regulates transcription, the loss of which, promotes the

expression of EMT genes and leads to early-stage breast cancer dissemination (Borgen et al., 2018; Rodriguez-Tirado et al., 2022). HNRNPCL1 is a nuclear ribonucleoprotein that may play a role in nucleosome assembly and mutations in this gene are associated with dicyclopatin resistance in prostate cancer (M. Liu et al., 2021). Telomerase reverse transcriptase (TERT) is responsible for maintaining telomeric ends and has contrary to our data, been associated with a poorer breast cancer prognosis and enables cancer cell prevent senescence (Dratwa et al., 2020; Gay-Bellile et al., 2017). A PARP1-KLF4 axis has been reported to promote telomerase expression (Hsieh et al., 2017). PARGi could drive TERT expression by this axis and warrants further investigation to determine what the implications are. TCEAL5 is involved in transcriptional regulation but despite elevated expression of this gene being associated with a favourable prognosis in our data, a report implicated TCEAL5 in increasing cellular proliferation (Gergics et al., 2016). KCNK16 is a potassium ion channel and its role in cancer has not been explored extensively. CD209 is a C-type lectin, indirectly regulated by C-MYC (Pello et al., 2012). Functional studies investigating CD209 roles in cancer have not been performed. Epithelial stromal interaction 1 (EPSTI1) has been linked to breast cancer invasion and metastasis, and warrants a investigation into the relationship between PARGi and EPSTI1 (T. Li et al., 2014; Nielsen et al., 2002).

Expression of the genes discussed may indicate a potential therapeutic use for PARGi in the relevant patient groups. However, there were also genes for which low expression was associated with poor survival and that PARGi downregulated. In addition, there were genes whose high expression was associated with poor survival and PARGi upregulated. These have not been discussed. Additionally, the upregulation of PPP1R1C, TERT, TCEAL5 and EPSTI1 emphasises the need for caution when using PARGi and further delineating what patient subgroups would most benefit from PARGi.

5.3.3 Validation of PARGi DEG's using qPCR was inconclusive however total E2F1 protein levels are reduced

A selection of DEG's were validated using qPCR based on their roles in the cytoskeleton, metabolism, and interactions with PARP1-3. However, there was a large amount of variation within the data, and the lack of consistency renders it difficult to draw conclusions. The lack of consistency is likely attributable to how many conditions and probes were attempted in parallel.

Pleasingly, total E2F1 proteins were downregulated in MDA-MB-231 in the presence of a PARGi, but not a PARPi or TNKSi, which is consistent with the PARGi microarray results. PARP1 regulates E2F1 expression (Simbulan-Rosenthal et al., 1999) but it was unclear whether PARGi could disrupt this. The automodification domain of PARP1 but not the catalytic site of PARP1, facilitates the PARP1-E2F1 interaction and they also bind to the promoter of E2F1 and drive E2F1 expression (Simbulan-Rosenthal et al., 2003). If the automodification domain of PARP1 is integral, then its absence could allosterically prevent the interaction with E2F1. Alternatively, perhaps poly(ADP-ribosylated) PARP1 is unable to interact with E2F1. Given the roles of E2F1 in driving metastasis and DNA repair, it warrants further characterisation and determining how this could best be utilised. Our result showing PARGi reducing E2F1 protein levels perhaps provides insight into the differences in repair dynamics observed between PARPi and PARGi in response to radiation (Gravells et al., 2018). PARGi treated MCF7 cells resolved DNA damage faster and had a rapid induction of DNA-PKcs foci which is consistent with E2F1 roles in HR (Gravells et al., 2018).

In summary, this details multiple transcriptional changes induced when PARG is inhibited but the functional relevance of this is still to be determined.

5.3.4 Limitations

E2F1 downregulation at the protein level was consistent with what the microarray predicted. Due to the lack of RT-PCR data, it cannot be ruled out that some of the DEG's are false positives and requires further validation. The same is true for the involvement of genes in enriched bioinformatics derived terms and biological processes. Additionally, when examining the prognostic impact of the DEG's on survival, the data was not split into breast cancer subtypes. The gene signatures of the subtypes are heterogenous, therefore examining the DEG's in the context of different subtypes may provide greater insight into what subtypes PARGi may have utility against or drawbacks against.

Chapter 6: Discussion

In this thesis, we provide evidence that inhibiting the catalytic activity of PARG using PDD decreases the migration and invasive capabilities of the TNBC cell line MDA-MB-231. This is consistent with a study that has examined the anti-migratory effects of PARGi in ovarian cancer, however they used high doses of PDD that they reported was cytotoxic, which could have accounted for the reduced migration (Matanes et al., 2021). Furthermore, we also depleted PARG111 using two different siRNA and this reduced single cell migration. Pleasingly, this was not enhanced when transfected cells were also treated with PDD. This is consistent with other studies in a range of cancer backgrounds that have shown that depleting PARG reduces migration and invasion (Fauzee et al., 2012; Q. Li et al., 2012; Marques et al., 2019; Pan et al., 2012). This is the first time the highly potent PARGi, COH34, which is also suitable for *in vivo* use, has been shown to exhibit an anti-migratory effect at doses as low as 0.1 nM. This collectively justifies investigating the anti-metastatic potential of PARGi *in vivo.*

Figure 6.1 is a model that depicts the possible mechanisms of how PARGi's reduce cellular migration. We noted in the live cell analysis that cells were rounder when treated with PDD. We quantified this and confirmed it. Depletion of PARG111 in MDA-MB-231 has also been noted to have this effect (Marques et al., 2019). Given that this was not a cytotoxic dose of PDD, we reasoned there could be two broad but interconnected explanations for this; cytoskeletal changes or a reversion of EMT. We reported evidence of both and this could account for the reduced migration when cells were treated with a PARGi (figure 6.1) First, the cytoskeletal results will be discussed. PDD treated MDA-MB-231 cells had elevated levels of F-actin and α-tubulin when examined on a fluorescent microscope. Cytoskeletal organisation and polymerisation were also hits retrieved by cluster profiler and DAVID.

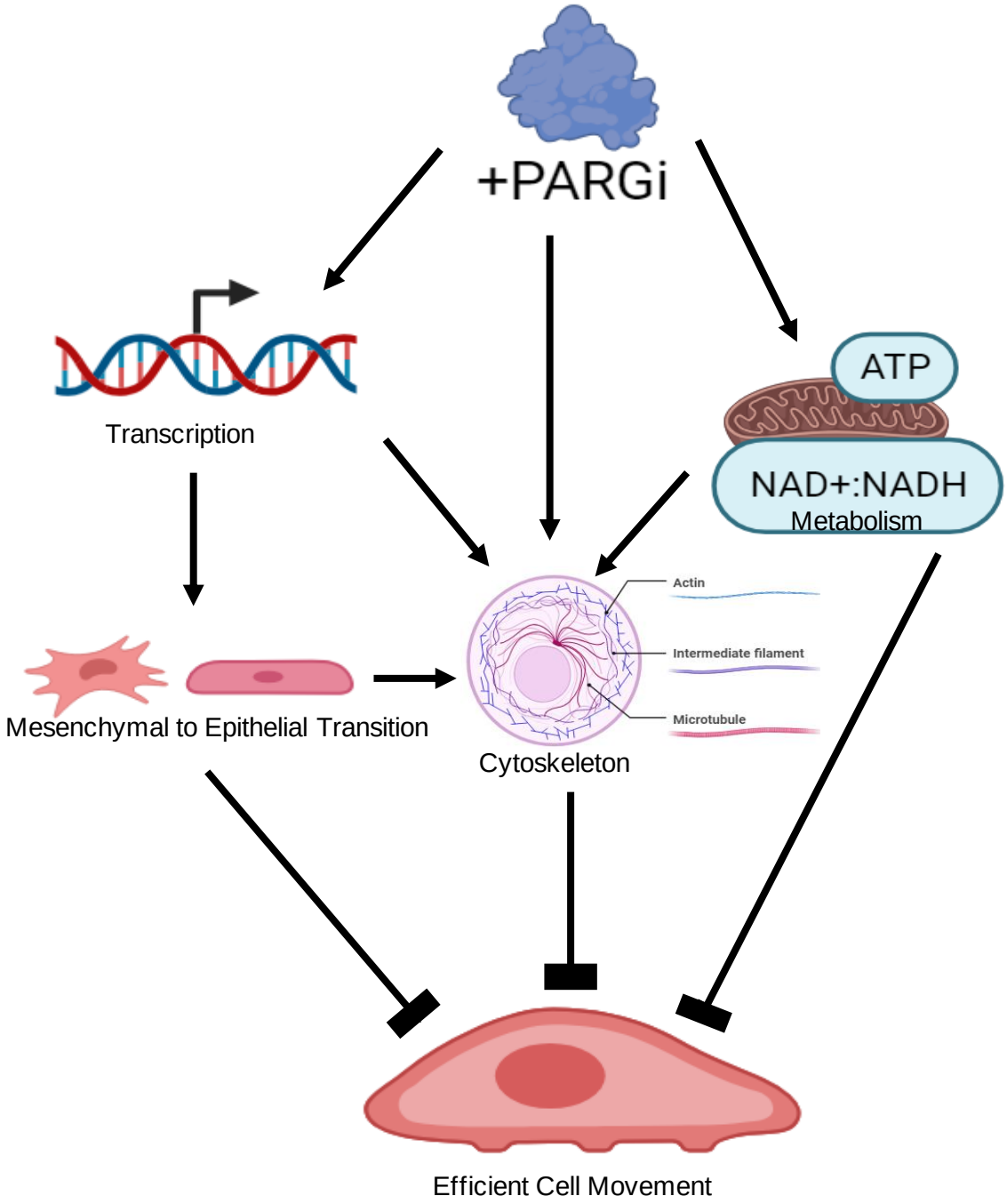

Figure 6.1 **Proposed model of how PARGi's potentially exert an anti-migratory effect.** PARGi's impact transcription, possibly PARylated proteins involved in coordinating the cytoskeleton and metabolism. Migration requires functional coordination and organisation of the cytoskeleton. Transcriptional changes could reduce the expression of cytoskeletal coordinating proteins and/or reduce the mesenchymal status of the cell, which collectively could reduce migration. Cytoskeleton organisation requires energy and PARGi's may disrupt the optimal metabolic conditions that favours migration, by impacting cytoskeleton dynamics or indirectly through other mechanism.

Therefore, its possible PARGi impacts the transcription of genes involved in the regulation of the cytoskeleton (figure 6.1). PARPi has been reported to reduce the ratio of F/G actin in monocytes (Rom et al., 2016). PARGi increasing F-actin is consistent with this. The authors also noted that PARPi decreased in the activity of the RhoA, a GTPase involved in stress fibre formation. We noted that as a percentage of the cell analysed, stress fibres amongst PARGi treated cells were more common. If PARPi decreased RhoA activity, its possible PARGi increases it and warrants further study. In support of this, the bioinformatics analysis of the PARGi DEG's retrieved positive regulation of GTPase activity in PANTHER and DAVID. These genes could provide insight into how PAR biology impacts GTPase activity and provides a plausible mechanism for how PARGi regulate GTPase activity directly or transcriptionally, or it's an indirect consequence of metabolic changes (figure 6.1). Vimentin is a marker of EMT that we observed to be downregulated when cells were treated with a PARGi. Vimentin is also involved in negatively regulating actin stress fibre formation (Jiu et al., 2017), so a decrease in vimentin could account for the increase in stress fibres we observed. We also noted a decrease in filopodia length and number of filopodia per cell. Furthermore, we observed an increase in the number of podosomes per cell when cells were treated with a PARGi. Investigating Cdc42, another Rho GTPase, that regulates filopodia formation and podosome dynamics, is another possible research avenue for PARGi. An alternative possibility is the Arp2/3 complex which is a TIP (Johnston et al., 2008) that is involved in podosome formation however its unknown what effect PARGi has on the Arp2/3 complex.

The second explanation for the change in morphology that could also contribute to the anti-migratory phenotype of PARGi will now be explored. When MDA-MB-231 cells were treated with PDD, we observed a reduction in the total protein of the following breast cancer EMT drivers: vimentin, C-MYC and β-catenin. Changes in the classical epithelial marker, E-cadherin, could not be determined however, so it cannot be definitively concluded that PARGi promotes MET per say using MDA-MB-231 as a model. However, mesenchymal

markers were reduced so perhaps it's a partial MET phenotype (figure 6.1). The E-cadherin promoter is hypermethylated in MDA-MB-231 cells (Amirabadi et al., 2019). PARP1 PARylation has been reported to inhibit DNA demethylation (Guastafierro et al., 2008) so its unlikely E-cadherin status will change in the presence of a PARG inhibitor. To confirm the MET status, increases in other epithelial markers would have to be investigated, along with decreases in other mesenchymal markers such as N-cadherin, snail, slug and twist. Depletion of PARG has been reported to reduce the total protein levels of snail and vimentin in MDA-MB-231 cells (Marques et al., 2019). We observed a reduction in the total protein levels of β-catenin when MDA-MB-231 cells were treated with PDD, which is another marker of EMT. Dai et al., (2019) provides support for a model whereby PARG mutant mice (+/-) decreased the expression of Wnt ligands and ultimately stabilised the DC, leading to decreased β-catenin. However, they did not specifically probe for phosphorylated β-catenin or phosphorylated members of the DC such as the APC, CK1 and Axin but it does warrant further investigation to confirm if this is how PARGi impacts β-catenin. Since we did not probe for phosphorylated β-catenin, we cannot rule out that the changes we observed are not due to other mechanisms. Interestingly, our bioinformatics interrogation of the DEG's retrieved positive regulation of Wnt signalling pathway in DAVID which could provide further insight into how PARGi modulates Wnt/β-catenin signalling and EMT via transcription (figure 6.1). C-MYC and vimentin were additional EMT markers that we observed to be reduced at the protein level in MDA-MB-231 PDD treated cells. PARP1 is involved in driving C-MYC and vimentin expression (Chu et al., 2007; Mostocotto et al., 2014). It would be interesting to determine what the effect of PARGi's are in this context by examining the levels of mRNA and if they are reduced at the mRNA level, investigate if PARP-DNA complexes at the C-MYC and vimentin promoter are affected in the presence of a PARGi. This is another possible mechanism PARGi are exerting transcriptional changes (figure 6.1). YAP1 is additional EMT marker involved in cellular mechano-regulation and we observed a reduction the total protein level. This may explain why we observed a reduction in nuclear YAP1 signal. However, p-127 YAP1 sequesters YAP1 in the cytoplasm and it would be interesting

to examine if PARGi impact YAP1 translocation via altering hippopathway activity and examining YAP1 mRNA levels to see ifs a consequence of transcriptional changes. Furthermore, YAP acts as a stiffness sensor and the changes in YAP1 total levels and nuclear localisation, could be reflective of this. Perhaps this warrants investigating the effect of PARGi on cell stiffness using atomic force microscopy. Interestingly, RhoA functions in the same pathway as YAP1 when sensing cell stiffness and as discussed previously, PARP/PARG may be playing a role here. The depletion of PARG has been reported to increase P-AKT (S473) signalling in colon carcinoma (Fauzee et al., 2012; Q. Li et al., 2012) and the authors concluded this underpinned their observations surrounding reduced migration and invasion when PARG was depleted. We observed no changes in P-AKT, T-AKT or in the ratio of the two when adjusted for GAPDH loading control. It would be interesting to investigate what the effect of PARG depletion is on P-AKT in breast cancer as this observation could a feature of absent PARG protein or unique to cell line/cancer background.

We also explored the mechanism underpinning the anti-migration phenotype of PARGi. Supplementing the cells with β-NMN prior to PARGi, rescued the anti-migration phenotype of PARGi but not PARPi suggesting metabolism is playing a role in the anti-migratory phenotype (figure 6.1). β-NMN is a part of the salvage pathway and it would be interesting to examine if supplementation with other NAD+ precursors also recused the anti-migration phenotype to gain further insight into what is metabolically disrupted. Regarding metabolism, given PARPs role in glycolysis (Andrabi et al., 2014) and TNKS role in glucose exocytosis (Sadler et al., 2019; Su et al., 2018; Yeh et al., 2007), it would be interesting to examine what effect PARGi have on glucose uptake and glycolytic flux. Co-treatment with a PARPi/TNKSi and PARGi also rescued the anti-migratory phenotype. These co-treatment strategies could be repeated using the EMT markers and cytoskeleton assays we have performed to determine which co-treatment reverses the effect. I.e., if co-treatment with a PARPi and PARGi but not a TNKSi and PARGi returns vimentin protein levels to normal and

stress fibres are reduces, then a greater insight into how PARPs/PARG is exerting the effect when PARGi is inhibited could be obtained. We also attempted to explore if the PARGi anti-migratory phenotype was PARP1 dependant using MEFs A19 (wt) and A11 (PARP-/-). Given that we have established the importance of PARPs vs PARG ratio in migration, it would provide further insight if each individual PARP1-5b were depleted and overexpressed in parallel in MDA-MB-231, with and without PARG treatment and assess how migration would be affected. Alternatively, PARP paired knockout cancer cell lines could be used, preferably in a range of cancer lines, as deletion of a PARP could decrease or increase migration depending on the genetic background and the role that PARP is playing in migration in any given cell line. This is an important consideration as have we established; it makes it difficult to examine the effects PARGi if the migration rates differ. This raises long term clinical questions as well as there will be inter-tumour heterogeneity with respect to each expression levels and the role PARPs are playing in any given cancer and this knowledge could improve outcomes if PARGi are used clinically. Given PARPi use in the clinic, it would also be worth while exploring the mechanism of anti-migration induced by PARPi that we have reported. Comparisons between PARPi inhibitors would also be interesting given their differential affinities for the PARylators (Carney et al., 2018) and differential off-target effects (Antolín & Mestres, 2014).

Additionally, we noted an increase in nuclear envelope ruptures, invaginations, and blebs when MDA-MB-231 cells were treated with a PARGi. Examining the stiffness of the nucleus using atomic force microscopy would provide insight what PARGi are mechanically doing to nucleus that may be causing this. We noted that Lamin A and B1 proteins were unaffected at the total protein level. PARG inhibitors anti-mitotic roles (J Ame et al., 2009) and PARP's involvement in chromatin (Krishnakumar & Kraus, 2010) are additional avenues that could be explored as to why the nucleus is in theory less stiff. However, the decrease in nuclear circularity and area that we observed in PARGi treated cells imply the nucleus could be stiffer. If it is, an explanation for this could be increased actomyosin contractility (Hatch,

2018; Maclejowski & Hatch, 2020), increasing the pressure on the nucleus which is possible given that we observed elevated levels of F-actin and α-tubulin but would require validation. Whilst the subject of this thesis has focused on the early stages of tumour dissemination, this does raise intriguing questions about nuclear integrity in the context of circulating tumour cells and intravascular pressure and whether this is something that is therapeutically exploitable.

A limitation of the dataset that examined the prognostic relevance of the DEG's, is that the tumours are not split into breast cancer subtypes. This is a regretful drawback because it could be used to examine which genes, once validated, play a role in how PARGi functions and elucidate what subtypes will be responsive or unresponsive to PARGi. This is likely given the heterogeneity within and between breast cancer subtypes. Therefore, it would be worthwhile examining the effects of PARPi/PARGi in parallel on models of all breast cancer subtypes, using more than one model for each to examine if there are differences at a transcriptional, protein and phenotypic level. Elevated levels of PARG expression are associated with a poorer prognosis in breast cancer, particularly within HER-2 positive and triple-negative sub types (Marques et al., 2019). It would be useful to examine if there is a relationship between PARG and HER2+ tumours, as HER2+ breast cancer has been reported to be sensitive to PARP inhibitors *in vitro* and *in vivo*, absent DNA repair defects and the same could be true for PARGi (Nowsheen et al., 2012; Wielgos et al., 2018), albeit via different or overlapping mechanisms. *In vitro* models of the TNBC subtypes have also been more thoroughly defined recently and examining the translational, protein and phenotypic observations we have reported here across these subtypes would further help determining which subtypes PARPi and PARGi will be most viable against (Espinosa Fernandez et al., 2020). MDA-MB-231 is classified as mesenchymal stem-like and its possible the reduction and possible (yet to validated) biological significance of reducing mesenchymal proteins on migration that we have reported here, will not necessarily be significant in other TNBC subtypes. The effects of PARPi and PARGi are multifaceted

however so until this is investigated more extensively across the TNBC subtypes, it remains to be seen.

In summary, PARPi, PARGi and TNKSi all reduced MDA-MB-231 migration, implying that these proteins are involved in regulating migration and that the ratio between PARylators and dePARylators must be balanced to promote it. This thesis has attempted elucidate why and what the effect of PARGi are but many questions remain and it will be exciting to see what answers future research will produce.

6.1 Future work

- Exploring the impact of PARGi on cell and nuclear stiffness using atomic force microscopy
- Examine cytoskeletal dynamics live in the presence of a PARG inhibitor with a transfected construct that expresses fluorescently labelled cytoskeletal monomers
- Explore the impact of PARGi on GTPase activity and assess the importance of relevant DEG's
- Examine the significance of PARGi on YAP1 and if it's a consequence of the hippopathway, RhoA, cell stiffness or transcription
- Examine if PARGi reduce C-MYC and vimentin mRNA and the status of PARP1 at their promoter sites
- Exploring the dependency of PARGi induced anti-migration on different PARylators using a range depletion and overexpression conditions
- Exploring the mechanism of PARPi anti-migration and compare different clinically approved PARPi
- Explore if any of the phenotypical or protein observations reported here are reversible with PARP/PARGi or TNKS/PARGi co-treatment or β-NMN pre-treatment

- Explore the role of PARGi on the phosphorylation status of β-catenin and DC members
- Validate relevant DEG's and further investigate their role within known PARP/PARG function
- Investigate the anti-migratory phenotype of PARPi/PARGi across other breast cancer subtypes, using more than one model for each
- Examine the validated differentially expressed genes across breast cancer subtypes and if the anti-tumour/migratory effects of PARGi are mediated by said genes

Bibliography

Abraham, J., Coleman, R., Elias, A., Holmes, F. A., Kalinsky, K., Kittaneh, M., Lower, E., Mahtani, R., Terry Mamounas, E., Pegram, M., & Vogel, C. (2018). Use of cyclin-dependent kinase (CDK) 4/6 inhibitors for hormone receptor-positive, human epidermal growth factor receptor 2-negative, metastatic breast cancer: a roundtable discussion by The Breast Cancer Therapy Expert Group (BCTEG). *Breast Cancer Research and Treatment*, *171*(1), 11–20. https://doi.org/10.1007/s10549-018-4783-1

Adamowicz, M., Hailstone, R., Demin, A. A., Komulainen, E., Hanzlikova, H., Brazina, J., Gautam, A., Wells, S. E., & Caldecott, K. W. (2021). XRCC1 protects transcription from toxic PARP1 activity during DNA base excision repair. *Nature Cell Biology*, *23*(12), 1287–1298. https://doi.org/10.1038/s41556-021-00792-w

Adamson, B., Smogorzewska, A., Sigoillot, F. D., King, R. W., & Elledge, S. J. (2012). A genome-wide homologous recombination screen identifies the RNA-binding protein RBMX as a component of the DNA-damage response. *Nature Cell Biology*, *14*(3), 318–328. https://doi.org/10.1038/ncb2426

Ahmed, S., Bott, D., Gomez, A., Tamblyn, L., Rasheed, A., Cho, T., Macpherson, L., Sugamori, K. S., Yang, Y., Grant, D. M., Cummins, C. L., & Matthews, J. (2015). Loss of the Mono-ADP-ribosyltransferase, Tiparp, Increases Sensitivity to Dioxin-induced Steatohepatitis and Lethality. *Journal of Biological Chemistry*, *290*(27), 16824–16840. https://doi.org/10.1074/jbc.m115.660100

Akiyama, T., Takasawa, S., Nata, K., Kobayashi, S., Abe, M., Shervani, N. J., Ikeda, T., Nakagawa, K., Unno, M., Matsuno, S., & Okamoto, H. (2001). Activation of Reg gene, a gene for insulin-producing β-cell regeneration: Poly(ADP-ribose) polymerase binds Reg promoter and regulates the transcription by autopoly(ADP-ribosyl)ation . *Proceedings of the National Academy of Sciences*, *98*(1), 48–53. https://doi.org/10.1073/pnas.98.1.48

Ali, A. A. E., Timinszky, G., Arribas-Bosacoma, R., Kozlowski, M., Hassa, P. O., Hassler, M., Ladurner, A. G., Pearl, L. H., & Oliver, A. W. (2012). The zinc-finger domains of PARP1 cooperate to recognize DNA strand breaks. *Nature Structural and Molecular Biology*, *19*(7), 685–692. https://doi.org/10.1038/nsmb.2335

Allinson, S. L., Dianova, I. I., & Dianov, G. L. (2003). Poly(ADP-ribose) polymerase in base excision repair: Always engaged, but not essential for DNA damage processing. *Acta Biochimica Polonica*, *50*(1), 169–179. https://doi.org/10.18388/abp.2003_3724

Alvarez-Gonzalez, R. (1988). 3'-Deoxy-NAD+ as a substrate for poly(ADP-ribose)polymerase and the reaction mechanism of poly(ADP-ribose) elongation. *The Journal of Biological Chemistry*, *263*(33), 17690–17696.

Alvarez-gonzalez, R., & Jacobson, M. K. (1987). Characterization of Polymers of Adenosine Diphosphate Ribose Generated in Vitro. *Biochemistry*, *26*(11), 3218–3224.

Amé, J.-C., Rolli, V., Schreiber, V., Niedergang, C., Apiou, F., Decker, P., Muller, S., Höger, T., Murcia, J. M.-D., & De Murcia, G. (1999). PARP-2, A Novel Mammalian DNA Damage-dependent Poly(ADP-ribose) Polymerase. *Journal of Biological Chemistry*, *274*(25), 17860–17868. https://doi.org/10.1074/jbc.274.25.17860

Amé, J.-C., Spenlehauer, C., & De Murcia, G. (2004). The PARP superfamily. *BioEssays*, *26*(8), 882–893. https://doi.org/10.1002/bies.20085

Ame, J, Apiou, F., Jacabson, E., & Jacobson, M. (1999). Assignment of the poly(ADP-

ribose) glycohydrolase gene (PARG) to human chromosome 10q11.23 and mouse chromosome 14B by in situ hybridization. *CYTOGENETIC AND CELL GENETICS*, *85*(3–4), 269–270.

Ame, J, Fouquerel, E., Gauthier, L. R., Biard, D., Boussin, F. D., Dantzer, F., De Murcia, G., & Schreiber, V. (2009). Radiation-induced mitotic catastrophe in PARG-deficient cells. *Journal of Cell Science*, *122*(12), 1990–2002. https://doi.org/10.1242/jcs.039115

Ame, Jean-christophe, Dolle, P., Rinaldi, B., & Murcia, G. De. (2002). Poly (ADP-ribose) Polymerase-2 (PARP-2) Is Required for Efficient Base Excision DNA Repair in Association with PARP-1 and XRCC1 * ´ rie Fraulob §, Josiane Me. *Journal of Biological Chemistry*, *277*(25), 23028–23036. https://doi.org/10.1074/jbc.M202390200

Amirabadi, H. E., Tuerlings, M., Hollestelle, A., Sahebali, S., Luttge, R., Donkelaar, C. C. Van, Martens, J. W. M., & Toonder, J. M. J. T. (2019). Characterizing the invasion of different breast cancer cell lines with distinct E-cadherin status in 3D using a microfluidic system. *Biomedical Microdevices*, *21*(101), 1–11.

Anderson, R. L., Balasas, T., Callaghan, J., Coombes, R. C., Evans, J., Hall, J. A., Kinrade, S., Jones, D., Jones, P. S., Jones, R., Marshall, J. F., Panico, M. B., Shaw, J. A., Steeg, P. S., Sullivan, M., Tong, W., Westwell, A. D., & Ritchie, J. W. A. (2019). A framework for the development of effective anti-metastatic agents. *Nature Reviews Clinical Oncology*, *16*(3), 185–204. https://doi.org/10.1038/s41571-018-0134-8

Andrabi, S. A., Dawson, T. M., & Dawson, V. L. (2008). Mitochondrial and Nuclear Cross Talk in Cell Death. *Annals of New York AAcademy of Sciences*, *1147*(1), 233–241. https://doi.org/10.1196/annals.1427.014

Andrabi, S. A., No, S. K., Yu, S. W., Wang, H., Koh, D. W., Sasaki, M., Klaus, J. A., Otsuka, T., Zhang, Z., Koehler, R. C., Hurn, P. D., Poirier, G. G., Dawson, V. L., & Dawson, T. M. (2006). Poly(ADP-ribose) (PAR) polymer is a signal. *Proceedings of the National Academy of Sciences of the United States of America*, *103*(48), 18308–18313. https://doi.org/10.1073/pnas.0606526103

Andrabi, S. A., Umanah, G. K. E., Chang, C., Stevens, D. A., Karuppagounder, S. S., Gagné, J. P., Poirier, G. G., Dawson, V. L., & Dawson, T. M. (2014). Poly(ADP-ribose) polymerase-dependent energy depletion occurs through inhibition of glycolysis. *Proceedings of the National Academy of Sciences of the United States of America*, *111*(28), 10209–10214. https://doi.org/10.1073/pnas.1405158111

Anthony, Vyas, S., Jennifer, Bhutkar, A., Phillip, & Chang, P. (2011). Poly(ADP-Ribose) Regulates Stress Responses and MicroRNA Activity in the Cytoplasm. *Molecular Cell*, *42*(4), 489–499. https://doi.org/10.1016/j.molcel.2011.04.015

Antolin, A. A., Ameratunga, M., Banerji, U., & Clarke, P. A. (2020). The kinase polypharmacology landscape of clinical PARP inhibitors. *Scientific Reports*, *10*(2585), 1–14. https://doi.org/10.1038/s41598-020-59074-4

Antolín, A. A., & Mestres, J. (2014). *Linking off-target kinase pharmacology to the differential cellular effects observed among PARP inhibitors*. *5*(10), 3023–3028. https://doi.org/10.18632/oncotarget.1814

Augustin, A., Spenlehauer, C., Dumond, H., Ménisier-de Murcia, J., Piel, M., Schmit, A. C., Apiou, F., Vonesch, J. L., Kock, M., Bornens, M., & de Murcia, G. (2003). PARP-3 localizes preferentially to the daughter centriole and interferes with the G1/S cell cycle progression. *Journal of Cell Science*, *116*(8), 1551–1562. https://doi.org/10.1242/jcs.00341

Bai, P., & Cantó, C. (2012). The Role of PARP-1 and PARP-2 Enzymes in Metabolic

Regulation and Disease. *Cell Metabolism*, *16*(3), 290–295. https://doi.org/10.1016/j.cmet.2012.06.016

Bai, P., Canto, C., Brunyánszki, A., Huber, A., Szántó, M., Cen, Y., Yamamoto, H., Houten, S. M., Kiss, B., Oudart, H., Gergely, P., Menissier-De Murcia, J., Schreiber, V., Sauve, A. A., & Auwerx, J. (2011). PARP-2 regulates SIRT1 expression and whole-body energy expenditure. *Cell Metabolism*, *13*(4), 450–460. https://doi.org/10.1016/j.cmet.2011.03.013

Bai, P., Cantó, C., Oudart, H., Brunyánszki, A., Cen, Y., Thomas, C., Yamamoto, H., Huber, A., Kiss, B., Houtkooper, R. H., Schoonjans, K., Schreiber, V., Sauve, A. A., Menissier-De Murcia, J., & Auwerx, J. (2011). PARP-1 inhibition increases mitochondrial metabolism through SIRT1 activation. *Cell Metabolism*, *13*(4), 461–468. https://doi.org/10.1016/j.cmet.2011.03.004

Bai, P., Houten, S. M., Huber, A., Schreiber, V., Watanabe, M., Kiss, B., De Murcia, G., Auwerx, J., & Ménissier-De Murcia, J. (2007). Peroxisome Proliferator-activated Receptor (PPAR)-2 controls adipocyte differentiation and adipose tissue function through the regulation of the activity of the retinoid X receptor/PPARγ heterodimer. *Journal of Biological Chemistry*, *282*(52), 37738–37746. https://doi.org/10.1074/jbc.M701021200

Bai, X., Ni, J., Beretov, J., Graham, P., & Li, Y. (2021). Triple-negative breast cancer therapeutic resistance: Where is the Achilles' heel? *Cancer Letters*, *497*, 100–111. https://doi.org/10.1016/j.canlet.2020.10.016

Bao, R., Christova, T., Song, S., Angers, S., Yan, X., & Attisano, L. (2012). Inhibition of Tankyrases Induces Axin Stabilization and Blocks Wnt Signalling in Breast Cancer Cells. *PLoS ONE*, *7*(11). https://doi.org/10.1371/journal.pone.0048670

Barkauskaite, E., Brassington, A., Tan, E. S., Warwicker, J., Dunstan, M. S., Banos, B., Lafite, P., Ahel, M., Mitchison, T. J., Ahel, I., & Leys, D. (2013). Visualization of poly(ADP-ribose) bound to PARG reveals inherent balance between exo- and endo-glycohydrolase activities. *Nature Communications*, *4*. https://doi.org/10.1038/ncomms3164

Beck, C., Boehler, C., Guirouilh Barbat, J., Bonnet, M.-E., Illuzzi, G., Ronde, P., Gauthier, L. R., Magroun, N., Rajendran, A., Lopez, B. S., Scully, R., Boussin, F. D., Schreiber, V., & Dantzer, F. (2014a). PARP3 affects the relative contribution of homologous recombination and nonhomologous end-joining pathways. *Nucleic Acids Research*, *42*(9), 5616–5632. https://doi.org/10.1093/nar/gku174

Beck, C., Boehler, C., Guirouilh Barbat, J., Bonnet, M. E., Illuzzi, G., Ronde, P., Gauthier, L. R., Magroun, N., Rajendran, A., Lopez, B. S., Scully, R., Boussin, F. D., Schreiber, V., & Dantzer, F. (2014b). PARP3 affects the relative contribution of homologous recombination and nonhomologous end-joining pathways. *Nucleic Acids Research*, *42*(9), 5616–5632. https://doi.org/10.1093/nar/gku174

Beneke, R., Geisen, C., Zevnik, B., Bauch, T., Müller, W.-U., Küpper, J.-H., & Möröy, T. (2000). DNA Excision Repair and DNA Damage-Induced Apoptosis Are Linked to Poly(ADP-Ribosyl)ation but Have Different Requirements for p53. *Molecular and Cellular Biology*, *20*(18), 6695–6703. https://doi.org/10.1128/mcb.20.18.6695-6703.2000

Beniey, M., Hubert, A., Haque, T., Cotte, A. K., Béchir, N., Zhang, X., Tran-Thanh, D., & Hassan, S. (2023). Sequential targeting of PARP with carboplatin inhibits primary tumour growth and distant metastasis in triple-negative breast cancer. *British Journal of Cancer*, *February*. https://doi.org/10.1038/s41416-023-02226-w

Benjamin, R. C., & Gill, D. M. (1980). Poly(ADP-ribose) synthesis in vitro programmed by damaged DNA. A comparison of DNA molecules containing different types of strand breaks. *Journal of Biological Chemistry*, *255*(21), 10502–10508.

Bergbold, N., & Lemberg, M. K. (2013). Emerging role of rhomboid family proteins in mammalian biology and disease. *Biochimica et Biophysica Acta*, *1828*(12), 2840–2848. https://doi.org/10.1016/j.bbamem.2013.03.025

Berger, N A. (1985). Poly(ADP-ribose) in the cellular response to DNA damage. *Radiation Research1*, *101*(1), 4–15.

Berger, Nathan A., Besson, V. C., Boulares, A. H., Bürkle, A., Chiarugi, A., Clark, R. S., Curtin, N. J., Cuzzocrea, S., Dawson, T. M., Dawson, V. L., Haskó, G., Liaudet, L., Moroni, F., Pacher, P., Radermacher, P., Salzman, A. L., Snyder, S. H., Soriano, F. G., Strosznajder, R. P., … Szabo, C. (2018). Opportunities for the repurposing of PARP inhibitors for the therapy of non-oncological diseases. *British Journal of Pharmacology*, *175*(2), 192–222. https://doi.org/10.1111/bph.13748

Berti, M., Chaudhuri, A. R., Thangavel, S., Gomathinayagam, S., Kenig, S., Vujanovic, M., Odreman, F., Glatter, T., Graziano, S., Mendoza-Maldonado, R., Marino, F., Lucic, B., Biasin, V., Gstaiger, M., Aebersold, R., Sidorova, J. M., Monnat, R. J., Lopes, M., & Vindigni, A. (2013). *Human RECQ1 promotes restart of replication forks reversed by DNA topoisomerase I inhibition*. *20*(3), 347–354. https://doi.org/10.1038/nsmb.2501

Bhardwaj, A., Yang, Y., Ueberheide, B., & Smith, S. (2017). Whole proteome analysis of human tankyrase knockout cells reveals targets of tankyrase-mediated degradation. *Nature Communications*, *8*(1). https://doi.org/10.1038/s41467-017-02363-w

Bindesbøll, C., Tan, S., Bott, D., Cho, T., Tamblyn, L., MacPherson, L., Grønning-Wang, L., Nebb, H. I., & Matthews, J. (2016). TCDD-inducible poly-ADP-ribose polymerase (TIPARP/PARP7) mono-ADP-ribosylates and co-activates liver X receptors. *Biochemical Journal*, *473*(7), 899–910. https://doi.org/10.1042/BJ20151077

Blenn, C., Felix, & Malanga, M. (2006). *Poly(ADP-ribose) glycohydrolase silencing protects against H 2 O 2 -induced cell death*. *396*(3), 419–429. https://doi.org/10.1042/bj20051696

Boamah, E. K., Kotova, E., Garabedian, M., Jarnik, M., & Tulin, A. V. (2012). Poly(ADP-ribose) polymerase 1 (PARP-1) regulates ribosomal biogenesis in Drosophila nucleoli. *PLoS Genetics*, *8*(1), 1–14. https://doi.org/10.1371/journal.pgen.1002442

Bock, F. J., Todorova, T. T., & Chang, P. (2015). RNA Regulation by Poly(ADP-Ribose) Polymerases. *Molecular Cell*, *58*(6), 959–969. https://doi.org/10.1016/j.molcel.2015.01.037

Boehler, C, Gauthier, L. R., Mortusewicz, O., Biard, D. S., Saliou, J.-M., Bresson, A., Sanglier-Cianferani, S., Smith, S., Schreiber, V., Boussin, F., & Dantzer, F. (2011). Poly(ADP-ribose) polymerase 3 (PARP3), a newcomer in cellular response to DNA damage and mitotic progression. *PNAS*, *108*(7), 2783–2788. https://doi.org/10.1073/pnas.1016574108

Boehler, Christian, Gauthier, L. R., Mortusewicz, O., Biard, D. S., Saliou, J. M., Bresson, A., Sanglier-Cianferani, S., Smith, S., Schreiber, V., Boussin, F., & Dantzer, F. (2011). Poly(ADP-ribose) polymerase 3 (PARP3), a newcomer in cellular response to DNA damage and mitotic progression. *Proceedings of the National Academy of Sciences of the United States of America*, *108*(7), 2783–2788. https://doi.org/10.1073/pnas.1016574108

Borgen, E., Rypdal, M. C., Sosa, M. S., Renolen, A., Schlichting, E., Lønning, P. E.,

Synnestvedt, M., Aguirre-Ghiso, J. A., & Naume, B. (2018). NR2F1 stratifies dormant disseminated tumor cells in breast cancer patients. *Breast Cancer Research*, *20*(1), 1–13. https://doi.org/10.1186/s13058-018-1049-0

Bouwman, P., Aly, A., Escandell, J. M., Pieterse, M., Bartkova, J., Van Der Gulden, H., Hiddingh, S., Thanasoula, M., Kulkarni, A., Yang, Q., Haffty, B. G., Tommiska, J., Blomqvist, C., Drapkin, R., Adams, D. J., Nevanlinna, H., Bartek, J., Tarsounas, M., Ganesan, S., & Jonkers, J. (2010). 53BP1 loss rescues BRCA1 deficiency and is associated with triple-negative and BRCA-mutated breast cancers. *Nature Structural & Molecular Biology*, *17*(6), 688–695. https://doi.org/10.1038/nsmb.1831

Breslin, C., Hornyak, P., Ridley, A., Rulten, S. L., Hanzlikova, H., Oliver, W., & Caldecott, K. W. (2015). The XRCC1 phosphate-binding pocket binds poly (ADP-ribose) and is required for XRCC1 function. *Nucleic Acids Research*, *43*(14), 6934–6944. https://doi.org/10.1093/nar/gkv623

Brochu, G., Duchaine, C., Thibeault, L., Lagueux, J., Shah, G. M., & Poirier, G. G. (1994). Mode of action of poly(ADP-ribose) glycohydrolase. *BIOCHIMICA ET BIOPHYSICA ACTA-GENE STRUCTURE AND EXPRESSION*, *1219*(2), 342–350. https://doi.org/10.1016/0167-4781(94)90058-2

Bryant, H. E., Petermann, E., Schultz, N., Jemth, A. S., Loseva, O., Issaeva, N., Johansson, F., Fernandez, S., McGlynn, P., & Helleday, T. (2009). PARP is activated at stalled forks to mediate Mre11-dependent replication restart and recombination. *EMBO Journal*, *28*(17), 2601–2615. https://doi.org/10.1038/emboj.2009.206

Bryant, H. E., Schultz, N., Thomas, H. D., Parker, K. M., Flower, D., Lopez, E., Kyle, S., Meuth, M., Curtin, N. J., & Helleday, T. (2005). Specific killing of BRCA2-deficient tumours with inhibitors of poly(ADP-ribose) polymerase. *Nature*, *434*(7035), 913–917. https://doi.org/10.1038/nature03443

Bunting, S. F., Callén, E., Wong, N., Chen, H.-T., Polato, F., Gunn, A., Bothmer, A., Feldhahn, N., Fernandez-Capetillo, O., Cao, L., Xu, X., Deng, C.-X., Finkel, T., Nussenzweig, M., Stark, J. M., & Nussenzweig, A. (2010). 53BP1 Inhibits Homologous Recombination in Brca1-Deficient Cells by Blocking Resection of DNA Breaks. *Cell*, *141*(2), 243–254. https://doi.org/10.1016/j.cell.2010.03.012

Callow, M. G., Tran, H., Phu, L., Lau, T., Lee, J., Sandoval, W. N., Liu, P. S., Bheddah, S., Tao, J., Lill, J. R., Hongo, J. A., Davis, D., Kirkpatrick, D. S., Polakis, P., & Costa, M. (2011). Ubiquitin ligase RNF146 regulates tankyrase and Axin to promote Wnt signaling. *PLoS ONE*, *6*(7). https://doi.org/10.1371/journal.pone.0022595

Canudas, S., Houghtaling, B. R., Kim, J. Y., Dynek, J. N., Chang, W. G., & Smith, S. (2007). Protein requirements for sister telomere association in human cells. *EMBO Journal*, *26*(23), 4867–4878. https://doi.org/10.1038/sj.emboj.7601903

Caprara, G., Prosperini, E., Piccolo, V., Sigismondo, G., Melacarne, A., Cuomo, A., Boothby, M., Rescigno, M., Bonaldi, T., & Natoli, G. (2018). PARP14 Controls the Nuclear Accumulation of a Subset of Type I IFN–Inducible Proteins. *The Journal of Immunology*, *200*(7), 2439–2454. https://doi.org/10.4049/jimmunol.1701117

Carney, B., Kossatz, S., Lok, B. H., Schneeberger, V., Gangangari, K. K., Pillarsetty, N. V. K., Weber, W. A., Rudin, C. M., Poirier, J. T., & Reiner, T. (2018). Target engagement imaging of PARP inhibitors in small-cell lung cancer. *Nature Communications*, *9*(1). https://doi.org/10.1038/s41467-017-02096-w

Catara, G., Grimaldi, G., Schembri, L., Spano, D., Turacchio, G., Lo Monte, M., Beccari, A. R., Valente, C., & Corda, D. (2017). PARP1-produced poly-ADP-ribose causes the PARP12 translocation to stress granules and impairment of Golgi complex functions.

Scientific Reports, *7*(1). https://doi.org/10.1038/s41598-017-14156-8

Chambon, P., Weill, J. D., Doly, J., Strosser, M. T., & Mandel, P. (1966). On the formation of a novel adenylic compound by enzymatic extracts of liver nuclei. *Biochemical and Biophysical Research Communications*, *25*(6), 638–643. https://doi.org/10.1016/0006-291x(66)90502-x

Chambon, P., Weill, J. D., & Mandel, P. (1963). Nicotinamide mononucleotide activation of a new DNA-dependent polyadenylic acid synthesizing nuclear enzyme. *Biochemical and Biophysical Research Communications*, *11*(1), 39–43. https://doi.org/10.1016/0006-291x(63)90024-x

Chang, H., Zhang, X., Li, B., & Meng, X. (2022). PARP1 Is Targeted by miR-519a-3p and Promotes the Migration, Invasion, and Tube Formation of Ovarian Cancer Cells. *Cancer Biotherapy & Radiopharmaceuticals*, *37*(9), 824–836. https://pubmed.ncbi.nlm.nih.gov/34009012/

Chang, P., Coughlin, M., & Mitchiso, T. (2009). Interaction between Poly(ADP-ribose) and NuMA Contributes to Mitotic Spindle Pole Assembly. *Molecular Biology of the Cell*, *20*, 4575–4585.

Chang, P., Coughlin, M., & Mitchison, T. J. (2005). Tankyrase-1 polymerization of poly(ADP-ribose) is required for spindle structure and function. *Nature Cell Biology*, *7*(11), 1133–1139. https://doi.org/10.1038/ncb1322

Chang, P., Jacobson, M. K., & Mitchison, T. J. (2004). Poly(ADP-ribose) is required for spindle assembly and structure. *Nature*, *432*(7017), 645–649. https://doi.org/10.1038/nature03061

Chang, W., Dynek, J. N., & Smith, S. (2005). NuMA is a major acceptor of poly (ADP-ribosyl) ation by tankyrase 1 in mitosis. *The Biochemical Journal*, *391*, 177–184. https://doi.org/10.1042/BJ20050885

Chaudhuri, A. R., Callen, E., Ding, X., Gogola, E., Duarte, A. A., Lee, J.-E., Wong, N., Lafarga, V., Calvo, J. A., Panzarino, N. J., John, S., Day, A., Crespo, A. V., Shen, B., Starnes, L. M., Ruiter, J. R. De, Daniel, J. A., Konstantinopoulos, P. A., Cortez, D., … Nussenzweig, A. (2016). Replication fork stability confers chemoresistance in BRCA-deficient cells. *Nature*, *535*(7612), 382–387. https://doi.org/10.1038/nature18325

Chen, H., Ruiz, P. D., Novikov, L., Casill, A. D., Park, J. W., & Gamble, M. J. (2014). MacroH2A1.1 and PARP-1 cooperate to regulate transcription by promoting CBP-mediated H2B acetylation. *Nature Structural & Molecular Biology*, *21*(11), 981–989. https://doi.org/10.1038/nsmb.2903

Chen, S.-H., & Yu, X. (2019). Targeting dePARylation selectively suppresses DNA repair–defective and PARP inhibitor–resistant malignancies. *Science Advances*, *5*(4), eaav4340. https://doi.org/10.1126/sciadv.aav4340

Chi, N. W., & Lodish, H. F. (2000). Tankyrase is a Golgi-associated mitogen-activated protein kinase substrate that interacts with IRAP in GLUT4 vesicles. *Journal of Biological Chemistry*, *275*(49), 38437–38444. https://doi.org/10.1074/jbc.M007635200

Choi, E. B., Yang, A. Y., Kim, S. C., Lee, J., Choi, J. K., Choi, C., & Kim, M. Y. (2016). PARP1 enhances lung adenocarcinoma metastasis by novel mechanisms independent of DNA repair. *Oncogene*, *35*(35), 4569–4579. https://doi.org/10.1038/onc.2016.3

Choi, E. H., & Kim, K. P. (2019). E2F1 facilitates DNA break repair by localizing to break sites and enhancing the expression of homologous recombination factors. *Experimental and Molecular Medicine*, *51*(9). https://doi.org/10.1038/s12276-019-0307-2

Choi, J.-R., Shin, K. S., Choi, C. Y., & Kang, S. J. (2016). PARP1 regulates the protein stability and proapoptotic function of HIPK2. *Cell Death & Disease*, *7*(10), e2438–e2438. https://doi.org/10.1038/cddis.2016.345

Chou, H.-Y. E., Chou, H. T., & Lee, S.-C. (2006). CDK-dependent Activation of Poly(ADP-ribose) Polymerase Member 10 (PARP10). *The Journal of Biological Chemistry*, *281*(22), 15201–15207. https://doi.org/10.1074/jbc.m506745200

Chowdhry, S., Zanca, C., Rajkumar, U., Koga, T., Diao, Y., Raviram, R., Liu, F., Turner, K., Yang, H., Brunk, E., Bi, J., Furnari, F., Bafna, V., Ren, B., & Mischel, P. S. (2019). NAD metabolic dependency in cancer is shaped by gene amplification and enhancer remodelling. *Nature*, *569*(7757), 570–575. https://doi.org/10.1038/s41586-019-1150-2

Chu, S., Xu, H., Ferro, T. J., & Rivera, P. X. (2007). Poly(ADP-ribose) polymerase-1 regulates vimentin expression in lung cancer cells. *American Journal of Physiology - Lung Cellular and Molecular Physiology*, *293*(5), 1127–1134. https://doi.org/10.1152/ajplung.00197.2007

Cortes, U., Tong, W.-M., Coyle, D. L., Meyer-Ficca, M. L., Meyer, R. G., Petrilli, V., Herceg, Z., Jacobson, E. L., Jacobson, M. K., & Wang, Z.-Q. (2004). Depletion of the 110-Kilodalton Isoform of Poly(ADP-Ribose) Glycohydrolase Increases Sensitivity to Genotoxic and Endotoxic Stress in Mice. *Molecular and Cellular Biology*, *24*(16), 7163–7178. https://doi.org/10.1128/mcb.24.16.7163-7178.2004

Dai, W., Fu, Y., Deng, Y., Zeng, Z., Gu, P., Liu, H., Liu, J., Xu, X., Wu, D., Luo, X., Yang, L., Zhang, J., Lin, K., Hu, G., & Huang, H. (2019). Regulation of Wnt Singaling Pathway by Poly (ADP-Ribose) Glycohydrolase (PARG) Silencing Suppresses Lung Cancer in Mice Induced by Benzo(a)pyrene Inhalation Exposure. *Frontiers in Pharmacology*, *10*. https://doi.org/10.3389/fphar.2019.00338

Daniel, J. G., & Panizzi, J. R. (2019). Spatiotemporal expression profile of embryonic and adult ankyrin repeat and EF-hand domain containing protein 1-encoding genes ankef1a and ankef1b in zebrafish. *Gene Expression Patterns*, *34*, 119069. https://doi.org/10.1016/j.gep.2019.119069

Dantzer, F., De La Rubia, G., Ménissier-De Murcia, J., Hostomsky, Z., De Murcia, G., & Schreiber, V. (2000). Base excision repair is impaired in mammalian cells lacking poly(ADP- ribose) polymerase-1. *Biochemistry*, *39*(25), 7559–7569. https://doi.org/10.1021/bi0003442

Dantzer, F., & Santoro, R. (2013). The expanding role of PARPs in the establishment and maintenance of heterochromatin. *The FEBS Journal*, *280*(15), 3508–3518. https://doi.org/10.1111/febs.12368

Dantzer, F., Schreiber, V., Niedergang, C., Trucco, C., Flatter, E., Rubia, G. D. La, Oliver, J., Rolli, V., Ménissier-de Murcia, J., & De Murcia, G. (1999). Involvement of poly(ADP-ribose) polymerase in base excision repair. *Biochimie*, *81*(1–2), 69–75. https://doi.org/10.1016/S0300-9084(99)80040-6

Davis, K., Banerjee, S., Friggeri, A., Bell, C., Abraham, E., & Zerfaoui, M. (2012). Poly(ADP-Ribosyl)ation of high mobility group box 1 (HMGB1) protein enhances inhibition of efferocytosis. *Molecular Medicine*, *18*(3), 359–369. https://doi.org/10.2119/molmed.2011.00203

de Murcia, G., & de Murcia, J. M. (1994). Poly(ADP-ribose) polymerase: a molecular nick-sensor. In *Trends in Biochemical Sciences* (Vol. 19, Issue 4, pp. 172–176). https://doi.org/10.1016/0968-0004(94)90280-1

Demin, A. A., Hirota, K., Tsuda, M., Adamowicz, M., Hailstone, R., Brazina, J., Gittens, W.,

Kalasova, I., Shao, Z., Zha, S., Sasanuma, H., Hanzlikova, H., Takeda, S., & Caldecott, K. W. (2021). XRCC1 prevents toxic PARP1 trapping during DNA base excision repair ll ll XRCC1 prevents toxic PARP1 trapping during DNA base excision repair. *Molecular Cell*, *81*(14), 3018–3030. https://doi.org/10.1016/j.molcel.2021.05.009

Dev, H., Chiang, T.-W. W., Lescale, C., De Krijger, I., Martin, A. G., Pilger, D., Coates, J., Sczaniecka-Clift, M., Wei, W., Ostermaier, M., Herzog, M., Lam, J., Shea, A., Demir, M., Wu, Q., Yang, F., Fu, B., Lai, Z., Balmus, G., … Jackson, S. P. (2018). Shieldin complex promotes DNA end-joining and counters homologous recombination in BRCA1-null cells. *Nature Cell Biology*, *20*(8), 954–965. https://doi.org/10.1038/s41556-018-0140-1

Di Giammartino, D. C., Shi, Y., & Manley, J. L. (2013). PARP1 Represses PAP and Inhibits Polyadenylation during Heat Shock. *Molecular Cell*, *49*(1), 7–17. https://doi.org/10.1016/j.molcel.2012.11.005

Di Paola, S., Micaroni, M., Di Tullio, G., Buccione, R., & Di Girolamo, M. (2012). PARP16/ARTD15 Is a Novel Endoplasmic-Reticulum-Associated Mono-ADP-Ribosyltransferase That Interacts with, and Modifies Karyopherin-ß1. *PLOS ONE*, *7*(6), e37352. https://doi.org/10.1371/journal.pone.0037352

Donnell, A. O., Yang, S., & Sharrocks, A. D. (2013). PARP1 orchestrates variant histone exchangein signal-mediated transcriptional activation. *EMBO Reports*, *14*(12), 1084–1091. https://doi.org/10.1038/embor.2013.164

Dratwa, M., Wysoczańska, B., Łacina, P., Kubik, T., & Bogunia-Kubik, K. (2020). TERT—Regulation and Roles in Cancer Formation. *Frontiers in Immunology*, *11*(November), 1–16. https://doi.org/10.3389/fimmu.2020.589929

Du, X., Matsumura, T., Edelstein, D., Rossetti, L., Zsengellér, Z., Szabó, C., & Brownlee, M. (2003). Inhibition of GAPDH activity by poly(ADP-ribose) polymerase activates three major pathways of hyperglycemic damage in endothelial cells. *Journal of Clinical Investigation*, *112*(7), 1049–1057. https://doi.org/10.1172/JCI18127

Dukacz, B. W., Omidiji, O., Gray, D. A., & Shall, S. (1980). (ADP-ribose)n participates in DNA excision repair. *Nature*, *283*(5747), 593–596.

Dupont, S., Morsut, L., Aragona, M., Enzo, E., Giulitti, S., Cordenonsi, M., Zanconato, F., Le Digabel, J., Forcato, M., Bicciato, S., Elvassore, N., & Piccolo, S. (2011). Role of YAP/TAZ in mechanotransduction. *Nature*, *474*(7350), 179–184. https://doi.org/10.1038/nature10137

Dutta, P., Paico, K., Gomez, G., Wu, Y., & Vadgama, J. V. (2020). Transcriptional regulation of CCL2 by parp1 is a driver for invasiveness in breast cancer. *Cancers*, *12*(5). https://doi.org/10.3390/cancers12051317

Dynek, J. N., & Smith, S. (2004). Resolution of Sister Telomere Association Is Required for Progression Through Mitosis. *Science*, *304*(5667), 97–100. https://doi.org/10.1126/science.1094754

El-Hamoly, T., Hegedűs, C., Lakatos, P., Kovács, K., Bai, P., El-Ghazaly, M. A., El-Denshary, E. S., Szabó, É., & Virág, L. (2014). Activation of poly(ADP-ribose) polymerase-1 delays wound healing by regulating keratinocyte migration and production of inflammatory mediators. *Molecular Medicine*, *20*(JULY-DECEMBER 2014), 363–371. https://doi.org/10.2119/molmed.2014.00130

El-Khamisy, S. F., Masutani, M., Suzuki, H., & Caldecott, K. W. (2003). A requirement for PARP-1 for the assembly or stability of XRCC1 nuclear foci at sites of oxidative DNA damage. *Nucleic Acids Research*, *31*(19), 5526–5533.

https://doi.org/10.1093/nar/gkg761

Eleazer, R., & Fondufe-mittendorf, Y. N. (2021). The multifaceted role of PARP1 in RNA biogenesis. *Wiley Interdisciplinary Reviews RNA*, *12*(2). https://doi.org/10.1002/wrna.1617

Erener, S., Hesse, M., Kostadinova, R., & Hottiger, M. O. (2012). Poly(ADP-ribose)polymerase-1 (PARP1) controls adipogenic gene expression and adipocyte function. *Molecular Endocrinology*, *26*(1), 79–86. https://doi.org/10.1210/me.2011-1163

Erener, S., Mirsaidi, A., Hesse, M., Tiaden, A. N., Ellingsgaard, H., Kostadinova, R., Donath, M. Y., Richards, P. J., & Hottiger, M. O. (2012). ARTD1 deletion causes increased hepatic lipid accumulation in mice fed a high-fat diet and impairs adipocyte function and differentiation . *The FASEB Journal*, *26*(6), 2631–2638. https://doi.org/10.1096/fj.11-200212

Espinosa Fernandez, J. R., Eckhardt, B. L., Lee, J., Lim, B., Pearson, T., Seitz, R. S., Hout, D. R., Schweitzer, B. L., Nielsen, T. J., Rayne Lawrence, O., Wang, Y., Rao, A., & Ueno, N. T. (2020). Identification of triple-negative breast cancer cell lines classified under the same molecular subtype using different molecular characterization techniques: Implications for translational research. *PLoS ONE*, *15*(4), 1–8. https://doi.org/10.1371/journal.pone.0231953

Eustermann, S., Brockmann, C., Mehrotra, P. V., Yang, J. C., Loakes, D., West, S. C., Ahel, I., & Neuhaus, D. (2010). Solution structures of the two PBZ domains from human APLF and their interaction with poly(ADP-ribose). *Nature Structural and Molecular Biology*, *17*(2), 241–243. https://doi.org/10.1038/nsmb.1747

Eustermann, S., Videler, H., Yang, J., Cole, P. T., Gruszka, D., Veprintsev, D., & Neuhaus, D. (2011). The DNA-Binding Domain of Human PARP-1 Interacts with DNA Single-Strand Breaks as a Monomer through Its Second Zinc Finger. *Journal of Molecular Biology*, *407*(1), 149–170. https://doi.org/10.1016/j.jmb.2011.01.034

Eustermann, S., Wu, W.-F., Langelier, M.-F., Yang, J.-C., Laura, Amanda, John, & Neuhaus, D. (2015). Structural Basis of Detection and Signaling of DNA Single-Strand Breaks by Human PARP-1. *Molecular Cell*, *60*(5), 742–754. https://doi.org/10.1016/j.molcel.2015.10.032

Fahrer, J., Kranaster, R., Altmeyer, M., Marx, A., & Bürkle, A. (2007). Quantitative analysis of the binding affinity of poly(ADP-ribose) to specific binding proteins as a function of chain length. *Nucleic Acids Research*, *35*(21). https://doi.org/10.1093/nar/gkm944

Fang, Y., Liu, T., Wang, X., Yang, Y. M., Deng, H., Kunicki, J., Traganos, F., Darzynkiewicz, Z., Lu, L., & Dai, W. (2006). BubR1 is involved in regulation of DNA damage responses. *Oncogene*, *25*(25), 3598–3605. https://doi.org/10.1038/sj.onc.1209392

Farmer, H., Mccabe, N., Lord, C. J., Tutt, A. N. J., Johnson, D. A., Richardson, T. B., Santarosa, M., Dillon, K. J., Hickson, I., Knights, C., Martin, N. M. B., Jackson, S. P., Smith, G. C. M., & Ashworth, A. (2005). Targeting the DNA repair defect in BRCA mutant cells as a therapeutic strategy. *Nature*, *434*(7035), 917–921. https://doi.org/10.1038/nature03445

Farrés, J., Llacuna, L., Martin-Caballero, J., Martínez, C., Lozano, J. J., Ampurdanés, C., López-Contreras, A. J., Florensa, L., Navarro, J., Ottina, E., Dantzer, F., Schreiber, V., Villunger, A., Fernández-Capetillo, O., & Yélamos, J. (2015). PARP-2 sustains erythropoiesis in mice by limiting replicative stress in erythroid progenitors. *Cell Death and Differentiation*, *22*(7), 1144–1157. https://doi.org/10.1038/cdd.2014.202

Fathers, C., Drayton, R. M., Solovieva, S., & Bryant, H. E. (2012). Inhibition of poly(ADP-

ribose) glycohydrolase (PARG) specifically kills BRCA2-deficient tumor cells. *Cell Cycle*, *11*(5), 990–997. https://doi.org/10.4161/cc.11.5.19482

Fauzee, N. J. S., Li, Q., Wang, Y.-L., & Pan, J. (2012). Silencing Poly (ADP-Ribose) Glycohydrolase (PARG) Expression Inhibits Growth of Human Colon Cancer Cells In Vitro via PI3K/Akt/NFκ-B Pathway. *Pathology Oncology Research*, *18*(2), 191–199. https://doi.org/10.1007/s12253-011-9428-1

Fehr, A. R., Singh, S. A., Kerr, C. M., Mukai, S., Higashi, H., & Aikawa, M. (2020). The impact of PARPs and ADP-ribosylation on inflammation and host-pathogen interactions. *Genes and Development*, *34*(5), 341–359. https://doi.org/10.1101/gad.334425.119

Fekete, J. T., & Győrffy, B. (2023). New Transcriptomic Biomarkers of 5-Fluorouracil Resistance. *International Journal of Molecular Sciences*, *24*(2), 1–12. https://doi.org/10.3390/ijms24021508

Felgueiras, J., Jerónimo, C., & Fardilha, M. (2020). Protein phosphatase 1 in tumorigenesis: is it worth a closer look? *Biochimica et Biophysica Acta - Reviews on Cancer*, *1874*(2), 188433. https://doi.org/10.1016/j.bbcan.2020.188433

Feng, X., Zhou, Y., Proctor, A. M., Hopkins, M. M., Liu, M., & Koh, D. W. (2012). Silencing of Apoptosis-Inducing factor and poly(ADP-ribose) glycohydrolase reveals novel roles in breast cancer cell death after chemotherapy. *Molecular Cancer*, *11*(1), 48. https://doi.org/10.1186/1476-4598-11-48

Ferro, A. M., & Olivera, B. M. (1982). Poly(ADP-ribosylation) in vitro. Reaction parameters and enzyme mechanism. *Journal of Biological Chemistry*, *257*(13), 7808–7813. https://doi.org/10.1016/s0021-9258(18)34453-3

Figueroa-Magalhães, M. C., Jelovac, D., Connolly, R. M., & Wolff, A. C. (2014). Treatment of HER2-positive breast cancer. *Breast*, *23*(2), 128–136. https://doi.org/10.1016/j.breast.2013.11.011

Finch, K. E., Knezevic, C. E., Nottbohm, A. C., Partlow, K. C., & Hergenrother, P. J. (2012). Selective Small Molecule Inhibition of Poly(ADP-Ribose) Glycohydrolase (PARG). *ACS Chemical Biology*, *7*(3), 563–570. https://doi.org/10.1038/jid.2014.371

Fischbach, A., Krüger, A., Hampp, S., Assmann, G., Rank, L., Hufnagel, M., Stöckl, M. T., Fischer, J. M. F., Veith, S., Rossatti, P., Ganz, M., Ferrando-May, E., Hartwig, A., Hauser, K., Wiesmüller, L., Bürkle, A., & Mangerich, A. (2018). The C-terminal domain of p53 orchestrates the interplay between non-covalent and covalent poly(ADP-ribosyl)ation of p53 by PARP1. *Nucleic Acids Research*, *46*(2), 804–822. https://doi.org/10.1093/nar/gkx1205

Fisher, A. E. O., Hochegger, H., Takeda, S., & Caldecott, K. W. (2007). Poly(ADP-Ribose) Polymerase 1 Accelerates Single-Strand Break Repair in Concert with Poly(ADP-Ribose) Glycohydrolase. *Molecular and Cellular Biology*, *27*(15), 5597–5605. https://doi.org/10.1128/mcb.02248-06

Flohr, C., Bürke, A., Radicella, J. P., & Epe, B. (2003). Poly(ADP-ribosyl)ation accelerates DNA repair in a pathway dependent on Cockayne syndrome B protein. *Nucleic Acids Research*, *31*(18), 5332–5337. https://doi.org/10.1093/nar/gkg715

Fouqin, A., Guirouilh-Barbat, J., Lopez, B., Hall, J., Amor-Gueret, M., & Pennaneach, V. (2017). PARP2 controls double-strand break repair pathway choice by limiting 53BP1 accumulation at DNA damage sites and promoting end-resection. *Nucleic Acids Research*, *45*(21), 12325–12339. https://doi.org/10.1093/nar/gkx881

Fouquerel, E., Goellner, E. M., Yu, Z., Gagné, J., Moura, M. B. De, Feinstein, T., Wheeler, D., Redpath, P., Li, J., Romero, G., Migaud, M., Houten, B. Van, Poirier, G. G., & Robert, W. (2014). ARTD1/PARP1 negatively regulates glycolysis by inhibiting hexokinase 1 independent of NAD+ depletion. *Cell Reports*, *8*(6), 1819–1831. https://doi.org/10.1016/j.celrep.2014.08.036.ARTD1/PARP1

Fujihara, H., Ogino, H., Maeda, D., Shirai, H., Nozaki, T., Kamada, N., Jishage, K., Tanuma, S., Takato, T., Ochiya, T., Sugimura, T., & Masutani, M. (2009). Poly(ADP-ribose) Glycohydrolase Deficiency Sensitizes Mouse ES Cells to DNA Damaging Agents. *Current Cancer Drug Targets*, *9*(8), 953–962. https://doi.org/10.2174/156800909790192419

Fujimoto, M., Takii, P., Takaki, E., Katiyar, A., Nakato, R., Shirahige, K., & Nakai, A. (2017). The HSF1–PARP13–PARP1 complex facilitates DNArepair and promotes mammary tumorigenesis. *Nature Communications*, *8*, 1638. https://doi.org/10.1038/s41467-017-01807-7

Gao, H., Coyle, D. L., Meyer-Ficca, M. L., Meyer, R. G., Jacobson, E. L., Wang, Z.-Q., & Jacobson, M. K. (2007). Altered poly(ADP-ribose) metabolism impairs cellular responses to genotoxic stress in a hypomorphic mutant of poly(ADP-ribose) glycohydrolase. *Experimental Cell Research*, *313*(5), 984–996. https://doi.org/10.1016/j.yexcr.2006.12.025

Gay-Bellile, M., Véronèse, L., Combes, P., Eymard-Pierre, E., Kwiatkowski, F., Dauplat, M. M., Cayre, A., Privat, M., Abrial, C., Bignon, Y. J., Mouret-Reynier, M. A., Vago, P., Penault-Llorca, F., & Tchirkov, A. (2017). TERT promoter status and gene copy number gains: Effect on TERT expression and association with prognosis in breast cancer. *Oncotarget*, *8*(44), 77540–77551. https://doi.org/10.18632/oncotarget.20560

Gergics, P., Christian, H. C., Choo, M. S., Ajmal, A., & Camper, S. A. (2016). Gene expression in mouse thyrotrope adenoma: Transcription elongation factor stimulates proliferation. *Endocrinology*, *157*(9), 3631–3646. https://doi.org/10.1210/en.2016-1183

Giansanti, V., Donà, F., Tillhon, M., & Scovassi, A. I. (2010). PARP inhibitors: New tools to protect from inflammation. *Biochemical Pharmacology*, *80*(12), 1869–1877. https://doi.org/10.1016/j.bcp.2010.04.022

Gibson, B. A., Zhang, Y., Jiang, H., Hussey, K. M., Shrimp, H. H., Lin, H., Schwede, F., Yu, Y., & Karus, W. L. (2016). Chemical Genetic Discovery of PARP Targets Reveals a Role for PARP-1 in Transcription Elongation. *Science (New York, N.Y.)*, *353*(6294), 45–50. https://doi.org/10.1053/j.gastro.2016.08.014.CagY

Gogola, E., Duarte, A. A., De Ruiter, J. R., Wiegant, W. W., Schmid, J. A., De Bruijn, R., James, D. I., Guerrero Llobet, S., Vis, D. J., Annunziato, S., Van Den Broek, B., Barazas, M., Kersbergen, A., Van De Ven, M., Tarsounas, M., Ogilvie, D. J., Van Vugt, M., Wessels, L. F. A., Bartkova, J., … Rottenberg, S. (2018). Selective Loss of PARG Restores PARylation and Counteracts PARP Inhibitor-Mediated Synthetic Lethality. *Cancer Cell*, *33*(6), 1078-1093.e12. https://doi.org/10.1016/j.ccell.2018.05.008

Goodall, J., Mateo, J., Yuan, W., Mossop, H., Porta, N., Miranda, S., Perez-Lopez, R., Dolling, D., Robinson, D. R., Sandhu, S., Fowler, G., Ebbs, B., Flohr, P., Seed, G., Rodrigues, D. N., Boysen, G., Bertan, C., Atkin, M., Clarke, M., … De Bono, J. S. (2017). Circulating Cell-Free DNA to Guide Prostate Cancer Treatment with PARP Inhibition. *Cancer Discovery*, *7*(9), 1006–1017. https://doi.org/10.1158/2159-8290.cd-17-0261

Gorden, N. T., Arts, H. H., Parisi, M. A., Coene, K. L. M., Letteboer, S. J. F., van Beersum, S. E. C., Mans, D. A., Hikida, A., Eckert, M., Knutzen, D., Alswaid, A. F., Özyurek, H.,

Dibooglu, S., Otto, E. A., Liu, Y., Davis, E. E., Hutter, C. M., Bammler, T. K., Farin, F. M., … Doherty, D. (2008). CC2D2A Is Mutated in Joubert Syndrome and Interacts with the Ciliopathy-Associated Basal Body Protein CEP290. *American Journal of Human Genetics*, *83*(5), 559–571. https://doi.org/10.1016/j.ajhg.2008.10.002

Gravells, P., Grant, E., Smith, K. M., James, D. I., & Bryant, H. E. (2017). Specific killing of DNA damage-response deficient cells with inhibitors of poly(ADP-ribose) glycohydrolase. *DNA Repair*, *52*, 81–91. https://doi.org/10.1016/j.dnarep.2017.02.010

Gravells, P., Neale, J., Grant, E., Nathubhai, A., Smith, K. M., James, D. I., & Bryant, H. E. (2018). Radiosensitization with an inhibitor of poly(ADP-ribose) glycohydrolase: A comparison with the PARP1/2/3 inhibitor olaparib. *DNA Repair*, *61*, 25–36. https://doi.org/10.1016/j.dnarep.2017.11.004

Grundy, G. J., Polo, L. M., Zeng, Z., Rulten, S. L., Hoch, N. C., Paomephan, P., Xu, Y., Sweet, S. M., Thorne, A. W., Oliver, A. W., Matthews, S. J., Pearl, L. H., & Caldecott, K. W. (2016). PARP3 is a sensor of nicked nucleosomes and monoribosylates histone H2B Glu2. *Nature Communications*, *7*. https://doi.org/10.1038/ncomms12404

Grundy, G. J., Rulten, S. L., Zeng, Z., Arribas-bosacoma, R., Iles, N., Manley, K., Oliver, A., & Caldecott, K. W. (2012). APLF promotes the assembly and activity of non-homologous end joining protein complexes. *The EMBO Journal*, *32*(1), 112–125. https://doi.org/10.1038/emboj.2012.304

Guastafierro, T., Cecchinelli, B., Zampieri, M., Reale, A., Riggio, G., Sthandier, O., Zupi, G., Calabrese, L., & Caiafa, P. (2008). CCCTC-binding factor activates PARP-1 affecting DNA methylation machinery. *Journal of Biological Chemistry*, *283*(32), 21873–21880. https://doi.org/10.1074/jbc.M801170200

Guo, H., Zhang, C., Liu, Q., Li, Q., Lian, G., Wu, D., Li, X., & Zhang, W. (2012). The Axin / TNKS complex interacts with KIF3A and is required for insulin-stimulated GLUT4 translocation. *Cell Research*, *22*(8), 1246–1257. https://doi.org/10.1038/cr.2012.52

Guo, N., Li, M. Z., Wang, L. M., Chen, H. D., Song, S. S., Miao, Z. H., & He, J. X. (2022). Repeated treatments of Capan-1 cells with PARP1 and Chk1 inhibitors promote drug resistance, migration and invasion. *Cancer Biology and Therapy*, *23*(1), 69–82. https://doi.org/10.1080/15384047.2021.2024414

Guo, T., Zuo, Y., Qian, L., Liu, J., Yuan, Y., Xu, K., Miao, Y., Feng, Q., Chen, X., Jin, L., Zhang, L., Dong, C., Xiong, S., & Zheng, H. (2019). ADP-ribosyltransferase PARP11 modulates the interferon antiviral response by mono-ADP-ribosylating the ubiquitin E3 ligase β-TrCP. *Nature Microbiology*, *4*(11), 1872–1884. https://doi.org/10.1038/s41564-019-0428-3

Guo, Y., Arciero, C. A., Jiang, R., Behera, M., Peng, L., & Li, X. (2020). Different Breast Cancer Subtypes Show Different Metastatic Patterns: A Study from A Large Public Database. *Asian Pacific Journal of Cancer Prevention*, *21*(12), 3587–3593. https://doi.org/10.31557/APJCP.2020.21.12.3587

Ha, G.-H., Kim, D.-Y., Breuer, E.-K., & Kim, C. K. (2018). Combination Treatment of Polo-Like Kinase 1 and Tankyrase-1 Inhibitors Enhances Anticancer Effect in Triple-negative Breast Cancer Cells. *Anticancer Research*, *1310*, 1303–1310. https://doi.org/10.21873/anticanres.12352

Ha, G. H., Kim, H. S., Go, H., Lee, H., Seimiya, H., Chung, D. H., & Lee, C. W. (2012). Tankyrase-1 function at telomeres and during mitosis is regulated by Polo-like kinase-1-mediated phosphorylation. *Cell Death and Differentiation*, *19*(2), 321–332. https://doi.org/10.1038/cdd.2011.101

Haikarainen, T., Krauss, S., & Lehtio, L. (2014). Tankyrases: Structure, Function and Therapeutic Implications in Cancer. *Current Pharmaceutical Design*, *20*(41), 6472–6488. https://doi.org/10.2174/1381612820666140630101525

Haince, J.-F., Ouellet, M.-E., Mcdonald, D., Hendzel, M. J., & Poirier, G. G. (2006). Dynamic relocation of poly(ADP-ribose) glycohydrolase isoforms during radiation-induced DNA damage. *BIOCHIMICA ET BIOPHYSICA ACTA*, *1763*(2), 226–237. https://doi.org/10.1016/j.bbamcr.2005.11.015

Hall, A. E., Lu, W. T., Godfrey, J. D., Antonov, A. V., Paicu, C., Moxon, S., Dalmay, T., Wilczynska, A., Muller, P. A. J., & Bushell, M. (2016). The cytoskeleton adaptor protein ankyrin-1 is upregulated by p53 following DNA damage and alters cell migration. *Cell Death and Disease*, *7*, 1–14. https://doi.org/10.1038/cddis.2016.91

Han, Yang, Jin, F., Xie, Y., Liu, Y., Hu, S., Liu, X. D., Guan, H., Gu, Y., Ma, T., & Zhou, P. K. (2019). DNA-PKcs parylation regulates DNA-PK kinase activity in the DNA damage response. *Molecular Medicine Reports*, *20*(4), 3609–3616. https://doi.org/10.3892/mmr.2019.10640

Han, Ye, Li, C.-W., Hsu, J.-M., Hsu, J. L., Chan, L.-C., Tan, X., & He, G.-J. (2019). Metformin reverses PARP inhibitors-induced epithelial-mesenchymal transition and PD-L1 upregulation in triple-negative breast cancer. *American Journal of Cancer Research*, *9*(4), 800–815. http://www.ncbi.nlm.nih.gov/pubmed/31106005%0Ahttp://www.pubmedcentral.nih.gov/articlerender.fcgi?artid=PMC6511636

Hanzlikova, H., Gittens, W., Krejcikova, K., Zeng, Z., & Caldecott, K. W. (2017). Overlapping roles for PARP1 and PARP2 in the recruitment of endogenous XRCC1 and PNKP into oxidized chromatin. *Nucleic Acids Research*, gkw1246. https://doi.org/10.1093/nar/gkw1246

Hanzlikova, H., Kalasova, I., Demin, A., Pennicot, L., Cihlarova, Z., & Caldecott, K. (2018). The Importance of Poly(ADP-Ribose) Polymerase asa Sensor of Unligated Okazaki Fragments during DNA Replication. *Molecular Cell*, *71*(2), 319–331. https://doi.org/10.1093/nar/gkx604

Hassa, P. O., & Hottiger, M. O. (2008). The diverse biological roles of mammalian PARPS, a small but powerful family of poly-ADP-ribose polymerases. *Frontiers in Bioscience: A Journal and Virtual Library*, *1*(13), 3046–3082.

Hatch, E. M. (2018). Nuclear envelope rupture: little holes, big openings. *Current Opinion in Cell Biology*, *52*, 66–72. https://doi.org/10.1053/j.gastro.2016.08.014.CagY

He, Y. J., Meghani, K., Caron, M.-C., Yang, C., Ronato, D. A., Bian, J., Sharma, A., Moore, J., Niraj, J., Detappe, A., Doench, J. G., Legube, G., Root, D. E., D'Andrea, A. D., Drané, P., De, S., Konstantinopoulos, P. A., Masson, J.-Y., & Chowdhury, D. (2018). DYNLL1 binds to MRE11 to limit DNA end resection in BRCA1-deficient cells. *Nature*, *563*(7732), 522–526. https://doi.org/10.1038/s41586-018-0670-5

Higgins, M. J., & Stearns, V. (2009). Understanding resistance to tamoxifen in hormone receptor-positive breast cancer. *Clinical Chemistry*, *55*(8), 1453–1455. https://doi.org/10.1373/clinchem.2009.125377

Hollern, D. P., Swiatnicki, M. R., Rennhack, J. P., Misek, S. A., Matson, B. C., McAuliff, A., Gallo, K. A., Caron, K. M., & Andrechek, E. R. (2019). E2F1 Drives Breast Cancer Metastasis by Regulating the Target Gene FGF13 and Altering Cell Migration. *Scientific Reports*, *9*(1), 1–13. https://doi.org/10.1038/s41598-019-47218-0

Holtlund, J., Kristensen, T., Stvold, A. Q., & Laland, S. G. (1980). On the presence of

poly(ADP-ribose) polymerase activity in metaphase chromosomes from HeLa S3 cells. *FEBS Letters*, *116*(1), 11–13.

Hopp, A. K., Grüter, P., & Hottiger, M. O. (2019). Regulation of glucose metabolism by NAD+ and ADP-ribosylation. *Cells*, *8*(11), 1–23. https://doi.org/10.3390/cells8111371

Hottiger, M. O., Hassa, P. O., Lüscher, B., Schüler, H., & Koch-Nolte, F. (2010). Toward a unified nomenclature for mammalian ADP-ribosyltransferases. *Trends in Biochemical Sciences*, *35*(4), 208–219. https://doi.org/10.1016/j.tibs.2009.12.003

Houl, J., Ye, Z., Brosey, C., Balapiti-Modarage, L., Namjoshi, S., Bacoola, A., Laverty, D., Walker, B., Yasin, P., Warden, L., Chinnam, N., Moiani, D., Stegeman, R., Chen, M.-K., Hung, M.-C., Nagel, Z., Ellenberger, T., Kim, I.-K., Jones, D., … Tainier, J. (2019). Selective small molecule PARG inhibitor causes replication fork stalling and cancer cell death. *Nature Communications*, *10*. https://doi.org/10.1038/s41467-019-13508-4

Hsieh, M. H., Chen, Y. T., Chen, Y. T., Lee, Y. H., Lu, J., Chien, C. L., Chen, H. F., Ho, H. N., Yu, C. J., Wang, Z. Q., & Teng, S. C. (2017). PARP1 controls KLF4-mediated telomerase expression in stem cells and cancer cells. *Nucleic Acids Research*, *45*(18), 10492–10503. https://doi.org/10.1093/nar/gkx683

Huang, D. W., Sherman, B. T., & Lempicki, R. A. (2009). Systematic and integrative analysis of large gene lists using DAVID bioinformatics resources. *Nature Protocols*, *4*(1), 44–57.

Huang, J. Y., Wang, K., Vermehren-Schmaedick, A., Adelman, J. P., & Cohen, M. S. (2016). PARP6 is a Regulator of Hippocampal Dendritic Morphogenesis. *Scientific Reports*, *6*, 18512. https://doi.org/10.1038/srep18512

Huang, K., Tidyman, W. E., Le, K. U. T., Kirsten, E., Kun, E., & Ordahl, C. P. (2004). Analysis of Nucleotide Sequence-Dependent DNA Binding of Poly (ADP-ribose) Polymerase in a Purified System. *Biochemistry*, *43*(1), 217–223. https://doi.org/10.1021/bi0301800

Huang, P., Chen, G., Jin, W., Mao, K., Wan, H., & He, Y. (2022). Molecular Mechanisms of Parthanatos and Its Role in Diverse Diseases. *International Journal of Molecular Sciences*, *23*(13). https://doi.org/10.3390/ijms23137292

Huang, S. M. A., Mishina, Y. M., Liu, S., Cheung, A., Stegmeier, F., Michaud, G. A., Charlat, O., Wiellette, E., Zhang, Y., Wiessner, S., Hild, M., Shi, X., Wilson, C. J., Mickanin, C., Myer, V., Fazal, A., Tomlinson, R., Serluca, F., Shao, W., … Cong, F. (2009). Tankyrase inhibition stabilizes axin and antagonizes Wnt signalling. *Nature*, *461*(7264), 614–620. https://doi.org/10.1038/nature08356

Huang, Z., Zhang, Z., Zhou, C., Liu, L., & Huang, C. (2022). Epithelial – mesenchymal transition : The history, regulatory mechanism, and cancer therapeutic opportunities. *MedComm*, *3*(2). https://doi.org/10.1002/mco2.144

Huletskyl, A., De, G., Mullerll, S., Hengartners, M., Menard, L., Lamarre, D., & Poirier, G. G. (1989). The Effect of Poly (ADP-ribosy1) ation on Native and H1-depleted Chromatin. *The Journal of Biological Chemistry*, *264*(15), 8878–8886. https://doi.org/10.1016/S0021-9258(18)81875-0

Hurst, V., Challa, K., Shimada, K., & Gasser, S. M. (2021). Cytoskeleton integrity influences XRCC1 and PCNA dynamics at DNA damage. *Molecular Biology of the Cell*, *32*(20), 1–11. https://doi.org/10.1091/mbc.E20-10-0680

Ikejima, M., Marsischky, G., & Gill, D. M. (1987). Direction of elongation of poly(ADP-ribose) chains. Addition of residues at the polymerase-proximal terminus. *Journal of Biological*

Chemistry, *262*(36), 17641–17650.

Illuzzi, G., Fouquerel, E., Amé, J.-C., Noll, A., Rehmet, K., Nasheuer, H.-P., Dantzer, F., & Schreiber, V. (2014). PARG is dispensable for recovery from transient replicative stress but required to prevent detrimental accumulation of poly(ADP-ribose) upon prolonged replicative stress. *Nucleic Acids Research*, *42*(12), 7776–7792. https://doi.org/10.1093/nar/gku505

Isabelle, M., Moreel, X., Gagné, J. P., Rouleau, M., Ethier, C., Gagné, P., Hendzel, M. J., & Poirier, G. G. (2010). Investigation of PARP-1, PARP-2, and PARG interactomes by affinity-purification mass spectrometry. *Proteome Science*, *8*, 1–11. https://doi.org/10.1186/1477-5956-8-22

Iwata, H., Goettsch, C., Sharma, A., Ricchiuto, P., Goh, W. W. Bin, Halu, A., Yamada, I., Yoshida, H., Hara, T., Wei, M., Inoue, N., Fukuda, D., Mojcher, A., Mattson, P. C., Barabási, A.-L., Boothby, M., Aikawa, E., Singh, S. A., & Aikawa, M. (2016). PARP9 and PARP14 cross-regulate macrophage activation via STAT1 ADP-ribosylation. *Nature Communications*, *7*(1), 12849. https://doi.org/10.1038/ncomms12849

Jain, A., Agostini, L. C., Mccarthy, G. A., Chand, S. N., Ramirez, A., Nevler, A., Cozzitorto, J., Schultz, C. W., Lowder, C. Y., Smith, K. M., Waddell, I. D., Raitses-Gurevich, M., Stossel, C., Gorman, Y. G., Atias, D., Yeo, C. J., Winter, J. M., Olive, K. P., Golan, T., … Brody, J. R. (2019). Poly (ADP) ribose glycohydrolase can be effectively targeted in pancreatic cancer. *Cancer Research*, canres.3645.201. https://doi.org/10.1158/0008-5472.can-18-3645

James, D., Fairweather, E., Griffiths, L., Hopkins, G., Jordan, A., Mcgonagle, A., Smith, K., Stowell, A., Waddell, I., & Ogilvie, D. (2016). Novel cell-permeable PARG inhibitors are selective and sensitize cells to alkylating DNA damage. *European Journal of Cancer*, *61*, S126. https://doi.org/10.1016/s0959-8049(16)61448-x

James, D. I., Smith, K. M., Jordan, A. M., Fairweather, E. E., Griffiths, L. A., Hamilton, N. S., Hitchin, J. R., Hutton, C. P., Jones, S., Kelly, P., Mcgonagle, A. E., Small, H., Stowell, A. I. J., Tucker, J., Waddell, I. D., Waszkowycz, B., & Ogilvie, D. J. (2016). First-in-Class Chemical Probes against Poly(ADP-ribose) Glycohydrolase (PARG) Inhibit DNA Repair with Differential Pharmacology to Olaparib. *ACS Chemical Biology*, *11*(11), 3179–3190. https://doi.org/10.1021/acschembio.6b00609

Janiszewska, M., Primi, M. C., & Izard, T. (2020). Cell adhesion in cancer: Beyond the migration of single cells. *The Journal of Biological Chemistry*, *295*(8), 2495–2505. https://doi.org/10.1074/jbc.REV119.007759

Jaspers, J. E., Sol, W., Kersbergen, A., Schlicker, A., Guyader, C., Xu, G., Wessels, L., Borst, P., Jonkers, J., & Rottenberg, S. (2015). *BRCA2-Deficient Sarcomatoid Mammary Tumors Exhibit Multidrug Resistance*. *75*(4), 732–741. https://doi.org/10.1158/0008-5472.can-14-0839

Ji, Y., & Tulin, A. V. (2010). The roles of PARP1 in gene control and cell differentiation. *Genes & Development*, *20*(5), 512–518. https://doi.org/10.1016/j.gde.2010.06.001

Jiu, Y., Peränen, J., Schaible, N., Cheng, F., Eriksson, J. E., Krishnan, R., & Lappalainen, P. (2017). Vimentin intermediate filaments control actin stress fiber assembly through GEF-H1 and RhoA. *Journal of Cell Science*, *130*(5), 892–902. https://doi.org/10.1242/jcs.196881

Johnston, S. A., Bramble, J. P., Yeung, C. L., Mendes, P. M., & Machesky, L. M. (2008). Arp2/3 complex activity in filopodia of spreading cells. *BMC Cell Biology*, *9*, 1–17. https://doi.org/10.1186/1471-2121-9-65

Joo, J. S., Cho, S. Y., Rou, W. S., Kim, J. S., Kang, S. H., Lee, E. S., Moon, H. S., Kim, S. H., Sung, J. K., Kwon, I. S., Eun, H. S., & Lee, B. S. (2020). SLC2A2 (GLUT2) as as a novel prognostic factor for hepatocellular carcinoma. *Oncology Reports*, *43*(6), 1785–1796. https://doi.org/10.3892/or.2020.7578

Jordan, A., Acton, B., Fairweather, E., Hamilton, N., Holt, S., Hitchin, J., Hutton, C., James, D., Jones, S., Mcgonagle, A., Small, H., Smith, K., Stowell, A., Waddell, I., Waszkowycz, B., & Ogilvie, D. (2014). 284 Poly(ADP-ribose) glycohydrolase (PARG) inhibitors increase nuclear poly(ADP-ribose) after methylating DNA damage. *European Journal of Cancer*, *50*, 94. https://doi.org/10.1016/s0959-8049(14)70410-1

Jungmichel, S., Rosenthal, F., Altmeyer, M., Lukas, J., Hottiger, M. O., & Nielsen, M. L. (2013). Proteome-wide identification of poly(ADP-Ribosyl)ation targets in different genotoxic stress responses. *Molecular Cell*, *52*(2), 272–285. https://doi.org/10.1016/j.molcel.2013.08.026

Jwa, M., & Chang, P. (2012). PARP16 is a tail-anchored endoplasmic reticulum protein required for the PERK- and IRE1α-mediated unfolded protein response. *Nature Cell Biology*, *14*(11), 1223–1230. https://doi.org/10.1038/ncb2593

Kamata, T., & Paschal, B. (2019). ADP-Ribosylation of the Ubiquitin C-Terminus by Dtx3L/Parp9. In *Ubiquitin Proteasome System - Current Insights into Mechanism Cellular Regulation and Disease*. IntechOpen. https://doi.org/10.5772/intechopen.81613

Kanai, M., Tong, W.-M., Sugihara, E., Wang, Z.-Q., Fukasawa, K., & Miwa, M. (2003). Involvement of Poly(ADP-Ribose) Polymerase 1 and Poly(ADP-Ribosyl)ation in Regulation of Centrosome Function. *Molecular and Cellular Biology*, *23*(7), 2451–2462. https://doi.org/10.1128/mcb.23.7.2451-2462.2003

Kanai, Y., Tanuma, S., & Sugimura, T. (1981). Immunofluorescent staining of poly (ADP-ribose) in situ in HeLa cell chromosomes in the M phase Biochemistry : *Proceedings of the National Academy of Sciences of the United States of America*, *78*(5), 2801–2804. https://doi.org/10.1073/pnas.78.5.2801

Kanu, N., Cerone, M. A., Goh, G., Zalmas, L. P., Bartkova, J., Dietzen, M., McGranahan, N., Rogers, R., Law, E. K., Gromova, I., Kschischo, M., Walton, M. I., Rossanese, O. W., Bartek, J., Harris, R. S., Venkatesan, S., & Swanton, C. (2016). DNA replication stress mediates APOBEC3 family mutagenesis in breast cancer. *Genome Biology*, *17*(1), 1–15. https://doi.org/10.1186/s13059-016-1042-9

Karch, K. R., Langelier, M., Pascal, M., & Garcia, B. A. (2017). The nucleosomal surface is the main target of histone ADP-ribosylation in response to DNA damage. *Molecular Biosystems*, *13*(12), 2660–2671. https://doi.org/10.1039/c7mb00498b

Karlberg, T., Klepsch, M., Thorsell, A., Andersson, C. D., & Linusson, A. (2015). Structural Basis for Lack of ADP-ribosyltransferase Activity in Poly (ADP-ribose) Polymerase-13 / Zinc Finger Antiviral. *Journal of Biological Chemistry*, *290*(12), 7336–7344. https://doi.org/10.1074/jbc.M114.630160

Karpova, Y., Johnson, S. J., Bordet, G., Guo, D., Ghatak, A., Markov, D. A., & Tulin, A. V. (2022a). Upregulation of PARG in prostate cancer cells suppresses their malignant behavior and downregulates tumor-promoting genes. *Biomedicine and Pharmacotherapy*, *153*(July), 113504. https://doi.org/10.1016/j.biopha.2022.113504

Karpova, Y., Johnson, S. J., Bordet, G., Guo, D., Ghatak, A., Markov, D. A., & Tulin, A. V. (2022b). Upregulation of PARG in prostate cancer cells suppresses their malignant behavior and downregulates tumor-promoting genes. *Biomedicine and Pharmacotherapy*, *153*(July), 113504. https://doi.org/10.1016/j.biopha.2022.113504

Kashima, L., Idogawa, M., Mita, H., Shitashige, M., Yamada, T., Ogi, K., Suzuki, H., Toyota, M., Ariga, H., Sasaki, Y., & Tokino, T. (2012). CHFR protein regulates mitotic checkpoint by targeting PARP-1 protein for ubiquitination and degradation. *Journal of Biological Chemistry*, *287*(16), 12975–12984. https://doi.org/10.1074/jbc.M111.321828

Kaufmann, T., Grishkovskaya, I., Polyansky, A., Kostrhon, S., Kukolj, E., Olek, K., Herbert, S., Beltzung, E., Mechtler, K., Peterbauer, Thomas Gotzman, J., Zhang, L., Hartl, M., Zagrovic, B., Elsayad, K., & Slade, D. (2017). A novel non-canonical PIP-box mediates PARGinteraction with PCNA. *Nucleic Acids Research*, *45*(19), 9741–9759. https://doi.org/10.1093/nar/gkx604

Ke, Wang, Zhang, Zhong, Wang, Zeng, & Ba. (2019). The Role of PARPs in Inflammation—and Metabolic—Related Diseases: Molecular Mechanisms and Beyond. *Cells*, *8*(9), 1047. https://doi.org/10.3390/cells8091047

Ke, Y., Han, Y., Guo, X., Wen, J., Wang, K., Jiang, X., Tian, X., Ba, X., Boldogh, I., & Zeng, X. (2017). PARP1 promotes gene expression at the post-transcriptiona level by modulating the RNA-binding protein HuR. *Nature Communications*, *8*. https://doi.org/10.1038/ncomms14632

Ke, Y., Zhang, J., Lv, X., Zeng, X., & Ba, X. (2019). Novel insights into PARPs in gene expression: regulation of RNA metabolism. *Cellular and Molecular Life Sciences*, *76*(17), 3283–3299. https://doi.org/10.1007/s00018-019-03120-6

Keil, C., Grobe, T., & Li Oei, S. (2006). MNNG-induced Cell Death Is Controlled by Interactions between PARP-1, Poly(ADP-ribose) Glycohydrolase, and XRCC1. *The Journal of Biological Chemistry*, *281*(45), 34394–34405. https://doi.org/10.1074/jbc.m606470200

Kennecke, H., Yerushalmi, R., Woods, R., Cheang, M. C. U., Voduc, D., Speers, C. H., Nielsen, T. O., & Gelmon, K. (2010). Metastatic behavior of breast cancer subtypes. *Journal of Clinical Oncology*, *28*(20), 3271–3277. https://doi.org/10.1200/JCO.2009.25.9820

Kidwell, W. R., & Mage, M. G. (1976). Changes in poly(adenosine diphosphate-ribose) and poly(adenosine diphosphate-ribose) polymerase in synchronous HeLa cells. *Biochemistry*, *15*(6), 1213–1217.

Kim, D., & Nam, H. J. (2022). PARP Inhibitors : Clinical Limitations and Recent Attempts to Overcome Them. *International Journal of Molecular Sciences*, *23*(15), 8412.

Kim, J. M. (2022). Molecular Link between DNA Damage Response and Microtubule Dynamics. *International Journal of Molecular Sciences*, *23*(13). https://doi.org/10.3390/ijms23136986

Kim, M. (2018). Novel insight into the function of tankyrase (Review). *Oncology Letters*. https://doi.org/10.3892/ol.2018.9551

Kim, M. K., Dudognon, C., & Smith, S. (2012). Tankyrase 1 regulates centrosome functionby controlling CPAP stability. *EMBO Reports*, *13*(8), 724–732. https://doi.org/10.1038/embor.2012.86

Kim, M. K., & Smith, S. (2014). Persistent telomere cohesion triggers a prolonged anaphase. *Molecular Biology of the Cell*, *25*(1), 30–40. https://doi.org/10.1091/mbc.E13-08-0479

Kim, M. Y., Mauro, S., Lis, J. T., Ge, N., & Kraus, W. L. (2004). NAD+-Dependent Modulation of Chromatin Structure and Transcription by Nucleosome Binding Properties of PARP-1. *Cell*, *119*(6), 803–814.

King, B. S., Cooper, K. L., Liu, K. J., & Hudson, L. G. (2012). Poly(ADP-ribose) contributes to

an association between Poly(ADP-ribose) polymerase-1 and xeroderma pigmentosum complementation group A in nucleotide excision repair. *Journal of Biological Chemistry*, *287*(47), 39824–39833. https://doi.org/10.1074/jbc.M112.393504

Kirby, I., Kojic, A., Arnold, M., Thorsell, A., Karlberg, T., Vermehren-Schmaedick, A., Sreenivasan, R., Schultz, C., Schuler, H., & Cohen, M. (2018). A Potent and Selective PARP11 Inhibitor Suggests Coupling between Cellular Localization and Catalytic Activity. *Cell Chemical Biology*, *25*(12), 1547–1553. https://doi.org/10.1016/j.chembiol.2018.09.011

Kiss, B., Szántó, M., Szklenár, M., Brunyánszki, A., Marosvölgyi, T., Sárosi, E., Remenyik, É., Gergely, P., Virág, L., Decsi, T., Rühl, R., & Bai, P. (2015). Poly(ADP) ribose polymerase-1 ablation alters eicosanoid and docosanoid signaling and metabolism in a murine model of contact hypersensitivity. *Molecular Medicine Reports*, *11*(4), 2861–2867. https://doi.org/10.3892/mmr.2014.3044

Ko, H. L., & Ren, E. C. (2012). Functional Aspects of PARP1 in DNA Repair and Transcription. *Biomolecules*, *2*(4), 524–548. https://doi.org/10.3390/biom2040524

Koh, D, Lawler, A. M., Poitras, M. F., Sasaki, M., Wattler, S., Nehls, M. C., Stoger, T., Poirier, G. G., Dawson, V. L., & Dawson, T. M. (2004). Failure to degrade poly(ADP-ribose) causes increased sensitivity to cytotoxicity and early embryonic lethality. *PNAS*, *101*(51), 17699–17704. https://doi.org/10.1073/pnas.0406182101

Koh, David. (2011). Synergistic cytotoxicity of N-methyl-N'-nitro-N-nitrosoguanidine and absence of poly(ADP-ribose) glycohydrolase involves chromatin decondensation. *International Journal of Oncology*. https://doi.org/10.3892/ijo.2011.1013

Koppensteiner, R., Samartzis, E. P., Noske, A., Teichman, A. Von, Dedes, I., Gwerder, M., Imesch, P., Ikenberg, K., Moch, H., Fink, D., Stucki, M., & Dedes, K. J. (2014). Effect of MRE11 Loss on PARP-Inhibitor Sensitivity in Endometrial Cancer In Vitro. *PLoS ONE*, *9*(6). https://doi.org/10.1371/journal.pone.0100041

Kowalik, M. A., Columbano, A., & Perra, A. (2017). Emerging Role of the Pentose Phosphate Pathway in Hepatocellular Carcinoma. *Frontiers in Oncology*, *7*. https://doi.org/10.3389/fonc.2017.00087

Krishnakumar, R., Gamble, M. J., Frizzell, K. M., Berrocal, J. G., Kininis, M., & Kraus, W. L. (2008). Reciprocal binding of PARP-1 and histone H1 at promoters specifies transcriptional outcomes. *Science*, *319*(5864), 819–821. https://doi.org/10.1126/science.1149250

Krishnakumar, R., & Kraus, W. L. (2010). PARP-1 Regulates Chromatin Structure and Transcription through a KDM5B-Dependent Pathway. *Molecular Cell*, *39*(5), 736–749. https://doi.org/10.1016/j.molcel.2010.08.014

Krukenberg, K. A., Kim, S., Tan, E. S., Maliga, Z., & Mitchison, T. J. (2015). Extracellular poly(ADP-ribose) is a pro-inflammatory signal for macrophages. *Chem Biol*, *22*(4), 446–452. https://doi.org/10.1053/j.gastro.2016.08.014.CagY

Kumar, A., Mazzanti, M., Mistrik, M., Kosar, M., Beznoussenko, G. V., Mironov, A. A., Garrè, M., Parazzoli, D., Shivashankar, G. V., Scita, G., Bartek, J., & Foiani, M. (2014). ATR mediates a checkpoint at the nuclear envelope in response to mechanical stress. *Cell*, *158*(3), 633–646. https://doi.org/10.1016/j.cell.2014.05.046

Lai, Y., Chen, Y., Watkins, S. C., Nathaniel, P. D., Guo, F., Clark, R. S. B., Kochanek, P. M., Jenkins, L. W., & Szabo, C. (2008). Identification of poly-ADP-ribosylated mitochondrial proteins after traumatic brain injury. *Journal of Neurochemistry*, *104*(6), 1700–1711. https://doi.org/10.1111/j.1471-4159.2007.05114.x

Langelier, M.-F., & Pascal, J. M. (2013). PARP-1 mechanism for coupling DNA damage detection to poly(ADP-ribose) synthesis. *Current Opinion in Structural Biology*, *23*(1), 134–143. https://doi.org/10.1016/j.sbi.2013.01.003.PARP-1

Lehmann, B. D., Bauer, J. A., Chen, X., Sanders, M. E., Chakravarthy, A. B., Shyr, Y., & Pietenpol, J. A. (2011). *Identification of human triple-negative breast cancer subtypes and preclinical models for selection of targeted therapies Brian D. Lehmann,1 Joshua A. Bauer,1 Xi Chen,2 Melinda E. Sanders,3 A. Bapsi Chakravarthy,4 Yu Shyr,2 and Jennifer A. Pietenpol1 1Dep*. *121*(7), 2750–2767. https://doi.org/10.1172/JCI45014DS1

Leung, A. K. L. (2020). Poly(ADP-ribose): A Dynamic Trigger for Biomolecular Condensate Formation. *Trends in Cell Biology*, *30*(5), 370–383. https://doi.org/10.1016/j.tcb.2020.02.002.Poly(ADP-ribose)

Li, B., Navarro, S., Kasahara, N., & Comai, L. (2004). Identification and Biochemical Characterization of A Werner's Syndrome Protein Complex with Ku70/80 and Poly(ADP-ribose) Polymerase-1. *Journal of Biological Chemistry*, *279*(14), 13659–13667. https://doi.org/10.1074/jbc.M311606200

Li, C., Zheng, X. U., Han, Y., Lv, Y. A. N., Lan, F. U., & Zhao, J. I. E. (2018). XAV939 inhibits the proliferation and migration of lung adenocarcinoma A549 cells through the WNT pathway. *Oncology Letters*, *15*, 8973–8982. https://doi.org/10.3892/ol.2018.8491

Li, H.-D., Chen, X., Xu, J.-J., Du, X., Yang, Y., Li, J.-J., Yang, X.-J., Huang, H.-M., Li, X.-F., Wu, M.-F., Zhang, C., Zhang, C., Li, Z., Wang, H., Meng, X.-M., Huang, C., & Li, J. (2020). DNMT3b-mediated methylation of ZSWIM3 enhances inflammation in alcohol-induced liver injury via regulating TRAF2-mediated NF-κB pathway. *Clinical Science*, *134*(14), 1935–1956.

Li, J., Saville, K. M., Ibrahim, M., Zeng, X., McClellan, S., Angajala, A., Beiser, A., Andrews, J. F., Sun, M., Koczor, C. A., Clark, J., Hayat, F., Makarov, M. V., Wilk, A., Yates, N. A., Migaud, M. E., & Sobol, R. W. (2021). NAD+bioavailability mediates PARG inhibition-induced replication arrest, intra S-phase checkpoint and apoptosis in glioma stem cells. *NAR Cancer*, *3*(4), 1–17. https://doi.org/10.1093/narcan/zcab044

Li, L., Zhao, H., Liu, P., Li, C., Quanquin, N., Ji, X., Sun, N., Du, P., Qin, C.-F., Lu, N., & Cheng, G. (2018). PARP12suppresses Zika virus infection through PARP-dependent degradation of NS1 and NS3 viral proteins. *Science Signaling*, *11*(535), eaas9332. https://doi.org/10.1126/scisignal.aas9332

Li, M., Lu, L. Y., Yang, C. Y., Wang, S., & Yu, X. (2013). The FHA and BRCT domains recognize ADP-ribosylation during DNA damage response. *Genes and Development*, *27*(16), 1752–1768. https://doi.org/10.1101/gad.226357.113

Li, M., & Yu, X. (2013). Function of BRCA1 in the DNA Damage Response Is Mediated by ADP-Ribosylation. *Cancer Cell*, *23*(5), 693–704. https://doi.org/10.1016/j.ccr.2013.03.025

Li, N., Wang, Y., Neri, S., Zhen, Y., Fong, L. W. R., Qiao, Y., Li, X., Chen, Z., Stephan, C., Deng, W., Ye, R., Jiang, W., Zhang, S., Yu, Y., Hung, M., Chen, J., & Lin, S. H. (2019). Tankyrase disrupts metabolic homeostasis andpromotes tumorigenesis by inhibiting LKB1-AMPKsignalling. *Nature Communications*, *10*(4363). https://doi.org/10.1038/s41467-019-12377-1

Li, N., Zhang, Y., Han, X., Liang, K., Wang, J., Feng, L., Wang, W., Songyang, Z., Lin, C., Yang, L., Yu, Y., & Chen, J. (2015). Poly-ADP ribosylation of PTEN by tankyrases promotes PTEN degradation and tumor growth. *Genes and Development*, *29*(2), 157–170. https://doi.org/10.1101/gad.251785.114

Li, Q., Li, M., Wang, Y.-L., Fauzee, N. J. S., Yang, Y., Pan, J., Yang, L., & Lazar, A. (2012). RNA Interference of PARG Could Inhibit the Metastatic Potency of Colon Carcinoma Cells via PI3-Kinase/Akt Pathway. *Cellular Phsiology and Biochemistry*, *29*(3–4), 361–372. https://doi.org/10.1159/000338491

Li, T., Lu, H., Shen, C., Lahiri, S. K., Wason, M. S., Mukherjee, D., Yu, L., & Zhao, J. (2014). Identification of epithelial stromal interaction 1 as a novel effector downstream of Krüppel-like factor 8 in breast cancer invasion and metastasis. *Oncogene*, *33*(39), 4746–4755. https://doi.org/10.1038/onc.2013.415

Liang, Y. C., Hsu, C. Y., Yao, Y. L., & Yang, W. M. (2013). PARP-2 regulates cell cycle-related genes through histone deacetylation and methylation independently of poly(ADP-ribosyl)ation. *Biochemical and Biophysical Research Communications*, *431*(1), 58–64. https://doi.org/10.1016/j.bbrc.2012.12.092

Lin, Y., Tang, X., Zhu, Y., Shu, T., & Han, X. (2011). Identification of PARP-1 as one of the transcription factors binding to the repressor element in the promoter region of COX-2. *Archives of Biochemistry and Biophysics*, *505*(1), 123–129. https://doi.org/10.1016/j.abb.2010.09.016

Linder, S., Cervero, P., Eddy, R., & Condeelis, J. (2023). Mechanisms and roles of podosomes and invadopodia. *Nature Reviews Molecular Cell Biology*, *24*(2), 86–106. https://doi.org/10.1038/s41580-022-00530-6

Liu, L., Zhang, X., Nan, C., Zhao, Z., Ma, S., Li, W., Hu, H., & Liang, Z. (2017). MicroRNA-182 targets protein phosphatase 1 regulatory inhibitor subunit 1C in glioblastoma. *Oncotarget*, *8*(70), 114677–114684. https://doi.org/10.18632/oncotarget.21309

Liu, M., Zhou, X., Liu, J., Lu, C., Zhang, G., Zhang, J., & Jiao, S. (2021). Predictive Biomarkers of Dicycloplatin Resistance or Susceptibility in Prostate Cancer. *Frontiers in Genetics*, *12*(July), 1–10. https://doi.org/10.3389/fgene.2021.669605

Loseva, O., Jemth, A.-S., Bryant, H. E., Schuler, H., Lehtio, L., Karlberg, T., & Helleday, T. (2010). PARP-3 Is a Mono-ADP-ribosylase That Activates PARP-1 in the Absence of DNA. *Biological Chemistry*, *285*(11), 8054–8060. https://doi.org/10.1074/jbc.m109.077834

Lu, H., Lei, Z., Lu, Z., Lu, Q., Lu, C. H. I., Chen, W., Wang, C., Tang, Q. I. U., & Kong, Q. (2013). Silencing tankyrase and telomerase promotes A549 human lung adenocarcinoma cell apoptosis and inhibits proliferation. *Oncology Reports*, *1*, 1745–1752. https://doi.org/10.3892/or.2013.2665

Lu, P., Takai, K., Weaver, V. M., & Werb, Z. (2011). Extracellular Matrix Degradation and Remodeling in Development and Disease. *Cold Spring Harbor Perspectives in Biology*, *3*(12).

Lu, X.-C. M., Massuda, E., Lin, Q., Li, W., Li, J.-H., & Zhang, J. (2003). Post-treatment With a Novel PARG Inhibitor Reduces Infarct in Cerebral Ischemia in the Rat. *Brain Research*, *18*(978), 99–103. https://doi.org/10.1016/s0006-8993(03)02774-4.

Luijsterburg, M. S., Lindh, M., Acs, K., Vrouwe, M. G., Pines, A., van Attikum, H., Mullenders, L. H., & Dantuma, N. P. (2012). DDB2 promotes chromatin decondensation at UV-induced DNA damage. *Journal of Cell Biology*, *197*(2), 267–281. https://doi.org/10.1083/jcb.201106074

Lupey-Green, L. N., Caruso, L. B., Madzo, J., Martin, K. A., Tan, Y., Hulse, M., & Tempera, I. (2018). PARP1 Stabilizes CTCF Binding and Chromatin Structure To Maintain Epstein-Barr Virus Latency Type. *Journal of Virology*, *92*(18). https://doi.org/10.1128/jvi.00755-18

Lupo, B., Vialard, J., Sassi, F., Angibaud, P., Puliafito, A., Pupo, E., Lanzetti, L., Comoglio, P. M., Bertotti, A., & Trusolino, L. (2016). Tankyrase inhibition impairs directional migration and invasion of lung cancer cells by affecting microtubule dynamics and polarity signals. *BMC Biology*, *14*(5). https://doi.org/10.1186/s12915-016-0226-9

Ma, Y., Zhang, P., Zhang, Q., Wang, X., Miao, Q., Lyu, X., Cui, B. O., & Ma, H. (2021). Dihydroartemisinin suppresses proliferation , migration , the Wnt / β - catenin pathway and EMT via TNKS in gastric cancer. *Oncology Letters*, *22*, 1–13. https://doi.org/10.3892/ol.2021.12949

Maclejowski, J., & Hatch, E. M. (2020). Nuclear Membrane Rupture and Its Consequences. *Annual Review of Cell and Developmental Biology*, *36*, 85–114. https://doi.org/10.1146/annurev-cellbio-020520-120627

Macpherson, L., Tamblyn, L., Rajendra, S., Bralha, F., Mcpherson, J. P., & Matthews, J. (2013). 2,3,7,8-Tetrachlorodibenzo-p-dioxin poly(ADP-ribose) polymerase (TiPARP, ARTD14) is a mono-ADP-ribosyltransferase and repressor of aryl hydrocarbon receptor transactivation. *Nucleic Acids Research*, *41*(3), 1604–1621. https://doi.org/10.1093/nar/gks1337

Madison, D. L., Stauffer, D., & Lundblad, J. R. (2011). The PARP inhibitor PJ34 causes a PARP1-independent, p21 dependent mitotic arrest. *DNA Repair*, *10*(10), 1003–1013. https://doi.org/10.1016/j.dnarep.2011.07.006

Maluchenko, N. V, Nilov, D. K., Pushkarev, S. V, Kotova, E. Y., Gerasimova, S., Kirpichnikov, M. P., Langelier, M., Pascal, J. M., Akhtar, S., Feofanov, A. V, & Studitsky, V. M. (2021). Mechanisms of Nucleosome Reorganization by PARP1. *International Journal of Molecular Sciences*, *22*(22), 12127.

Mani, R. S., Fanta, M., Karimi-Busheri, F., Silver, E., Virgen, C. A., Caldecott, K. W., Cass, C. E., & Weinfield, M. (2007). XRCC1 Stimulates Polynucleotide Kinase by Enhancing Its Damage Discrimination and Displacement from DNA Repair Intermediates * □. *The Journal of Biological Chemistry*, *282*(38), 28004–28013. https://doi.org/10.1074/jbc.M704867200

Mann, M., Kumar, S., Chauhan, S. S., Bhatla, N., Kumar, S., Bakhshi, S., Gupta, R., Sharma, A., & Kumar, L. (2019). Correction: PARP-1 inhibitor modulate β-catenin signaling to enhance cisplatin sensitivity in cancer cervix (Oncotarget (2019) 10 (4262-4275) DOI: 10.18632/oncotarget.27008). *Oncotarget*, *10*(46), 4802.

Mao, X., Du, S., Yang, Z., Zhang, L., Peng, X., Jiang, N., & Zhou, H. (2017). Inhibitors of PARP-1 exert inhibitory effects on the biological characteristics of hepatocellular carcinoma cells in vitro. *Molecular Medicine Reports*, *16*(1), 208–214. https://doi.org/10.3892/mmr.2017.6568

Mariotti, L., Pollock, K., & Guettler, S. (2017a). Regulation of Wnt/β-catenin signalling by tankyrase-dependent poly(ADP-ribosyl)ation and scaffolding. *British Journal of Pharmacology*, *174*(24), 4611–4636. https://doi.org/10.1111/bph.14038

Mariotti, L., Pollock, K., & Guettler, S. (2017b). Regulation of Wnt/β-catenin signalling by tankyrase-dependent poly(ADP-ribosyl)ation and scaffolding. *British Journal of Pharmacology*, *174*(24), 4611–4636. https://doi.org/10.1111/bph.14038

Marques, M., Jangal, M., Wang, L.-C., Kazanets, A., Daniela da Silva, S., Zhao, T., Lovato, A., Yu, H., Jie, S., del Rincon, S., Mackey, J., Damaraju, S., Alaoui-Jamali, M., & Witcher, M. (2019). Oncogenic activity of poly (ADP-ribose) glycohydrolase. *Oncogene*, *38*, 2177–2191. https://doi.org/10.1038/s41388-018-0568-6

Martin, L., Cheng, T., James, D. I., Begum, H., Smith, K. M., Jordan, A., Waddell, I., Vaidya,

K., Fischer, M., Yao, B., Drummond, J., Cleary, L., Martinez, R., Sutton, J., Ravindran, N., Joseph, J., Venetsanakos, E., Dillon, M., Hager, J. H., & Belmont, L. D. (2018). Abstract 1943: PARG inhibitors exhibit synthetic lethality with XRCC1 deficiency and a cellular mechanism of action that is distinct from PARP inhibition. *American Association for Cancer Research*. https://doi.org/10.1158/1538-7445.am2018-1943

Martinez-Zamudio, R., & Ha, H. C. (2012). Histone ADP-Ribosylation Facilitates Gene Transcription by Directly Remodeling Nucleosomes. *Molecular and Cellular Biology*, *32*(13), 2490–2502. https://doi.org/10.1128/mcb.06667-11

Márton, J., Fodor, T., Nagy, L., Vida, A., Kis, G., Brunyánszki, A., Antal, M., Lüscher, B., & Bai, P. (2018). PARP10 (ARTD10) modulates mitochondrial function. *PLOS ONE*, *13*(1), e0187789. https://doi.org/10.1371/journal.pone.0187789

Márton, J., Péter, M., Balogh, G., Bódi, B., Vida, A., Szántó, M., Bojcsuk, D., Jankó, L., Bhattoa, H. P., Gombos, I., Uray, K., Horváth, I., Török, Z., Balint, B. L., Papp, Z., Vígh, L., & Bai, P. (2018). Poly(ADP-ribose) polymerase-2 is a lipid-modulated modulator of muscular lipid homeostasis. *Biochimica et Biophysica Acta - Molecular and Cell Biology of Lipids*, *1863*(11), 1399–1412. https://doi.org/10.1016/j.bbalip.2018.07.013

Masson, M., Niedergang, C., Schreiber, V., Muller, S., Menissier-De Murcia, J., & De Murcia, G. (1998). XRCC1 Is Specifically Associated with Poly(ADP-Ribose) Polymerase and Negatively Regulates Its Activity following DNA Damage. *Molecular and Cellular Biology*, *18*(6), 3563–3571. https://doi.org/10.1128/mcb.18.6.3563

Masutani, M., Nozaki, T., Nakamoto, K., Nakagama, H., Suzuki, H., Kusuoka, O., Tsutsumi, M., & Sugimura, T. (2000). The response of Parp knockout mice against DNA damaging agents. *Mutation Research - Reviews in Mutation Research*, *462*(2–3), 159–166. https://doi.org/10.1016/S1383-5742(00)00033-8

Matanes, E., López-Ozuna, V. M., Octeau, D., Baloch, T., Racovitan, F., Dhillon, A. K., Kessous, R., Raban, O., Kogan, L., Salvador, S., Lau, S., Gotlieb, W. H., & Yasmeen, A. (2021). Inhibition of Poly ADP-Ribose Glycohydrolase Sensitizes Ovarian Cancer Cells to Poly ADP-Ribose Polymerase Inhibitors and Platinum Agents. *Frontiers in Oncology*, *11*(October), 1–12. https://doi.org/10.3389/fonc.2021.745981

Matsumoto, Y., Dimitriou, I. D., Rose, J. La, Lim, M., Camilleri, S., Law, N., Adissu, H. A., Tong, J., Moran, M. F., Chruscinski, A., He, F., Asano, Y., Katsuyama, T., Sada, K., & Wada, J. (2022). Tankyrase represses autoinflammation through the attenuation of TLR2 signaling. *The Journal of Clinical Investigation*, *132*(7).

Matveeva, E. A., Al-Tinawi, Q. M. H., Rouchka, E. C., & Fondufe-Mittendorf, Y. N. (2019). Coupling of PARP1-mediated chromatin structural changes to transcriptional RNA polymerase II elongation and cotranscriptional splicing. *Epigenetics and Chromatin*, *12*(1). https://doi.org/10.1186/s13072-019-0261-1

Matveeva, E., Maiorano, J., Zhang, Q., Eteleeb, A. M., Convertini, P., Chen, J., Infantino, V., Stamm, S., Wang, J., Rouchka, E. C., & Fondufe-Mittendorf, Y. N. (2016). Involvement of PARP1 in the regulation of alternative splicing. *Cell Discovery*, *2*, 1–19. https://doi.org/10.1038/celldisc.2015.46

Mayr, M., Hu, Y., Hainaut, H., & Xu, Q. (2002). Mechanical stress-induced DNA damage and rac-p38MAPK signal pathways mediate p53-dependent apoptosis in vascular smooth muscle cells. *The FASEB Journal : Official Publication of the Federation of American Societies for Experimental Biology*, *16*(11), 1423–1425. https://doi.org/10.1096/fj.02-0042fje

Mcgurk, L., Gomes, E., Guo, L., Kalb, R. G., Shorter, J., Bonini, N. M., Mcgurk, L., Gomes, E., Guo, L., Mojsilovic-petrovic, J., Tran, V., & Kalb, R. G. (2018). Poly (ADP-Ribose)

Prevents Pathological Phase Separation of TDP-43 by Promoting Liquid Demixing and Stress Granule Localization Article Poly (ADP-Ribose) Prevents Pathological Phase Separation of TDP-43 by Promoting Liquid Demixing and Stress Granule . *Molecular Cell*, *71*(5), 703-717.e9. https://doi.org/10.1016/j.molcel.2018.07.002

Meisterernst, M., Stelzer, G., & Roeder, R. G. (1997). Poly (ADP-ribose) polymerase enhances activator-dependent transcription in vitro. *PNAS*, *94*(6), 2261–2265. https://doi.org/10.1073/pnas.94.6.2261

Melikishvili, M., Chariker, J. H., Rouchka, E. C., & Fondufe-Mittendorf, Y. N. (2017). Transcriptome-wide identification of the RNA-binding landscape of the chromatin-associated protein PARP1 reveals functions in RNA biogenesis. *Cell Discovery*, *3*, 1–21. https://doi.org/10.1038/celldisc.2017.43

Menissier De Murcia, J. (2003). Functional interaction between PARP-1 and PARP-2 in chromosome stability and embryonic development in mouse. *The EMBO Journal*, *22*(9), 2255–2263. https://doi.org/10.1093/emboj/cdg206

Ménissier De Murcia, J., Niedergang, C., Trucco, C., Ricoul, M., Dutrillaux, B., Mark, M., Oliver, F. J., Masson, M., Dierich, A., Lemeur, M., Walztinger, C., Chambon, P., & De Murcia, G. (1997). Requirement of poly(ADP-ribose) polymerase in recovery from DNA damage in mice and in cells. *Proceedings of the National Academy of Sciences of the United States of America*, *94*(14), 7303–7307. https://doi.org/10.1073/pnas.94.14.7303

Meyer-Ficca, M. L., Meyer, R. G., Coyle, D. L., Jacobson, E. L., & Jacobson, M. K. (2004). Human poly(ADP-ribose) glycohydrolase is expressed in alternative splice variants yielding isoforms that localize to different cell compartments. *Experimental Cell Research*, *297*(2), 521–532. https://doi.org/10.1016/j.yexcr.2004.03.050

Meyer, R. G., Meyer-Ficca, M. L., Whatcott, C. J., Jacobson, E. L., & Jacobson, M. K. (2007). Two small enzyme isoforms mediate mammalian mitochondrial poly(ADP-ribose) glycohydrolase (PARG) activity. *Experimental Cell Research*, *313*(13), 2920–2936. https://doi.org/10.1016/j.yexcr.2007.03.043

Meyer, R., Müller, M., Beneke, S., Küpper, J. H., & Bürkle, A. (2000). Negative regulation of alkylation-induced sister-chromatid exchange by poly(ADP-ribose) polymerase-1 activity. *International Journal of Cancer*, *88*(3), 351–355. https://doi.org/10.1002/1097-0215(20001101)88:3<351::AID-IJC5>3.0.CO;2-H

Mi, H., Muruganujan, A., Huang, X., Guo, X., & Thomas, P. D. (2016). Protocol Update for large-scale genome and gene function analysis with the PANTHER. *Nature Protocols*, *14*, 703–721. https://doi.org/10.1038/s41596-019-0128-8

Min, W., Cortes, U., Herceg, Z., Tong, W.-M., & Wang, Z.-Q. (2010). Deletion of the nuclear isoform of poly(ADP-ribose) glycohydrolase (PARG) reveals its function in DNA repair, genomic stability and tumorigenesis. *Carcinogenesis*, *31*(12), 2058–2065. https://doi.org/10.1093/carcin/bgq205

Mirman, Z., Lottersberger, F., Takai, H., Kibe, T., Gong, Y., Takai, K., Bianchi, A., Zimmermann, M., Durocher, D., & De Lange, T. (2018). 53BP1–RIF1–shieldin counteracts DSB resection through CST- and Polα-dependent fill-in. *Nature*, *560*(7716), 112–116. https://doi.org/10.1038/s41586-018-0324-7

Miwa, M., Saikawa, N., Yamaizumi, Z., Nishimura, S., & Sugimura, T. (1979). Structure of poly(adenosine diphosphate ribose): identification of 2'-[1''-ribosyl-2''-(or 3''-)(1'''-ribosyl)]adenosine-5',5'',5'''-tris(phosphate) as a branch linkage. *Proceedings of the National Academy of Sciences*, *76*(2), 595–599. https://doi.org/10.1073/pnas.76.2.595

Miwa, M., & Sugimura, T. (1971). Splitting of the ribose-ribose linkage of poly(adenosine

diphosphate-robose) by a calf thymus extract. *Journal of Biological Chemistry*.

Miwa, M., Tanaka, M., Matsushima, T., & Sugimura, T. (1974). Purification and properties of a glycohydrolase from calf thymus splitting ribose ribose linkages of poly(adenosine diphosphate ribose). *Journal of Biological Chemistry*.

Miyake, Y., Nakamura, M., Nabetani, A., Shimamura, S., Tamura, M., Yonehara, S., Saito, M., & Ishikawa, F. (2009). RPA-like Mammalian Ctc1-Stn1-Ten1 Complex Binds to Single-Stranded DNA and Protects Telomeres Independently of the Pot1 Pathway. *Molecular Cell*, *36*(2), 193–206. https://doi.org/10.1016/j.molcel.2009.08.009

Molloy-Simard, V., St-Laurent, J.-F., Vigneault, F., Gaudreault, M., Dargis, N., Guérin, M.-C., Leclerc, S., Morcos, M., Black, D., Molgat, Y., Bergeron, D., De Launoit, Y., Boudreau, F., Desnoyers, S., & Guérin, S. (2012). Altered Expression of the Poly(ADP-Ribosyl)ation Enzymes in Uveal Melanoma and Regulation of PARG Gene Expression by the Transcription Factor ERM. *Biochemistry and Molecular Biology*, *53*(10), 6219. https://doi.org/10.1167/iovs.11-8853

Mortusewicz, O., Fouquerel, E., Ame, J.-C., Leonhardt, H., & Schreiber, V. (2011). PARG is recruited to DNA damage sites through poly(ADP-ribose)- and PCNA-dependent mechanisms. *Nucleic Acids Research*, *39*(12), 5045–5056. https://doi.org/10.1093/nar/gkr099

Mostocotto, C., Carbone, M., Battistelli, C., Ciotti, A., Amati, P., & Maione, R. (2014). Poly(ADP-Ribosyl)ation is required to modulate chromatin changes at c-MYC promoter during emergence from quiescence. *PLoS ONE*, *9*(7), 1–11. https://doi.org/10.1371/journal.pone.0102575

Munnur, D., Bartlett, E., Mikolčević, P., Kirby, I. T., Gregor, J., Mikoč, A., Cohen, M. S., & Ahel, I. (2019). Reversible ADP-ribosylation of RNA. *Nucleic Acids Research*, *47*(11), 5658–5669. https://doi.org/10.1093/nar/gkz305

Murai, J., Huang, S. N., Das, B. B., Renaud, A., Zhang, Y., Doroshow, J. H., Ji, J., Takeda, S., & Pommier, Y. (2012). Trapping of PARP1 and PARP2 by Clinical PARP Inhibitors. *Cancer Research*, *72*(33), 5588–5599. https://doi.org/10.1158/0008-5472.CAN-12-2753

Murai, J., Huang, S. Y. N., Renaud, A., Zhang, Y., Ji, J., Takeda, S., Morris, J., Teicher, B., Doroshow, J. H., & Pommier, Y. (2014). Stereospecific PARP trapping by BMN 673 and comparison with olaparib and rucaparib. *Molecular Cancer Therapeutics*, *13*(2), 433–443. https://doi.org/10.1158/1535-7163.MCT-13-0803

Murai, J., Tankg, S.-W., Leo, E., Baechler, S. A., Redon, C. E., Zhang, H., Abo, M. Al, Rajapakse, V. N., Nakamura, E., Jenkins, L. M. M., Aladjem, M. I., & Pommier, Y. (2018). SLFN11 blocks stressed replication forks independently of ATR. *Molecular Cell*, *69*(3), 371–384. https://doi.org/doi:10.1016/j.molcel.2018.01.012.

Murata, M. M., Kong, X., Moncada, E., Chen, Y., Imamura, H., Wang, P., Berns, M. W., Yokomori, K., & Digman, M. A. (2019). NAD+ consumption by PARP1 in response to DNA damage triggers metabolic shift critical for damaged cell survival. *Molecular Biology of the Cell*, *30*(20), 2584–2597. https://doi.org/10.1091/mbc.E18-10-0650

Murcia, G. D. E., & Murcia, J. M. D. E. (1995). A dominant-negative mutant of human poly (ADP-ribose) polymerase affects cell recovery , apoptosis , and sister chromatid exchange following DNA damage. *Proceedings of the National Academy of Sciences of the United States of America*, *92*(11), 4753–4757. https://doi.org/10.1073/pnas.92.11.4753

Murcial, G. De, Jongstra-bilen, J., Ittel, M., Mandel, P., & Delain, E. (1983). Poly (ADP-ribose) polymerase auto-modification and interaction with DNA : electron microscopic

visualization. *The EMBO Journal*, *2*(4), 543–548. https://doi.org/10.1002/j.1460-2075.1983.tb01460.x

Muthurajan, U. M., Hepler, M. R. D., Hieb, A. R., Clark, N. J., Kramer, M., Yao, T., & Luger, K. (2014). Automodification switches PARP-1 function from chromatin architectural protein to histone chaperone. *Proceedings of the National Academy of Sciences of the United States of America*. https://doi.org/10.1073/pnas.1405005111

Nagashima, H., Lee, C. K., Tateishi, K., Higuchi, F., Rafferty, S., Melamed, L., Miller, J. J., Wakimoto, H., & Cahill, D. P. (2021). Poly(ADP-ribose) glycohydrolase inhibition sequesters NAD+ to potentiate the metabolic lethality of alkylating chemotherapy in IDH mutant tumor cells. *Cancer Discovery*, *10*(11), 1672–1689. https://doi.org/10.1158/2159-8290.CD-20-0226.Poly(ADP-ribose)

Nakadate, Y., Kodera, Y., Kitamura, Y., Tachibana, T., Tamura, T., & Koizumi, F. (2013). Silencing of poly(ADP-ribose) glycohydrolase sensitizes lung cancer cells to radiation through the abrogation of DNA damage checkpoint. *Biochemical and Biophysical Research Communications*, *441*(4), 793–798. https://doi.org/10.1016/j.bbrc.2013.10.134

Nalabothula, N., Al-Jumaily, T., Eteleeb, A. M., Flight, R. M., Xiaorong, S., Moseley, H., Rouchka, E. C., & Fondufe-Mittendorf, Y. N. (2015). Genome-wide profiling of PARP1 reveals an interplay with gene regulatory regions and DNA methylation. *PLoS ONE*, *10*(8), 1–22. https://doi.org/10.1371/journal.pone.0135410

Nathubhai, A., Haikarainen, T., Koivunen, J., Murthy, S., Koumanov, F., Lloyd, M. D., Holman, G. D., Pihlajaniemi, T., Tosh, D., Lehtiö, L., & Threadgill, M. D. (2017). Highly Potent and Isoform Selective Dual Site Binding Tankyrase/Wnt Signaling Inhibitors That Increase Cellular Glucose Uptake and Have Antiproliferative Activity. *Journal of Medicinal Chemistry*, *60*(2), 814–820. https://doi.org/10.1021/acs.jmedchem.6b01574

Navas, L. E., & Carnero, A. (2021). NAD+ metabolism, stemness, the immune response, and cancer. *Signal Transduction and Targeted Therapy*, *6*(1). https://doi.org/10.1038/s41392-020-00354-w

Newman, L. A., Reis-Filho, J. S., Morrow, M., Carey, L. A., & King, T. A. (2015). The 2014 Society of Surgical Oncology Susan G. Komen for the Cure Symposium: Triple-Negative Breast Cancer. *Annals of Surgical Oncology*, *22*(3), 874–882. https://doi.org/10.1245/s10434-014-4279-0

Nielsen, H. L., Ronnov-Jessen, L., Villadsen, R., & Petersen, O. W. (2002). Identification of EPSTI1, a novel gene induced by epithelial-stromal interaction in human breast cancer. *Genomics*, *79*(5), 703–710. https://doi.org/10.1006/geno.2002.6755

Niere, M, Mashimo, M., Agledal, L., Dolle, C., Kasamatsu, A., Kato, J., Moss, J., & Ziegler, M. (2012). ADP-ribosylhydrolase 3 (ARH3), Not Poly(ADP-ribose) Glycohydrolase (PARG) Isoforms, Is Responsible for Degradation of Mitochondrial Matrix-associated Poly(ADP-ribose). *The Journal of Biological Chemistry*, *287*(20), 16088–16102. https://doi.org/10.1074/jbc.m112.349183

Niere, Marc, Kernstock, S., Koch-nolte, F., & Ziegler, M. (2008). Functional Localization of Two Poly (ADP-Ribose) -Degrading Enzymes to the Mitochondrial Matrix □. *Mol*, *28*(2), 814–824. https://doi.org/10.1128/MCB.01766-07

Noll, A., Illuzzi, G., Amé, J.-C., Dantzer, F., & Schreiber, V. (2016). PARG deficiency is neither synthetic lethal with BRCA1 nor PTEN deficiency. *Cancer Cell International*, *16*(1). https://doi.org/10.1186/s12935-016-0333-2

Noordermeer, S. M., Adam, S., Setiaputra, D., Barazas, M., Pettitt, S. J., Ling, A. K., Olivieri,

M., Álvarez-Quilón, A., Moatti, N., Zimmermann, M., Annunziato, S., Krastev, D. B., Song, F., Brandsma, I., Frankum, J., Brough, R., Sherker, A., Landry, S., Szilard, R. K., … Durocher, D. (2018). The shieldin complex mediates 53BP1-dependent DNA repair. *Nature*, *560*(7716), 117–121. https://doi.org/10.1038/s41586-018-0340-7

Noordermeer, S. M., & Van Attikum, H. (2019). PARP Inhibitor Resistance: A Tug-of-War in BRCA-Mutated Cells. *Trends in Cell Biology*, *29*(10), 820–834. https://doi.org/10.1016/j.tcb.2019.07.008

Nowsheen, S., Cooper, T., Bonner, J. A., LoBuglio, A. F., & Yang, E. S. (2012). HER2 overexpression renders human breast cancers sensitive to PARP inhibition independently of any defect in homologous recombination DNA repair. *Cancer Research*, *72*(18), 4796–4806. https://doi.org/10.1158/0008-5472.CAN-12-1287.HER2

Oikawa, A., Tohda, H., Kanai, M., Miwa, M., & Sugimura, T. (1980). Inhibitors of poly(adenosine diphosphate ribose) polymerase induce sister chromatid exchanges. *Biochemical and Biophysical Research Communications*, *97*(4), 1311–1316.

Okano, S., Lan, L., Caldecott, K. W., Mori, T., & Yasui, A. (2003). Spatial and Temporal Cellular Responses to Single-Strand Breaks in Human Cells. *Molecular and Cellular Biology*, *23*(15), 5472–5472. https://doi.org/10.1128/mcb.23.15.5472.2003

Otake, H., Miwa, M., Fujimura, S., & Sugimura, T. (1969). Binding of ADP-ribose polymer with histone. *Journal of Biochemistry*, *65*(1), 145–146.

Ozaki, Y., Matsui, H., Asou, H., Nagamachi, A., Aki, D., Honda, H., Yasunaga, S., Takihara, Y., Yamamoto, T., Izumi, S., Ohsugi, M., & Inaba, T. (2012). Poly-ADP Ribosylation of Miki by tankyrase-1 Promotes Centrosome Maturation. *Molecular Cell*, *47*(5), 694–706. https://doi.org/10.1016/j.molcel.2012.06.033

Pachkowski, B. F., Tano, K., Afonin, V., Elder, R. H., Takeda, S., Watanabe, M., Swenberg, H. A., & Nakamura, J. (2009). Cells deficient in PARP1 show an accelerated accumulation of DNA single strand breaks, but not AP sites, over the PARP1- proficient cells exposed to MMS. *Mutation Research*, *671*(1–2), 93–99. https://doi.org/10.1016/j.mrfmmm.2009.09.006.Cells

Pan, J., Fauzee, N. J. S., Wang, Y.-L., Sheng, Y.-T., Tang, Y., Wang, J.-Q., Wu, W.-Q., Yan, J.-X., & Xu, J. (2012). Effect of silencing PARG in human colon carcinoma LoVo cells on the ability of HUVEC migration and proliferation. *Cancer Gene Therapy*, *19*(10), 715–722. https://doi.org/10.1038/cgt.2012.48

Park, J. S., Burckhardt, C. J., Lazcano, R., Solis, L. M., Isogai, T., Li, L., Chen, C. S., Gao, B., Minna, J. D., Bachoo, R., DeBerardinis, R. J., & Danuser, G. (2020). Mechanical regulation of glycolysis via cytoskeleton architecture. *Nature*, *578*(7796), 621–626. https://doi.org/10.1038/s41586-020-1998-1

Park, S. B., Hwang, K. T., Chung, C. K., Roy, D., & Yoo, C. (2020). Causal Bayesian gene networks associated with bone, brain and lung metastasis of breast cancer. *Clinical and Experimental Metastasis*, *37*(6), 657–674. https://doi.org/10.1007/s10585-020-10060-0

Parker, J. S., Mullins, M., Cheung, M. C. U., Leung, S., Voduc, D., Vickery, T., Davies, S., Fauron, C., He, X., Hu, Z., Quackenhush, J. F., Stijleman, I. J., Palazzo, J., Marron, J. S., Nobel, A. B., Mardis, E., Nielsen, T. O., Ellis, M. J., Perou, C. M., & Bernard, P. S. (2009). Supervised Risk Predictor of Breast Cancer Based on Intrinsic Subtypes. *Journal of Clinical Oncology*, *27*(8), 1160–1167. https://doi.org/10.1200/JCO.2008.18.1370

Parra, J. G. (2012). PARP1 expression in breast cancer and effects of its inhibition in preclinical models. *Dissertation, Universitat Pompey Fabra*.

Pazzaglia, S., & Pioli, C. (2020). Multifaceted role of parp-1 in dna repair and inflammation: Pathological and therapeutic implications in cancer and non-cancer diseases. *Cells*, *9*(1). https://doi.org/10.3390/cells9010041

Pello, O. M., De Pizzol, M., Mirolo, M., Soucek, L., Zammataro, L., Amabile, A., Doni, A., Nebuloni, M., Swigart, L. B., Evan, G. I., Mantovani, A., & Locati, M. (2012). Role of c-MYC in alternative activation of human macrophages and tumor-associated macrophage biology. *Blood*, *119*(2), 411–421. https://doi.org/10.1182/blood-2011-02-339911

Perou, C. M., Sorlie, T., Eisen, M. B., Rijn, M. Van De, Jeffrey, S. S., Rees, C. A., Pollack, J. R., Ross, D. T., Johnsen, H., Akslen, L. A., Fluge, I., Pergamenschikov, A., Williams, C., Zhu, S. X., Lonning, P. E., Borresen-Dale, A., Brown, P. O., & Botstein, D. (2000). Molecular Portraits of Human Breast Tumours. *Nature*, *406*(6797), 747–752. www.stanford.edu/molecularportraits/

Petermann, E., Orta, M. L., Issaeva, N., Schultz, N., & Helleday, T. (2010). Hydroxyurea-Stalled Replication Forks Become Progressively Inactivated and Require Two Different RAD51-Mediated Pathways for Restart and Repair. *Molecular Cell*, *37*(4), 492–502. https://doi.org/10.1016/j.molcel.2010.01.021

Pettitt, S. J., Krastev, D. B., Brandsma, I., Dréan, A., Song, F., Aleksandrov, R., Harrell, M. I., Menon, M., Brough, R., Campbell, J., Frankum, J., Ranes, M., Pemberton, H. N., Rafiq, R., Fenwick, K., Swain, A., Guettler, S., Lee, J.-M., Swisher, E. M., … Lord, C. J. (2018). Genome-wide and high-density CRISPR-Cas9 screens identify point mutations in PARP1 causing PARP inhibitor resistance. *Nature Communications*, *9*(1). https://doi.org/10.1038/s41467-018-03917-2

Pfeifer, C. R., Xia, Y., Zhu, K., Liu, D., Irianto, J., Morales García, V. M., Santiago Millán, L. M., Niese, B., Harding, S., Deviri, D., Greenberg, R. A., & Discher, D. E. (2018). Constricted migration increases DNA damage and independently represses cell cycle. *Molecular Biology of the Cell*, *29*(16), 1948–1962. https://doi.org/10.1091/mbc.E18-02-0079

Pillay, N., Tighe, A., Nelson, L., Littler, S., Coulson-Gilmer, C., Bah, N., Golder, A., Bakker, B., Spierings, D. C. J., James, D. I., Smith, K. M., Jordan, A. M., Morgan, R. D., Ogilvie, D. J., Foijer, F., Jackson, D. A., & Taylor, S. S. (2019). DNA Replication Vulnerabilities Render Ovarian Cancer Cells Sensitive to Poly(ADP-Ribose) Glycohydrolase Inhibitors. *Cancer Cell*, *35*(3), 519-533.e8. https://doi.org/10.1016/j.ccell.2019.02.004

Pines, A., Vrouwe, M. G., Marteijn, J. A., Typas, D., Luijsterburg, M. S., Cansoy, M., Hensbergen, P., Deelder, A., de Groot, A., Matsumoto, S., Sugasawa, K., Thoma, N., Vermeulen, W., Vrieling, H., & Mullenders, L. (2012). PARP1 promotes nucleotide excision repair through DDB2 stabilization and recruitment of ALC1. *Journal of Cell Biology*, *199*(2), 235–249. https://doi.org/10.1083/jcb.201112132

Piskunova, T. S., Yurova, M. N., Ovsyannikov, A. I., Semenchenko, A. V., Zabezhinski, M. A., Popovich, I. G., Wang, Z.-Q., & Anisimov, V. N. (2008). Deficiency in Poly(ADP-ribose) Polymerase-1 (PARP-1) Accelerates Aging and Spontaneous Carcinogenesis in Mice. *Current Gerontology and Geriatrics Research*. https://doi.org/10.1155/2008/754190

Plasilova, M. L., Hasyse, B., Killelea, B. K., Horowitz, N. R., Chag[ar, A. B., & Lannin, D. R. (2016). Features of Triple Negative Breast Cancer. *Medicine*, *95*(35). https://doi.org/10.37015/audt.2018.180005

Poirier, G. G., Murciat, G. D. E., Jongstra-bilent, J., & Niedergangt, C. (1982). Poly(ADP-ribosyl)ation of polynucleosomes causes relaxation of chromatin structure. *Proceedings*

of the National Academy of Sciences of the United States of America, *79*(June), 3423–3427. https://doi.org/10.1073/pnas.79.11.3423

Polo, L. M., Xu, Y., Hornyak, P., Caldecott, K. W., Oliver, A. W., Pearl, L. H., Polo, L. M., Xu, Y., Hornyak, P., Garces, F., Zeng, Z., & Hailstone, R. (2019). Efficient Single-Strand Break Repair Requires Binding to Both Poly (ADP-Ribose) and DNA by the Central BRCT Domain of XRCC1 Report Efficient Single-Strand Break Repair Requires Binding to Both Poly (ADP-Ribose) and DNA by the Central BRCT Domain of XR. *Cell Reports*, *26*(3), 573–581. https://doi.org/10.1016/j.celrep.2018.12.082

Prat, A., Pineda, E., Adamo, B., Galván, P., Fernández, A., Gaba, L., Díez, M., Viladot, M., Arance, A., & Muñoz, M. (2015). Clinical Implications of the Intrinsic Molecular Subtypes of Breast Cancer. *Breast*, *24*, S26–S35. https://doi.org/10.1016/j.breast.2015.07.008

Pu, H., Horbinski, C., Hensley, P. J., Matuszak, E. A., Atkinson, T., & Kyprianou, N. (2014). PARP-1 regulates epithelial-mesenchymal transition (EMT) in prostate tumorigenesis. *Carcinogenesis*, *35*(11), 2592–2601. https://doi.org/10.1093/carcin/bgu183

Quiñonero, F., Mesas, C., Muñoz-Gámez, J. A., Jiménez-Luna, C., Perazzoli, G., Prados, J., Melguizo, C., & Ortiz, R. (2022). PARP1 inhibition by Olaparib reduces the lethality of pancreatic cancer cells and increases their sensitivity to Gemcitabine. *Biomedicine and Pharmacotherapy*, *155*(August). https://doi.org/10.1016/j.biopha.2022.113669

Raj-Kumar, P. K., Liu, J., Hooke, J. A., Kovatich, A. J., Kvecher, L., Shriver, C. D., & Hu, H. (2019). PCA-PAM50 improves consistency between breast cancer intrinsic and clinical subtyping reclassifying a subset of luminal A tumors as luminal B. *Scientific Reports*, *9*(1), 1–13. https://doi.org/10.1038/s41598-019-44339-4

Raval-Fernandes, S. (2005). Increased Susceptibility of Vault Poly(ADP-Ribose) Polymerase-Deficient Mice to Carcinogen-Induced Tumorigenesis. *Cancer Research*, *65*(19), 8846–8852. https://doi.org/10.1158/0008-5472.can-05-0770

Ray Chaudhuri, A., Ahuja, A. K., Herrador, R., & Lopes, M. (2015). Poly(ADP-Ribosyl) Glycohydrolase Prevents the Accumulation of Unusual Replication Structures during Unperturbed S Phase. *Molecular and Cellular Biology*, *35*(5), 856–865. https://doi.org/10.1128/mcb.01077-14

Ray Chaudhuri, A., Hashimoto, Y., Herrador, R., Neelsen, K. J., Fachinetti, D., Bermejo, R., Cocito, A., Costanzo, V., & Lopes, M. (2012). Topoisomerase I poisoning results in PARP-mediated replication fork reversal. *Nature Structural and Molecular Biology*, *19*(4), 417–423. https://doi.org/10.1038/nsmb.2258

Ray Chaudhuri, A., & Nussenzweig, A. (2017). The multifaceted roles of PARP1 in DNA repair and chromatin remodelling. *Nature Reviews Molecular Cell Biology*, *18*(10), 610–621. https://doi.org/10.1038/nrm.2017.53

Reber, J. M., Božić-Petković, J., Lippmann, M., Mazzardo, M., Dilger, A., Warmers, R., Bürkle, A., & Mangerich, A. (2022). PARP1 and XRCC1 exhibit a reciprocal relationship in genotoxic stress response. *Cell Biology and Toxicology*, *39*(1), 345–364. https://doi.org/10.1007/s10565-022-09739-9

Rein, I. D., Landsverk, K. S., Micci, F., Patzke, S., Stokke, T., Dale, I., Landsverk, K. S., Micci, F., Patzke, S., Rein, I. D., Landsverk, K. S., Micci, F., Patzke, S., & Stokke, T. (2015). Replication-induced DNA damage after PARP Replication-induced DNA damage after PARP inhibition causes G 2 delay , and cell line-dependent apoptosis , necrosis and multinucleation. *Cell Cycle*, *14*(20), 3248–3260. https://doi.org/10.1080/15384101.2015.1085137

Reynolds, P., Cooper, S., Lomax, M., & O'Neill, P. (2015). Disruption of PARP1 function inhibits base excision repair of a sub-set of DNA lesions. *Nucleic Acids Research*, *43*(8), 4028–4038. https://doi.org/10.1093/nar/gkv250

Richard, I. A., Burgess, J. T., O'Byrne, K. J., & Bolderson, E. (2022). Beyond PARP1: The Potential of Other Members of the Poly (ADP-Ribose) Polymerase Family in DNA Repair and Cancer Therapeutics. *Frontiers in Cell and Developmental Biology*, *9*(January), 1–11. https://doi.org/10.3389/fcell.2021.801200

Robert, I., Dantzer, F., & Reina-San-Martin, B. (2009). Parp1 facilitates alternative NHEJ, whereas Parp2 suppresses IgH/c-myc translocations during immunoglobulin class switch recombination. *Journal of Experimental Medicine*, *206*(5), 1047–1056. https://doi.org/10.1084/jem.20082468

Robu, M., Shah, R. G., Petitclerc, N., Brind'amour, J., Kandan-Kulangara, F., & Shah, G. M. (2013). Role of poly(ADP-ribose) polymerase-1 in the removal of UV-induced DNA lesions by nucleotide excision repair. *Proceedings of the National Academy of Sciences of the United States of America*, *110*(5), 1658–1663. https://doi.org/10.1073/pnas.1209507110

Rodriguez-Tirado, C., Kale, N., Carlini, M. J., Shrivastava, N., Rodrigues, A. A., Khalil, B. D., Bravo-Cordero, J. J., Hong, Y., Alexander, M., Ji, J., Behbod, F., & Sosa, M. S. (2022). NR2F1 Is a Barrier to Dissemination of Early-Stage Breast Cancer Cells. *Cancer Research*, *82*(12), 2313–2326. https://doi.org/10.1158/0008-5472.CAN-21-4145

Rodríguez-Vargas, J. M., Oliver-Pozo, F. J., & Dantzer, F. (2019). PARP1 and Poly(ADP-ribosyl)ation Signaling during Autophagy in Response to Nutrient Deprivation. *Oxidative Medicine and Cellular Longevity*, *2019*, 1–15. https://doi.org/10.1155/2019/2641712

Rolli, V., O'Farrell, M., Ménissier-De Murcia, J., & De Murcia, G. (1997). Random Mutagenesis of the Poly(ADP-ribose) Polymerase Catalytic Domain Reveals Amino Acids Involved in Polymer Branching †. *Biochemistry*, *36*(40), 12147–12154. https://doi.org/10.1021/bi971055p

Rom, S., Zuluaga-Ramirez, V., Reichenbach, N. L., Dykstra, H., Gajghate, S., Pacher, P., & Persidsky, Y. (2016). PARP inhibition in leukocytes diminishes inflammation via effects on integrins/cytoskeleton and protects the blood-brain barrier. *Journal of Neuroinflammation*, *13*(1), 1–16. https://doi.org/10.1186/s12974-016-0729-x

Rondinelli, B., Gogola, E., Yücel, H., Duarte, A. A., Van De Ven, M., Van Der Sluijs, R., Konstantinopoulos, P. A., Jonkers, J., Ceccaldi, R., Rottenberg, S., & D'Andrea, A. D. (2017). EZH2 promotes degradation of stalled replication forks by recruiting MUS81 through histone H3 trimethylation. *Nature Cell Biology*, *19*(11), 1371–1378. https://doi.org/10.1038/ncb3626

Ronson, G. E., Piberger, A. L., Higgs, M. R., Olsen, A. L., Stewart, G. S., McHugh, P. J., Petermann, E., & Lakin, N. D. (2018). PARP1 and PARP2 stabilise replication forks at base excision repair intermediates through Fbh1-dependent Rad51 regulation. *Nature Communications*, *9*(746). https://doi.org/10.1038/s41467-018-03159-2

Rosado, M. M., Bennici, E., Novelli, F., & Pioli, C. (2013). Beyond DNA repair, the immunological role of PARP-1 and its siblings. *Immunology*, *139*(4), 428–437. https://doi.org/10.1111/imm.12099

Rottenberg, S., Jaspers, J. E., Kersbergen, A., Van Der Burg, E., Nygren, A. O. H., Zander, S. A. L., Derksen, P. W. B., De Bruin, M., Zevenhoven, J., Lau, A., Boulter, R., Cranston, A., O'Connor, M. J., Martin, N. M. B., Borst, P., & Jonkers, J. (2008). High sensitivity of BRCA1-deficient mammary tumors to the PARP inhibitor AZD2281 alone and in combination with platinum drugs. *Proceedings of the National Academy of*

Sciences, *105*(44), 17079–17084. https://doi.org/10.1073/pnas.0806092105

Rouleau, M., McDonald, D., Gagné, P., Ouellet, M. E., Droit, A., Hunter, J. M., Dutertre, S., Prigent, C., Hendzel, M. J., & Poirier, G. G. (2007). PARP-3 associates with polycomb group bodies and with components of the DNA damage repair machinery. *Journal of Cellular Biochemistry*, *100*(2), 385–401. https://doi.org/10.1002/jcb.21051

Roy, S., Liu, F., & Arav-boger, R. (2016). Human Cytomegalovirus Inhibits the PARsylation Activity of Tankyrase — A Potential Strategy for Suppression of the Wnt Pathway. *Viruses*, *8*(1), 8. https://doi.org/10.3390/v8010008

Ruf, A., Rolli, Â., Murcia, G. De, Schulz, G. E., Breisgau, F., & Supe, E. (1998). The Mechanism of the Elongation and Branching Reaction of Poly (ADP-ribose) Polymerase as Derived From Crystal Structures and Mutagenesis. *Journal of Molecular Biology*, *278*, 57–65.

Rulten, S. L., Cortes-ledesma, F., Guo, L., Iles, N. J., & Caldecott, K. W. (2008). APLF (C2orf13) Is a Novel Component of Poly (ADP- Ribose) Signaling in Mammalian Cells APLF (C2orf13) Is a Novel Component of Poly (ADP-Ribose) Signaling in Mammalian Cells □. *Molecular and Cellular Biologyl*, *28*(14), 4620–4628. https://doi.org/10.1128/MCB.02243-07

Rulten, S. L., Fisher, A. E. O., Robert, I., Zuma, M. C., Rouleau, M., Ju, L., Poirier, G., Reina-san-martin, B., & Caldecott, K. W. (2011). PARP-3 and APLF Function Together to Accelerate Nonhomologous End-Joining. *Molecular Cell*, *41*(1), 33–45. https://doi.org/10.1016/j.molcel.2010.12.006

Sadler, J. B. A., Lamb, C. A., Cassie, R. W., Adamson, I. S., Dimitrios, K., Chi, N., Gould, G. W., & Bryant, N. J. (2019). The deubiquitinating enzyme USP25 binds tankyrase and regulates trafficking of the facilitative glucose transporter GLUT4 in adipocytes. *Scientific Reports*, *February*, 1–7. https://doi.org/10.1038/s41598-019-40596-5

Sahu, S., Sridhar, D., Abnave, P., Kosaka, N., Dattani, A., Thompson, J. M., Hill, M. A., & Aboobaker, A. (2021). Ongoing repair of migration-coupled dna damage allows planarian adult stem cells to reach wound sites. *ELife*, *10*, 1–20. https://doi.org/10.7554/ELIFE.63779

Saleh-gohari, N., Bryant, H. E., Schultz, N., Parker, K. M., Cassel, T. N., Helleday, T., Bryant, H. E., Schultz, N., Saleh-gohari, N., Bryant, H. E., Schultz, N., Parker, K. M., Cassel, T. N., & Helleday, T. (2005). Spontaneous Homologous Recombination Is Induced by Collapsed Replication Forks That Are Caused by Endogenous DNA Single-Strand Breaks Spontaneous Homologous Recombination Is Induced by Collapsed Replication Forks That Are Caused by Endogenous DNA Single-S. *Molecular and Cellular Biology*, *25*(16), 7158–7169. https://doi.org/10.1128/MCB.25.16.7158-7169.2005

Sasaki, Y., Fujimori, H., Hozumi, M., Onodera, T., Nozaki, T., Murakami, Y., Ashizawa, K., Inoue, K., Koizumi, F., & Masutani, M. (2019). Dysfunction of poly(ADP-ribose) glycohydrolase induces a synthetic lethal effect in dual specificity phosphatase 22-deficient lung cancer cells. *Cancer Research*, canres.1037.201. https://doi.org/10.1158/0008-5472.can-18-1037

Satoh, M. S., & Lindahl, T. (1992). Role of poly(ADP-ribose) formation in DNA repair. *Nature*, *356*(6367), 356–358. https://doi.org/10.1038/356356a0

Saxena, A, Saffery, R., Wong, L. H., Kalitsis, P., & Choo, K. H. A. (2002). *Centromere Proteins Cenpa, Cenpb, and Bub3 Interact with Poly(ADP-ribose) Polymerase-1 Protein and Are Poly(ADP-ribosyl)ated*. *277*(30), 26921–26926. https://doi.org/10.1074/jbc.m200620200

Saxena, Alka, Saffery, R., Wong, L. H., Kalitsis, P., & Choo, K. H. A. (2002). Centromere Proteins Cenpa , Cenpb , and Bub3 Interact with Poly (ADP-ribose) Polymerase-1 Protein and Are Poly (ADP-ribosyl) ated *. *Journal of Biological Chemistry*, *277*(30), 26921–26926. https://doi.org/10.1074/jbc.M200620200

Schleicher, E. M., Galvan, A. M., Imamura-Kawasawa, Y., Moldovan, G.-L., & Nicolae, C. M. (2018). PARP10 promotes cellular proliferation and tumorigenesis by alleviating replication stress. *Nucleic Acids Research*, *46*(17), 8908–8916. https://doi.org/10.1093/nar/gky658

Schoen, I., Aires, L., Ries, J., & Vogel, V. (2017). Nanoscale invaginations of the nuclear envelope: Shedding new light on wormholes with elusive function. *Nucleus*, *8*(5), 506–514. https://doi.org/10.1080/19491034.2017.1337621

Schultz, N., Lopez, E., Saleh-gohari, N., & Helleday, T. (2003). Poly (ADP-ribose) polymerase (PARP-1) has a controlling role in homologous recombination. *Nucleic Acids Research*, *31*(17), 4959–4964. https://doi.org/10.1093/nar/gkg703

Schweiker, S. S., Tauber, A. L., Sherry, M. E., & Levonis, S. M. (2018). Structure, Function and Inhibition of Poly(ADP-ribose)polymerase, Member 14 (PARP14). *Mini-Reviews in Medicinal Chemistry*, *18*(19), 1659–1669. https://doi.org/10.2174/1389557518666180816111749

Sfeir, Agnel J, de Lange, T. (2012). Removal of Shelterin Revelas the Telomere End-Replication Problem. *Science*, *336*(6081), 593–597. https://doi.org/10.1126/science.1218498.Removal

Shah, P., Hobson, C. M., Cheng, S., Colville, M. J., Paszek, M. J., Superfine, R., & Lammerding, J. (2021). Nuclear Deformation Causes DNA Damage by Increasing Replication Stress. *Current Biology*, *31*(4), 753-765.e6. https://doi.org/10.1016/j.cub.2020.11.037

Shah, P., Wolf, K., & Lammerding, J. (2017). Bursting the bubble – nuclear envelope rupture as a path to genomic instability? *Trends in Cell Biologys*, *27*(8), 546–555. https://doi.org/10.1053/j.gastro.2016.08.014.CagY

Shamloo, B., Kumar, N., Owen, R. H., Reemmer, J., Ost, J., Serene Perkins, R., & Shen, H. Y. (2019). Dysregulation of adenosine kinase isoforms in breast cancer. *Oncotarget*, *10*(68), 7238–7250. https://doi.org/10.18632/oncotarget.27364

Shan, L., Li, X., Liu, L., Ding, X., Wang, Q., Zheng, Y., Duan, Y., Xuan, C., Wang, Y., Yang, F., Shang, Y., & Shi, L. (2014). GATA3 cooperates with PARP1 to regulate CCND1 transcription through modulating histone H1 incorporation. *Oncogene*, *33*(24), 3205–3216. https://doi.org/10.1038/onc.2013.270

Shebzukhov, Y. V, Lavrik, I. N., Karbach, J., Khlgatian, S. V, Koroleva, E. P., Belousov, P. V, Kashkin, K. N., Knuth, A., Jager, E., Dmitry, N. C., & Sergei, V. K. (2008). Human tankyrases are aberrantly expressed in colon tumors and contain multiple epitopes that induce humoral and cellular immune responses in cancer patients. *Cancer Immunology, Immunotherapy*, *57*(8), 871–881. https://doi.org/10.1007/s00262-007-0423-z

Sherman, B. T., Hao, M., Qiu, J., Jiao, X., Baseler, M. W., Lane, H. C., Imamichi, T., & Chang, W. (2022). DAVID : a web server for functional enrichment analysis and functional annotation of gene lists (2021 update). *Nucleic Acids Research*, *50*(March), 216–221.

Shibata, A., Maeda, D., Ogino, H., Tsutsumi, M., Nohmi, T., Nakagama, H., Sugimura, T., Teraoka, H., & Masutani, M. (2009). *Role of Parp-1 in suppressing spontaneous*

deletion mutation in the liver and brain of mice at adolescence and advanced age. *664*(1–2), 20–27. https://doi.org/10.1016/j.mrfmmm.2009.02.001

Shieh, W. M., Amé, J. C., Wilson, M. V., Wang, Z. Q., Koh, D. W., Jacobson, M. K., & Jacobson, E. L. (1998). Poly(ADP-ribose) polymerase null mouse cells synthesize ADP-ribose polymers. *Journal of Biological Chemistry*, *273*(46), 30069–30072. https://doi.org/10.1074/jbc.273.46.30069

Shimokawa, T., Masutani, M., Nozaki, T., Nakagama, H., Araki, S., Aoki, Y., & Sugimura, T. (1998). The human poly(ADP-ribose) glycohydrolase maps to chromosome 10q11.23-21.1 by fluorescence in situ hybridization. *Human Cell*, *11*(4), 243–246.

Shirai, H, Poetsch, A. R., Gunji, A., Maeda, D., Fujimori, H., Fujihara, H., Yoshida, T., Ogino, H., & Masutani, M. (2013). PARG dysfunction enhances DNA double strand break formation in S-phase after alkylation DNA damage and augments different cell death pathways. *Cell Death & Disease*, *4*(6), e656. https://doi.org/10.1038/cddis.2013.133

Shirai, Hidenori, Fujimori, H., Gunji, A., Maeda, D., Hirai, T., Poetsch, A. R., Harada, H., Yoshida, T., Sasai, K., Okayasu, R., & Masutani, M. (2013). Parg deficiency confers radio-sensitization through enhanced cell death in mouse ES cells exposed to various forms of ionizing radiation. *Biochemical and Biophysical Research Communications*, *435*(1), 100–106. https://doi.org/10.1016/j.bbrc.2013.04.048

Shiu, J., Wu, C., Chang, S., Sun, Y., Chen, Y., Lai, C., Chiu, W., Chang, W., Myung, K., Su, W., & Liaw, H. (2020). The HLTF – PARP1 interaction in the progression and stability of damaged replication forks caused by methyl methanesulfonate. *Oncogenesis*, *9*(104). https://doi.org/10.1038/s41389-020-00289-5

Simanov, G., Dang, I., Fokin, A. I., Oguievetskaia, K., Cherfils, J., & Gautreau, A. M. (2021). Arpin Regulates Migration Persistence by Interacting with Both Tankyrases and the Arp2 / 3 Complex. *International Journal of Molecular Sciences*, *22*(8).

Simbulan-Rosenthal, C. M., Rosenthal, D. S., Luo, R. B., Samara, R., Espinoza, L. A., Hassa, P. O., Hottiger, M. O., & Smulson, M. E. (2003). PARP-1 binds E2F-1 independently of its DNA binding and catalytic domains, and acts as a novel coactivator of E2F-1-mediated transcription during re-entry of quiescent cells into S phase. *Oncogene*, *22*(52), 8460–8471. https://doi.org/10.1038/sj.onc.1206897

Simbulan-Rosenthal, C. M., Rosenthal, D. S., Luo, R. B., & Smulson, M. E. (1999). Poly(ADP-ribose) polymerase upregulates E2F-1 promoter activity and DNA pol α expression during early S phase. *Oncogene*, *18*(36), 5015–5023. https://doi.org/10.1038/sj.onc.1202900

Simoneau, A., Xiong, R., & Zou, L. (2021). The trans cell cycle effects of PARP inhibitors underlie their selectivity toward BRCA1 / 2-deficient cells. *Genes & Developments*, *35*(17–18), 1271–1289. https://doi.org/10.1101/gad.348479.121.2013

Slama, J. T., Aboul-Ela, N., Goli, D. M., Cheesman, B. V, Simmons, A. M., & Jacobson, M. K. (1995). *Specific Inhibition of Poly(ADP-ribose) Glycohydrolase by Adenosine Diphosphate (Hydroxymethyl)pyrrolidinediol*. *38*(2), 389–393. https://doi.org/10.1021/jm00002a021

Slatterys, E., Dignamg, D., Matsuit, T., & Roederjl, R. G. (1983). Purification and Analysis of a Factor Which Suppresses Nick-induced Transcription by RNA Polymerase I1 and Its Identity with Poly(ADP-ribose) Polymerase*. *The Journal of Biological Chemistry*, *258*(9), 5955–5959. https://doi.org/10.1016/S0021-9258(20)81989-9

Smith, S. (2015). TIPs: Tankyrase Interacting Proteins. In *PARP Inhibitors for Cancer Therapy* (pp. 79–97).

Spano, D., Heck, C., De Antonellis, P., Christofori, G., & Zollo, M. (2012). Molecular networks that regulate cancer metastasis. *Seminars in Cancer Biology*, *22*(3), 234–249. https://doi.org/10.1016/j.semcancer.2012.03.006

Stakheev, D., Taborska, P., Strizova, Z., Podrazil, M., & Bartunkova, J. (2019). The WNT / β -catenin signaling inhibitor XAV939 enhances the elimination of LNCaP and PC-3 prostate cancer cells by prostate cancer patient lymphocytes in vitro. *Scientific Reports*, *9*(4761). https://doi.org/10.1038/s41598-019-41182-5

Stein, L. R., & Imai, S.-I. (2012). The dynamic regulation of NAD metabolism in mitochondria. *Trends in Endocrinology & Metabolism*, *23*(9), 420–428. https://doi.org/10.1016/j.tem.2012.06.005

Stephens, A. D., Liu, P. Z., Banigan, E. J., Almassalha, L. M., Backman, V., Adam, S. A., Goldman, R. D., & Marko, J. F. (2018). Chromatin histone modifications and rigidity affect nuclear morphology independent of lamins. *Molecular Biology of the Cell*, *29*(2), 220–233. https://doi.org/10.1091/mbc.E17-06-0410

Stratford, E. W., Daffinrud, J., Munthe, E., Castro, R., Waaler, J., Krauss, S., & Myklebost, O. (2013). The tankyrase-specific inhibitor JW74 affects cell cycle progression and induces apoptosis and differentiation inosteosarcoma cell lines. *Cancer Medicine*. https://doi.org/10.1002/cam4.170

Ström, C. E., Johansson, F., Uhlén, M., Szigyarto, C. A. K., Erixon, K., & Helleday, T. (2011). Poly (ADP-ribose) polymerase (PARP) is not involved in base excision repair but PARP inhibition traps a single-strand intermediate. *Nucleic Acids Research*, *39*(8), 3166–3175. https://doi.org/10.1093/nar/gkq1241

Su, Z., Deshpande, V., James, D. E., & Stöckli, J. (2018). Tankyrase modulates insulin sensitivity in skeletal muscle cells by regulating the stability of GLUT4 vesicle proteins. *Journal of Biological Chemistry*, *293*(27), 8578–8587. https://doi.org/10.1074/jbc.RA117.001058

Sugimura, K., Takebayashi, S. I., Taguchi, H., Takeda, S., & Okumura, K. (2008). PARP-1 ensures regulation of replication fork progression by homologous recombination on damaged DNA. *Journal of Cell Biology*, *183*(7), 1203–1212. https://doi.org/10.1083/jcb.200806068

Sung, H., Ferlay, J., Siegel, R. L., Laversanne, M., Soerjomataram, I., Jemal, A., & Bray, F. (2021). Global Cancer Statistics 2020: GLOBOCAN Estimates of Incidence and Mortality Worldwide for 36 Cancers in 185 Countries. *CA: A Cancer Journal for Clinicians*, *71*(3), 209–249. https://doi.org/10.3322/caac.21660

Szántó, M., Brunyánszki, A., Kiss, B., Nagy, L., Gergely, P., Virág, L., & Bai, P. (2012). Poly(ADP-ribose) polymerase-2: emerging transcriptional roles of a DNA-repair protein. *Cellular and Molecular Life Sciences*, *69*(24), 4079–4092. https://doi.org/10.1007/s00018-012-1003-8

Szántó, M., Brunyánszki, A., Márton, J., Vámosi, G., Nagy, L., Fodor, T., Kiss, B., Virág, L., Gergely, P., & Bai, P. (2014). Deletion of PARP-2 induces hepatic cholesterol accumulation and decrease in HDL levels. *Biochimica et Biophysica Acta - Molecular Basis of Disease*, *1842*(4), 594–602. https://doi.org/10.1016/j.bbadis.2013.12.006

Taglialatela, A., Alvarez, S., Leuzzi, G., Sannino, V., Ranjha, L., Huang, J. W., Madubata, C., Anand, R., Levy, B., Rabadan, R., Cejka, P., Costanzo, V., & Ciccia, A. (2017). Restoration of Replication Fork Stability in BRCA1- and BRCA2-Deficient Cells by Inactivation of SNF2-Family Fork Remodelers. *Molecular Cell*, *68*(2), 414-430.e8. https://doi.org/10.1016/j.molcel.2017.09.036

Tang, X., Zhang, H., Long, Y., Hua, H., Jiang, Y., & Jing, J. (2018). PARP9 is overexpressed in human breast cancer and promotes cancer cell migration. *Oncology Letters*, *16*, 4073–4077. https://doi.org/10.3892/ol.2018.9124

Taniguchi, T. (1987). Reaction mechanism for automodification of poly(ADP-ribose) synthetase. *Biochemical and Biophysical Research Communications*, *147*(3), 1008–1012. https://doi.org/10.1016/S0006-291X(87)80170-5

Tatsuka, M. (2012). PARP6, a mono(ADP-ribosyl) transferase and a negative regulator of cell proliferation, is involved in colorectal cancer development. *INTERNATIONAL JOURNAL OF GYNECOLOGICAL CANCER*, *41*, 2079–2086. https://doi.org/10.3892/ijo.2012.1652

Taylor, R. M., Thistlethwaite, A., & Caldecott, K. W. (2002). Central Role for the XRCC1 BRCT I Domain in Mammalian DNA Single-Strand Break Repair Central Role for the XRCC1 BRCT I Domain in Mammalian DNA Single-Strand Break Repair. *Molecular and Cellular Biology*, *22*(8), 2556–2563. https://doi.org/10.1128/MCB.22.8.2556

Teloni, F., & Altmeyer, M. (2016). Readers of poly(ADP-ribose): Designed to be fit for purpose. *Nucleic Acids Research*, *44*(3), 993–1006. https://doi.org/10.1093/nar/gkv1383

Tentori, L., Leonetti, C., Scarsella, M., Muzi, A., Vergati, M., Forini, O., Lacal, P. M., Ruffini, F., Gold, B., Li, W., Zhang, J., & Graziani, G. (2005). Poly(ADP-ribose) glycohydrolase inhibitor as chemosensitiser of malignant melanoma for temozolomide. *European Journal of Cancer*, *41*(18), 2948–2957. https://doi.org/10.1016/j.ejca.2005.08.027

Ter Brugge, P., Kristel, P., Van Der Burg, E., Boon, U., De Maaker, M., Lips, E., Mulder, L., De Ruiter, J., Moutinho, C., Gevensleben, H., Marangoni, E., Majewski, I., Jóźwiak, K., Kloosterman, W., Van Roosmalen, M., Duran, K., Hogervorst, F., Turner, N., Esteller, M., … Jonkers, J. (2016). Mechanisms of Therapy Resistance in Patient-Derived Xenograft Models of BRCA1-Deficient Breast Cancer. *Journal of National Cancer Institute*, *108*(11), djw148. https://doi.org/10.1093/jnci/djw148

Thomas, P. D., & Mushayahama, T. (2022). PANTHER : Making genome-scale phylogenetics accessible to all. *Protein Society*, *31*(1), 8–22. https://doi.org/10.1002/pro.4218

Tian, Xiao-hong, Hou, W., Fang, Y., Fan, J., Tong, H., Bai, S., Chen, Q., Xu, H., & Li, Y. (2013). XAV939, a tankyrase 1 inhibitior, promotes cell apoptosis in neuroblastoma cell lines by inhibiting Wnt / β -catenin signaling pathway. *Journal of Experimental & Clinical Cancer Research*, 1–9.

Tian, Xiaohong, Hou, W., Bai, S., Fan, J., Tong, H., & Bai, Y. (2014). XAV939 promotes apoptosis in a neuroblastoma cell line via telomere shortening. *Oncology Reports*, *32*(5), 1999–2006. https://doi.org/10.3892/or.2014.3460

Tian, Xiaohong, Hou, W., Bai, S., Fan, J. U. N., Tong, H. A. O., & Xu, H. E. (2014). XAV939 inhibits the stemness and migration of neuroblastoma cancer stem cells via repression of tankyrase 1. *Internation Journal of Oncology*, 121–128. https://doi.org/10.3892/ijo.2014.2406

Todorova, T., Bock, F. J., & Chang, P. (2014). PARP13 regulates cellular mRNA post-transcriptionally and functions as a pro-apoptotic factor by destabilizing TRAILR4 transcript. *Nature Communications*, *5*(1), 5362. https://doi.org/10.1038/ncomms6362

Todorova, T., Bock, F. J., & Chang, P. (2015). Poly(ADP-ribose) polymerase-13 and RNA regulation in immunity and cancer. *Trends in Molecular Medicine*, *21*(6), 373–384. https://doi.org/10.1016/j.molmed.2015.03.002

Tong, W. M., Yang, Y. G., Cao, W. H., Galendo, D., Frappart, L., Shen, Y., & Wang, Z. Q. (2007). Poly (ADP-ribose) polymerase-1 plays a role in suppressing mammary tumourigenesis in mice. *Oncogene*, *26*, 3857–3867. https://doi.org/10.1038/sj.onc.1210156

Troilo, A., Benson, E. K., Esposito, D., Garibsingh, R. A. A., Reddy, E. P., Mungamuri, S. K., & Aaronson, S. A. (2016). Angiomotin stabilization by tankyrase inhibitors antagonizes constitutive TEAD-dependent transcription and proliferation of human tumor cells with Hippo pathway core component mutations. *Oncotarget*, *7*(20), 28765–28782. https://doi.org/10.18632/oncotarget.9117

Tsai, Y. J., Abe, H., Maruta, H., Hatano, T., Nishina, H., Sakagami, H., Okuda, T., & Tanuma, S. I. (1991). Effects of chemically defined tannins on Poly(ADP-ribose) glycohydrolase activity. *Biochemistry International*, *24*(5), 889–897.

Uchiumi, F. (2013). PARP1 gene expression is downregulated by knockdown of PARG gene. *Oncology Reports*, *29*, 1683–1688. https://doi.org/10.3892/or.2013.2321

Vaidyanathan, A., Sawers, L., Gannon, A.-L., Chakravarty, P., Scott, A. L., Bray, S. E., Ferguson, M. J., & Smith, G. (2016). ABCB1 (MDR1) induction defines a common resistance mechanism in paclitaxel- and olaparib-resistant ovarian cancer cells. *British Journal of Cancer*, *115*(4), 431–441. https://doi.org/10.1038/bjc.2016.203

Vaitsiankova, A., Burdova, K., Sobol, M., Gautam, A., Benada, O., Hanzlikova, H., & Caldecott, K. W. (2022). PARP inhibition impedes the maturation of nascent DNA strands during DNA replication. *Nature Structural and Molecular Biology*, *29*(4), 329–338. https://doi.org/10.1038/s41594-022-00747-1

Van Zon, A., Mossink, M. H., Scheper, R. J., Sonneveld, P., & Wiemer, E. A. C. (2003). The vault complex. *Cellular and Molecular Life Sciences (CMLS)*, *60*(9), 1828–1837. https://doi.org/10.1007/s00018-003-3030-y

Verma, A. (2021). Tankyrase inhibitors: emerging and promising therapeutics for cancer treatment. *Medicinal Chemistry Research*, *30*, 50–73. https://doi.org/10.1007/s00044-020-02657-7

Vodenicharov, M. D., Sallmann, F. R., Satoh, M. S., & Poirier, G. G. (2000). Base excision repair is efficient in cells lacking poly(ADP-ribose) polymerase 1. *Nucleic Acids Research*, *28*(20), 3887–3896. https://doi.org/10.1093/nar/28.20.3887

Vyas, S., Matic, I., Uchima, L., Rood, J., Zaja, R., Hay, R. T., Ahel, I., & Chang, P. (2014). Family-wide analysis of poly(ADP-ribose) polymerase activity. *Nature Communications*, *5*(1). https://doi.org/10.1038/ncomms5426

Waaler, J., Mygland, L., Tveita, A., Strand, M. F., Solberg, N. T., Olsen, P. A., Aizenshtadt, A., Fauskanger, M., Lund, K., Brinch, S. A., Lycke, M., Dybing, E., Nygaard, V., Bøe, S. L., Heintz, K., Hovig, E., Hammarström, C., Corthay, A., & Krauss, S. (2020). Tankyrase inhibition sensitizes melanoma to PD-1 immune checkpoint blockade in syngeneic mouse models. *Communications Biology*, *3*(1), 196. https://doi.org/10.1038/s42003-020-0916-2

Wang, D. Y., Jiang, Z., Ben-David, Y., Woodgett, J. R., & Zacksenhaus, E. (2019). Molecular stratification within triple-negative breast cancer subtypes. *Scientific Reports*, *9*(1), 1–10. https://doi.org/10.1038/s41598-019-55710-w

Wang, J., Tang, Y., Li, Q., Xiao, M., Li, M., Sheng, Y., Yang, Y., & Wang, Y. (2019). PARG regulates the proliferation and differentiation of DCs and T�cells via PARP/NF-κB in tumour metastases of colon carcinoma. *Oncology Reports*. https://doi.org/10.3892/or.2019.7051

Wang, W., Li, N., Li, X., Tran, M. K., Han, X., & Chen, J. (2015). Tankyrase Inhibitors Target YAP by Stabilizing Angiomotin Family Proteins. *Cell Reports*, *13*(3), 524–532. https://doi.org/10.1016/j.celrep.2015.09.014

Wang, Y., An, R., Umanah, G. K., Park, H., Eacker, S. M., Kim, B., Bao, L., Harraz, M. M., Chen, R., Wang, J. E., Kam, T., Jeong, J. S., Xie, Z., Neifert, S., Qian, J., Andrabi, S. A., & Blackshaw, S. (2016). A nuclease that mediates cell death induced by DNA damage and poly(ADP-ribose) polymerase-1. *Science*, *354*(6308), 1–29. https://doi.org/10.1126/science.aad6872.A

Wang, Y., Kim, N. S., Haince, J.-F., Kang, H., David, K. K., Andrabi, S. A., Poirier, G. G., Dawson, V. L., & Dawson, T. M. (2011). Poly (ADP-ribose) (PAR) Binding to Apoptosis-Inducing Factor Is Critical For PAR Polymerase-1-Dependent Cell Death (Parthanatos). *Science Signaling*, *4*(167), ra20. https://doi.org/10.1126/scisignal.2000902.Poly

Wang, Z., Guo, M. qi, Cui, Q. ke, Yuan, H., Shan-ji Fu, Liu, B., Xie, F., Qiao, W., Cheng, J., Wang, Y., & Zhang, M. xiang. (2021). PARP1 deficiency protects against hyperglycemia-induced neointimal hyperplasia by upregulating TFPI2 activity in diabetic mice. *Redox Biology*, *46*, 102084. https://doi.org/10.1016/j.redox.2021.102084

Wasyluk, W., & Zwolak, A. (2021). Parp inhibitors: An innovative approach to the treatment of inflammation and metabolic disorders in sepsis. *Journal of Inflammation Research*, *14*, 1827–1844. https://doi.org/10.2147/JIR.S300679

Wei, L., Nakajima, S., Hsieh, C. L., Kanno, S., Masutani, M., Levine, A. S., Yasui, A., & Lan, L. (2013). Damage response of XRCC1 at sites of DNA single strand breaks is regulated by phosphorylation and ubiquitylation after degradation of poly(ADP-ribose). *Journal of Cell Science*. https://doi.org/10.1242/jcs.128272

Weigert, V., Jost, T., Hecht, M., Knippertz, I., Heinzerling, L., Fietkau, R., & Distel, L. V. (2020). PARP inhibitors combined with ionizing radiation induce different effects in melanoma cells and healthy fibroblasts. *BMC Cancer*, *20*(1). https://doi.org/10.1186/s12885-020-07190-9

Welsby, I., Hutin, D., Gueydan, C., Kruys, V., Rongvaux, A., & Leo, O. (2014). PARP12, an Interferon-stimulated Gene Involved in the Control of Protein Translation and Inflammation. *Journal of Biological Chemistry*, *289*(38), 26642–26657. https://doi.org/10.1074/jbc.m114.589515

Westera, L., Jennings, A. M., Maamary, J., Schwemmle, M., García-Sastre, A., & Bortz, E. (2019). Poly-ADP Ribosyl Polymerase 1 (PARP1) Regulates Influenza A Virus Polymerase. *Advances in Virology*, *2019*, 1–11. https://doi.org/10.1155/2019/8512363

Whatcott, C. J., Meyer-Ficca, M. L., Meyer, R. G., & Jacobson, M. K. (2009). A specific isoform of poly(ADP-ribose) glycohydrolase is targeted to the mitochondrial matrix by a N-terminal mitochondrial targeting sequence. *Experimental Cell Research*, *315*(20), 3477–3485. https://doi.org/10.1016/j.yexcr.2009.04.005

Whitehouse, C. J., Taylor, R. M., Thistlethwaite, A., Zhang, H., Karimi-Busheri, F., Lasko, D. D., Weinfeld, M., & Caldecott, K. W. (2001). XRCC1 stimulates human polynucleotide kinase activity at damaged DNA termini and accelerates DNA single-strand break repair. *Cell*, *104*(1), 107–117. https://doi.org/10.1016/S0092-8674(01)00195-7

Wielgos, M. E., Zhang, Z., Rajbhandari, R., Cooper, T. S., Zeng, L., Forero, A., Esteva, F. J., Osborne, C. K., Schiff, R., Albert, L. F., Nozell, S. E., & Yang, E. S. (2018). Trastuzumab-Resistant HER2+ Breast Cancer Cells Retain Sensitivity to Poly (ADP-Ribose) Polymerase (PARP) Inhibition. *Molecular Cancer Therapeutics*, *17*(5), 921–930. https://doi.org/10.1158/1535-7163.MCT-17-0302.Trastuzumab

Winstall, E., Affar, E. B., Shah, R., Bourassa, S., Scovassi, I. A., & Poirier, G. G. (1999). Preferential Perinuclear Localization of Poly(ADP-ribose) Glycohydrolase. *Experimental Cell Research*, *251*(2), 372–378. https://doi.org/10.1006/excr.1999.4594

Wu, P., Takai, H., & Titia. (2012). Telomeric 3′ Overhangs Derive from Resection by Exo1 and Apollo and Fill-In by POT1b-Associated CST. *Cell*, *150*(1), 39–52. https://doi.org/10.1016/j.cell.2012.05.026

Wu, W. J., Xiao, F., Xiong, Y., Sun, G. F., Guo, Y., Zhou, X., Hu, W., Huang, K., & Guo, H. (2023). N6-methyladenosine (m6A)-connected lncRNAs are linked to survival and immune infiltration in glioma patients. *Bioscience Reports*, *43*(5).

Wu, W., Wang, M., Mussfeldt, T., & Iliakis, G. (2008). Enhanced Use of Backup Pathways of NHEJ in G2 in Chinese Hamster Mutant Cells with Defects in the Classical Pathway of NHEJ. *Radiation Research*, *170*(4), 512–520.

Xu, Y., Shi, M.-L., Zhang, Y., Kong, N., Wang, C., Xiao, Y.-F., Du, S.-S., Zhu, Q.-Y., & Lei, C.-Q. (2022). Tankyrases inhibit innate antiviral response by PARylating VISA / MAVS and priming it for RNF146-mediated ubiquitination and degradation. *Proceedings of the National Academy of Sciences of the United States of America*, *119*(26). https://doi.org/10.1073/pnas.2122805119/-/DCSupplemental.Published

Yamashita, S., Tanaka, M., Ida, C., Kouyama, K., Nakae, S., Matsuki, T., Tsuda, M., Shirai, T., Kamemura, K., Nishi, Y., Moss, J., & Miwa, M. (2022). Physiological levels of poly(ADP-ribose) during the cell cycle regulate HeLa cell proliferation. *Experimental Cell Research*, *417*(1), 113163. https://doi.org/10.1016/j.yexcr.2022.113163

Yang, G., Chen, Y., Wu, J., Chen, S. H., Liu, X., Singh, A. K., & Yu, X. (2020). Poly(ADP-ribosyl)ation mediates early phase histone eviction at DNA lesions. *Nucleic Acids Research*, *48*(6), 3001–3013. https://doi.org/10.1093/nar/gkaa022

Yang, Hong-yi, Shen, J., Wang, Y., Liu, Y., Shen, D., & Quan, S. (2019a). Tankyrase Promotes Aerobic Glycolysis and Proliferation of Ovarian Cancer through Activation of Wnt / ? -Catenin Signaling. *Biomed Research International*, *2019*.

Yang, Hong-yi, Shen, J., Wang, Y., Liu, Y., Shen, D., & Quan, S. (2019b). Tankyrase Promotes Aerobic Glycolysis and Proliferation of Ovarian Cancer through Activation of Wnt / ? -Catenin Signaling. *Biomed Research International*. https://doi.org/10.1155/2019/2686340

Yang, Hong, Wang, R., Zeng, F., Zhao, J., Peng, S., Ma, Y., Chen, S., Ding, S., Zhong, L., Guo, W., & Wang, W. (2020). Impact of molecular subtypes on metastatic behavior and overall survival in patients with metastatic breast cancer: A single-center study combined with a large cohort study based on the surveillance, epidemiology and end results database. *Oncology Letters*, *20*(4). https://doi.org/10.3892/ol.2020.11948

Yang, Lin, Yang, G., Ding, Y., Huang, Y., Liu, S., Zhou, L., Wei, W., Wang, J., & Hu, G. (2018). Combined treatment with PI3K inhibitor BKM120 and PARP inhibitor olaparib is effective in inhibiting the gastric cancer cells with ARID1A deficiency. *Oncology Reports*, *40*(1), 479–487. https://doi.org/10.3892/or.2018.6445

Yang, Liu, Huang, K., Li, X., Du, M., Kang, X., Luo, X., Gao, L., Wang, C., Zhang, Y., Zhang, C., Tong, Q., Huang, K., Zhang, F., & Huang, D. (2013). Identification of Poly(ADP-Ribose) Polymerase-1 as a Cell Cycle Regulator through Modulating Sp1 Mediated Transcription in Human Hepatoma Cells. *PLOS ONE*, *8*(12), e82872. https://doi.org/10.1371/journal.pone.0082872

Yang, Lu, Sun, L., Teng, Y., Chen, H., Gao, Y., Levine, A. S., Nakajima, S., & Lan, L. (2017). Tankyrase1-mediated poly(ADP-ribosyl)ation of TRF1 maintains cell survival after

telomeric DNA damage. *Nucleic Acids Research*, *45*(7), 3906–3921. https://doi.org/10.1093/nar/gkx083

Yao, J., Deng, K., Huang, J., Zeng, R., & Zuo, J. (2020). Progress in the Understanding of the Mechanism of Tamoxifen Resistance in Breast Cancer. *Frontiers in Pharmacology*, *11*, 1–9. https://doi.org/10.3389/fphar.2020.592912

Yeh, T. J., Sbodio, J. I., & Chi, N. (2006). Mitotic phosphorylation of tankyrase, a PARP that promotes spindle assembly, by GSK3. *Biochemical and Biophysical Research Communications*, *350*(3), 574–579. https://doi.org/10.1016/j.bbrc.2006.09.080

Yeh, T. J., Sbodio, J. I., Tsun, Z., Luo, B., & Chi, N. (2007). Insulin-stimulated exocytosis of GLUT4 is enhanced by IRAP and its partner tankyrase. *The Biochemical Journal*, *290*, 279–290. https://doi.org/10.1042/BJ20060793

Ying, S., Hamdy, F. C., & Helleday, T. (2012). Mre11-Dependent Degradation of Stalled DNA Replication Forks Is Prevented by BRCA2 and PARP1. *American Association for Cancer Research*, *72*(11), 2814–2821. https://doi.org/10.1158/0008-5472.CAN-11-3417

Ying, W., Chen, Y., Alano, C. C., & Swanson, R. A. (2002). Tricarboxylic acid cycle substrates prevent PARP-mediated death of neurons and astrocytes. *Journal of Cerebral Blood Flow and Metabolism*, *22*(7), 774–779. https://doi.org/10.1097/00004647-200207000-00002

Yu, Mengbin, Zhang, C., Yang, Y., Yang, Z., Zhao, L., Xu, L., Wang, R., Zhou, X., & Huang, P. (2011). The interaction between the PARP10 protein and the NS1 protein of H5N1 AIV and its effect on virus replication. *Virology Journal*, *8*(1), 546. https://doi.org/10.1186/1743-422x-8-546

Yu, Mincheng, Chen, Z., Zhou, Q., Zhang, B., Huang, J., Jin, L., Zhou, B., Liu, S., Yan, J., Li, Zx., Zhang, W., Liu, C., Hu, B., Fu, P., Zhou, C., Xu, Y., Xiao, Y., Zhou, J., Fan, J., … Ye, Q. (2022). PARG inhibition limits HCC progression and potentiates the ef fi cacy of immune checkpoint therapy. *Journal of Hepatology*, *77*(1), 140–151. https://doi.org/10.1016/j.jhep.2022.01.026

Yu, S.-W. (2002). Mediation of Poly(ADP-Ribose) Polymerase-1-Dependent Cell Death by Apoptosis-Inducing Factor. *Science*, *297*(5579), 259–263. https://doi.org/10.1126/science.1072221

Yu, S.-W., Andrabi, S. A., Wang, H., Kim, N. S., Poirier, G. G., Dawson, T. M., & Dawson, V. L. (2006). Apoptosis-inducing factor mediates poly(ADP-ribose) (PAR) polymer-induced cell death. *PNAS*, *103*(48), 18314–18319. https://doi.org/10.1073/pnas.0606528103

Zahradka, P., & Ebisuzaki, K. (1982). A Shuttle Mechanism for DNA-Protein Interactions. The Regulation of Poly(ADP-ribose) Polymerase. *European Journal of Biochemistry*, *127*(3), 579–585. https://doi.org/10.1111/j.1432-1033.1982.tb06912.x

Zanotelli, M. R., Goldblatt, Z. E., Miller, J. P., Bordeleau, F., Li, J., & Garcia, A. J. (2018). Regulation of ATP utilization during metastatic cell migration by collagen architecture. *Molecular Biology of the Cell*, *29*(1), 1–9. https://doi.org/10.1091/mbc.E17-01-0041

Zarkovic, G., Belousova, E. A., Talhaoui, I., Saint-Pierre, C., Kutuzov, M. M., Matkarimov, B. T., Biard, D., Gasparutto, D., Lavrik, O. I., & Ishchenko, A. A. (2018). Characterization of DNA ADP-ribosyltransferase activities of PARP2 and PARP3: new insights into DNA ADP-ribosylation. *Nucleic Acids Research*, *46*(5), 2417–2431. https://doi.org/10.1093/nar/gkx1318

Zha, S., Li, Z., Cao, Q., Wang, F., & Liu, F. (2018). PARP1 inhibitor (PJ34) improves the function of aging-induced endothelial progenitor cells by preserving intracellular NAD+

levels and increasing SIRT1 activity. *Stem Cell Research & Therapy*, *9*(1). https://doi.org/10.1186/s13287-018-0961-7

Zhang, J., Dawson, V. L., Dawson, T. M., & Snyder, S. H. (1994). Nitric Oxide Activation of Poly(ADP-Ribose) Synthetase in Neurotoxicity. *Science*, *263*(5147), 687–690.

Zhang, R., Wang, T., & Lin, J. (2021). Synergistic effect of bazedoxifene and parp inhibitor in the treatment of ovarian cancer regardless of brca mutation. *Anticancer Research*, *41*(5), 2277–2286. https://doi.org/10.21873/ANTICANRES.15003

Zhao, B., Li, L., Tumaneng, K., Wang, C. Y., & Guan, K. L. (2010). A coordinated phosphorylation by Lats and CK1 regulates YAP stability through SCFβ-TRCP. *Genes and Development*, *24*(1), 72–85. https://doi.org/10.1101/gad.1843810

Zhao, H., Sifakis, E. G., Sumida, N., Millán-Ariño, L., Scholz, B. A., Svensson, J. P., Chen, X., Ronnegren, A. L., Mallet de Lima, C. D., Varnoosfaderani, F. S., Shi, C., Loseva, O., Yammine, S., Israelsson, M., Rathje, L. S., Németi, B., Fredlund, E., Helleday, T., Imreh, M. P., & Göndör, A. (2015). PARP1- and CTCF-Mediated Interactions between Active and Repressed Chromatin at the Lamina Promote Oscillating Transcription. *Molecular Cell*, *59*(6), 984–997. https://doi.org/10.1016/j.molcel.2015.07.019

Zhao, Y., Hu, X., Wei, L., Song, D., Wang, J., You, L., Saiyin, H., Li, Z., Yu, W., Yu, L., Ding, J., & Wu, J. (2018). PARP10 suppresses tumor metastasis through regulation of AuroraA activity. *Oncogene*, *37*, 2921–2935. https://doi.org/10.1038/s41388-018-0168-5

Zhen, Y., & Yu, Y. (2018). Proteomic Analysis of the Downstream Signaling Network of PARP1. *Biochemistry*, *57*(4), 429–440. https://doi.org/10.1021/acs.biochem.7b01022

Zhou, Y., Feng, X., & Koh, D. W. (2010). Enhanced DNA Accessibility and Increased DNA Damage Induced by the Absence of Poly(ADP-ribose) Hydrolysis. *Biochemistry*, *49*(34), 7360–7366. https://doi.org/10.1021/bi100979j

Zhou, Y., Feng, X., & Koh, D. W. (2011). Activation of Cell Death Mediated by Apoptosis-Inducing Factor Due to the Absence of Poly(ADP-ribose) Glycohydrolase. *Biochemistry*, *50*(14), 2850–2859. https://doi.org/10.1021/bi101829r